PROGRAM 631A   VOLUME VI

TECHNICAL REPORT

EXPERIMENT D 8:   RADIATION IN SPACECRAFT

Prepared by:

MARION F. SCHNEIDER
1st Lt USAF
AFWL

JOSEPH F. JANNI
1st Lt USAF
AFWL

B. BRENTNALL
Maj USAF
SSD Det 2

MAY 1966

Bioastronautics Group

Biophysics Branch
Air Force Weapons Laboratory
Kirtland AFB, New Mexico

and

Space Systems Division
Det 2
MSC, Houston, Texas

PROGRAM 631A   VOLUME VI

TECHNICAL REPORT

EXPERIMENT D 8:   RADIATION IN SPACECRAFT

Prepared by:

MARION F. SCHNEIDER
1st Lt USAF
AFWL

JOSEPH F. JANNI
1st Lt USAF
AFWL

B. BRENTNALL
Maj USAF
SSD Det 2

MAY 1966

Bioastronautics Group

Biophysics Branch
Air Force Weapons Laboratory
Kirtland AFB, New Mexico

and

Space Systems Division
Det 2
MSC, Houston, Texas

FOREWORD

This document describes in technical detail the Air Force Radiation Experiment D8, carried out as a part of the 631A Program on the NASA Gemini flights. This experiment was concerned with gathering dose data and developing techniques furthering the art of manned spacecraft radiation dosimetry systems. Information from D8 should be of significant value in insuring manned mission safety and success in the future. From this effort new and highly sophisticated space-flight-worthy radiac systems have evolved. Their versatility in manned space operations was demonstrated for the first time on Gemini IV. D8 was the initial effort to place a complete dosimetry system on-board a manned spacecraft. This radiation experiment consisted of the latest available passive devices complimentary to (and correlated with) active ionization chambers giving instantaneous dose data. The information gathered in this experiment has been used to perform vital empirical checks on existing computational techniques and is presently providing corrections for application to theoretical prediction capabilities for radiation hazards associated with future manned spaceflights.

The authors wish to express their thanks to the following individuals:

1. Captain John W. Donahue, whose timely guidance and advice as the Systems Command Field Office Project Officer between the Air Force and NASA proved invaluable in successfully integrating the experiment on the Gemini spacecraft.

2. Mr. Robert Seick of NASA, who gave untiringly of his time to keep things running smoothly during the prelaunch checkout of the spacecraft.

3. Mr. Ray Roten, who helped reduced the data from the active part of the experiment.

i

4. Mr. Benton C. Clark, who initiated the experimental program at the Air Force Weapons Laboratory, whose sound technical guidance made this experiment possible.

5. To all personnel at AFWL, especially Mr. Glenn C. Ainsworth, George Radke, and Mr. Charles Coombs, whose team effort helped bring this experiment to a successful completion.

This technical report has been reviewed and is approved.

Wilbur A. Ballentine
Colonel, USAF
Commander, Det 2 SSD AFSCFO

ABSTRACT

A prerequisite to the successful completion of Manned Space Missions is the gathering of adequate data concerning the radiation environment and its inter-action properties with the matter comprising the spacecraft system. It has been demonstrated that the most important parameters associated with the radia-tion field are a measure of the time, depth, and accumulated absorbed dose dis-tributions in a tissue equivalent material. The Gemini 4 and 6 flights provided the initial opportunity to perform these critical dose measurements under the actual environmental conditions of space and within realistic spacecraft shield-ing configurations. The important properties of the space radiation environment which governed the design and extent of the experiment are discussed in detail in this report. The experiment was divided into two separate instrument systems to accomplish the fundamental measurements. A specially designed active tissue equivalent ionization chamber system incorporating portable sensors was utilized. The active system measured all absorbed dose levels above 0.1 millirad/hour at many astronaut body shielding and spacecraft cabin locations. The most sensi-tive currently available passive dosimeters, e.g. thermoluminescent devices were coupled with film emulsion packs and activation foils to record the radiation within the Gemini spacecraft. Measurements of Primary Cosmic and Inner Van Allen Belt Radiation provided excellent agreement between the response of the active and passive dosimetry systems. The total dose received on the Gemini 4 Mission was measured to be 82 millirad while for the Gemini 6 Mission only 20 millirad was recorded. The instantaneous dose rate reached a level of 107 millirad/hour during revolution 7 of the Gemini 4 Mission. The highest dose rate recorded on the Gemini 6 Mission was 73 millirad/hour during a pass through the Inner Belt. The spacecraft shielding was found to have influenced dose levels by more than a factor of two on both missions. Film emulsion data coupled with

special shielding experiments conducted using the active dosimeters show that
the doses received on both the Gemini 4 and 6 Missions were predominately a result
of the energetic proton component of the Inner Van Allen Belt and point out the
dangers of manned operations deeper in the radiation belts.

TABLE OF CONTENTS

LIST OF TABLES

LIST OF ILLUSTRATIONS

I. INTRODUCTION:

I.A. <u>Title of Experiment</u>: DOD Experiment, D-8: Radiation in Spacecraft

I.B. <u>Purpose of Experiment</u>:

It was the purpose of this experiment to perform a series of precision radiation measurements to obtain reliable empirical dosimetry data for use in spaceflight planning studies where accurate prediction and interpretation of biological radiation effects produced in man are vitally important. The gathering of adequate data concerning the radiation environment, shielding interactions, and dose rate levels encountered in space is a fundamental prerequisite to successful space mission planning. It provides the only means of insuring astronaut protection against an often hostile radiation environment.

I.C. <u>General Description of Experiment</u>:

The specific measurements performed in this effort comprise a quantitative and qualitative characterization of the spacecraft interior radiation levels encountered in the Gemini missions. The expected radiation environment consisted largely of the energetic protons and electrons previously observed in the Inner Van Allen Belt. The spacecraft encountered this Belt each time it passed through the South Atlantic Anomaly: that part of the belt which dips close to the earth due to an anomalously low strength of the earth's magnetic field. The low altitude of this trapped radiation region and the short duration of the mission through it provided an excellent opportunity to study radiation interaction characteristics without exposing Gemini astronauts to the undesirably high levels encountered deeper in the Inner Belt. For these reasons, the instruments designed for the experiment were optimized for response to the radiation levels anticipated in this geomagnetic anomaly. The dynamic range of the instrumentation

1

was extended in lower sensitivity limits to detect all energy deposition rates above 0.1 millirad/hour. This permitted measurement of the very low cosmic radiation intensities that contribute in lesser degree to the total mission dose.

The experiment also determined the ionizing and penetrating power of the various primary and secondary radiation present in the Gemini capsule as well as measuring the contribution to dose according to profile, particle type, time and position or location within the spacecraft.

The experiment was accomplished through the use of two distinct types of dosimetry systems. One system had active response to ionizing radiation, while the other provided a passive response. The design, fabrication, testing, spacecraft integration, flight plan incorporation, and final data analysis program associated with each type of dosimeter system will be discussed in the following sections of the report.

II. BACKGROUND:

II.A. Source of Experiment:

The problem of space radiation has posed a potential obstacle to space missions for many years. Radiation likely to be encountered in space missions is, moreover, quite complex when compared to sources available on earth; the effects on biological systems exposed to it are also complex. The parameters associated with the biological effects of ionizing radiation were, therefore, the primary concern of this experiment.

The knowledge of radiation effects on biological targets has been observed over the last half century, beginning with the introduction of the X-ray machine as a research device with primates, mice, guinea pigs, rabbits, sheep, and other animals. The effects of radiation in man were first observed in the early 1900's, when persons working with X-rays and naturally radioactive radium became exposed to their ionizing fields and developed a variety of symptoms common to

2

radiation sickness. Early observations and resultant experiments provided several avenues to describe the effects of ionizing radiation on matter. One is the assessment of the total energy deposited by the radiation field in the irradiated material. Another is the local microscopic or spatial distribution of ionization density of the radiation. The latter concept determines the quality or effectiveness of the total energy deposited in producing a given effect. Comparison subsequently showed the total energy deposited, that is, the "dose", to be the most important single measurable factor associated with the radiation field in determining fundamental biological effects.

For the purposes of this report space radiation may be divided into three categories: Van Allen radiation, cosmic radiation, and solar flare radiation.

II.A.1 Van Allen Radiation:

The Van Allen particles, although a relatively recent discovery, have been subject to intense study and measurement since 1958. The existence of the Van Allen particles, however, was predicted by Störmer from studies of the trapping mechanisms associated with dipole fields as far back as 1955. Van Allen radiation populates a large region near the earth and is divided into two separate regions or belts. Figure 1 shows a cut-away view of the Belts and their general composition.

Störmer, in 1907, (Ref 1) formulated the problem of charged particle motion in dipole fields to study the behavior of cosmic radiation and auroral phenomena. Störmer's theory was later utilized to predict the existence of trapped particles in the earth's magnetic field.

According to Störmer, a particle will spiral about a magnetic line of force in a dipole field as shown in Figure 2.

3
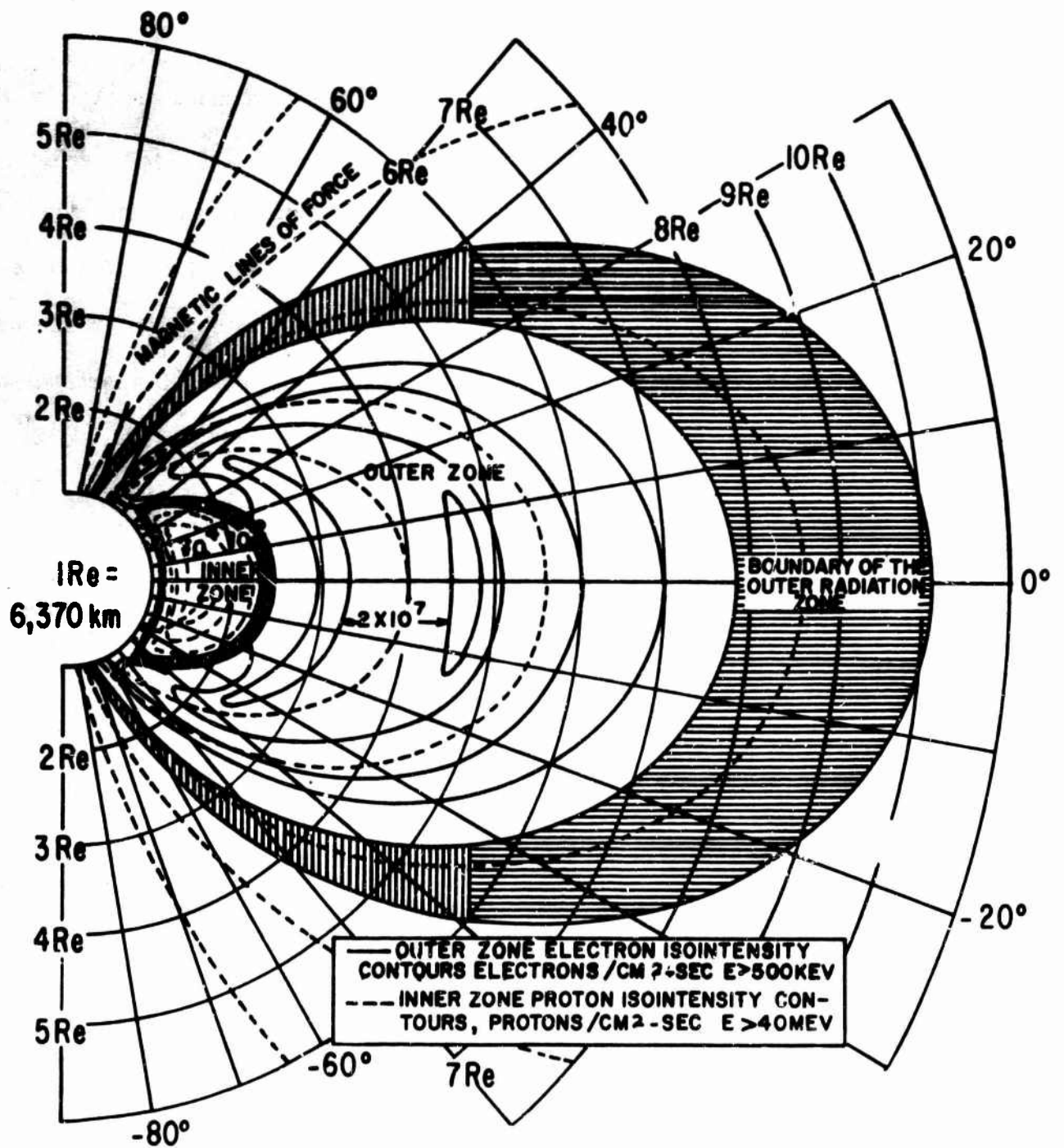
GEOMAGNETIC MERIDIAN PROJECTION MAP OF THE SPACE
RADIATION ENVIRONMENT ILLUSTRATING THE OUTER AND
THE INNER ZONE.

Figure 1

4

COORDINATE REPRESENTATION OF A TRAPPED CHARGED PARTICLE IN A DIOPOLE FIELD
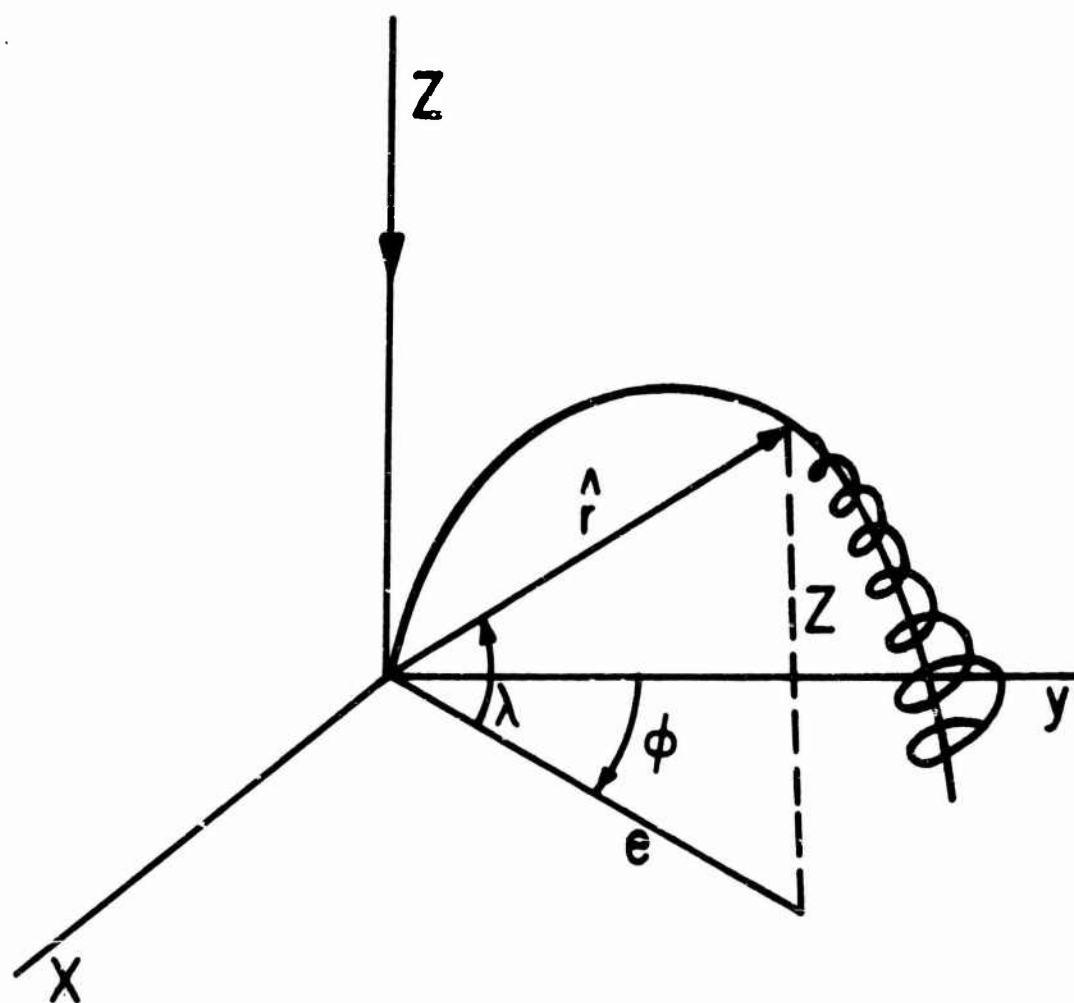
Figure 2

The particle gyrates about the guiding line of force

$$r = r_c \cos^2 \lambda$$

·with a cyclotron frequency

$$\omega = \frac{qB}{\gamma M}$$

where

$$\gamma = \left(1 - \frac{v^2}{c^2}\right)^{-\frac{1}{2}}$$

$$\hat{B} = \hat{\nabla} \times \hat{A}$$

$$\hat{A} = \phi M \rho \, r^{-3}$$

$$B = \frac{m}{r^3} (1 + 3 \sin^2 \lambda)^{\frac{1}{2}}$$

M = down·ard magnetic moment of Figure 2.

The particle moves along the line of force which imparts to it helical motion.
In addition, when the particle moves into a region of stronger magnetic field
at higher latitudes, it is reflected back toward the equator. The point at
which a charged particle is reflected back by the converging lines of force
is called a mirror point. The value of the magnetic field at this point is
shown to be $B_m = B/\sin^2 \alpha$. The particles will drift slowly west if they are
positively charged, east if they are negative. They trace a shell around

6

the earth. The two dimensional equations of motion for a system of trapped particles is given by

$$\ddot{Z} + \frac{1}{\rho^6} (\rho - 1) Z = \Phi(Z^3)$$

$$\ddot{\rho} + \frac{1}{\rho^5} (\rho - 1)(2 - \rho) = \Phi(Z^2)$$

The equations of motion form a non-linear system of coupled, second order differential equations, for which no simple solutions exist. One very useful method of describing trapped particle motion of this type is given by the guiding center approximation vectorially illustrated in Figure 3.

$$\hat{b} = \frac{\hat{B}}{B} \qquad\qquad\qquad \hat{\gamma}_c = \frac{c}{B_e}(\hat{b}x\hat{P})$$

$$P\ C = B_e \gamma_c$$

$$r_c = P\ C/B_e$$

$$\tilde{r}_c = P\ C/B_e \left(\frac{\hat{b} \times \hat{P}}{P}\right)$$

Using this approximation, the following expression for the average drift velocity of the guiding center of the particle can be written:

$$\frac{d\hat{R}}{dt} = \hat{v}_{//} + \hat{b} \ x \ \frac{c}{e} \left[m\ \frac{1}{B}\ \hat{\nabla}\ B + 2m\ \frac{P^2}{P^2}_{//}\ \frac{\partial \hat{b}}{\partial s} + \frac{P_{//}}{B}\ \frac{\partial \hat{b}}{\partial t} \right] + \frac{c}{B^2}\ (\hat{E}x\hat{B}) + \hat{b}$$

This expression may be written in another useful manner by a transformation. In order to accomplish this transform, we note first that the magnitude of the field due to a dipole of strength μ can be written:

$$B = \frac{\mu}{r^3} \sqrt{3 \cos^2 \theta + 1}$$

7

GUIDING LINE OF FORCE

$\vec{B}$

R_c

$\vec{M}$

$\vec{F}_\perp$

$\vec{T}_c$

$\vec{R}$

$\vec{V}_\perp$

$\vec{V}_\parallel$

$\vec{T}$
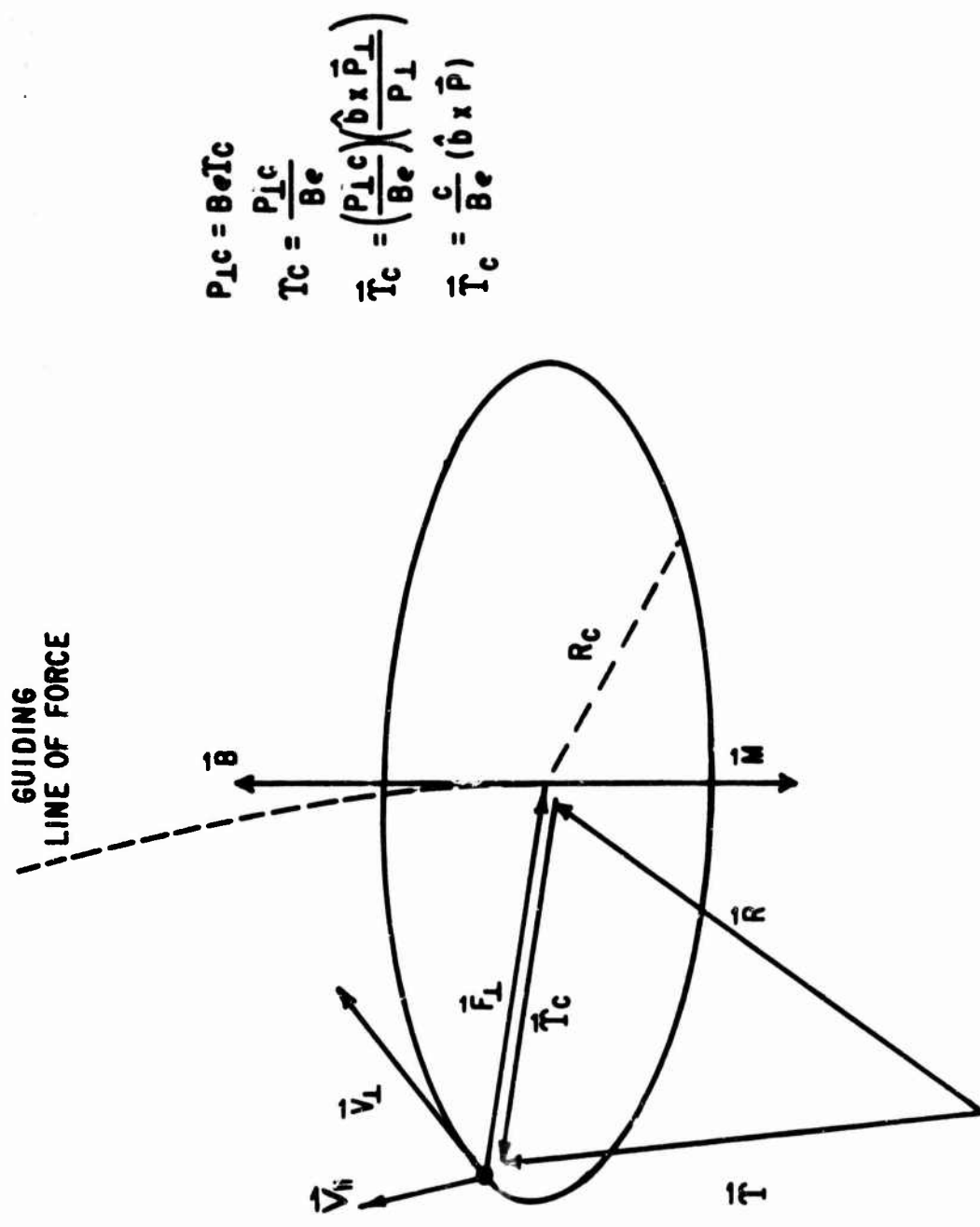
$$P_{\perp c} = BeT_c$$

$$T_c = \frac{P_{\perp c}}{Be}$$

$$\vec{T}_c = \left(\frac{P_{\perp c}}{Be}\right)\left(\frac{\hat{b} \times \vec{P}_\perp}{P_\perp}\right)$$

$$\vec{T}_c = \frac{c}{Be}(\hat{b} \times \vec{P})$$

Cyclotron Motion of a Particle in a Magnetic Field Around a Guiding Center of Force

Figure 3

Where r is the distance from the dipole and θ is the polar angle or the angle that the position vector of the particle makes with the axis of the dipole. If we choose the time t = 0 to be the time that the particle is in the equatorial plane and define ψ so that the angle the particle momentum makes with the magnetic field at t = 0 is $\frac{\pi}{2} - \psi$, the equation is transformed into the following quantity:

$$r^3 = r_o^3 \cos^2 \sqrt{1 + 3 \cos^2 \theta}$$

This equation expresses the altitude, r, at which reflection occurs in terms of the polar angle at reflection θ and altitude r_o and pitch angle ψ when the particle is in the equatorial plane. This means that the particle injected at a high altitude with a pitch angle which is not too large will remain at high altitudes, oscillating along a field line with a relatively small amplitude. Figure 4 illustrates the spiralling motion of a typical case for a trapped charged particle, where $\hat{v}_{\parallel}$ is the velocity component parallel to $\hat{B}$.

$$\hat{b} \left[\frac{c}{e} \ m \ \frac{\hat{B}_o \ \nabla \times \hat{B}}{B^3} \right] = \text{correction to B due to curvature of the field lines.}$$

$$\frac{c(\hat{E} \times \hat{B})}{B^2} = \text{Hall current drift.}$$

$$\hat{b} \times \frac{c}{e} \ (m \ \frac{1}{B} \ \nabla \ \hat{B}) = \text{Drift current arising from the variation of the Larmor radius during the cyclotron motion.}$$

$$\hat{b} \times \frac{c}{e} \ \left[2m \ \frac{P^2_{\parallel}}{P^2_{\perp}} \ \frac{\partial \hat{b}}{\partial s} + \frac{P_{\parallel}}{B} \ \frac{\partial \hat{b}}{\partial t} \right] = \text{a term arising from the inertial effects of } P_{\parallel} \text{ motion which carries particles across the field lines.}$$

9
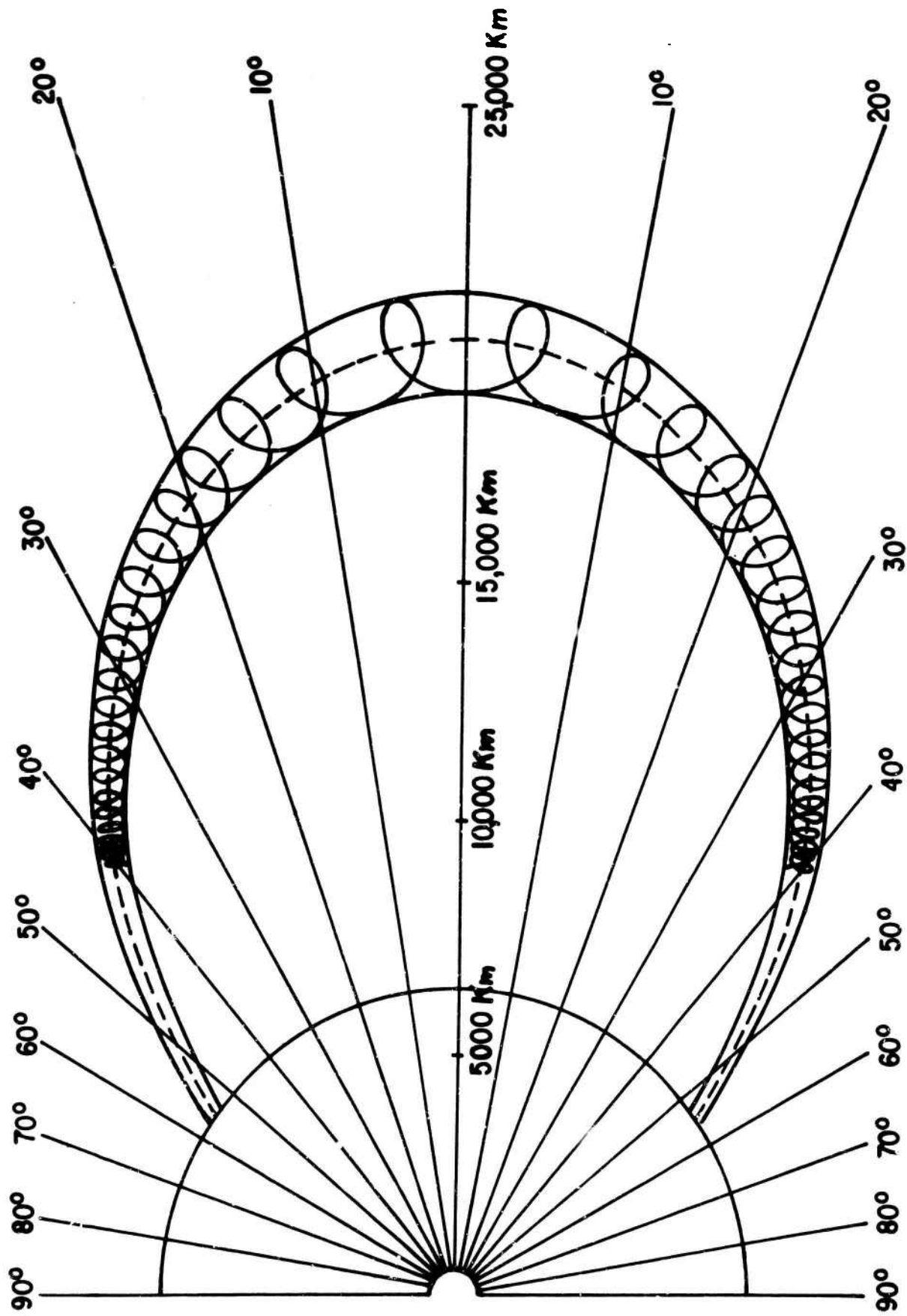
MOTION OF A TRAPPED PARTICLE BETWEEN ITS MIRROR POINTS ON A LINE OF FORCE TYPICAL OF THE GEOMAGNETIC FIELD.

Figure 4

10

It can be shown that for motion in a pure magnetic field the energy of a particle is constant. This leads to the adiabatic invariant $\underline{m}$ which is defined by

$$ m = \frac{p^2}{2mB} $$

The point on a field line at which reflection occurs is given by

$$ \frac{p^2}{2mB} = \frac{p^2}{2mB} \Bigg|_{t=0} $$

The second or longitudinal invariant is defined by:

$$ I = \int \sqrt{1 - \frac{B}{B_m}} \; ds $$

The integration is taken along the guiding center path between the mirror points. This invariant restricts the drift of a charged particle to field lines on which I is a constant, and occurs only for slow perturbations. This slow variance means that the time variations of the field must be small compared to the mirror period, that is, the time it takes a particle to complete an oscillation from one mirror point to the opposite one and back. Since a particle makes many gyrations around a field line in each bounce period, the second adiabatic invariant is more easily disturbed than the first, in a time dependent field for instance, and may lead to the particle's loss in the atmosphere.

The third adiabatic invariant is the total flux or the magnetic "B" field inside the surface formed by the particle as it drifts in longitude. This invariant guarantees that the surface will be closed. The magnetic flux is is invariant only when the field is almost constant for the time it takes the particles to drift in longitude around the earth, or its drift period. Thus, a total of three adiabatic invariants can be used to predict the behavior of trapped particles in the earth's magnetic field. Since the trapped particles

11

are confined to a shell of magnetic field lines having a constant I and B, these two parameters may be used instead of geographical coordinates for mapping the fluxes of particles. By using I and B as the basic coordinates, the number of necessary coordinates is reduced from three to two. McIlwain formulated the concept of a parameter which retained the geomagnetic significance of I and also was approximately constant on a given line of force. In a dipole field such a parameter is called R_o, the radial distance to the point where the field line crosses the magnetic equator. It follows that trapped radiation in a dipole field can be entirely specified in terms of R_o and B, where R_o specifies a field line and B specifies a point on that field line. Since a dipole field constrains the particles to motion along field lines having the same R_o, and oscillations in a manner such that their pitch angles are the same at the same value of B (as a result of the magnetic moment), the flux at a point in space having magnetic coordinates (B, R_o) is the same as the flux at every other point having the same geomagnetic coordinates.

The real geomagnetic field is, unfortunately, not a dipole field. McIlwain, however, devised the magnetic field parameter L which is analogous to the dipole parameter R_o. The real field is in practice approximated by a multi-term expansion given by Jensen and Cain. This expansion was used by McIlwain to calculate B and I and in turn L, which is generally found to vary by less than one per cent along a field line. A reverse transformation leads to the following relationship between the real and the B - L coordinates:

$$B = \frac{M}{r^3} \sqrt{4 - \frac{3r}{L}} = L \cos^2\lambda$$

The B - L coordinate system is based on the assumption of the conservation of the adiabatic invariants, which is not valid during large geomagnetic or solar storms or at high latitudes and altitudes where the magnetic field lines are

12

distorted by the solar wind. However, the concept of B - L mapping of the
Van Allen Belts is very useful and has made it possible to relate widely
different experimental measurements of the spectra of charged particles in the
radiation belts.

The most reliable proton energy spectrum for the Inner Van Allen Belt
protons is given by McIlwain and Pizzella and takes into account the softening
of the spectrum with increasing L. This spectrum is:

$$J_{proton}(E) \, dE = Ke - \frac{E}{E_0} \, dE$$

where

$$E_0 = (306 \pm 28) \; |E^{-}_{\nu} \, (5.2 \pm 0.2)_{mev}$$

Using this proton spectrum, a flux distribution similar to the one shown in
Figure 5 is obtained. Figure 6 shows the character of the Inner Belt spectrum
of protons as measured for an L of 1.6 earth radii from Explorer IV and
Explorer XV data.

It has been found that a safe upper limit for the natural electron flux
can be represented through the altitude independent integral spectrum of the
form given by Holly (Ref 5):

$$J_{electron}(>E) = K, E^{-0.5} \qquad 30 < E < 200 \quad KEV$$

$$J_{electron}(>E) = K_2 E^{-4.0} \qquad 0.2 < E < \quad 5 \quad MEV$$

Using this spectral representation of the natural electron field, one
obtains an electron distribution in B - L space such as is shown in Figure 7.

In July, 1962, a nuclear device designated "Starfish" was detonated at
an altitude of nearly 400 km over Johnston Island on the L = 1.12 geomagnetic
field line. This device is estimated to have injected some 10^{25} electrons with
energies between 0.5 and 10 Mev in trapped orbits in the geomagnetic field.
The peak flux at L = 1.2 to 1.3 on the equator was given as over 10^9 per cm^2 sec

Figure 5

OMNIDIRECTIONAL PROTON FLUX Jp (40<E<110MeV) IN B-L COORDINATES

14

OMNIDIRECTIONAL PROTON FLUX AT L = 1.6 (40 < E < 110 MeV)

Figure 6

15
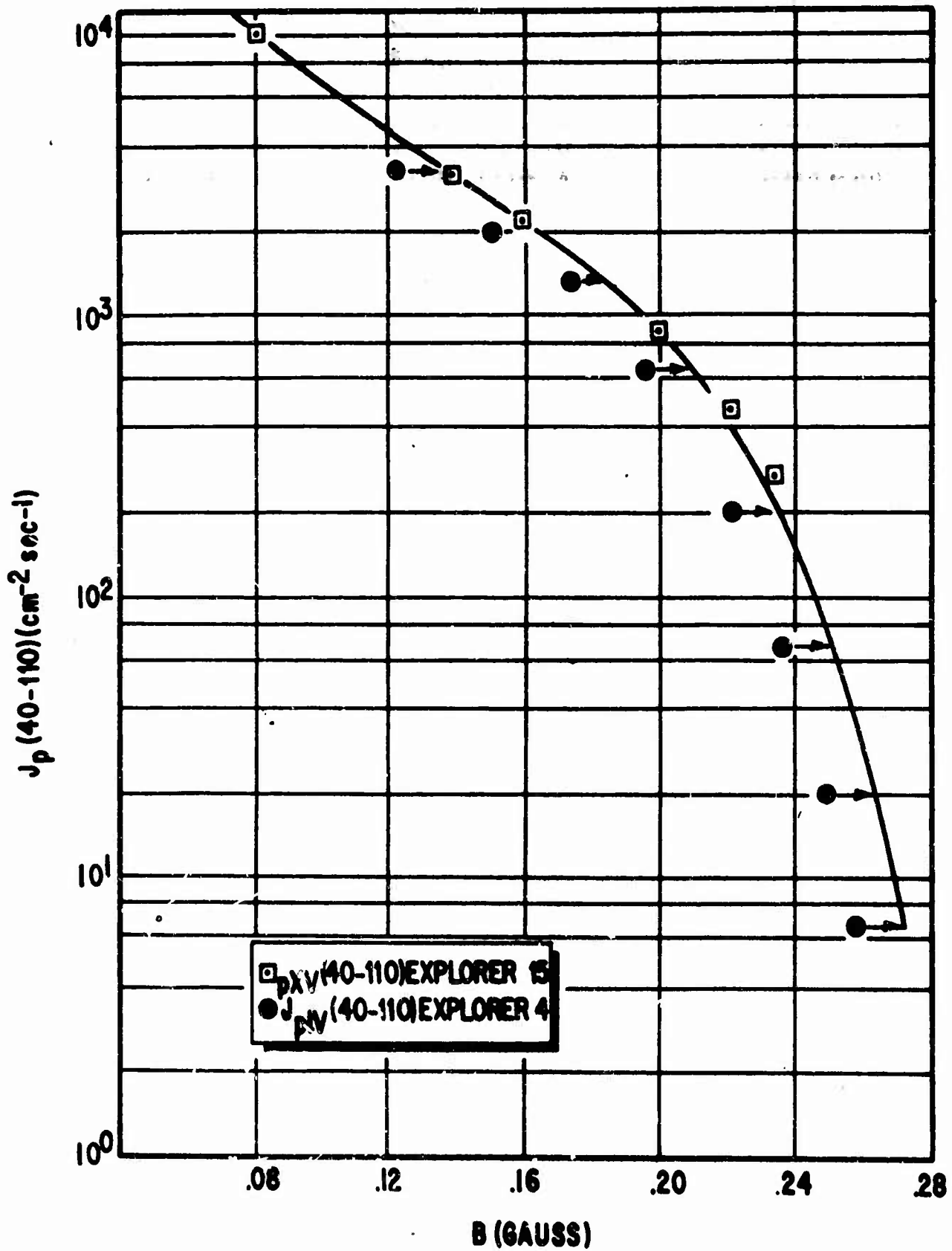
CODIRECTIONAL ELECTRON FLUX J_e (E 0.5 MeV) IN B-L COORDINATES

Figure 7

16
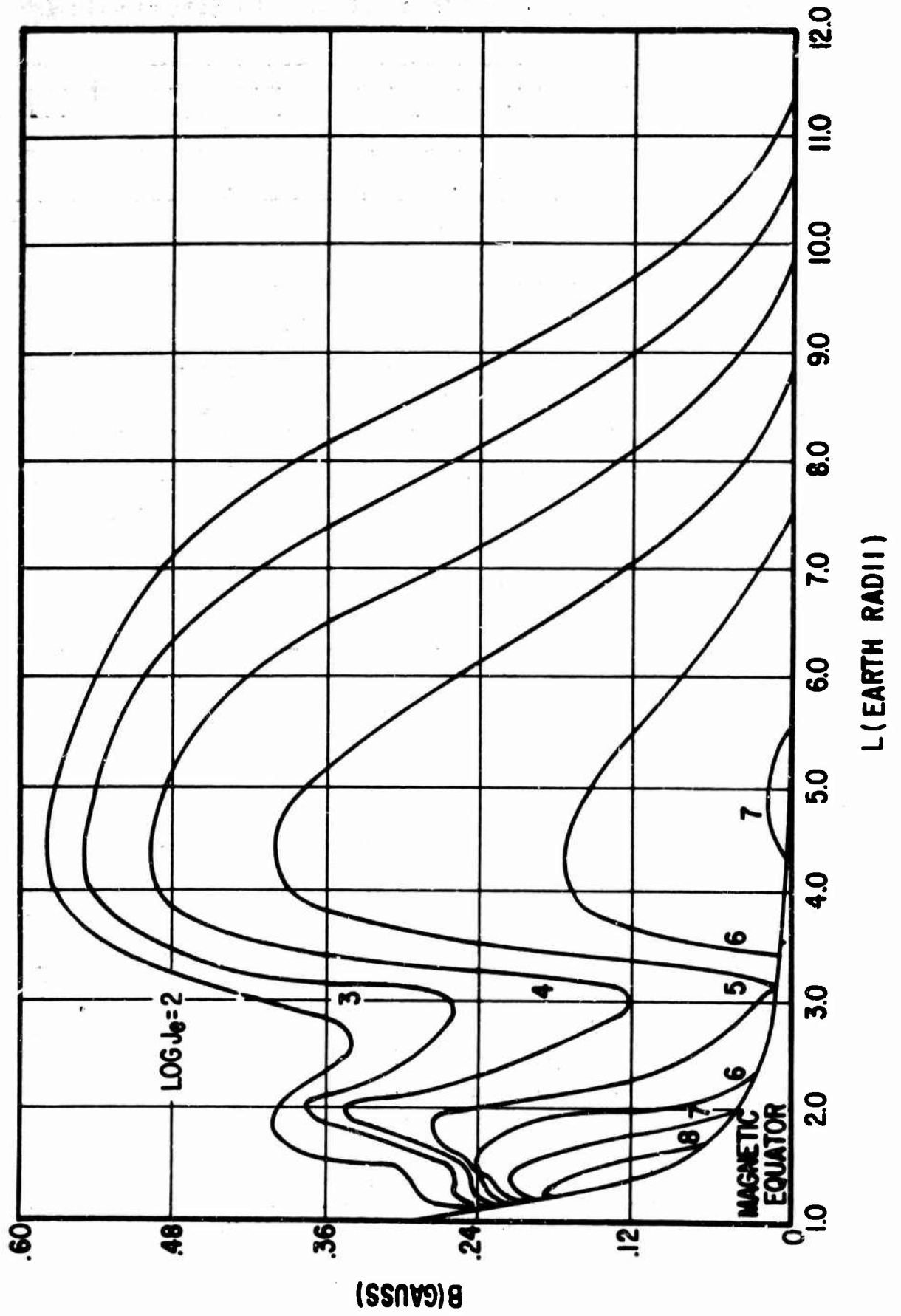
with large fluxes as low as 100 km. Since the Starfish burst was so large, the energy density in the particle cloud was greater than the energy density in the magnetic field, disrupting the magnetic field and allowing the electrons which would have been contained by the field to be distributed over a large range of L values, particularly L values larger than 1.12. Electrons diffusing to lower L values were quickly lost in the atmosphere. Later measurements showed that the peak fluxes had shifted to an L value of approximately 1.2.

II.A.2   Cosmic Radiation:

The most energetic source of space radiation now known to exist is found in the primary cosmic radiation fluxes that reach the solar system from outside. Particles resulting from cosmic radiation have been measured with energies extending up to 10^{-18} electron volts. These particles are found to be isotropically distributed throughout the solar system. The origin of cosmic radiation is galactic; hence, the name galactic cosmic radiation is often used synonymously with cosmic radiation. The tracks of cosmic radiation have been observed since the discovery of the cloud chamber at the beginning of this century. Extensive research into the nature and behavior of cosmic radiation was carried out in balloons and other high-altitude devices prior to the launching of probes and rockets in the late 1950's. Cosmic radiation has long provided researchers in nuclear physics with a ready source of high energy particles for experiments before the existence of high energy accelerators. The composition of cosmic radiation is similar to that of matter that is thought to make up the universe as a whole. It is primarily composed of hydrogen nuclei or protons which make up about 87 percent of the flux. Alpha particles or stripped helium nuclei make up about 10 percent, and the remaining 3 percent is made up

17

of heavier nuclei particularly nitrogen, carbon, and oxygen. Nuclei of iron and calcium have also been observed in small traces in cosmic radiation. The flux of cosmic radiation is extremely low in comparison to the other two contributors to space radiation, having a value of only about 2.5 particles per cm^2 per sec in free space or at high altitudes over the poles. At lower latitudes, cosmic radiation is subject to magnetic cutoff from the earth's field, and the value of the flux is greatly reduced. Cosmic radiation is significant in that it possesses an extremely high penetrating ability as a result of its ultra-high velocity and is difficult to shield against in many operations. This extremely high energy also leads to a rather large and complicated spectrum of secondary products which in some instances could be dangerous, especially if a system is exposed to it over any great period of time. Temporal variations in cosmic radiation have been observed during periods of solar activity. The cycles show a decrease in the flux below the 2.5 particles per cm^2 per sec observed during quiet periods. This decrease is attributed to magnetic disturbances in the solar magnetic fields which deflect many of the cosmic particles. The energy spectrum of the galactic protons is represented by the expression:

$$N \ (> E) \ = \frac{0.3}{1+E} \ 1.5 \ particles/cm^2 \ sec \ steradian$$

This expression is valid over the range 500 Mev to 20 Bev. E in the above expression is in Bev. It has been shown that this equation also represents the energy spectrum per nucleon for the other components of cosmic radiation.

II.A.3   Solar Flare Radiation:

Solar flare particles are the remaining constituent of the space radiation of present concern. Solar flare particles were initially detected and identified from a combination of research into cosmic radiation and later

18

BLANK

can be represented by the expression $N \ (> E) = KE^{-\Gamma} t^{-x}$ where Γ is between 3.5 and 5.0.

Proton peak intensities for the larger events described by the formula show an intensity of 1.5×10^5 protons/cm^2 sec at 1.2 days. Over a one-day period the total flux above 30 Mev was approximately 5×10^9 protons/cm^2. It has been observed that the yearly average production rate is on the order of 10^8 protons/cm^2 above 100 Mev, or 10^{10} protons/cm^2 per year above 30 Mev. This corresponds to a dose of about 3,000 rads absorbed dose in unit density material which shows that the solar flare dose could be dangerously high in a lightly shielded operation. The alpha particle component of the relativistic flares has been observed to constitute as much as ten percent of the total flux in some of the flares. The alpha particles have a much higher ion density than protons, varying approximately as the square of the charge of the particle, and such could add significantly to the effective biological hazard of a given flare.

At this time no adequate warning system exists for detemining the nature and extent of a flare. There exists a great need to equip space-ships that will travel at greater distances from the earth with instantaneous radiation monitoring equipment to provide directly the biologically-significant parameters generated by such radiation, (i.e., a measurement of the total and specific ionization of the emitted radiation). On-board dosimetry equipment would not rely on theoretical predictions based on scanty input data of the flare fluxes to provide instantaneous measurements of the determining mission go or no-go parameters.

Table I illustrates some of the more important space experiments that have been carried out in the field of radiation research since 1958. Space radiation research was initiated with the flying of Geiger counters whose saturation indicated the presence of the radiation belts and has evolved into a whole

20

series of experiments flown on satellites, whose specific missions are to perform
sophisticated directional and omnidirectional spectral measurements in conjunction
with simultaneously measurable depth dose patterns in phantoms. The first series
of unmanned satellites set out to define the nature and extent of the radiation belts.
With the ejection of fission-formed electrons into the Van Allen regions, forming the
artificial belts, emphasis was also placed on determining the dose levels. The later
satellites, were designed with the idea of complete coverage of the radiation field
and its biological effects and, hence, were set up to measure both dose and spectra.
Since 1962, manned spaceflight has emerged as a prime instrument of space research.
Experiments like D8 usher in new and different techniques of assessing the radiation
problem. These techniques and results are only a beginning of more advanced and
refined methods of attacking the problem of space radiation as man reaches further out
in space.

Thus, in attempting to predict the biological effects of space radiation,
two main factors face the researcher:

1. The radiation environment itself is highly complex and oftentimes
poorly defined--even unpredictable in many instances.

2. The complex way in which radiation interacts with matter makes the
determination and measurement of dose very difficult when complex spectra of
radiation impinge on matter. It was in dealing with these problems that this
experiment was initially conceived.

Table I.
PARTIAL LIST OF RADIATION TYPE SATELLITES AND PROBES

TABLE

NAME & DESCRIPTION	ALTITUDE (MAX. KM)	EXPERIMENTAL EQUIPMENT	TYPE AND ENERGY OF PARTICLE	EXPERIMENTER
Explorer I, 1958	120	Geiger Counter	Electrons - 3 Kev to 100 Kev	Van Allen
Explorer III, 1958	180	Geiger Counter Proton Electron Spectrometer	Electrons - 30 Kev to 100 Kev Protons - 50 Kev to 1.5 Mev	Davis
Pioneer I, 1958	60,000	Ionization Chamber	Dose rate of electrons & protons	Rosen
Sputnik III, 1958	1,500	Geiger Counters and Spectrometers	Electrons - 80 Kev to 650 Kev Protons - 28 Mev to 200 Mev	Vernov
Lunik I, 1959	Solar Orbit	Geiger Counters and Scintillators	Electrons greater than 2 Mev Protons greater than 30 Mev	Vernov
Atlas Pod, 1959	900	Geiger Counters with Shields and Magnets	Electrons - 30 Kev to 6 Mev	Holly
Atlas Pod, 1959	1,100	Nuclear Emulsions	Protons greater than 40 Mev	Yogoda
Atlas Pod, 1959	1,200	Nuclear Emulsions	Protons greater than 75 Mev	Freden & White
Explorer IV, 1959	2,000	Scintillator	Electrons and protons greater than 35 Kev	Rosen
Sputnik V, 1960	300	Scintillator and Geiger Telescope	Electrons greater than 8 Mev Protons greater than 60 Mev	Vernov
Ballistic Flight, 1960	1,155	Ionization Chamber 5.75 grams of shielding	390 millirad/hour electrons and protons	Parker
Explorer XII, 1961	77,000	Scintillator, Proportional and Geiger Counters	Electron isointensity contours and temporal variations in Outer Belt established during solar flares	Imhof
Rocket Probe, 1961	2,100	Ionization Chamber .75 grams of shielding	500 millirad/hour protons and and electrons	Tinney
Alpha Upsilon I, 1962	609	Ionization Chamber Shielded	1000 r/hour electrons	Clark
Beta Kappa I, 1962	5,198	Ionization Chamber, Shielded	23,000 r/hour electrons	Clark

II. B. **Scientific Need for Experiment:**

Since 1962 there have been an increasing number of unmanned satellites which have been programmed to carry dosimetric equipment into space. Scientific interest in space radiation dosimetry was spurred by two factors:

1. Nuclear detonations by the Soviet Union and the United States led to the creation of a new artificial radiation environment known as the Starfish Radiation Belts. The Starfish radiation consisted of fission spectrum electrons of very high flux density which were subject to magnetic trapping and led to large charged particle populations in regions of possible manned space operations, such as the South Atlantic anomaly. Since no accurate measurements of the electron population or its rate of decay were readily available at the time, it was necessary to measure the dose or energy deposition directly to satisfy various spacecraft design and operational criteria which were being formulated by the Air Force and NASA. The two agencies set out to solve the problem of measuring this high electron environment in two different ways. NASA instrumented their planned Mercury flights with passive dosimetry interior to the spacecraft and Geiger counters external to the capsule. The Air Force on the other hand pursued a program of unmanned satellites flying shielded and un-shielded tissue equivalent ionization chamber dosimeters. Neither method of measurement proved successful in assessing the exact radiation hazard properties of the space particle environment, and by late 1963 it was realized that there existed a need to fly a specially designed tissue responding active dosimetry system in conjunction with an elaborate passive dosimetry network within the cabin of a manned space vehicle in order to examine closely the behavior of charged particles with space systems.

2. Due to intense interest in the possible hazards associated with the trapped radiation environment and the solar flare eruptions, theoretical

radiation transport codes known as shielding codes were developed by various groups concerned with space flight. These codes utilized mathematical models of the radiation interaction properties of matter combined with various simple geometries such as spheres and cylinders to predict the expected dose levels within the interior of various spacecraft. The initial codes used homogeneous materials such as water, tungsten, and aluminum to obtain the dose at the center point of the spacecraft. Existing flux maps of the radiation environment were utilized as the input data for each code. Later codes were improved and the order of sophistication of the prediction capability was increased by "second generation methods," which allowed the dose to be calculated in existing spacecraft geometries at many locations within the vehicle. With the development of more refined prediction methods which account for specific geometries of the spacecraft and provided versatility in the dose predictions, empirical dose data were necessary for known radiation environments to perform corrections in the codes. This type of data was not available in any usable form. Furthermore, the dose measurements that would be required for a complete experimental verification of the codes would of necessity have to be carried out at various depths in an astronaut simulating phantom placed in the actual spacecraft and exposed to a well known environment. This is required because the radiation sensitive organs of the body are generally all located at some depth, protected by the body self-shielding, and the skin dose would not suffice in determining any hazards that might arise from the radiation fields. In charged particle environments such as are found in space, the depth dose profiles are most often very steep and can vary by several orders of magnitude across the dimensions of the astronaut. These factors pointed out a critical need for shielding experiments with active dosimeters which had never been performed before this. Lack of definition in the flux maps that were being used as input data for the codes was recognized as a

further major obstacle to placing confidence in the prediction capability of the codes. In order to update theoretical work in the field of space radiation effects and protection, there existed the need for an experimental program which would accomplish the following: (1) the measurement of the true tissue dose from a mixed radiation field; (2) the determination of the dose at a number of varying depths in a tissue type phantom, and at various locations within the exact spacecraft shielding configuration; (3) simultaneous spectral measurements made in conjunction with the dose measurements to insure the correctness of the input data to the transport codes. If these three criteria could be satisfied, then a verification of the existing computer codes would be possible; and the confidence level of such codes to predict the hazards in other environments could be increased greatly. With these three factors to consider, the Air Force Weapons Laboratory embarked on a program of instrumentation that would permit the fulfillment of these scientific needs.

The Gemini program called for an orbital pattern which would carry the spacecraft through the South Atlantic or Brazilian anomaly of the inner Van Allen radiation belt. In this region the spacecraft would pass for a few minutes through a charged particle radiation environment whose intensity was quite measurable in terms of dose and spectra and yet would not pose any hazard to the experimenting astronauts. NASA had programmed the use of spectrometers capable of measuring the external environment for selected Gemini flights. In order to obtain a complement of dose and spectral measurements which would permit simultaneous comparison, however, it was deemed advantageous to fly the dosimetry experimental system on flights also equipped by versatile charged particle spectrometers exterior to the spacecraft.

Besides obtaining empirical data on the dose profiles, there was also a widespread need to test existing passive dosimetry equipment, such as

thermoluminescent phospers, photoluminescent glass, activation foils, discharge chambers, and newly developed heavy particle detectors which would, when exposed to a complex field of space radiation, determine their suitability for mixed field dosimetry. Environments of the type found in the Gemini operating situations could not be successfully or practically duplicated on earth. Although it is true that a limited part of the radiation environment could be simulated,

the large number of accelerator facilities required for such a project could be obtained neither at reasonable cost nor in sufficiently short time. It was proposed that dosimetric chemicals and phospers be simultaneously exposed and then be recovered as a parasite experiment on a manned flight such as the Gemini. Their response to space radiation thus could be determined economically and easily.

II.C. Military Need for Experiment.

1. Military manned spacecraft will not be, in general, constrained to operations in radiation environments that are void of hostile components. In the light of this fact, it becomes extremely important to equip such spacecraft with elaborate dosimetry systems capable of warning the ship's crew of possible dangerous radiation environment. Such a military system of necessity must be designed to cover all possible ranges of radiation that might be encountered. This dictates that the dosimetry system be capable of detecting all types of known particles and energy that might constitute such an environment in space. Particle detection would have to cover all natural radiation environments as well as any created from nuclear weapon discharge. Furthermore, any military dosimetry system must be extremely rugged, long lasting, portable, and unsusceptible to the ambient conditions of free space pressure and temperature. Prior to design of this experiment dosimetry systems were not available to the military which would meet all of the criteria described above. This required the design and testing of an entirely new

system of hardware compatible with military space needs. The only way to completely insure the feasibility of new instrument systems would be to flight test the hardware under actual space flight conditions. The Gemini program was ideal in this respect, for it would allow the testing of military space hardware in flight and provide the Air Force with tried, tested flight items -in being- for future military manned systems.

2. There was a military need to test the new proposed Manned Space Dosimetry System more than environmentally. Any system used for space flight should be tested from the point of view of human engineering. This can only be accomplished through active astronaut participation in instrument design evaluation where the instrument is mated in realistic spacecraft packaging configurations with other spacecraft systems. Since no military spacecraft program was available at the time design was initiated in 1963, the only way that this military need could be satisfied was to participate in an extensive manned space program of the type available on the Gemini spacecraft series.

3. Another extremely important requirement in any military spacecraft program is the existence of technical personnel trained in the methods of equipment design, testing, integration, and data analysis, who are familiar with the management and operation of a mission oriented space program. There was at the time of the conception of this experiment a total lack of familiarity by Air Force laboratory personnel of Manned Space Systems Program Management. The 631A Gemini Program provided the opportunity for AFWL personnel to become familiar with the mechanics of operating as part of a large manned space program from its beginning to completion. This experience will be directly applicable to future military needs.

27

III. THEORY;

    III.A. <u>Active Dosimetry—Tissue Equivalent Sensor Head and Cavity Design</u>:

        1. <u>Bragg-Gray Theory</u>: The Bragg-Gray relationship derived in
Appendix A provides a most convenient method of directly measuring radiation dose
in rads absorbed in a given material. Ionization of a gas in a cavity contained
in a medium may be related to absorbed dose in the medium by the following
relation:

$$E_m = S_m \, W \, J_{gas}$$

where E_m = Energy absorption in ev/gm-sec

           S_m = Mass stopping power of the wall material relative to
                the cavity gas

           W = Energy required to form an ion pair

           J_{gas} = Ion current in ion pairs/gm-sec

The basic criteria necessary in a system for which the Bragg-Gray relation is
to hold are as follows:

        a. The cavity dimensions must be chosen so that only a small
fraction of the particle energy is dissipated in it. This means also that only
a very small portion of the ionizing particles will enter the cavity with a range
shorter than the cavity dimensions.

        b. Ionization due to direct absorption of quantum radiation by the
gas in the cavity must be negligible.

        c. The cavity must be surrounded by an "equilibrium thickness" of
the solid medium so that all particles transversing the cavity can be said to
originate in the medium.

        d. The energy dissipation by the ionizing particles must be reason-
ably uniform throughout the medium which surrounds the cavity. A radiation source

28

must be far enough from the cavity to make beam divergence over the cavity dimensions negligible.

If the gas and the surrounding medium are of identical atomic composition, the cavity may be large without disturbing the flux of secondary particles. It has been shown that: In a medium of given composition exposed to a uniform flux of primary radiation, the flux of secondary radiation is also uniform and independent of the density of the medium, as well as of density variations from point to point.   The cavity ionization principle, therefore, permits a determination of energy absorption in a solid medium from the measured ionization in a small gas-filled cavity.   This principle is the basis for most present-day energy deposition dosimetry, and provides the basis for the development of the advanced dosimetry systems discussed in this paper, and utilized to perform the active measurements accomplished on the Gemini spacecraft.

A series of calculations comparing the tissue equivalency of various materials for a wide variety of charged particles and quanta to the standard muscle compound have been carried out by Janni at AFWL. The following standard muscle composition as defined by the International Committee on Radiological Units was employed:

Element	Atomic number	Atoms/ Molecule	Percent by weight	Atomic weight
H	1	10.11905	10.20	1.01
C	6	1.02415	12.30	12.01
N	7	0.24986	3.50	14.01
O	8	4.55625	72.90	16.00
Na	11	0.00348	0.08	23.00
Mg	12	0.00082	0.02	24.33
P	15	0.00646	0.20	30.98
S	16	0.01559	0.50	32.07
K	19	0.00767	0.30	39.11
Ca	20	0.00017	0.01	40.09

Calculations for 0.5 to 1000 Mev protons in Shonka plastic were found to deviate from those for ICRU muscle by not more than 5.16%, and for electrons by not more than 3.65%. Shonka plastic also provided a true tissue response for gamma and X-ray radiation within 12% for energies between 0.01 and 100 Mev. The composition of Shonka plastic follows:

Element	Percent by weight
C	1.024
H	10.2
O	4.556
N	0.25
Na	0.0035
Mg	0.0008
P	0.0065
Si	0.0756
K	0.0077
Ca	0.00017

Shonka plastic was chosen for the sensor material of the active instruments due to its desirable atomic matching to tissue which was required to provide the radiation response dictated by Bragg-Gray criteria. The use of Shonka plastic as a sensor wall material provides a radical improvement in measurement of the tissue dose which could never be realized by the use of metals such as aluminum or stainless steel which are often used to measure the energy deposition and provide at best, extrapolations to the true tissue dose. For example, aluminum which is commonly used in dosimeter chamber walls, will provide an under-response to true tissue energy absorption that varies from 68.2% at 0.50 Mev to 113.4% at 100 Mev for protons. Stainless steel is even worse, for it departs in tissue equivalency from the standard muscle composition by 334.4% for 0.50 Mev protons and 451.8% for 100 Mev protons. It might appear that corrections could be made in the readings obtained by the non-tissue dosimeter for any under or over responses to radiation that are present at the point of dose measurement. Correction could be readily accomplished for monoenergetic beams of ionizing charged particles; however, for mixed fields of protons, heavy

particles, electrons, and gamma radiation that are commonly encountered in space-flight, the task would indeed be formidable if not impossible to accomplish with the desired accuracy which is required in empirical data gathering processes. A fundamental requirement to perform any corrections would be that the spectrum of particles causing the dose be accurately known at the point of dose measurement. This would require extremely sophisticated and cumbersome spectrometry hardware to be utilized at that same dose point each time an energy deposition measurement is performed. This would be an extremely costly and inconvenient process. In order to avoid having to apply significant correction factors, it was decided to perform direct tissue dose measurements by use of the material previously described which then allows for an unperturbed tissue response to be realized at all points of interest.

III.A2. **Filling Gas**:

In order to provide an ionization chamber cavity capable of measuring rad doses in a tissue equivalent medium, the chamber wall and gas should be matched atomically to this medium. A suitable nonexplosive tissue equivalent gas comprising methane, carbon dioxide and nitrogen, in the following proportions, was initially employed inside the chamber:

C	45.6% (by weight)
O_2	40.8%
H_2	10.1%
N_2	3.5%

Observations of the gamma and neutron sensitivity of a TEIC using this filling gas have indicated a stability within the measuring accuracy of $\pm2\%$ over a period of more than six months, thus demonstrating that no measurable change in the filling gas occurs through diffusion or absorption losses in the cavity wall for this period of time.

Since the relative mass stopping power of the wall to the gas is unity, the Bragg-Gray relation reduces to: $E = W_m J_{gas}$

A summary of recently measured values of W for the gases of
interest are presented in Table II. The errors quoted are not those of individual
contributors, but are chosen so that the confidence limits include all the best
values used to establish a mean for a particular gas. A value of 34.0 electron
volts/ion air was chosen as the mean value for ionization to energy conversion.
This i discussed in Appendix D.

A restriction based on NASA Gemini qualification requirements was
placed on the use of tissue gas in the flight dosimeters and it was necessary to
fill the sensing elements with dry air. The air replacement of the tissue gas
resulted in a negligible change in sensor response to cobalt-60 and cesium-137
gamma radiation which was used in calibrating the instrument. Because air and
tissue gas are closely matched interaction-wise to the radiation measured, negligible
error was introduced in the final measurements by substituting air for the tissue
gas.

TABLE II

ION-PAIR ENERGY REQUIREMENTS (W) FOR VARIOUS GASES

Gas	Formula	W, Electrons X-rays and γ-rays	W Protons	W, Alpha Particles	ThC Recoil Atoms	ThC' Recoil Atoms
Air		32.0 ± 0.5	$36.0 \pm .8$	35.1 ± 0.7	...	...
Carbon Dioxide	CO_2	33.0 ± 0.5	34.9 ± 0.7	34.2 ± 0.7	102	99
Methane	CH_4	$27.7 - 0.9$	...	29.4 ± 0.8	111	96
Nitrogen	N_2	34.8 ± 0.5	36.6 ± 0.5	36.4 ± 0.4	...	...
Tissue		...	30.5 ± 0.4	...	...	...
Equivalent	30.01% CO_2					
Gas	1.74% N_2 Percent					
	67.92% CH_4 by partial					
	0.33% C_2H_6 pressure					

W is in electron volts/ion pair

33

III.B Passive Dosimeter Theory of Operation:

The Passive Dosimeters in each Passive Dosimetry Unit can be best described in terms of the solid state phenomena which govern the operation of each separate dosimeter. These are:

1. Photoluminescence

2. Thermoluminescence

3. Formation of developable grains by charged particle energy deposition in nuclear emulsions.

4. Nuclear activation

These four general changes in the physical properties of selected materials will be discussed in terms of their theory of operation. The pertinent information concerning response to various types of radiation will be given in graphical form.

III.B.1 Photoluminescent Glasses:

Glass of both the silver activated phosphate and cobalt activated borosilicate types may be used as radiation dosimeters by optically measuring the transmission of light through these glasses after exposure to radiation. Although the optical density method provides good accuracy with excellent reproducibility it was not used because such a system works only with radiation doses far higher than were anticipated on either the Gemini-4 or Gemini-6 mission.

Two very practical dosimetry systems using the photoluminescent properties of silver activated phosphate glass have been developed. The two systems actually used on Gemini 4 and 6 were the small "glass needle system" produced by Bausch and Lomb, and the "Toshiba" glass system. The principle of both types rests on the formation of permanent centers within the glass following exposure to radiation. Although several centers are formed, the one used in photoluminescent dosimetry absorbs ultraviolet light and then continuously re-radiates orange light when exposed to ultraviolet light. A photomultiplier tube with an associated amplification system is used to record the intensity of the orange light upon exposure to

34

a constant intensity ultraviolet light used to excite the orange luminescence.

The accuracy of such systems is usually near 5% for total dosages above 1 rad, but this accuracy decreases rapidly at lower doses. The glass needle system is unusable below 1 rad and the accuracy of the "Toshiba" system is about 20% at 30 millirads.

The glass needles are 1mm in diameter and 6mm in length, and thus provide a very small and lightweight dosimetry system where expected doses are above the sensitivity threshold of 1 rad. The "Toshiba" system consists of small rectangular blocks of glass approximately 6 by 6 by 3 millimeters on a side, and is also reasonably lightweight.

In addition to being lightweight, needle and Toshiba systems have the advantage that their response is much more stable as a function of time after exposure than would be given using the optical density method. The photoluminescent dosimeter must not be read out immediately after exposure, because a rise of about 15% in the photoluminescent property of the glass occurs a few hours after irradiation, and then stabilizes. The total dose fading of the glass after this initial increase is on the order of 1% per week and was negligible in the Gemini measurements because of the rapid recovery and evaluation of the passive dosimetry packages.

Unfortunately, the photoluminescent light emission per rad for various types and energies of radiation is not constant. Some experimental information has been taken by Tochilin (Ref. 6) and is available for primary protons (Figure 8.) The response per rad of the unshielded glass exhibits an increase per roentgen of exposure as the energy of incident gamma or X radiation is lowered.

Figure 8

LET (KEV/MICRON)

EQUIVALENT PROTON ENERGY (MEV)

DOSE RESPONSE

TOSHIBA GLASS

RESPONSE PER RAD (TISSUE)
OF TOSHIBA GLASS

36
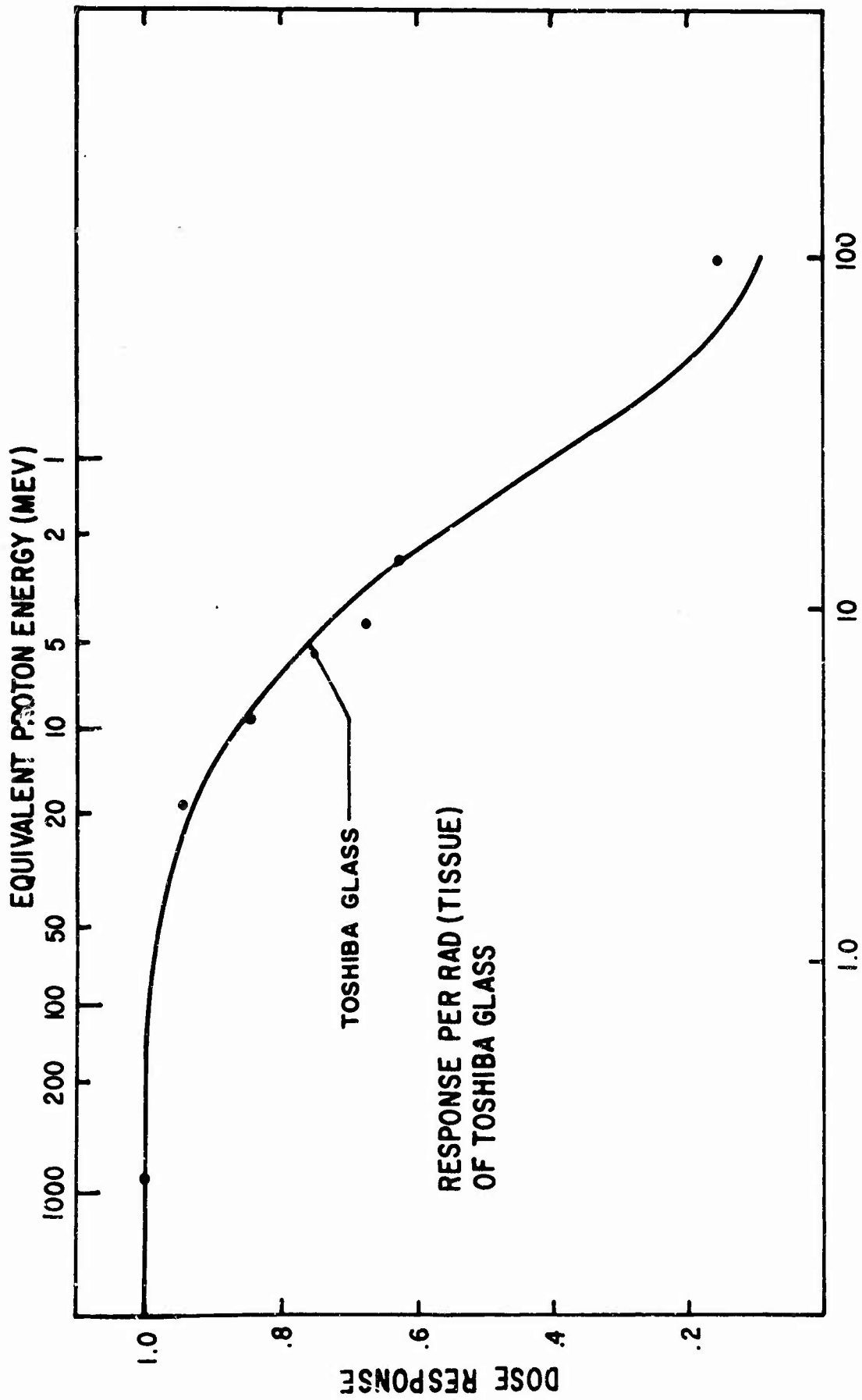
This effect is of little importance in the Gemini measurements because the active dose was the result of charged particles. However, various types of shielding have been developed to compensate for this behavior, and this shielding was employed on half of the dosimeters used.

The photoluminescent properties of the glass have been shown to be dose rate independent. This has been established experimentally for dose rates up to 10^5 rads per second.

Photoluminescent glasses are usually insensitive to neutrons because they detect only the secondary products from the primary neutron bombardment. Two significant modes of interaction are the nuclear activation of the elements within the glass, primarily the silver, and the elastic recoils of structure atoms. Such recoils are generally low in occurrence unless hydrogen is present, which is not the case for glass. No problem existed on Gemini where no significant neutron population was expected, and where neutron detectors in the form of activation foils and the Li_6 isotope were specifically included within each passive dosimetry package.

III.B.2 Thermoluminescent Devices:

Two types of dosimeters acting upon the principle of thermoluminescence were employed in D8: LiF and both shielded and unshielded CaF_2. When a thermoluminescent material is irradiated, electrons are released within the crystalline solid which become trapped at lattice imperfections throughout the solid. This trapping is relatively stable at normal ambient temperature, on the order of 70 degrees F, but addition of large amounts of thermal energy cause the electrons which were trapped within the imperfections of the solid to be thermally agitated to a sufficient degree to allow them to combine with charge carriers of the opposite sign. Visible light is emitted in this process which is measured by a photomultiplier tube and can be correlated with the amount of absorbed energy that has been deposited

within the material by radiation. After this reading out process, a thorough reheating or annealing removes the majority of the charge carriers trapped in the lattice imperfections thus allowing the powder to be reused.

Two types of thermoluminescent materials have been investigated and are presently being widely used as dosimetry systems.

The first system employs manganese activated calcium fluoride, CaF_2, which is uniformly coated on a heating element which is sealed within a vacuum container. The coating of the powder on an ohmic heater allows a known quantity of heat to be uniformly applied to this powder, and also makes for a very high degree of reproducibility in the system. The powder must be heated in a vacuum or a pure inert gas atmosphere to eliminate spurious luminescence peaks which would occur otherwise. The vacuum technique also eliminates errors due to inaccurate weighing, chemical change, or handling. The emitted light is blue-green and is again measured using a photo-multiplier tube and associated electronics to determine the intensity of the light emission. This system is quite sensitive and can record total doses as low as 3 millirad with accuracies near 10 percent. It should be noted that the accuracy of this system improves rapidly as the dose increases and is about 5% at 50 millirads. This system is also independent of dose-rate up to rates as high as 10^5 rads per hour. The response of unshielded and shielded CaF_2 dosimeters to protons is shown in Figure 9. The electron response is shown in Figures 10 and 11, and the gamma response is illustrated in Figure 12.

The storage of energy in calcium fluoride is not entirely stable with time at normal room temperatures. Fading of a few percent in the first 16 hours after exposure and of 1% per day for several days thereafter occurs. This effect can be removed by the use of proper calibration techniques and careful control of the readout times. The energy dependence response of the calcium fluoride is roughly

38

RESPONSE BEHIND .091 GM/CM^2

RESPONSE BEHIND .871 GM/CM^2

RELATIVE PROTON RESPONSE OF
CALCIUM FLUORIDE DOSIMETERS

100

10

1

ARBITRARY UNITS

10   100   1000

PROTON ENERGY (MEV)

Figure 9

39

RESPONSE PER CM² PER
ELECTRON OF CALCIUM FLOURIDE
DOSIMETERS BEHIND .091
GM/CM² SHIELDING

SHIELDING

.091 GM/CM² GLASS

Figure 10

RESPONSE PER CM^2 PER
ELECTRON OF CALCIUM FLOURIDE
DOSIMETERS BEHIND .871
GM/CM^2 SHIELDING

SHIELDING

.091 GM/CM^2 GLASS,
.516 GM/CM^2 LEAD,
.117 GM/CM^2 TIN,
.147 GM/CM^2 ALUMINUM.

TOTAL .871 GM/CM^2

EXPERIMENTAL POINTS

RAD X 10^{-12}/ELECTRON/CM^2

INCIDENT ELECTRON ENERGY (MEV)

Figure 11

47

RESPONSE PER CM² PER PHOTON OF CALCIUM FLOURIDE DOSIMETERS

—— RESPONSE BEHIND .091 GM/CM² GLASS,
- - - RESPONSE BEHIND .516 GM/CM² LEAD,
.117 GM/CM² TIN,
.147 GM/CM² ALUMINUM.

TOTAL .871 GM/CM²

RAD X 10⁻¹⁰/PHOTON/CM²

PHOTON ENERGY (MEV)

e 12

the same as that for the silver activated phosphate glass and can be flattened by appropriate shielding. Such shielding was used on several of the CaF_2 dosimeters where the weight and space limitations permitted. Response to thermal neutrons is also about the same as that of the glass. Fast neutron response has not yet been determined.

The other compound commonly employed for use as a radiation dosimeter and used on Gemini is lithium fluoride, LiF. It is not as sensitive as the calcium fluoride system, being able to record doses only down to 10 millirads with accuracies of 50% at this minimum level. At very low doses, an inert gas blanket must be used around the LiF powder to reduce tribothermoluminescent effects which mask the low doses. The accuracy of this system improves with increasing dosage, being approximately 20% near 50 millirads.

Lithium fluoride has a good energy response because it contains only low atomic number elements, and thus it is a relatively good dosimeter from the point of view of tissue equivalency. The response per rad of the LiF powder is illustrated in Figure 13. The response of the LiF dosimeter itself versus kinetic energy is shown in Figure 14. The rate of dose fading after exposure is very small, and is less than 5% per year at room temperatures. The following relation adequately expresses the time required for loss of half of the dose as a function of the temperature:

$$F = 8.8 \times 10^7 \ e^{-.1 \ T(^oC)}$$

About 6% of the LiF powder contains the lithium isotope Li_6 and will respond to ionizing radiation as well as to thermal neutrons. Since the other isotope of lithium, Li_7, was used in half of the dosimeters, and has practically zero neutron cross-section, the difference between the readings obtained on these two isotopes can be used to determine the neutron radiation component within the

Figure 13

RESPONSE PER RAD (TISSUE)
OF LITHIUM FLOURIDE

144

RELATIVE PROTON RESPONSE OF LITHIUM FLUORIDE DOSIMETERS

RESPONSE BEHIND .22 GM/CM^2
RESPONSE BEHIND .43 GM/CM^2
RESPONSE BEHIND .64 GM/CM^2

ARBITRARY UNITS

PROTON ENERGY (MEV)

Figure 14

45
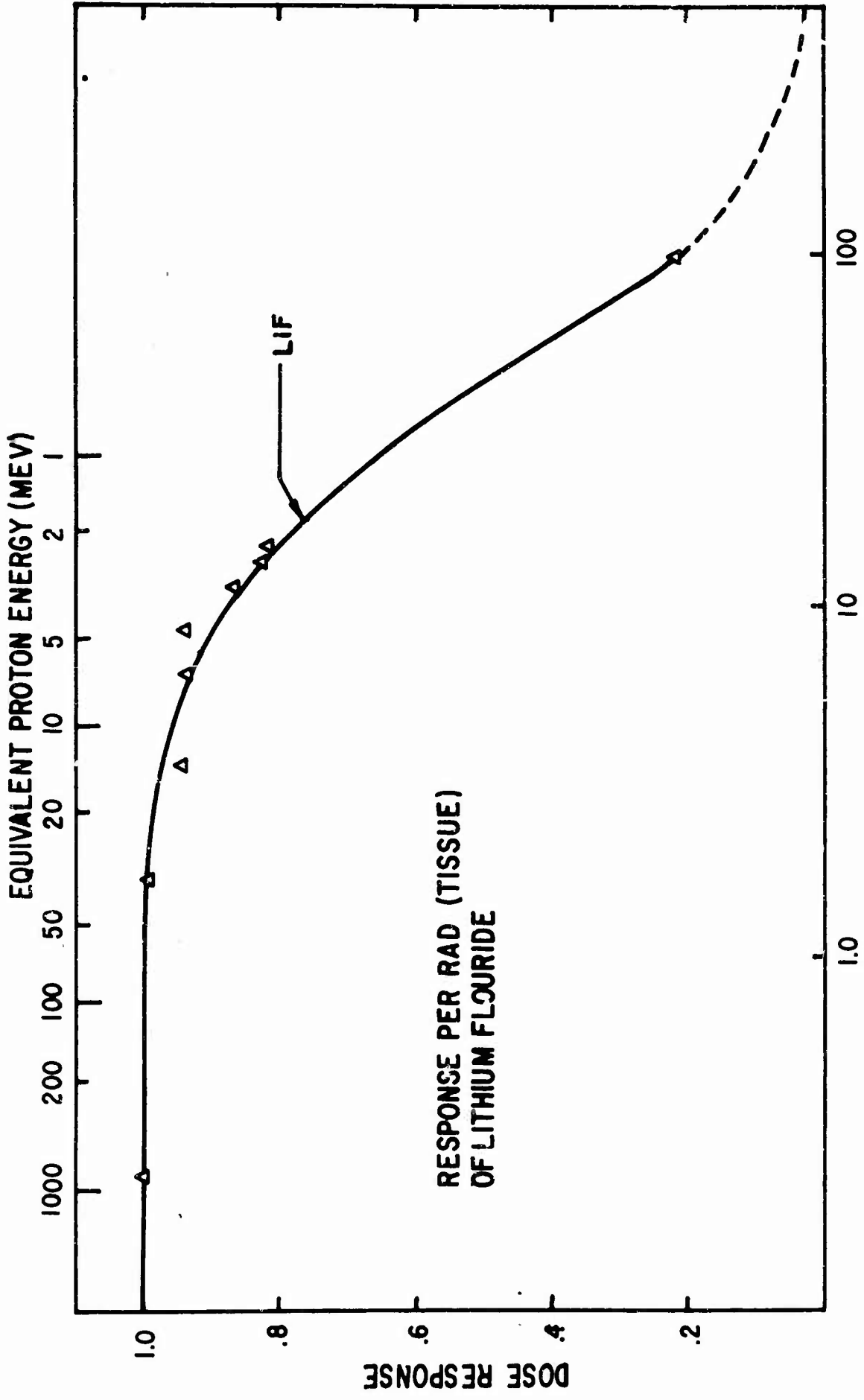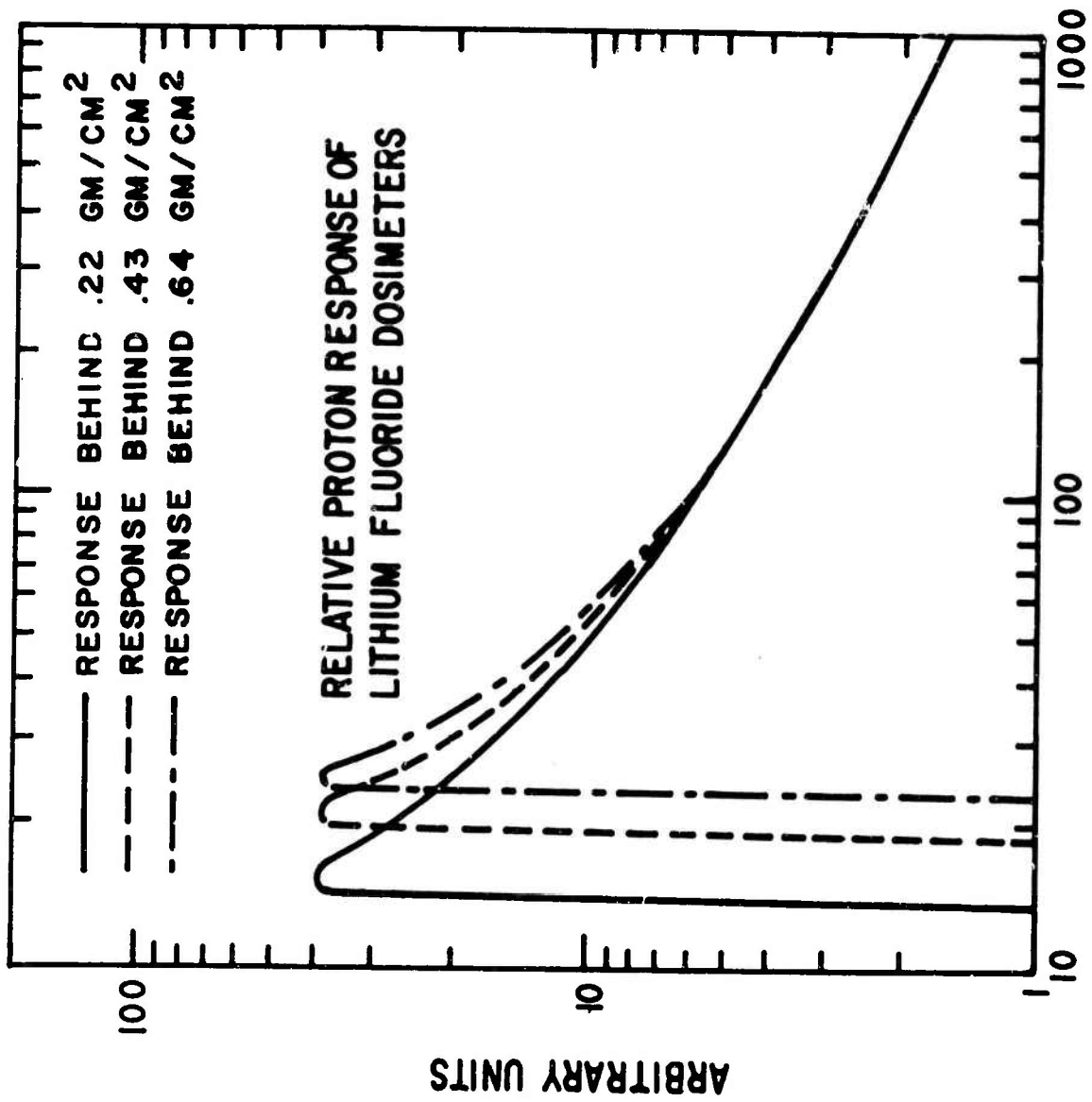
spacecraft cabin. The feasibility of this approach was tested following exposure
in the fission spectrum of the Godiva pulsed neutron reactor located at Albuquer-
que, New Mexico, and was found to be a practical neutron dosimetry system.

III.B.3. Nuclear Emulsion:

Nuclear emulsions of the Ilford G-5, K-2, and Kodak
NTA types were selected for use aboard GT-4 and GT-6. This combination allows
detection of electrons, protons, and alpha particles from very high linear energy
transfer at low energies up to the relativistic minimum ionization point, and
beyond. This is accomplished by visually examining the individual particle tracks
in the developed emulsion. The blob count and grain density are then used to
establish the atomic number of the charged particle, while the straggling and
scattering differentiate electrons from the heavier protons and alphas.

The energy loss of protons in emulsion parallels that of tissue,
as is illustrated in Figure 15.

III.B.4 Activation Foils:

A complete set of activation foils was also included in each
passive dosimetry package aboard Gemini-4 for the purpose of determining
the presence, or the absence of neutrons. These foils were chosen for de-
tection of neutrons over a wide range of energies, including thermal energies.
They were: zirconium, sulfur, tantalum, gold, cobalt, and aluminum. None
of these foils indicated the presence of neutrons during the GT-4 mission.

The energy range, dominant reaction, and half life of each foil are out-
lined in the following table:

Foil & Reaction	Energy Range	Half Life
$Co^{59}(N, \gamma) Co^{60}$	Thermal	5.26 years
Au^{197} & Cd covered Au^{197} (N, γ)	Thermal	2.7 days
$S^{32}(N, P) P^{32}$	Over 3.0 Mev	14.3 days
$Al^{27} (N, \alpha) Na^{24}$	Over 8 Mev	14.67 hours
$Zr^{90} (N, 2N) Zr^{89}$	Over	3.13 days

46

EMULSION (ILFORD G.5)
------- MUSCLE TISSUE

PROTON ENERGY (MEV)

ENERGY LOSS (MEV/GM/CM2)
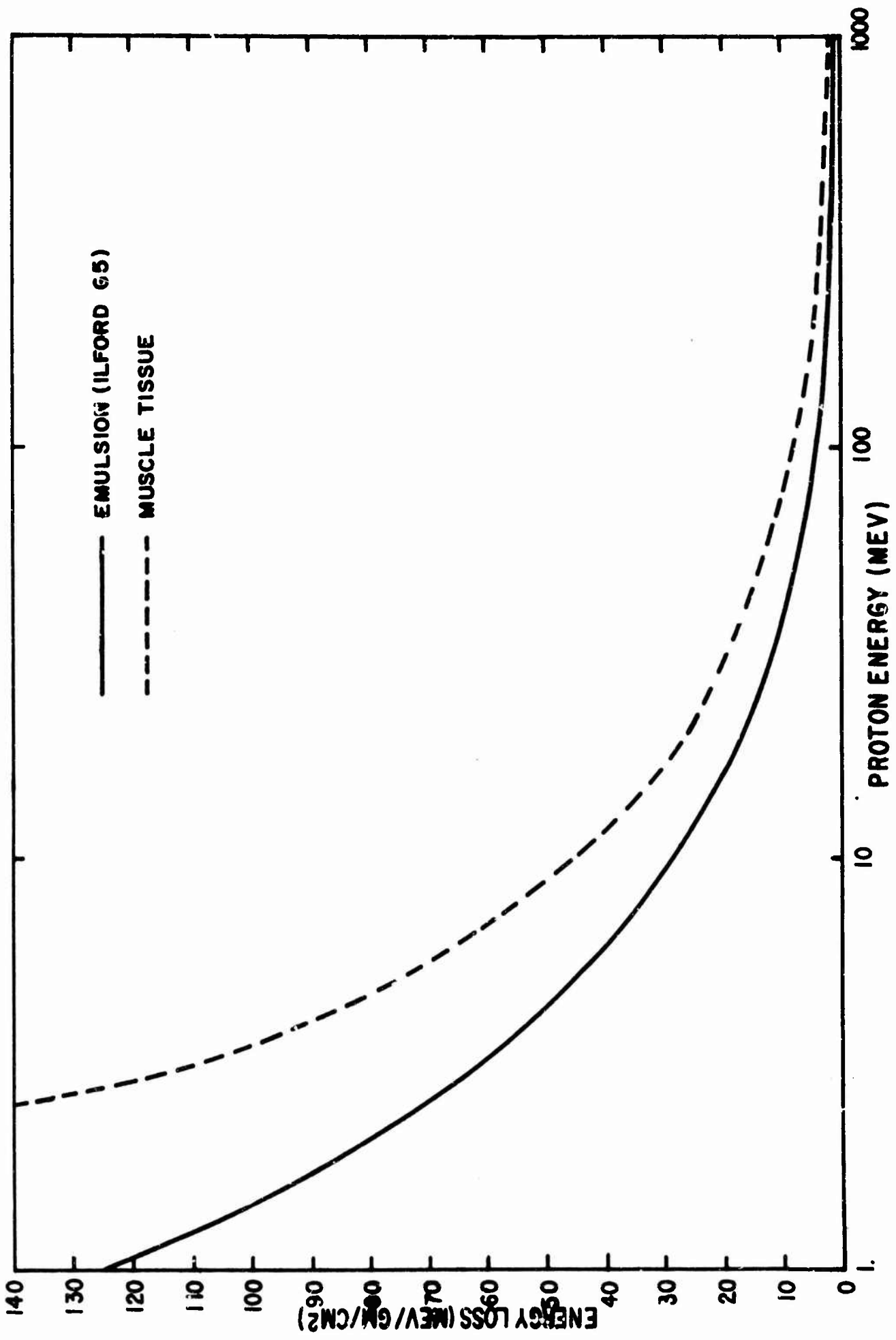
Figure 15

47

Co^{60} and Au^{198} are both thermal neutron detectors. Detectability of these foils was on the order of 5×10^5 neutrons per square centimeter. Sulfur is a fast neutron detector with a threshold of 3 MeV. Burning of the sulfur prior to evaluation allows an order of magnitude increase in the net counting efficiency because the self-shielding of the detector has been greatly reduced. Aluminum is another high energy neutron foil which has a detectability of 10^9 neutrons per square centimeter. Zirconium is a very high energy neutron threshold foil having a large effective cross section and a reaction threshold of 14 MeV.

All of the foils were counted for long durations using low background techniques. Many of the foils were evaluated using both beta and gamma counters.

All of the above dosimeters are illustrated in Figure 16.
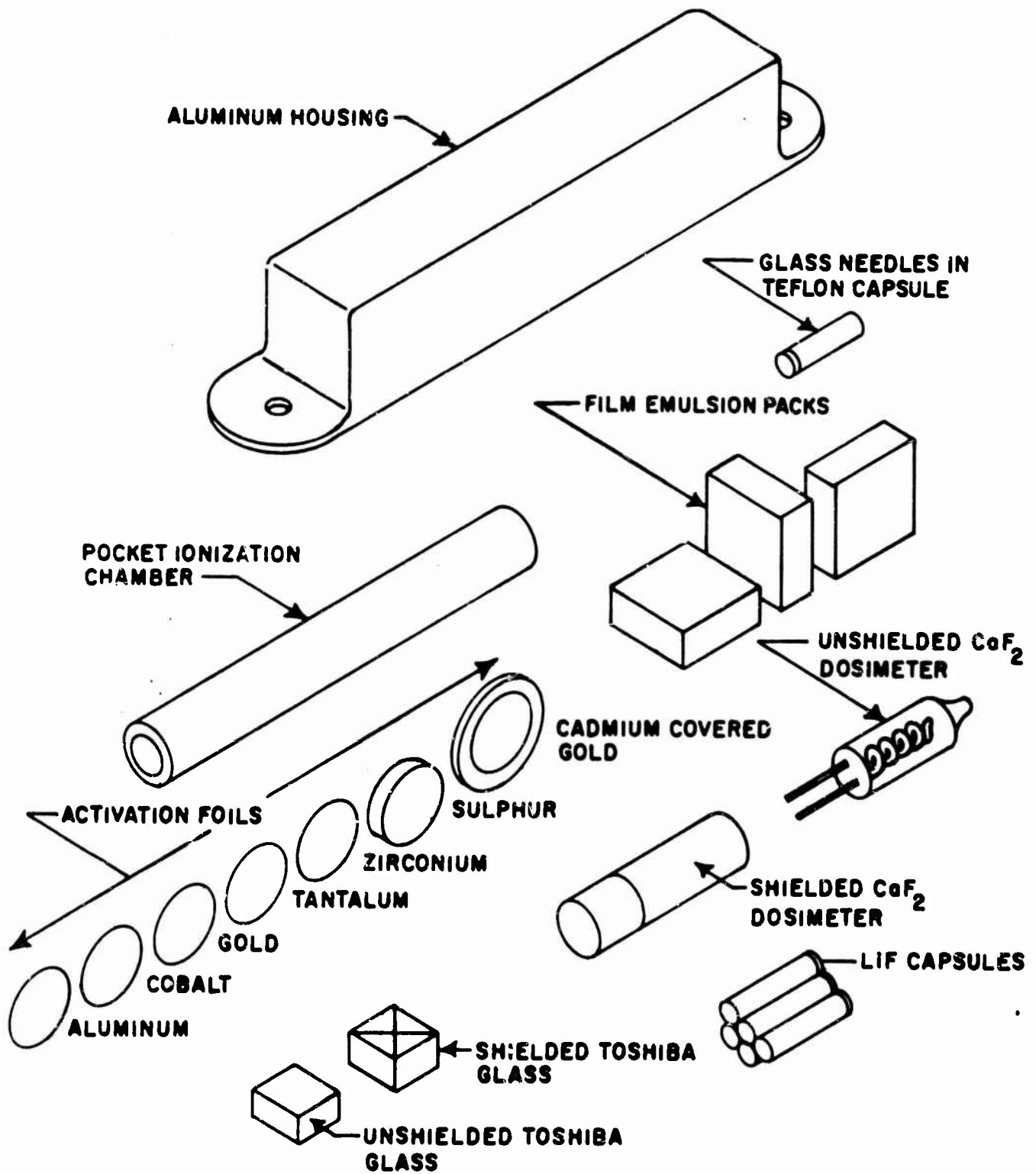
Passive Dosimeter Contents within Cannister

Figure 16

IV. EQUIPMENT:

   IV.A. Equipment Description and Design:

   IV.A.1. Nomenclature and Function:

   Table III presents the complete breakdown of all hardware employed
in experiment D-8 for Gemini spacecraft 4 and 6. Active units bearing the same
Air Force part number are identical mechanically and electrically. Passive
units are mechanically identical, but require no spacecraft telemetry or power.
The first two items in the table are the active dosimeter checkout system and as
such are AGE equipment and not flight or flight test equipment. A breakdown
of the design and specifications of the AGE equipment and each of the active and
passive units will be presented in detail later in this section.

TABLE III

Experiment D-8 Hardware Description and Serial Number List

Gemini Flights 4 and 6

Parts and Serial Number List
Active Dosimetry Units

ITEM	PART NO.	SERIAL NO.
Test Fixture (For use at MAC)	AF 67,960	SN-1
Test Fixture (Cape Kennedy)	AF 67,970	SN-1
Cricket I (Sled Test Prototype)	AF 67,951	SN-1
Cricket V (Sled Test Prototype)	AF 67,955	SN-1
Cricket I (CTU)	AF 67,961	SN-1
Cricket V (CTU)	AF 67,965	SN-2
Cricket I (For Gemini Mock-up)	AF 67,971	SN-1
Cricket I (For trainer)	AF 67,971	SN-2
Cricket I (GT-4, SST unit)	AF 67,971	SN-4
Cricket I (GT 6, SST Unit)	AF 67,971	SN-3
Cricket I (GT-4, Flight unit)	AF 67,971	SN-5
Cricket I (GT-6, Flight unit)	AF 67,971-1	SN-6
Cricket I (Flight unit Back-up)	AF 67,971-1	SN-7
Cricket V (For Gemini Mock-up)	AF 67,975	SN-1
Cricket V (For Trainer)	AF 67,975	SN-2
Cricket V (GT-4, SST unit)	AF 67,975	SN-4
Cricket V (GT-6, SST unit)	AF 67,975	SN-3
Cricket V (GT-4, Flight unit)	AF 67,975	SN-5
Cricket V (GT-6, Flight unit)	AF 67,975	SN-6
Cricket V (Flight Unit Back-up)	AF 67,975	SN-7

Passive Dosimetry Units

ITEM	PART NO.	SERIAL NO.
GT-4 SST Unit	AF 67,983	SN-101
GT-4 SST Unit	AF 67,983	SN-102
GT-4 SST Unit	AF 67,983	SN-103
GT-4 SST Unit	AF 67,983	SN-104
GT-4 SST Unit	AF 67,983	SN-105
GT-4 Flight Unit	AF 67,983	SN-111
GT-4 Flight Unit	AF 67,983-1	SN-112
GT-4 Flight Unit	AF 67,983	SN-113
GT-4 Flight Unit	AF 67,983	SN-114
GT-4 Flight Unit	AF 67,983	SN-115
GT-6 SST Unit	AF 67,983	SN-106
GT-6 SST Unit	AF 67,983	SN-107
GT-6 SST Unit	AF 67,983	SN-108
GT-6 SST Unit	AF 67,983	SN-109
GT-6 SST Unit	AF 67,983	SN-110
GT-6 Flight Unit	AF 67,983	SN-116
GT-6 Flight Unit	AF 67,983-1	SN-117
GT-6 Flight Unit	AF 67 983	SN-118
GT-6 Flight Unit	AF67,983	SN-119
GT-6 Flight Unit	AF 67,983	SN-120

IV.A.2. Physical Description:

a. Active Dosimeter: The active dosimetry system may be thought of
as being divided into two subassemblies: the sensor and the electronic parts.
The sensor subassembly includes the tissue equivalent gas cavity surrounded by a
conducting spherical tissue equivalent plastic wall, an internal radiation source,
and a tetrode electrometer vacuum-tube preamplifier operated as a floating grid
logarithmic triode (previously described in section III).

Sensing Element: The mechanical design of the sensing element
(cavity shape, size, etc.) was dictated by the need for optimal collection with
minimum capacity. These factors were, in turn, influenced by sensitivity, speed
of response, and power limitations on the system. In Figures 17 through 24 are
presented the engineering drawings of the design of all the active chamber types.
Cavity volume was established by determining the ionization current produced at
the lowest measurable range and application of these current values to the lowest
compatible with the logarithmic response of the 5889 electrometer tube.

A 1.59 millimeter thick sphere, the cavity wall, envelopes the
sensitive volume. Shonka Type a-150 conductive tissue equivalent plastic has
been chosen for the fabrication of this cavity wall because of the following of
its characteristics: 1) Its radiation absorption is quite exactly matched to
that of tissue and it reproduces tissue absorption coefficients as recommended by
the International Commission on Radiological Units; 2) It has a volume resistivity
of only 10^4 ohm-cm; 3) It is machinable; 4) It has a chemically inert polyethylene
base. The sizes of the sensitive volumes have been chosen to satisfy operational
trade-off between low radiation level sensitivity and system response time.
Table IV is a tabulation of volumes for each sensor, the ion current at lowest
measured radiation level, and the experimentally determined saturation voltage at
maximum measured radiation rate.

53
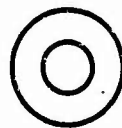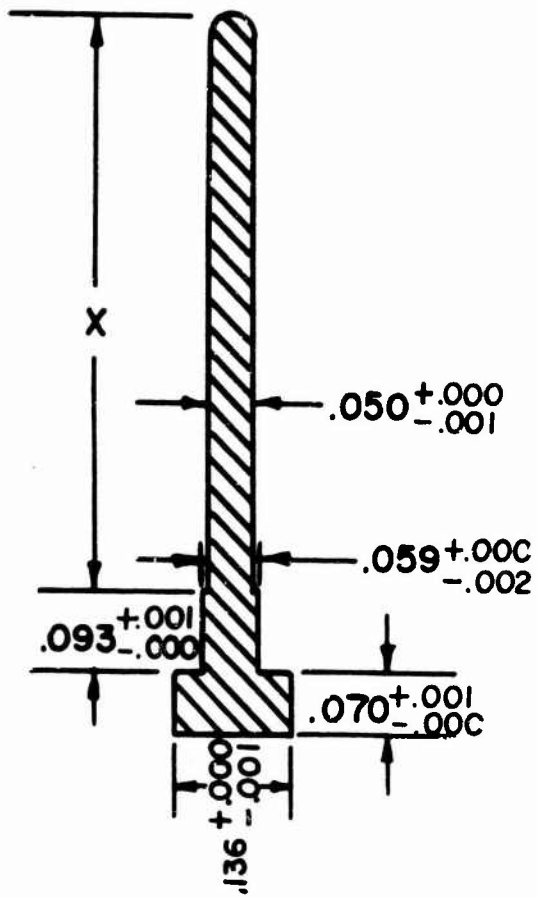
SMALL CHAMBER: X = .449 +.001 -.000
MEDIUM CHAMBER: X = .747 +.00 -.000
LARGE CHAMBER: X = 1.548 +.001 -.000

T.E. PLASTIC

Tissue Equivalent Collecting Electrode

Figure 17.

GUARD ELECTRODE CONNECTOR

.015⁺·⁰⁰¹₋·⁰⁰⁰

.325±.002 D

.475⁺·⁰⁰⁰₋·⁰⁰² D

NICKEL

LUCITE
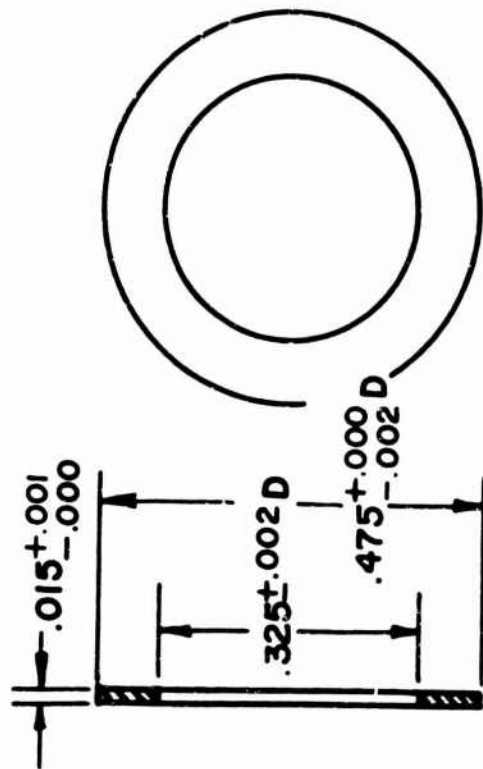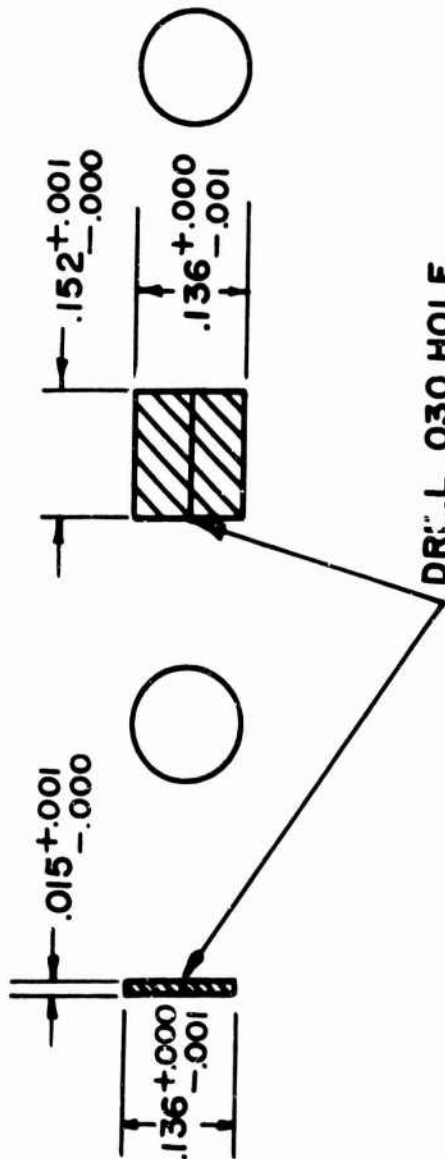
DRILL .030 HOLE

COLLECTING ELECTRODE CONNECTOR

.152⁺·⁰⁰¹₋·⁰⁰⁰

.136⁺·⁰⁰⁰₋·⁰⁰¹

.015⁺·⁰⁰¹₋·⁰⁰⁰

.136⁺·⁰⁰⁰₋·⁰⁰¹

Guard Electrode Assembly

Figure 18.

55

SEAT TO FIT RUBBER TIP OF NEEDLE VALVE

40 THREADS PER INCH

4-40 BOLT HOLE

.375 +.002 -.000 D

.150 +.001 -.000

.100 +.001 -.001

.400 +.001 -.000

LUCITE

.750 +.000 -.002 D

.250 +.002 -.000 D
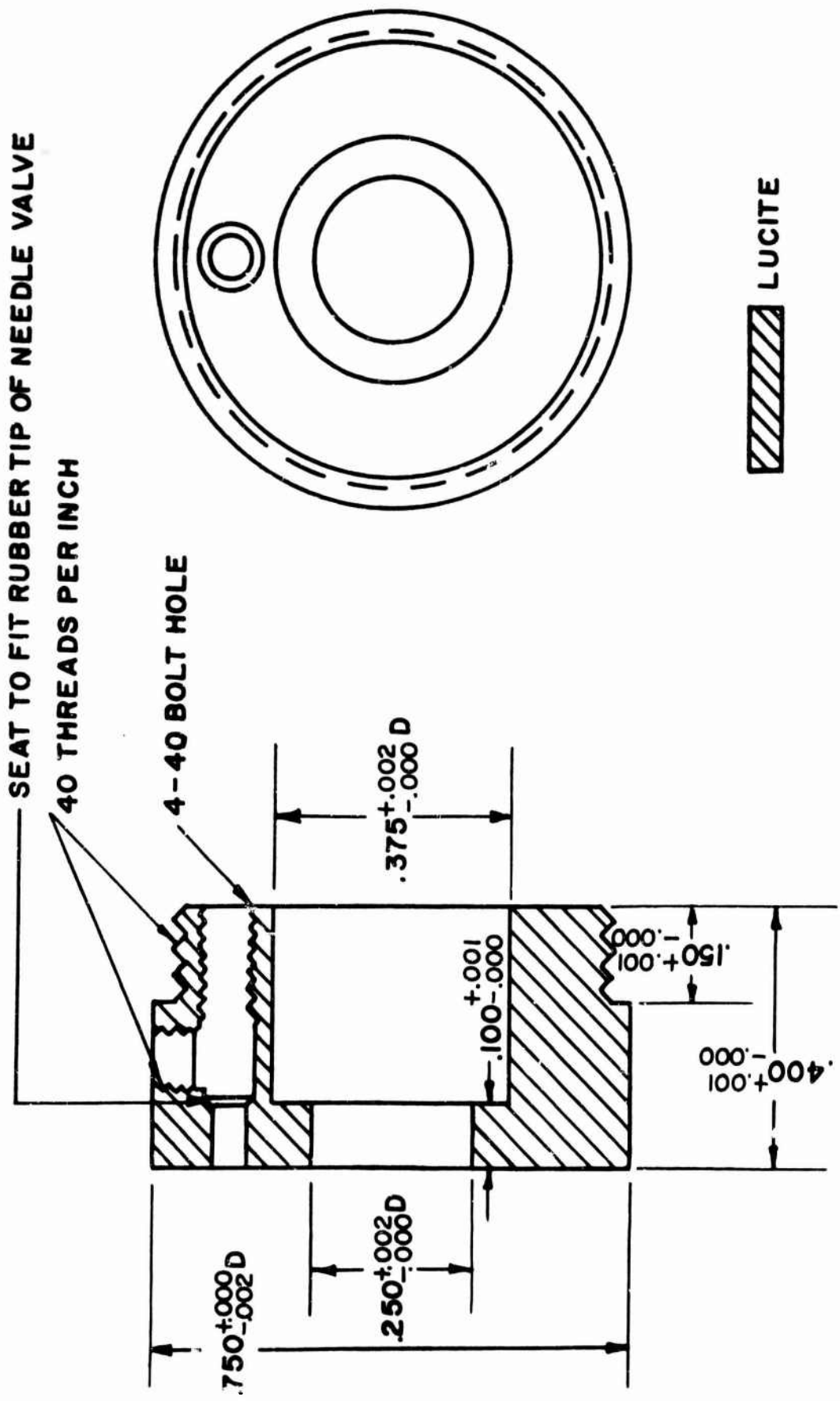
COMPLETE ASSEMBLY WITH HEMISPHERE BEFORE DRILLING GAS FILLING HOLE

Figure 19.

56
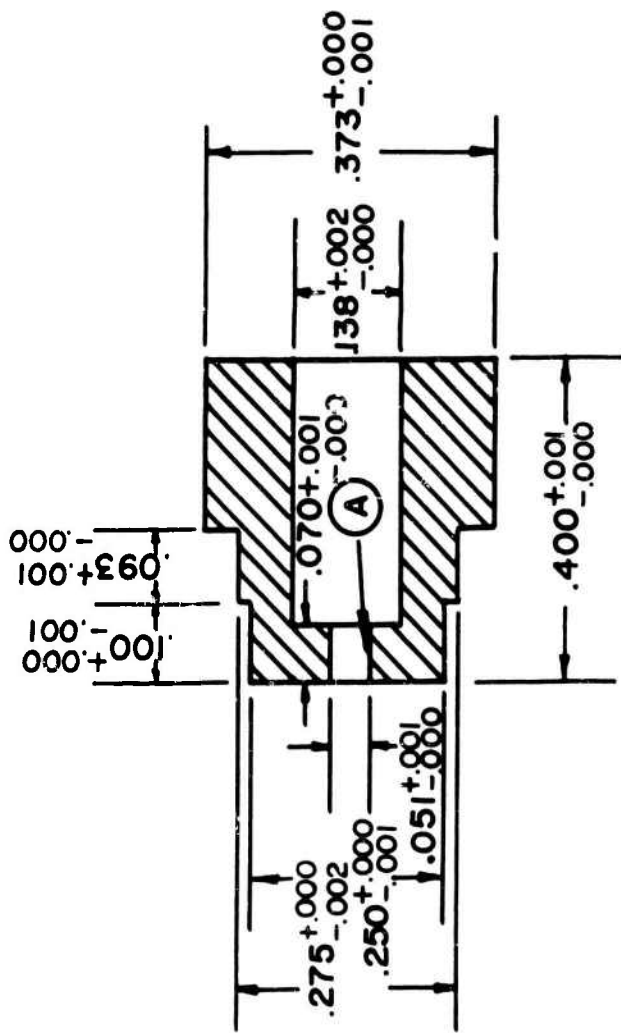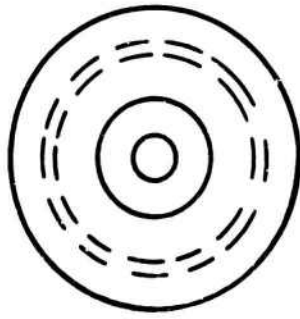
FLARE HOLE TO A
LARGER DIAMETER
BY .005 – .007 FOR
SHOCK RESISTANCE

.051$^{+.001}_{-.000}$

← INSIDE

DETAIL A

POLYSTYRENE

.373$^{+.000}_{-.001}$

.138$^{+.002}_{-.000}$

.070$^{+.001}_{-.003}$

(A)

.400$^{+.001}_{-.000}$

.093$^{+.001}_{-.000}$

.001$^{+.001}_{-.000}$

.275$^{+.000}_{-.002}$

.250$^{+.000}_{-.001}$

.051$^{+.001}_{-.000}$
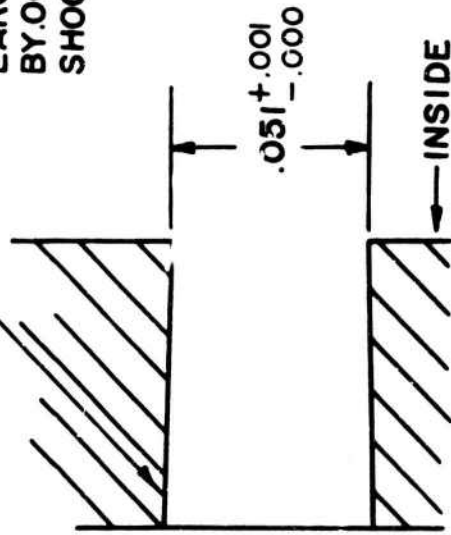
Collecting Electrode Mount

Figure 20.

5.

SMALL HEMISPHERES MACHINED FROM TISSUE EQUIVALENT CONDUCTING PLASTIC
SEAL AFTER COUPLE ASSEMBLY

TYPE V   TYPE I
(PORTABLE SENSOR)   (FIXED SENSOR)
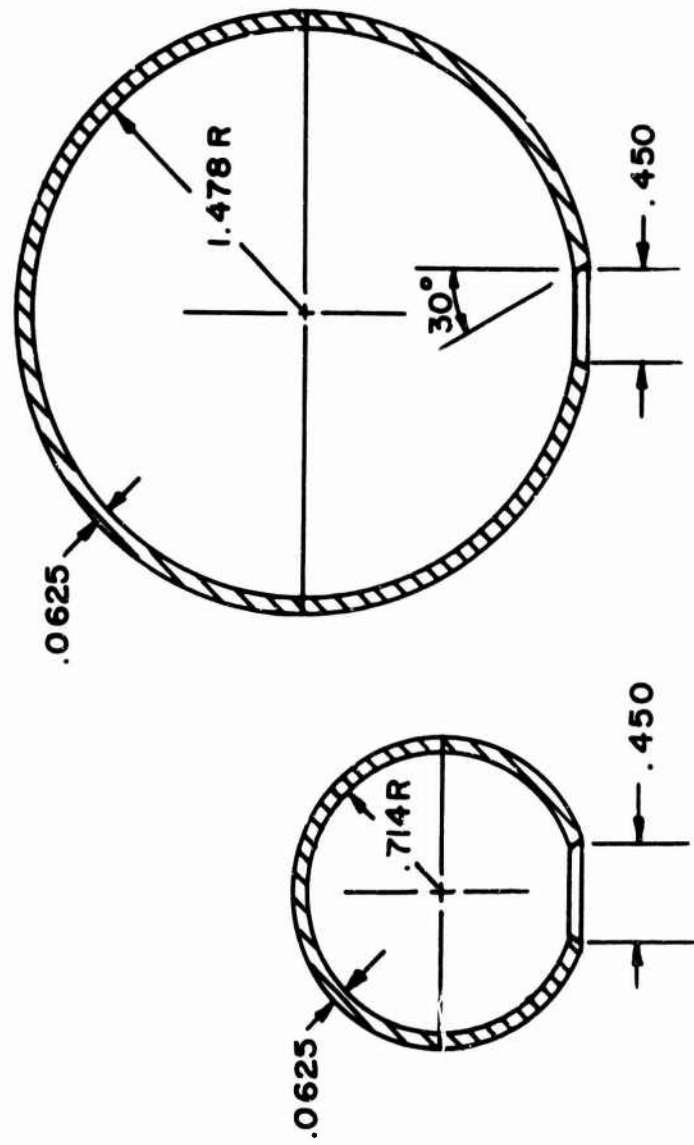
T.E. PLASTIC

TypeI and TypeV Hemisphere Design

Figure 21.

58

DETAILS OF INTERFACE BETWEEN SPHERES AND INSULATORS
COMPLETE THIS ASSEMBLY BEFORE DRILLING GAS FILLING HOLE

Figure 22.

59
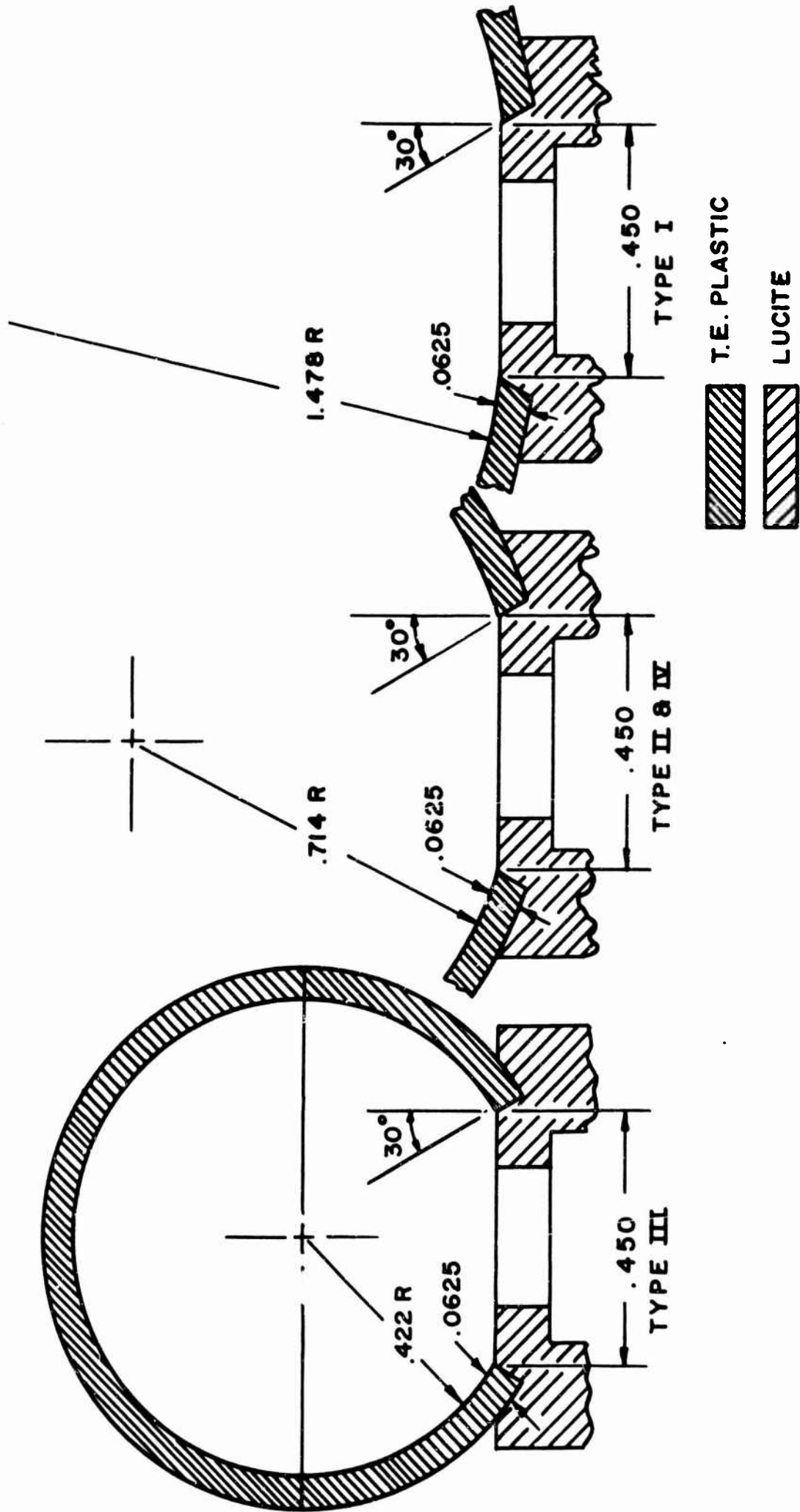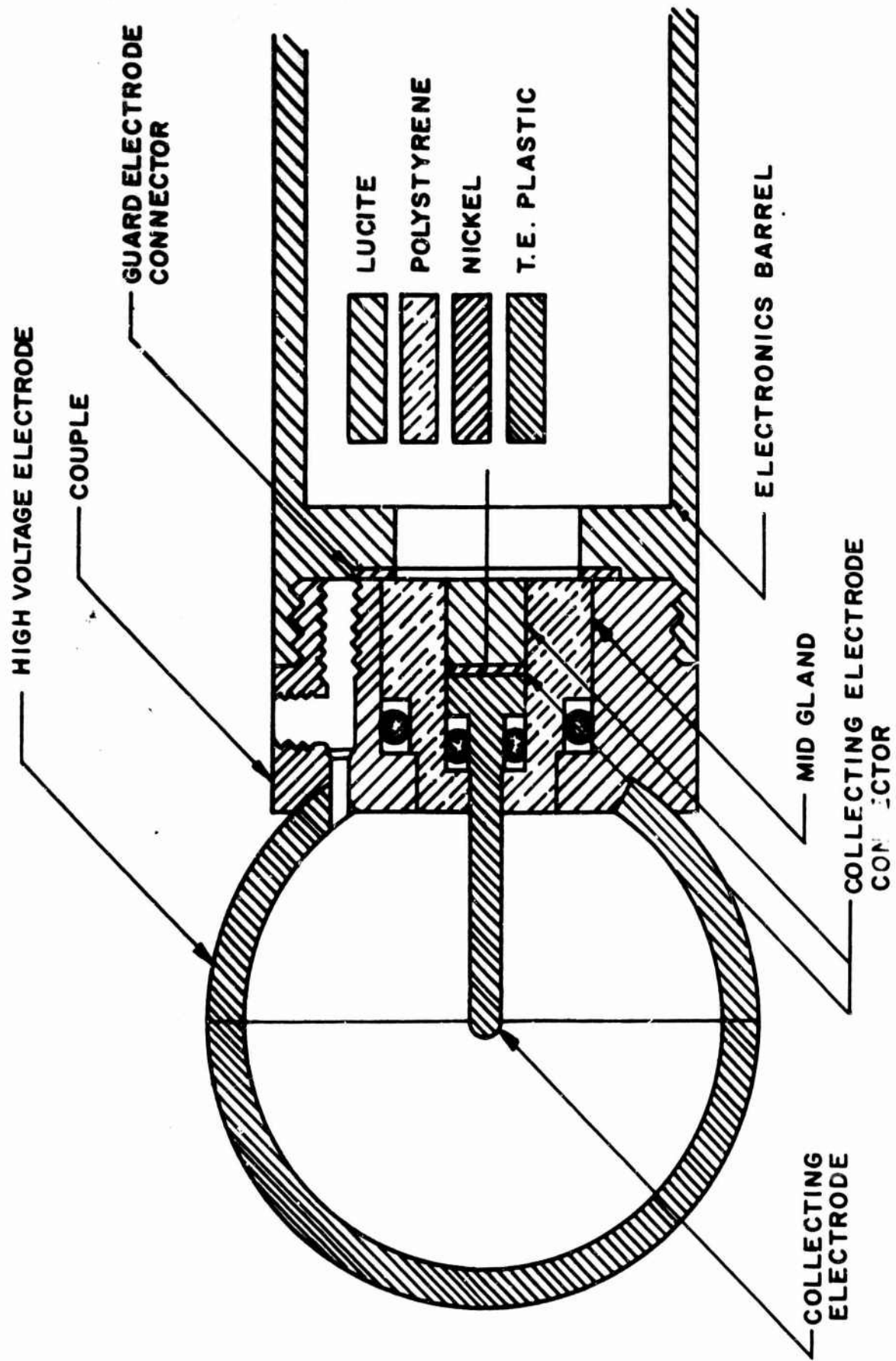
Complete Sphere and Barrel Assembly

Figure 23.

60
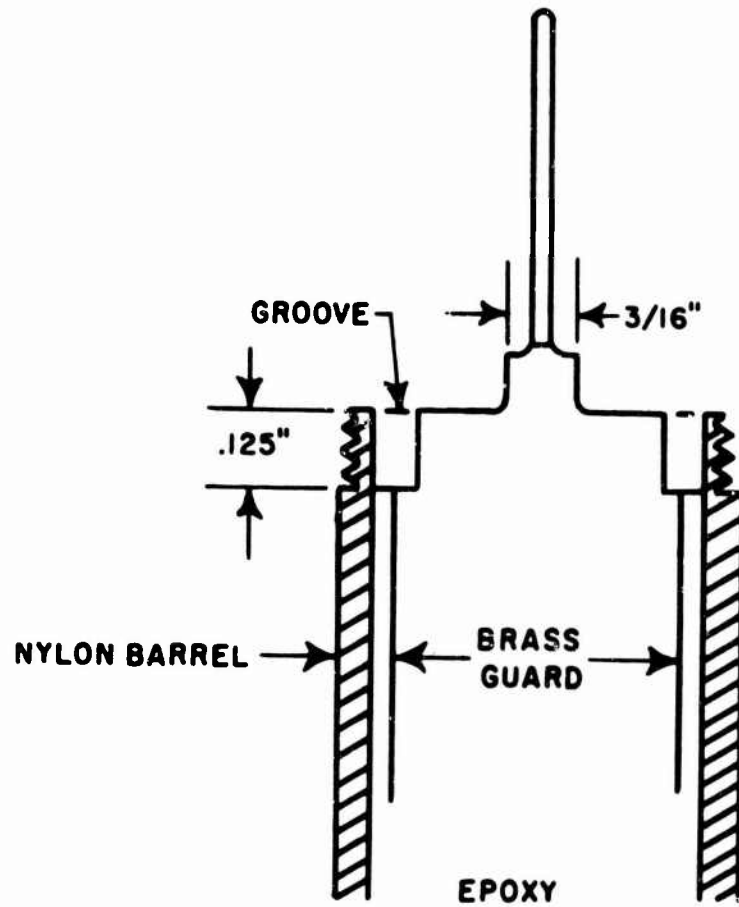
Figure 24   Machining of Barrel

TABLE IV

Chamber Type	Volume	Minimum Radiation Level	Minimum Ion Current	Experimental Saturation Voltage
Type I	221 cc	5×10^{-4} rad/hr	1×10^{-14} amp	120v @ 1 rad/m
Type V	25 cc	1×10^{-2} rad/hr	2.3×10^{-14} amp	280v @ 10^4 rad/m

An extrapolation experiment was performed to test the equivalency between the mass absorption of the cavity walls and that of the filling gas. The cavity gas pressure in the Type I sensor was reduced by fixed increments and extrapolated to zero pressure. It was thereby shown that ionization per unit mass of gas is a constant regardless of gas pressure. X rays of HVL-2.0 mm of Aluminum were used in the experiments, the results of which are displayed in figure 25.

Collecting Electrode: A conducting tissue equivalent plastic is used as a collecting electrode to transfer the current induced by ionizing radiation from the ion cavity to the electrometer of the sensor. The electrode base is housed in a cylindrical polystyrene insulator and electrically connected to the grid lead of a CK 5889 electrometer tube.

Insulating Material: The temperature properties of various insulating materials were investigated in order to ascertain which one would be best for use in space temperature environment. Table V displays the results thus obtained for the material examined.

62

221 c.c. Ion Cavity

60 KVCP X-rays, No Filters

Half-Value-Layers: 2.0 mm Al

RELATIVE IONS PER UNIT MASS OF GAS

100
90
80
70
60
50
40
30
20
10
0

0   0.1   0.2   0.3   0.4   0.5   0.6   0.7   0.8   0.9   1.0

PRESSURE   (atmospheres)
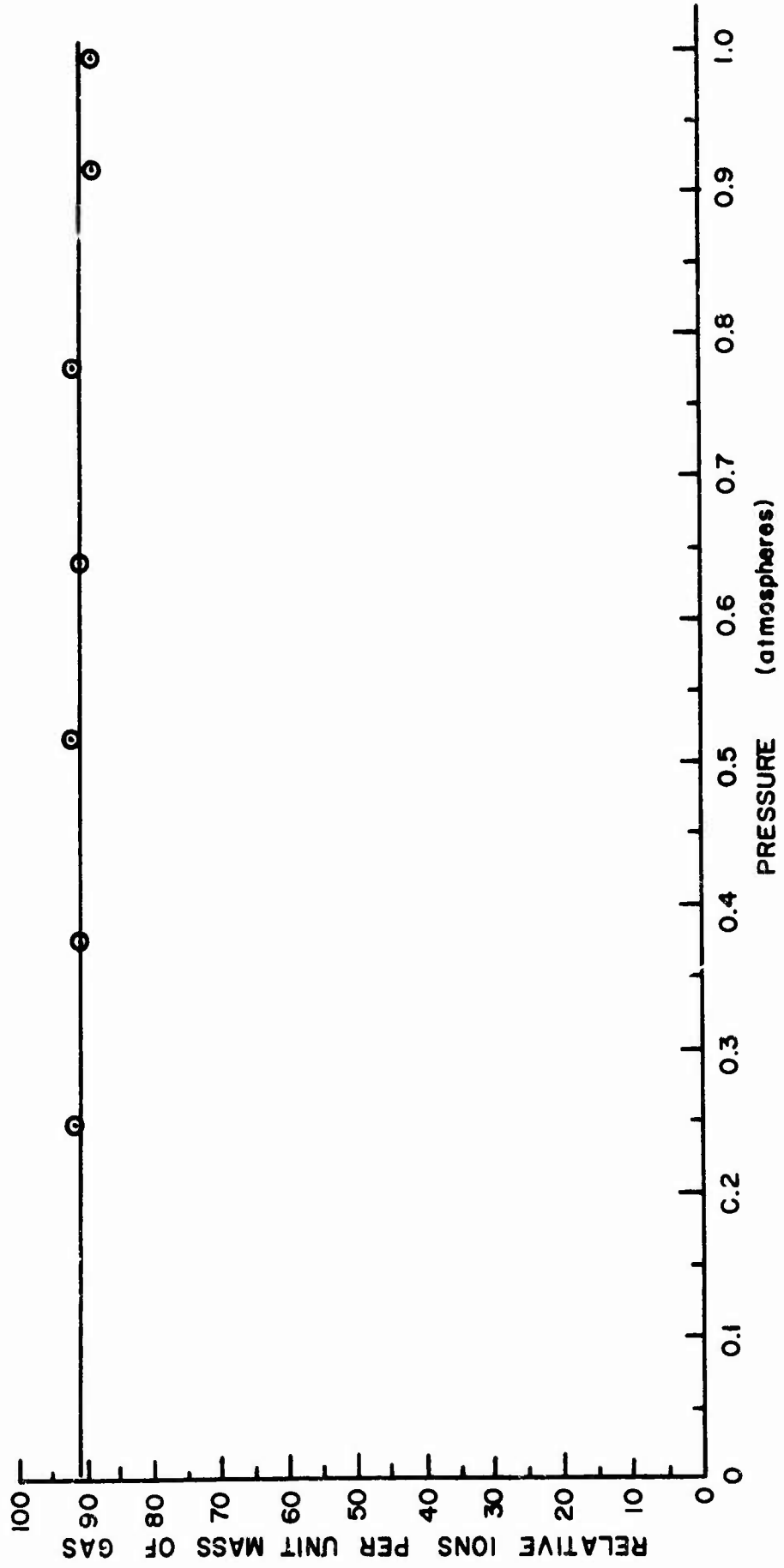
Figure 25   Gas-Wall Equivalence Test

63

TABLE V

Volume Resistivities of Insulators

	25°C	60°C	100°C
Ceresin Wax	>10^{19} ohm-cm	3×10^{13}	liquid
Polystyrene	$10^{18} - 10^{19}$	10^{18}	phase change
Teflon	2×10^{18}	10^{18}	5×10^{17}
Synthetic Mica	10^{17}	5×10^{16}	10^{16}
(Supramica 600)			
Tri-bond 3104 Epoxy	3.1×10^{16}	1×10^{16}	6×10^{15}

At temperatures below 60°C, the upper limit for design accuracy, polystyrene insulates best and has hence been chosen for the electrode insulator. Tri-bond epoxy is employed in encapsulation at the electrometer tube.

Guard Electrode: As shown in Figure 26, the outer surface of the insulator is made into a conductive guard electrode by coating it with colloidal graphite. It is connected to the electrometer cathode so that there exists a maximum two volts potential between the collecting and guard electrodes, thus minimizing leakage currents through the insulation. The insertion procedure for the tube and guard assembly into the rubber mold for fabricating the barrel of the sensor is shown in figure 27. Figure 28 shows the resistor and pin assembly at the barrel entrance after molding.

Electrometer Tubes: The filament of the electrometer tubes should be operated at the lowest voltage commensurate with adequate electrometer emission, because it reduces the production of photo-electrons from other elements of the tube, and because it lengthens the life of the tube and reduces system operating power. Operation of the electrometers at low plate voltage also tends to

CONDUCTIVE EPOXY
(MAKE CONTACT
WITH GUARD RING
ON TUBE)

2.200

CONDUCTIVE
EPOXY
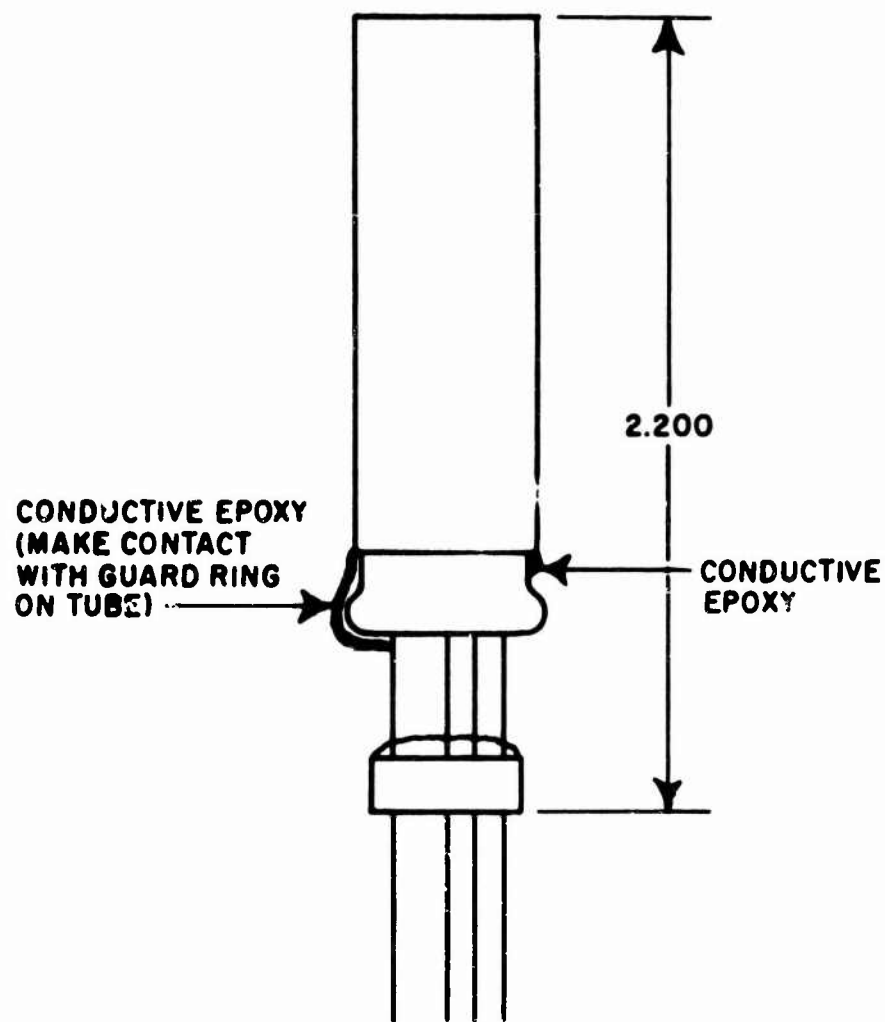
Figure 26   Electrometer Tube Mounting Epoxy

STEP 1

STEP 2

INSERT

GROUND WIRE HOLE

STEP 3

FILL WITH EPOXY TO JUST COVER PROJECTION

EPOXY

66
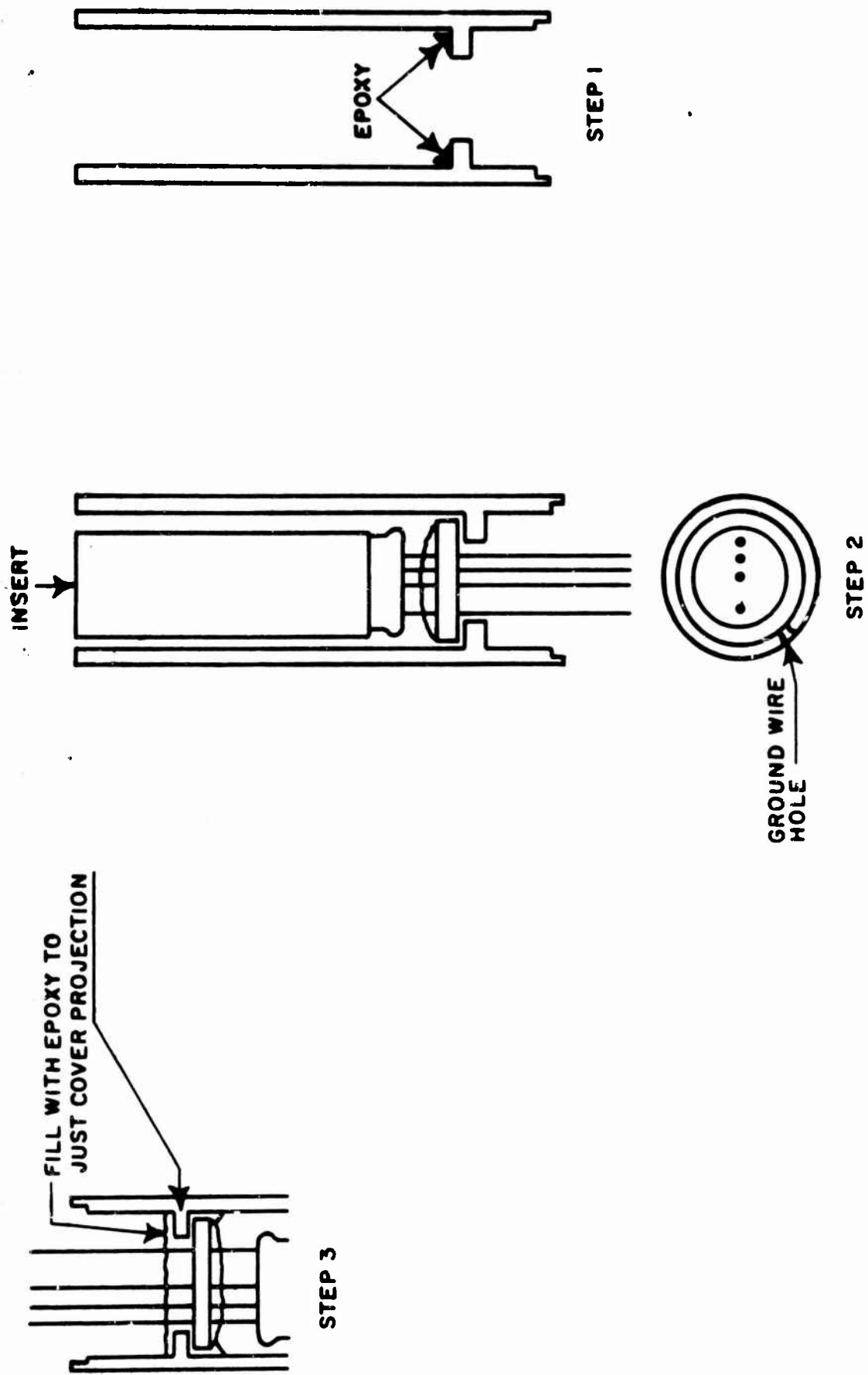
Figure 27   Hysol Epoxy Application for Barrel Mounting

TYPE V

TYPE I

A - PLATE
B - CATHODE
C - GROUND
D - FILAMENT

EPOXY

INSERT
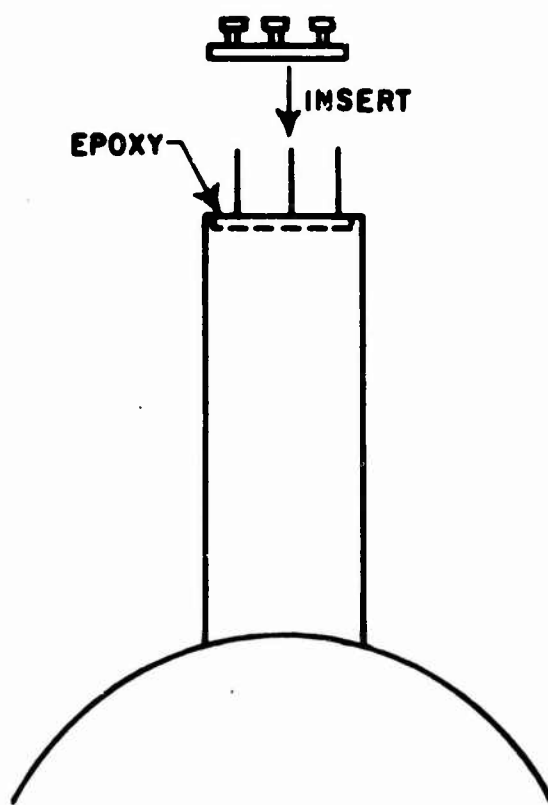
Figure 28   Connector Installation

67

reduce internal ionization by photons and charged particles of residual gas in the tube, and to lower the shot noise component of the plate current.

Tubes operated at low plate and filament voltage, however, become increasingly filament temperature dependent as the energy acquired by traversing electrons approaches the values of initial emission energies: approximately 3 ev If the tube can be made to operate independently of temperature, the following conditions are obtained: As filament temperature increases, the greater emission tends to increase plate current. A stronger negative grid voltage also results, however, in order to maintain equilibrium between electron current and ion current at the grid. The change in grid voltage thus affects the tendency toward increased tube transconductance and results in a stable plate-versus-grid current characteristic over a wide range of input currents.

The logarithmic triode mode of operation was used to eliminate temperature dependence of the preamplifier. This mode of operation involves the "floating grid" of a CK 5889 triode at voltages which allow some of the electrons committed to arrive at the grid. When the ion chamber and "floating grid" attain equilibrium, the flow of positive ions from the cavity neutralizes the flow of filament electrons arriving at the grid, and the following relation holds:

$$i_p = s\log_{10} i_g + g$$

Additional benefits which accrue to the operation of a floating grid log triode are: 1) Obviation of a high value grid resistor, decreasing grid parasitic capacitance and attendant response time as well as lowering the practical limit in ion current sensitivity and making for a simpler chamber/electrometer interface, fewer electrical connections and smaller physical size; 2) Increase in inherent response speed by virtue of logarithmic input impedance; 3) Minimizing of aging and temperature effects upon the electrometer; and 4) A wide range (approximately 7 decades) logarithmic response.

The optimum filament voltage for temperature-independent electrometer response has been experimentally found to be close to 1.00 volt, 20 percent lower than nominal for the CK 5889; and this results in approximately 30 percent lower tube power drain over standard operation and an estimated 200 percent increase in tube lifetime. A method of determining the optimum operating point for the electrometer tubes utilized in the design of the chambers is presented in appendix (B).

Electronic Subassembly: The electronic subassembly, although physically separate from the sensor subassembly, is jointed to it by a four-lead wire cable. It includes a coarse magnetic amplifier, a fine magnetic amplifier, a switching type regulator, a voltage comparator for voltage regulation, an electronic conversion unit for supplying all required operational voltages, a calibration circuit for periodically pulsing the ionization chamber high voltage, and a decade switcher for supplying a variable bias current to the fine magnetic amplifier. The complete system is illustrated in block form in figure 29.

An advanced concept using magnetic amplifiers was developed by Amey to meet the stringent restrictions placed on unit weight, size, and power consumption; while maintaining high output stability and reliability.

The coarse amplifier, schematically illustrated by Figure 30 has two tasks to perform: (1) bias the quiescent electrometer tube plate current such that zero ambient radiation provides a near zero output voltage and (2) transpose the radiation created increase in electrometer tube plate current at minus collecting voltage potential to a voltage output of 0 to 5 volts full scale at ground potential.

The voltage operating level transposition is accomplished by use of a full wave, self-saturable magnetic amplifier connected in a push-pull configuration; and since there is no current path between input control windings 11-12 and output voltage windings 7-8, it is possible to operate the input at any voltage

69
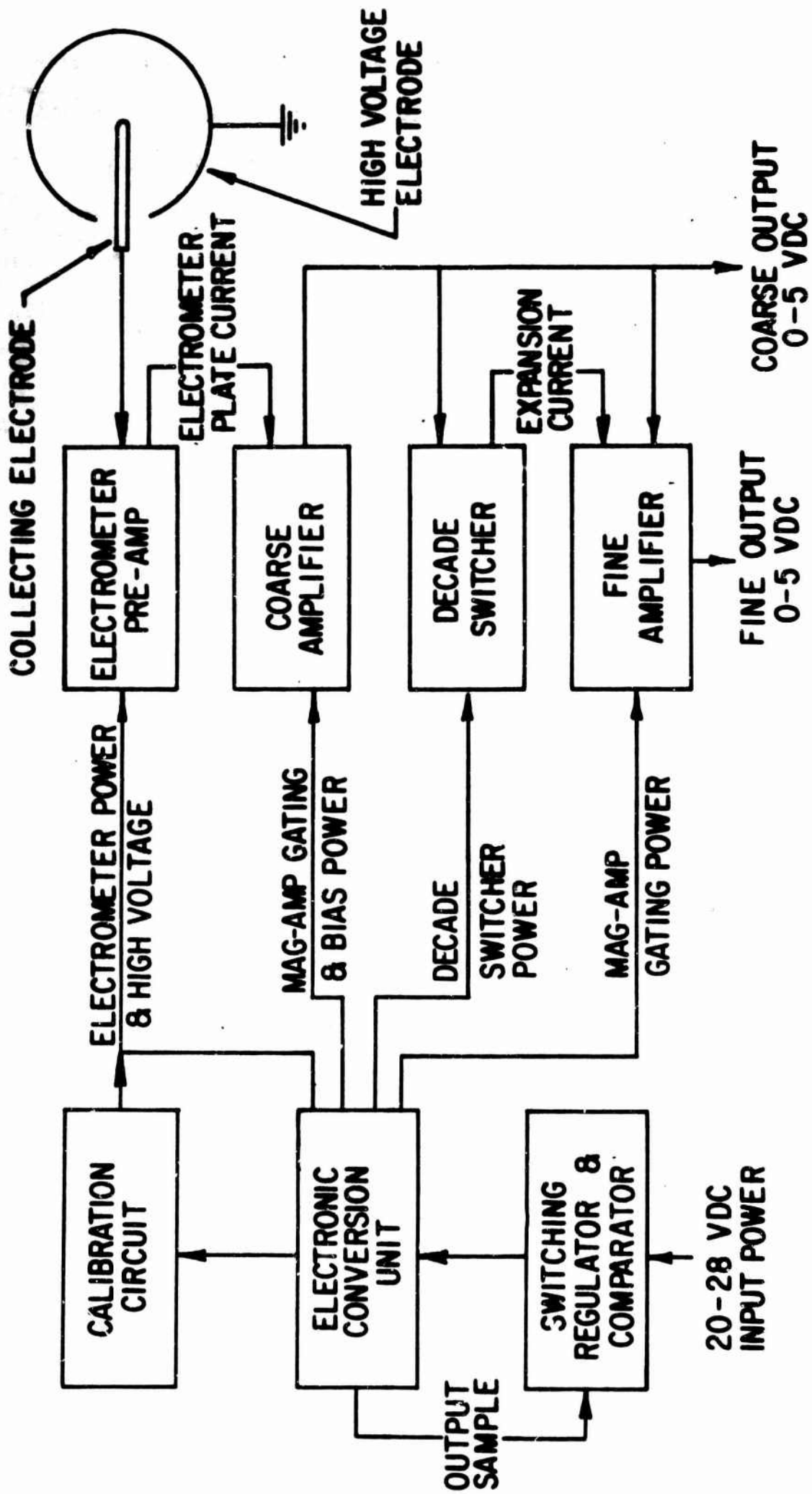
Figure 29   Electronic Subassembly

70
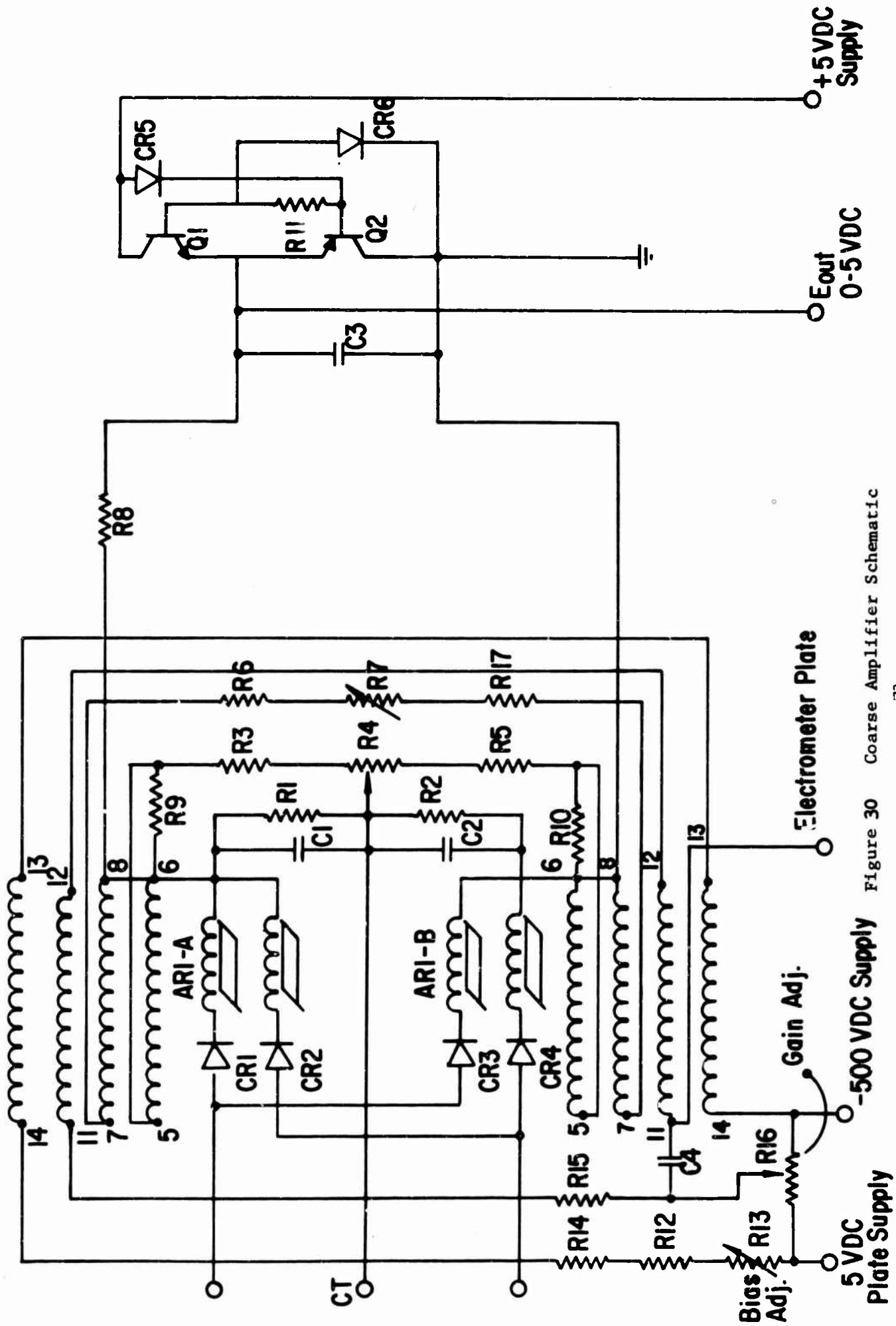
Figure 30   Coarse Amplifier Schematic

71

level less than insulation breakdown. Thus, the electrometer preamplifier plate and filament voltages are referenced to minus collection voltage potential and the control windings in series with resistor R15 constitute the electrometer tube plate load impedance.

To provide zero output voltage with quiescent plate current flowing through the input control windings, an offset current is applied to windings 13-14 and the amount of this current is controlled by potentiometer R13.

Gain adjustment is accomplished by varying the plate voltage potential at potentiometer R16. Both bias and gain adjustments are externally accessible and are used to match a particular electrometer tube to a fixed gain amplifier. Resistors R1 and R2 are summing resistors and R8 in conjunction with C1, C2, and C3 furnish the necessary output filtering Self-biasing of each half of the amplifier to a proper operating point is accomplished by resistors R9, R3, R5, R10, and potentiometer R4. The adjustment and temperature compensation of the amplifier gain is accomplished by resistor R6, potentiometer R7 and Balco resistor R17. The network, consisting of diodes CR5 and CR6, resistor R11 and transistors Q1 and Q2, provides hard limiting at zero and +5 vdc. The 0 to 5 vdc output of the coarse amplifier is monitored by both the fine amplifier and the decade switcher.

For a detailed discussion of magnetic amplifier theory, the reader is referred to Self-Saturating Magnetic Amplifiers by Gordon E. Lynn, Thadders J. Pulo, John F. Ringelman, & Frederick G. Timmel, McGraw-Hill, 1960.

The fine amplifier in conjunction with a decade switcher provides expansion of the coarse amplifier output. Referring to Figure 31, the input signal is from coarse amplifier output. Since this amplifier has a voltage gain of five, the fine output goes from 0 to +5 volts when the coarse output goes to one volt. The amplifier zero reference is shifted by the decade switcher in four discrete steps to expand different levels of the coarse output.

72

Figure 31   Fine Magnetic Amplifier Schematic

73

The decade switcher, schematically illustrated in Figure 32 is a four stage, level sensing circuit with a step current output. Each stage is identical except for the divider resistors which establish the trigger level. The switching circuits consist of a Schmitt trigger which drives a constant current generator. The trigger level is established by divider resistors R2, R5, and R6. Transistor Q2 samples the coarse amplifier output and causes the circuit to switch when the sample voltage reaches one volt. Transistor A1 is a constant current generator which turns on when the switching circuit triggers and off when the switching circuit returns to its original state. The second, third, and fourth stages operate in the same manner as the first, except for switching at coarse amplifier output levels of 2, 3, and 4 volts, respectively.

The decade switcher has a step function current output, which increases the current through windings 9-10 by integral multiples. In this manner, at 1, 2, 3, and 4 volts switching is accomplished.

The electronic conversion unit is a combination d.c. - d.c. converter and d.c. - a.c. inverter. The d.c. converter portion supplies high voltage for collection potential, electrometer plate and filament currents and power for the decade switcher. The a.c. inverter supplies gating voltage at 3 kc to the magnetic amplifier. Figure 33 is a schematic of this unit. Switches Q1 and Q2 are silicon planar epitaxial transistors selected for low saturated collector voltage and fast switching time. Both switching time and saturated collector voltage have been optimized for maximum efficiency. The transformer is fabricated from nyleze magnet wire and a permalloy number 80 magnetic core. Transistors Q3 and Q4 are also planar-planar epitaxial and are used as gated rectifiers. Both have been chosen to improve efficiency and reduce temperature effects on the 1.5 volt filament supply. It should be noted that the 5 volt plate supply and 1.5 volt filament supply are referenced to the high voltage supply.

74
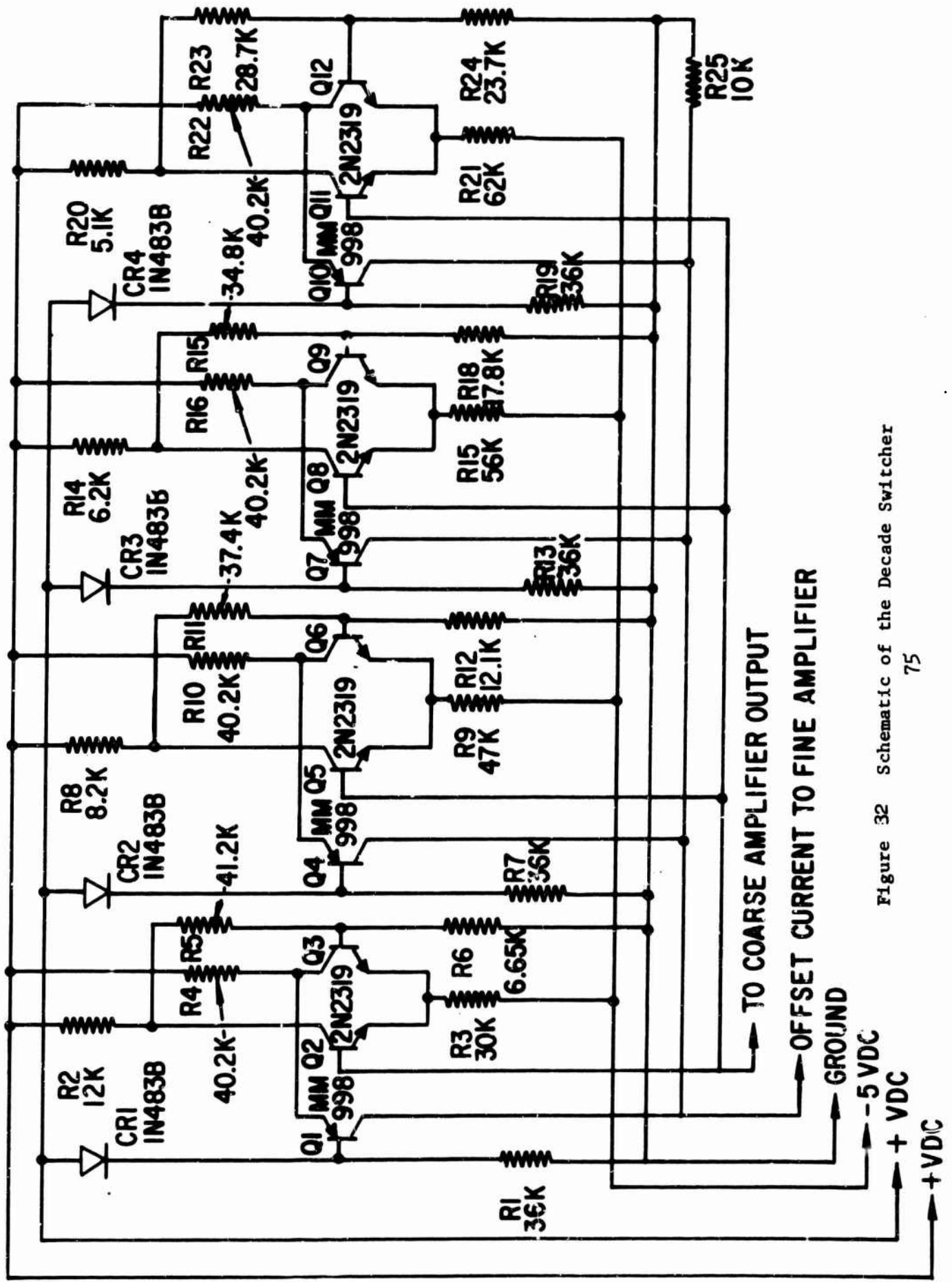
Figure 32   Schematic of the Decade Switcher

75
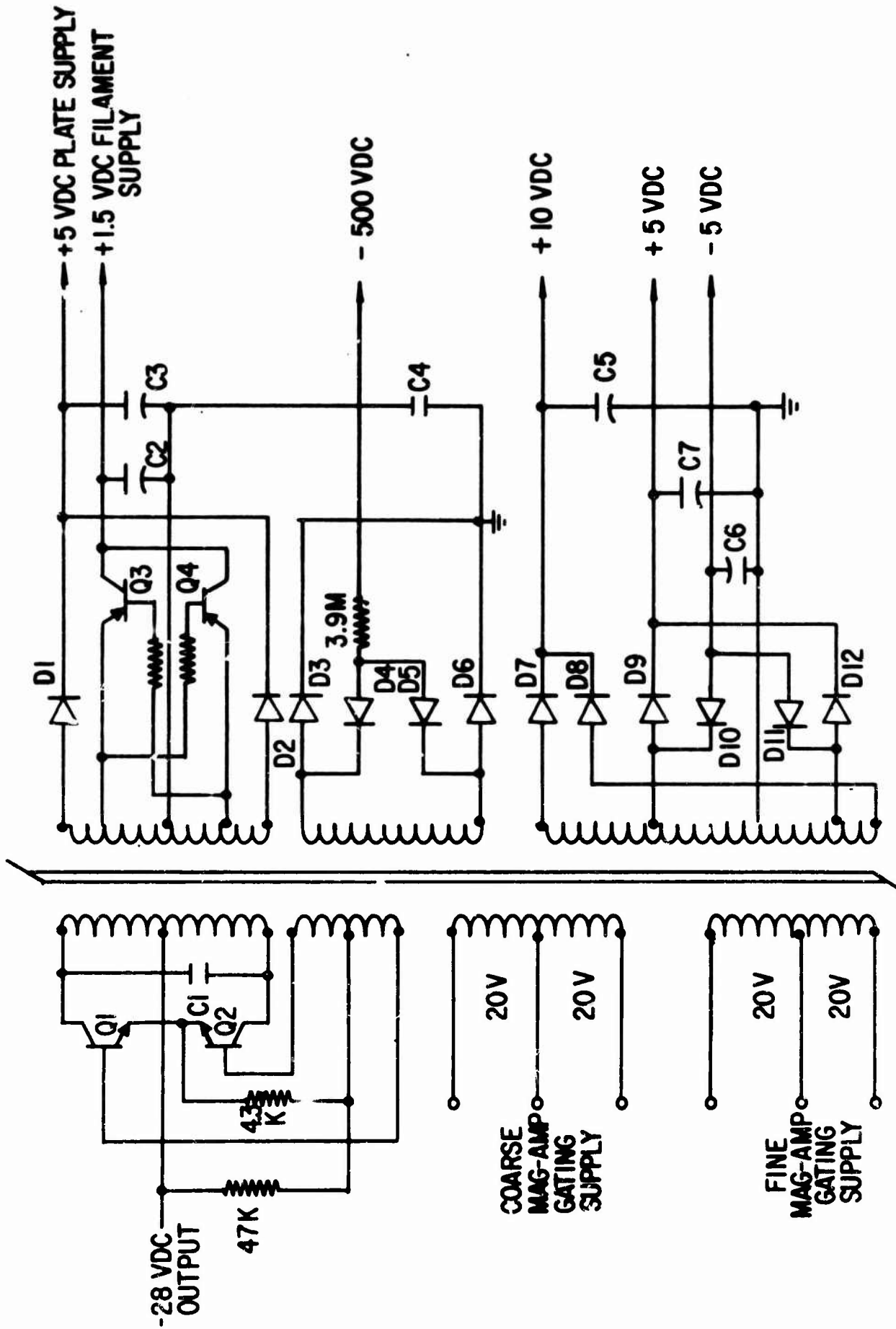
Figure 33   Schematic of the Electronic Conversion Unit (ECU)

76

To attain high efficiency with the specified input voltage variation, a switching type regulator is used. A schematic of the regulator circuit is illustrated in Figure 34. The circuit functions in the following manner. Transistors Q1 and Q2 form a comparator circuit which differentially compares a sample of the ECU output to a reference voltage. The reference voltage is developed across CR1 which is a temperature compensated zener diode. The error signal from the comparator is amplified in Q3 and applied to the base of Q4. Transistor Q4 controls the repetition rate of the power switch Q5 so as to maintain a constant output voltage from the regulator.

The calibration circuit (Figure 35) consists of a relaxation oscillator and a flip-flop. The oscillator has a period of 6 minutes and switches the state of the flip-flop when it fires. Capacitor C14 and resistor R28 form the long-time constant R-C network of the oscillator. Transistor Q12 is used to reduce the leakage current across C14 which unijunction transistor Q13 would create. Transistor Q13 is the oscillator switch which generates the pulse for control of the flip-flop. Transistor Q10 and Q11 form a conventional flip-flop, the state of which is read across divider resistors R17 and R18. When the flip-flop changes state, the negative collection voltage at the electrometer tube cathode is alternately increased or decreased by 0.8 volt.

The method developed for automatic calibration of the ionization chamber system is similar in operation to that of a gold leaf electrometer or Neher type ionization chamber since it employs the time-of-charge technique of measuring ionization current.

By introducing a pulsed step change to the ionization chamber collection potential, a fixed charge is introduced into the collecting grid of the electrometer. This establishes a relationship for the transfer function Q_{in} versus E_{out} of the system; and, at the same time, it provides a linear rather than

77
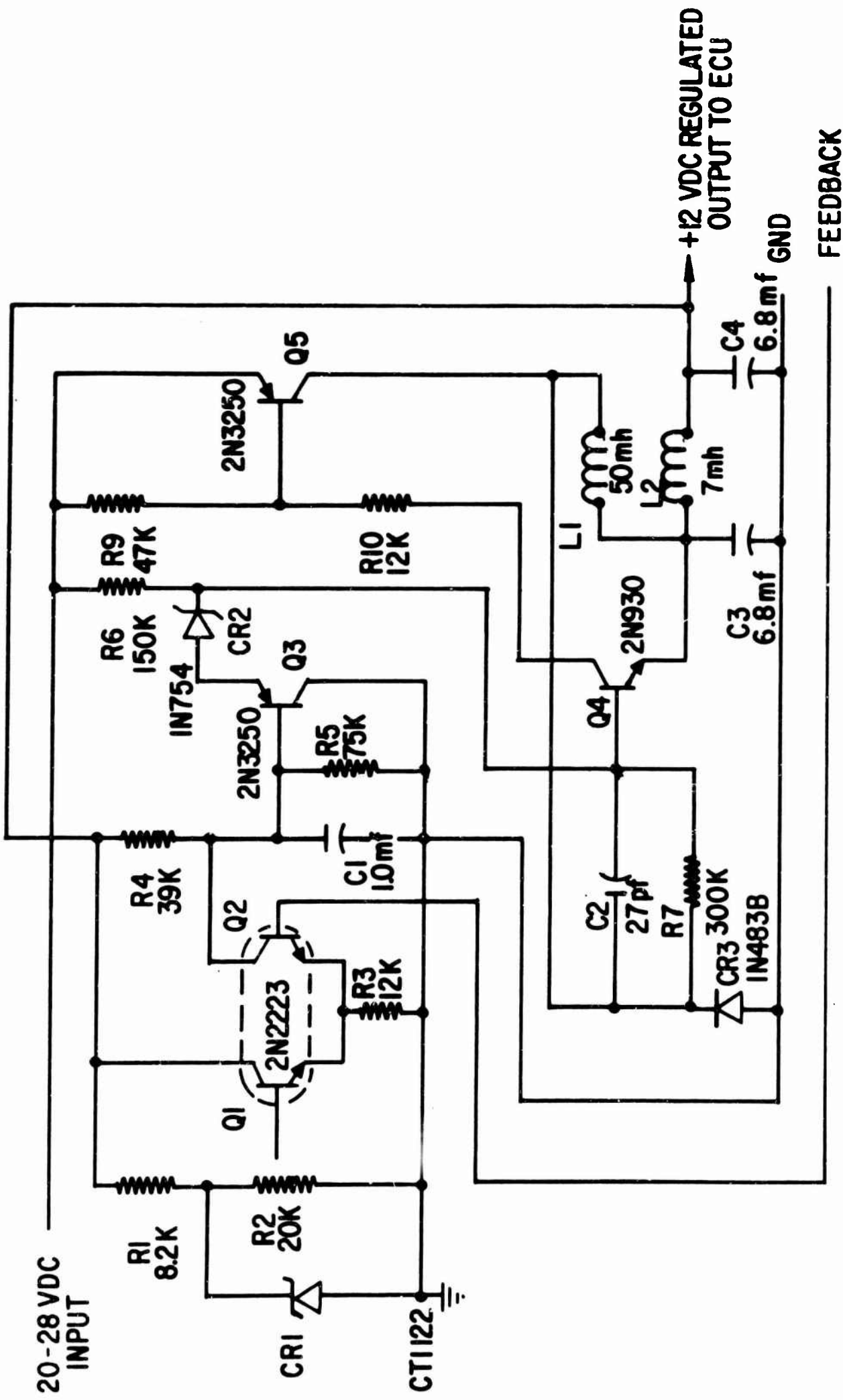
Figure 34   Schematic of the Switching Regulator

78
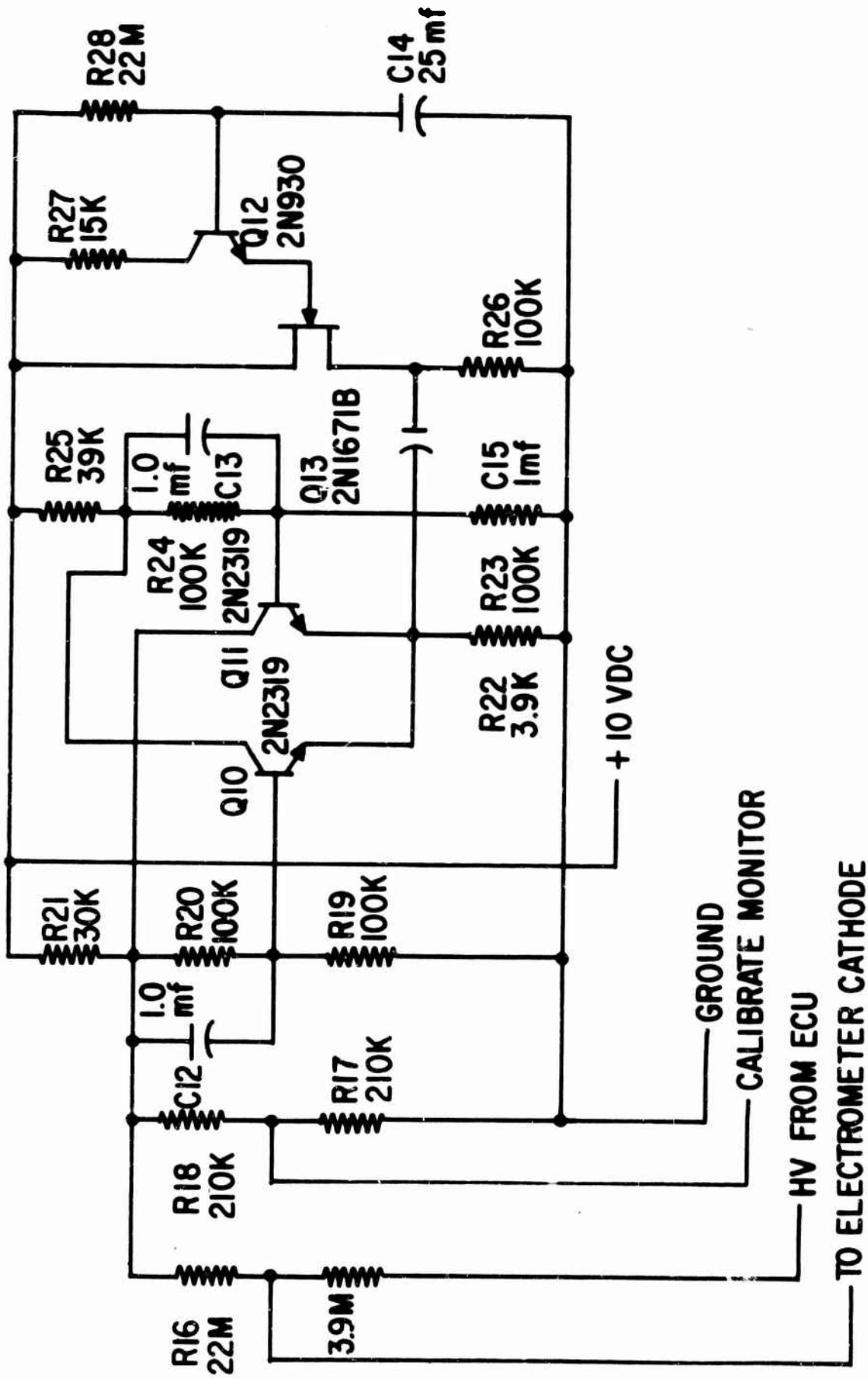
Figure 35   Calibration Timing Circuit Schematic

79

logarithmic measurement of the ambient radiation via observation of the rate of change of the output signal. In addition, the presence of a near point source (20 to 50 pico curies) of Pb^{210} placed on the cavity wall allows an indirect measurement of cavity gas pressure at zero external radiation.

The zero ambient electrometer input current is calculated from

$$I = \frac{6.8 \times 10^{-13}}{T}$$

where T is a linear projection of the time decay curve after a step decrease in output. For a step increase in output, the input current is calculated from

$$I = \frac{2.1 \times 10^{-13}}{\tau}$$

where τ is the time for E_{out} to decrease to half maximum value.

Calling the initial time, t_o, ambient radiation is zero. At t_o, a step decrease in collection potential of 0.8 volt creates a decrease in output of 0.25 volt. Projection of the linear portion of the curve to equilibrium output results in a value for T of 63 seconds; thus,

$$I = 1.1 \times 10^{-14} \text{ amp}$$

IV.A. 3. <u>System Description and Operation</u>:

Although each active dosimeter was encased in a similar package, the Type V dosimeter was fitted with a movable locking barrel and sensor assembly and an extendable, spring-loaded cord in order to provide a movable sensor. The Type I and Type V dosimeters were mounted symmetrically on the right and left hatches respectively as shown in Figure 36 The mechanical envelope for the Type V unit is shown in Figure 37; that of the Type I unit, in Figure 38.
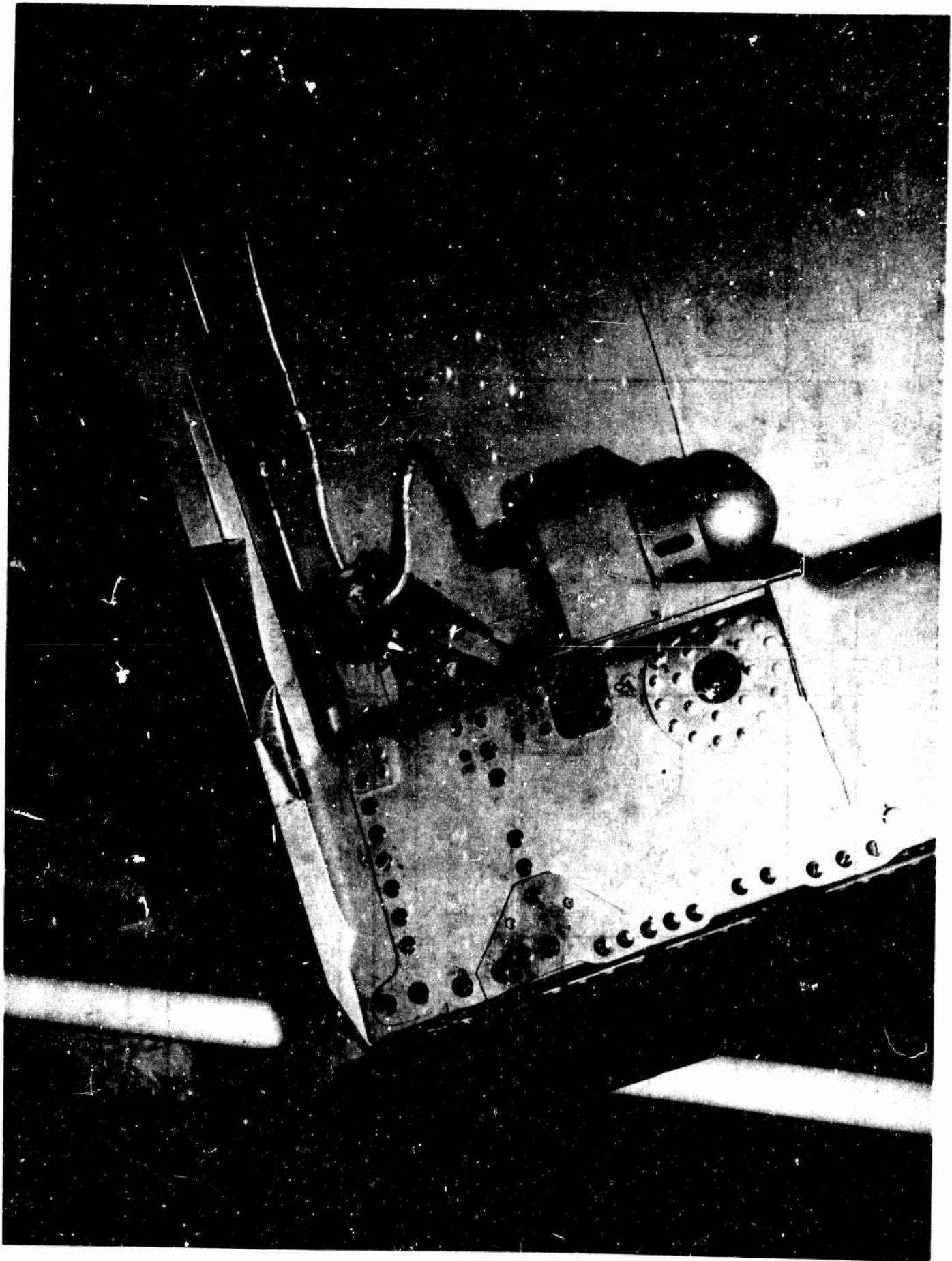
Type V Active Dosimeter on Gemini Hatch
Figure 36.

MAXIMUM ENVELOPE AND ATTACH POINTS, DOSE RATE INDICATOR (TYPE V)
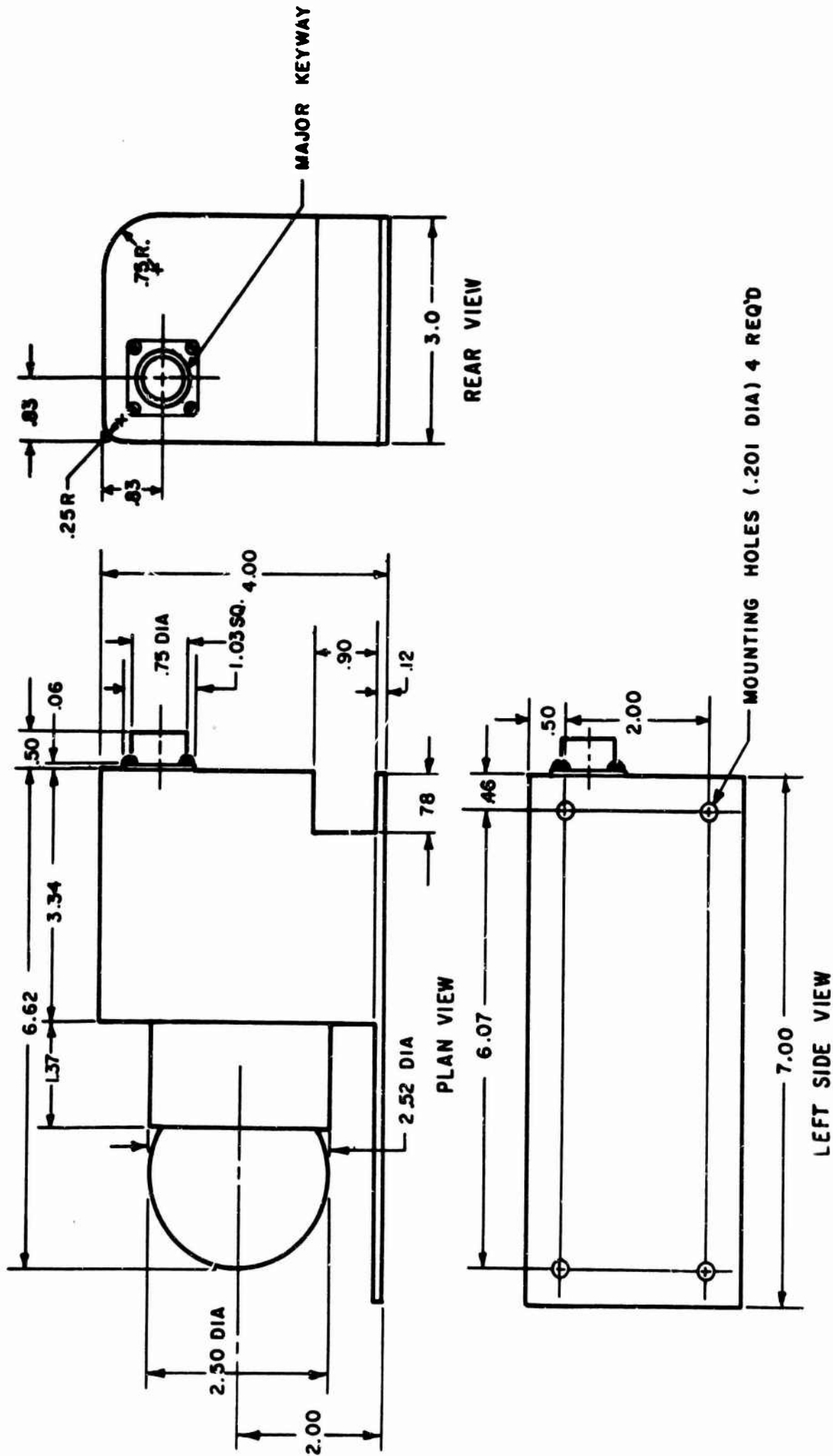
Figure 37

82

MAXIMUM ENVELOPE AND ATTACH POINTS, DOSE RATE INDICATOR (TYPE I)

MOUNTING HOLES (.201 DIA) 4 REQ.

RIGHT SIDE

MAJOR KEYWAY

REAR VIEW

PLAN VIEW

Figure 38

83
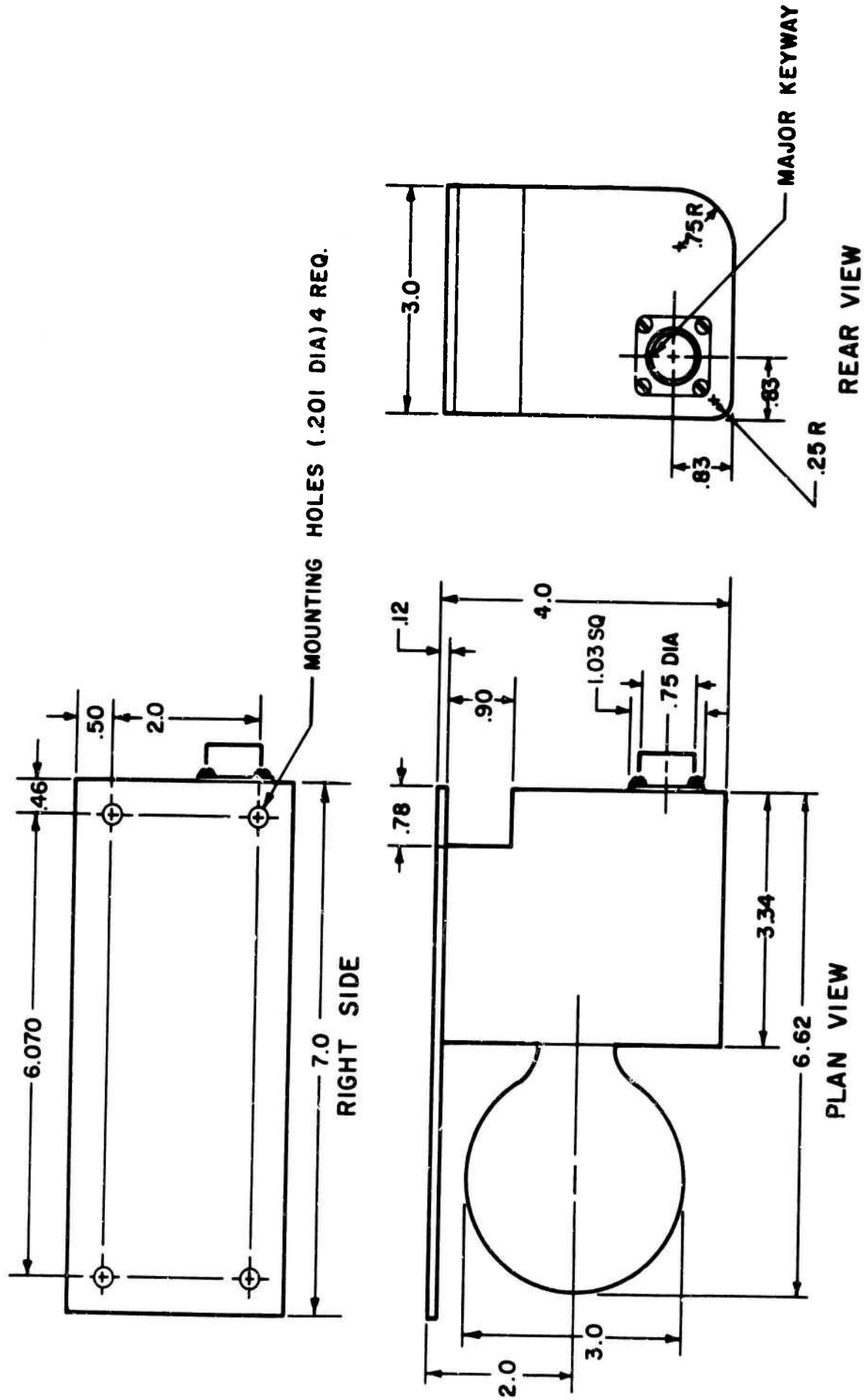
For Gemini 6 the Type I active dosimeter was redesigned to perform depth dose measurements during passage of the spacecraft through the inner radiation belt. The Type I unit was fitted with a removable one-eighth inch brass shield to simulate a depth dose at 2.5 grams/cm^2 of material. In order to accommodate the brass shield, a set of tracks and a special locking mechanism was fitted to the Type I envelope used on Gemini 4. The brass shield and the Type I dosimeter are pictured in Figure 39. The shield is fitted on the side with a piece of Velcro tape by means of which it can be hung on the spacecraft wall when depth dose measurements were not being performed.

The passive dosimetry system consisted of five small aluminum cannisters one thirty-second of an inch thick (Fig. 16). Each unit was hermetically sealed and contained the thermoluminescent and photoluminescent dosimeters described earlier. The units were placed at selected locations within the spacecraft cabin (Figure 40), the same mechanical configuration being used for spacecraft 4 and 6. Figure 41 displays the mechanical envelope of each passive dosimeter.

No electrical power or telemetry were required for the passive portion of this experiment.

It was mentioned earlier that each tissue equivalent active dosimeter is equipped with two radiation rate electronic shaping circuits: a coarse and a fine output. For Experiment D-8 the Type I unit outputs designated XB01 and XB02; and for the Type V unit they were labeled XB03 and XB18. Each channel ranged from 0.0 to 5.0 volts D.C. They were fitted with impedences to operate into telemetry systems whose input impedence is greater than 100,000 ohms. The Type I unit was also equipped with a temperature sensor located in the power supply section of the electronics. This output pin is also a 0.0 to 5.0 volts D.C. in range and is designated XB06. The other output pin for the Type I dosimeter is labeled XB17 and monitors on a 0.0 to 5.0 volt D.C. scale the cali- brate timing circuit voltage which activates the automatic calibration of the sensor described previously. The electrical system schematic of the active

Gemini 6 Active Dosimeter with Accompanying Depth Dose Shield

Figure 39.

85
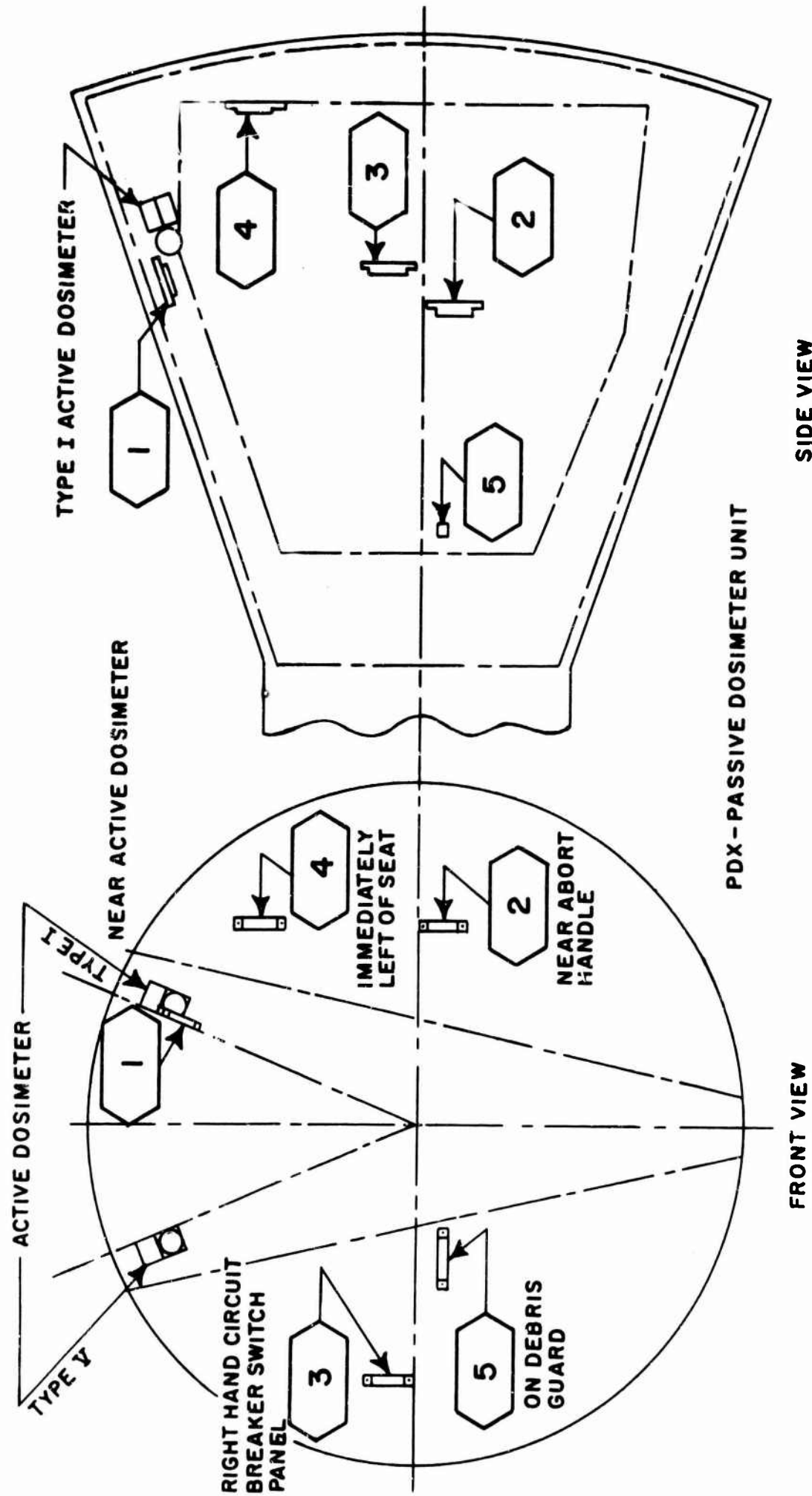
Figure 40 - Passive dosimeter locations in spacecraft.

MAXIMUM ENVELOPE AND ATTACH POINTS, PASSIVE DOSIMETERS

#10 HOLES

1.00

1.00

5.38

4.50

6.00

.50

.31

Figure 41.

87
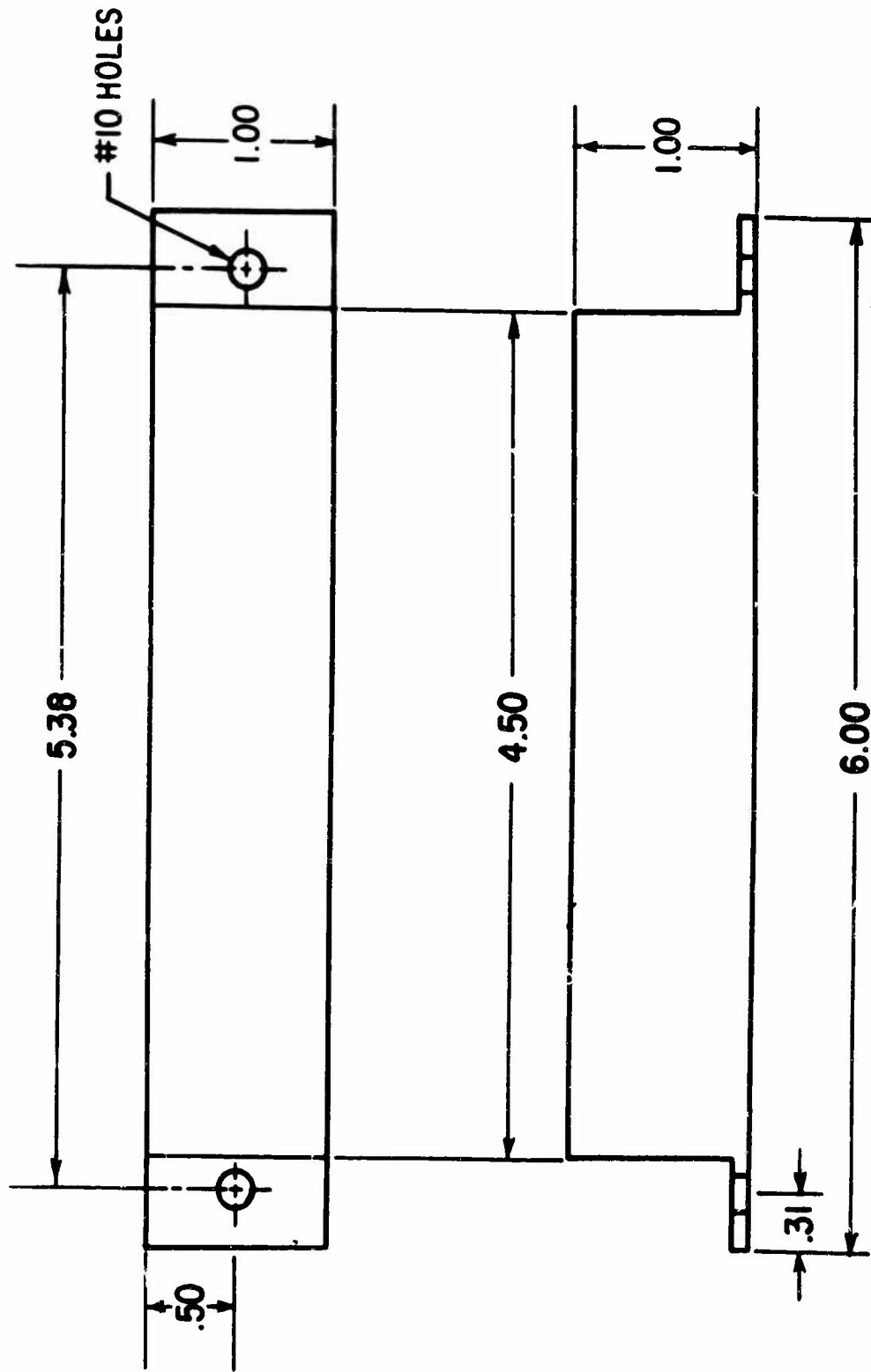
portion of Experiment D-8 is shown in Figure 42. A block diagram of the active

dosimetry spacecraft data storage and power supply system is shown in Figure 43.

IV. B. Development (Technological Chronology of Design)

IV. B. 1. Schedule:

A CPIF contract, AF 29 (601)-6346, was let with the AVCO Corpora-

tion of Tulsa, Oklahoma on February 24, 1964, for the design and development of

the active dosimetry system for Experiment D-8. The passive dosimetry portion

of the experiment was completely designed, tested, and fabricated in-house by

the Biophysics Branch of the Air Force Weapons Laboratory.

Two types of active dosimeters were proposed and designed for

use on the Gemini Spacecraft. One is designated Type I and employs a fixed

sensor, that is, one which cannot be removed from the electronics package.

The other dosimeter, the Type V, uses a removable sensor. It was planned to

couple the Type V to a meter which would give a direct measurement of the dose

to the astronaut. These design plans, including the electronic design based upon

technical data compiled under a previous contract, were submitted to the Air Force

by the contractor on 15 January 1964 as part of the contract proposal. The active

units were to have 4 distinct, hermetically sealed modules consisting of one de-

cade switcher, a power supply, and a set of coarse and fine magnetic amplifiers.

The initially proposed weight of each unit was 3.00 lbs. Electronic breadboarding

was begun on 1 March and the bench test procedures given in Appendix (C) were

submitted to the Air Force on that date.

EXPERIMENT D-B ELECTRICAL SCHEMATIC

Figure 42.

89

EXPERIMENT D-8   BLOCK DIAGRAM

DOSE RATE INDICATOR

DOSE RATE INDICATOR

PCM PROGRAMMER

+ 24V REG.

DC-DC CONV.
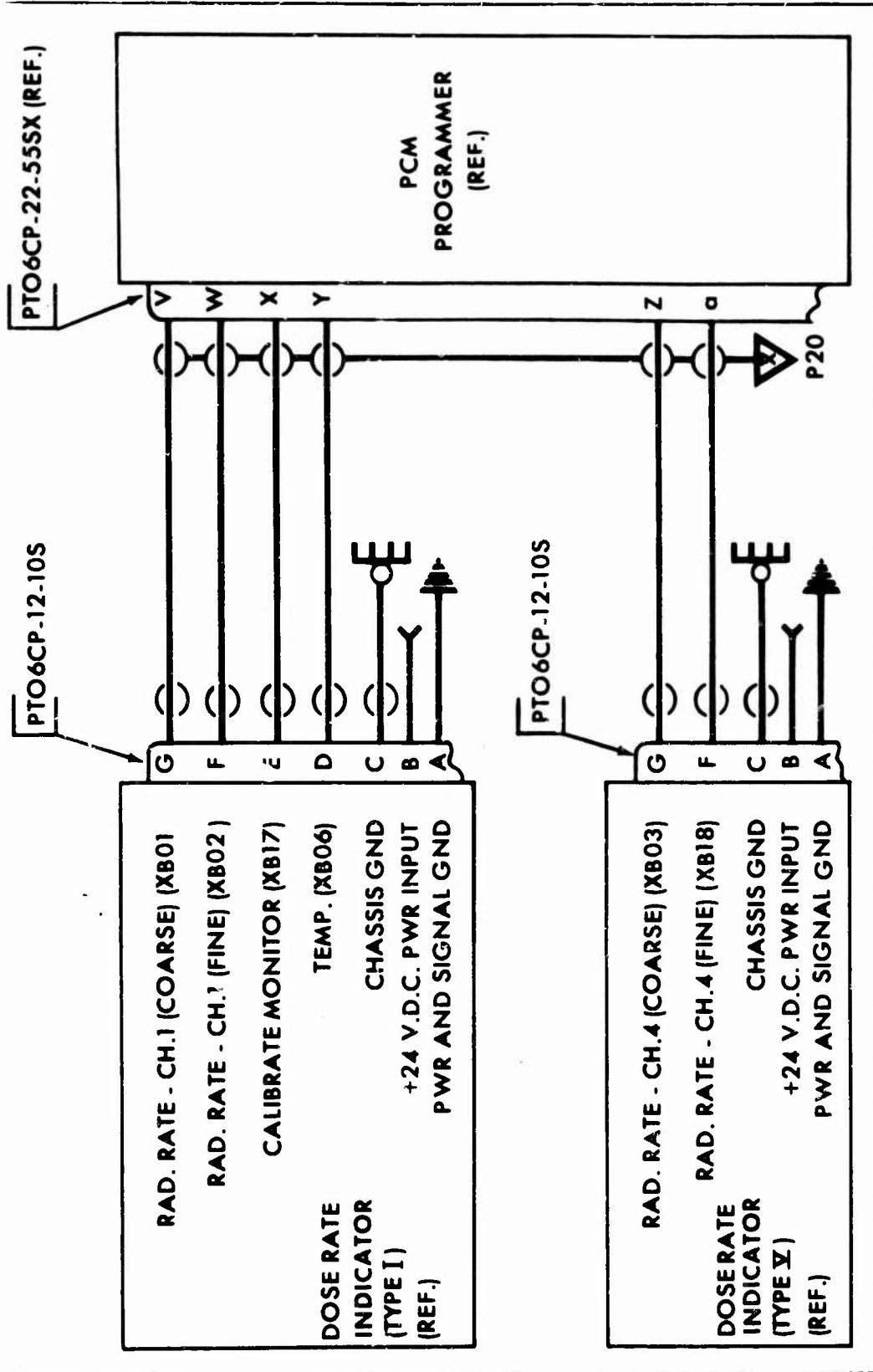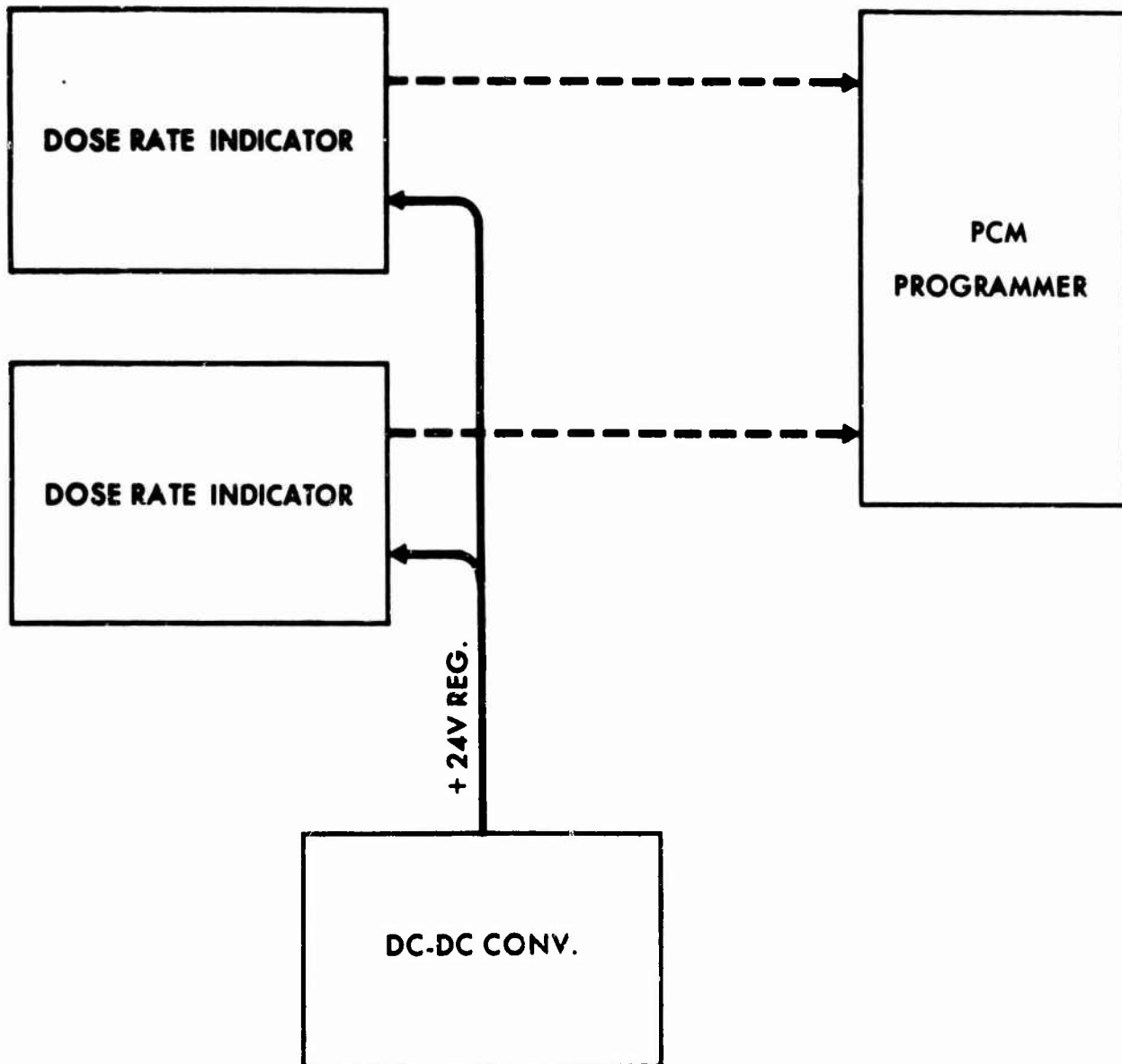
Figure 43.

On March 7, 1964, the contractor contacted Weston Meters, Inc. and learned that no flight-qualified meters could be made available for inclusion in the final mechanical sled test unit or the first flight units. It was also learned that the pricing of the meters whenever they became available, would be excessive. It was decided to change the design of the Type V meter so that no meters would be required for any of the hardware on Spacecraft 4 and 6. With this change, the mechanical design of the active dosimeters was then modified and submitted to the Air Force technical monitor by the contractor. Testing of this unit was performed by the contractor on 15 March 1964.

The Air Force and McDonnell approved the mechanical envelope drawings for the two active instruments on 20 March 1964. The mechanical drawing of the integrated experiment for both the Type I and the Type V dosimeters was designated 453D1-003. Approval was given on 23 March 1964 to fix the sensor operating voltages at 100 volts rather than the 300 volts initially proposed because of corona discharge problems encountered at the higher voltage. The mechanical sled test unit was delivered to McDonnell Aircraft on 30 March 1964. The final shock testing at China Lake, California was scheduled for late April. This test was delayed until May, however, because of technical difficulties at McDonnell.

The first spacecraft systems test (SST) unit was fabricated on 15 April 1964. This unit incorporated the final design of the flight items with one exception: The method of sensor and barrel assembly which was changed in August of 1964. The changes consisted in corona epoxy molding the barrel and cavity ionization chamber when it was discovered that the chamber had suffered leaks in preliminary vibration testing of the unit. Delay of vibration testing until August was necessitated by the short delivery date of the first SST unit.

With sensor and barrel assembly change the SST-6 active units were successfully qualified by 15 November 1964 and the final flight units were fabricated identical to those units. Delivery of the units to the Air Force was effected 1 March 1965. At that time all Gemini hardware fabrication and delivery to the Air Force was completed.

IV.B.2. Testing:

A three-phase program of pre-delivery and pre-installation acceeptance testing was associated with the integration of the active dosimetry system into the Gemini spacecraft. Initial testing was begun at the vendor's facility immediately after the sensors were constructed.

IV.B.2.a. Design Testing:

Preliminary testing was conducted to establish operating conditions for each type of sensor used in the program: Figure 25, discussed earlier, illustrates the results of the first test run on the Type I dosimeter. Its purpose was to establish the tissue equivalence of the ionizing cavity. In this test, the number of ions per mass of gas in the chamber was plotted against the gas pressure. The linearity of this curve demonstrated that the ionization chambers were operating in the Bragg-Gray mode, as predicted in the theoretical considerations by Fano's Theorem. Figures 44 and 45 show a plot of the saturation curves for the Type V Dosimeter. This data was gathered using varying energies of X Radiation to determine the optimum voltage operating point of the ionization cavity. Figures 46 and 47 show the effects of the type and length of the collecting electrode on the saturation curves of the Type V Dosimeter for 80 to 120 kcvp X rays. A long tissue equivalent plastic center electrode was utilized in the final flight items because of the flat behavior of its saturation curves which distinguish it from the sharp bending experienced by the other commonly used probe types. It should be noted that this feature was incorporated as a result of data generated in initial tests and was not theoretically predicted.
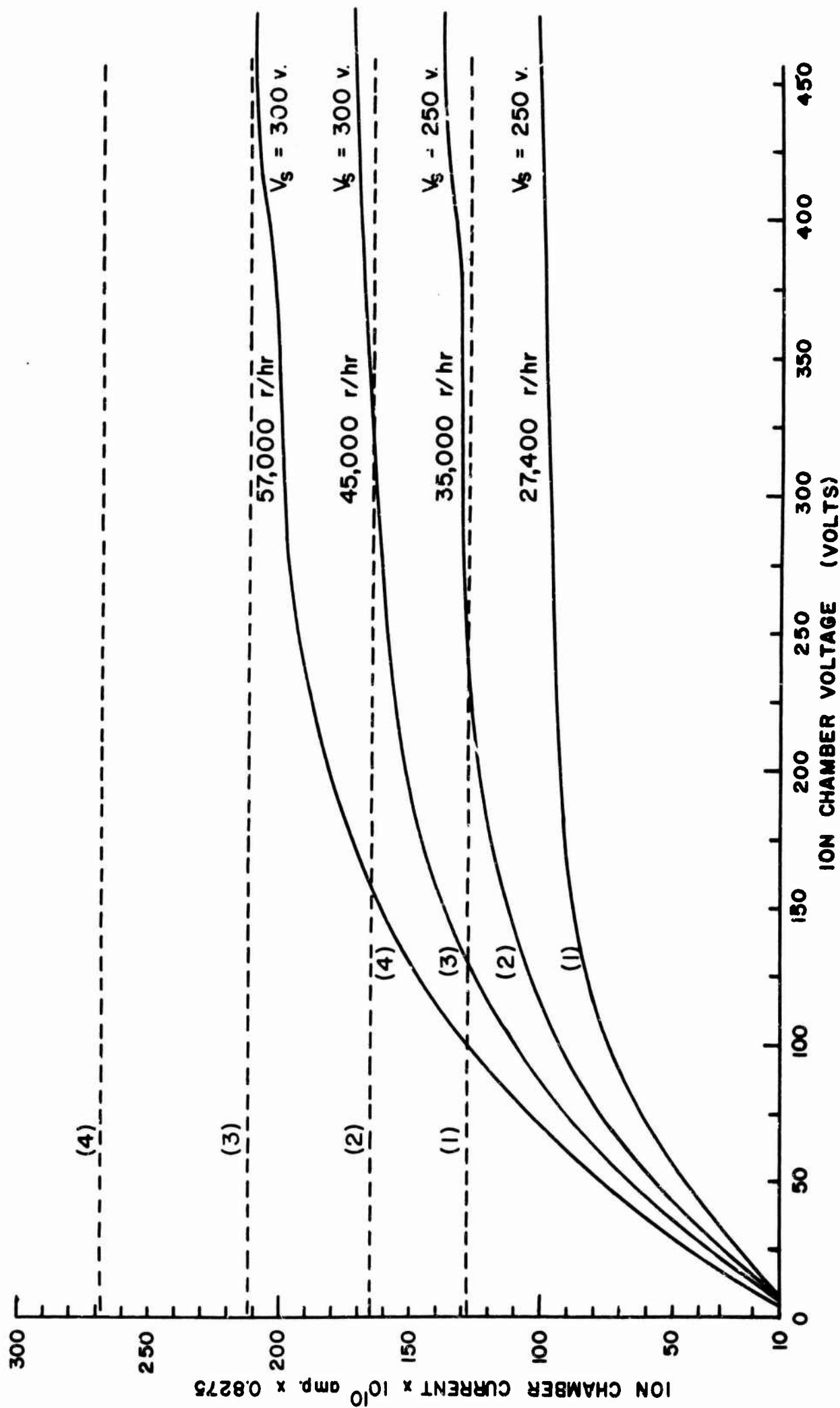
Figure 44. Saturation Voltage versus Collection Current for 80 KVCP X Rays

93
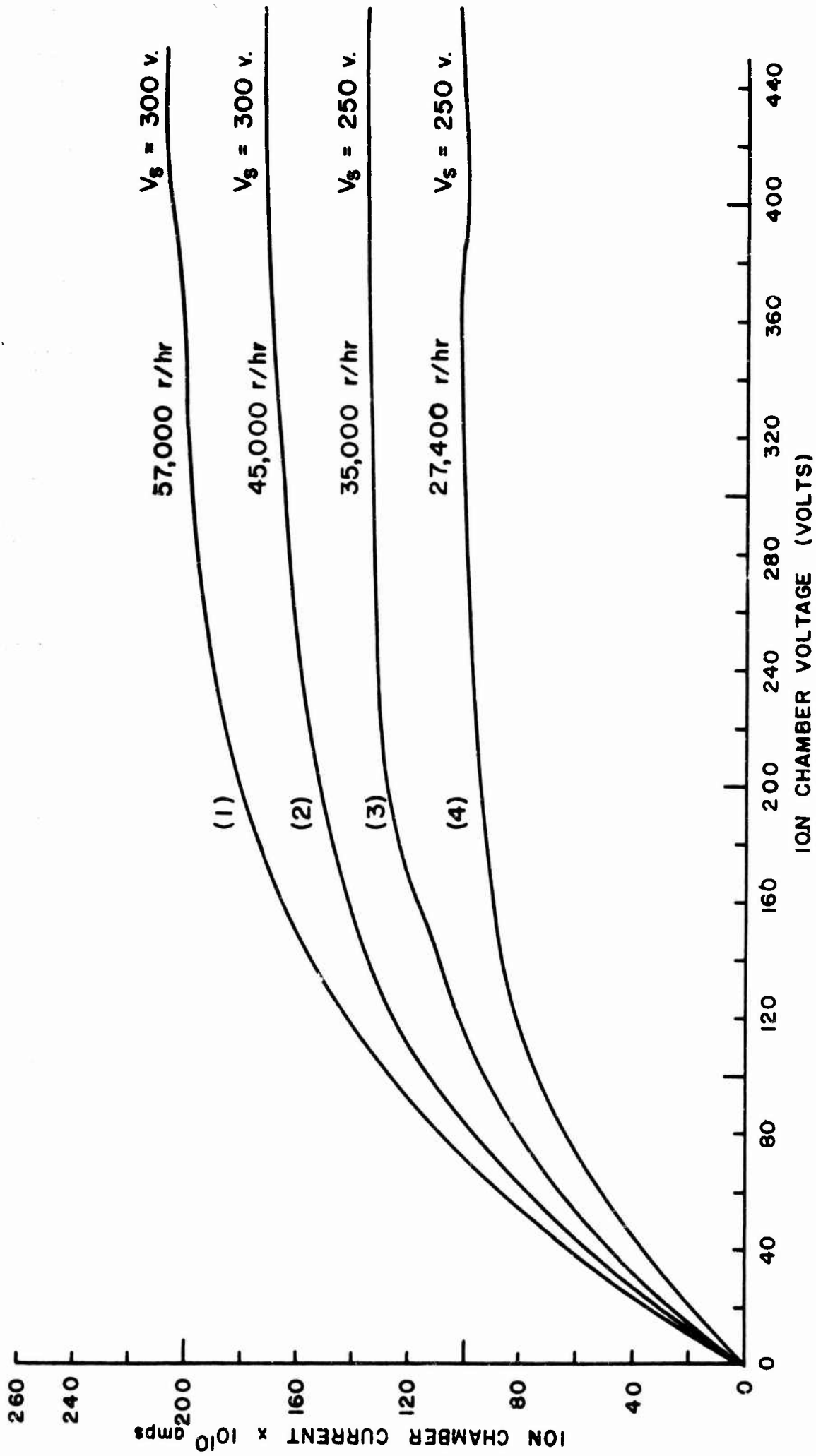
Figure 45. Saturation Voltage versus Collection Current for 120 KVCP X Rays

94
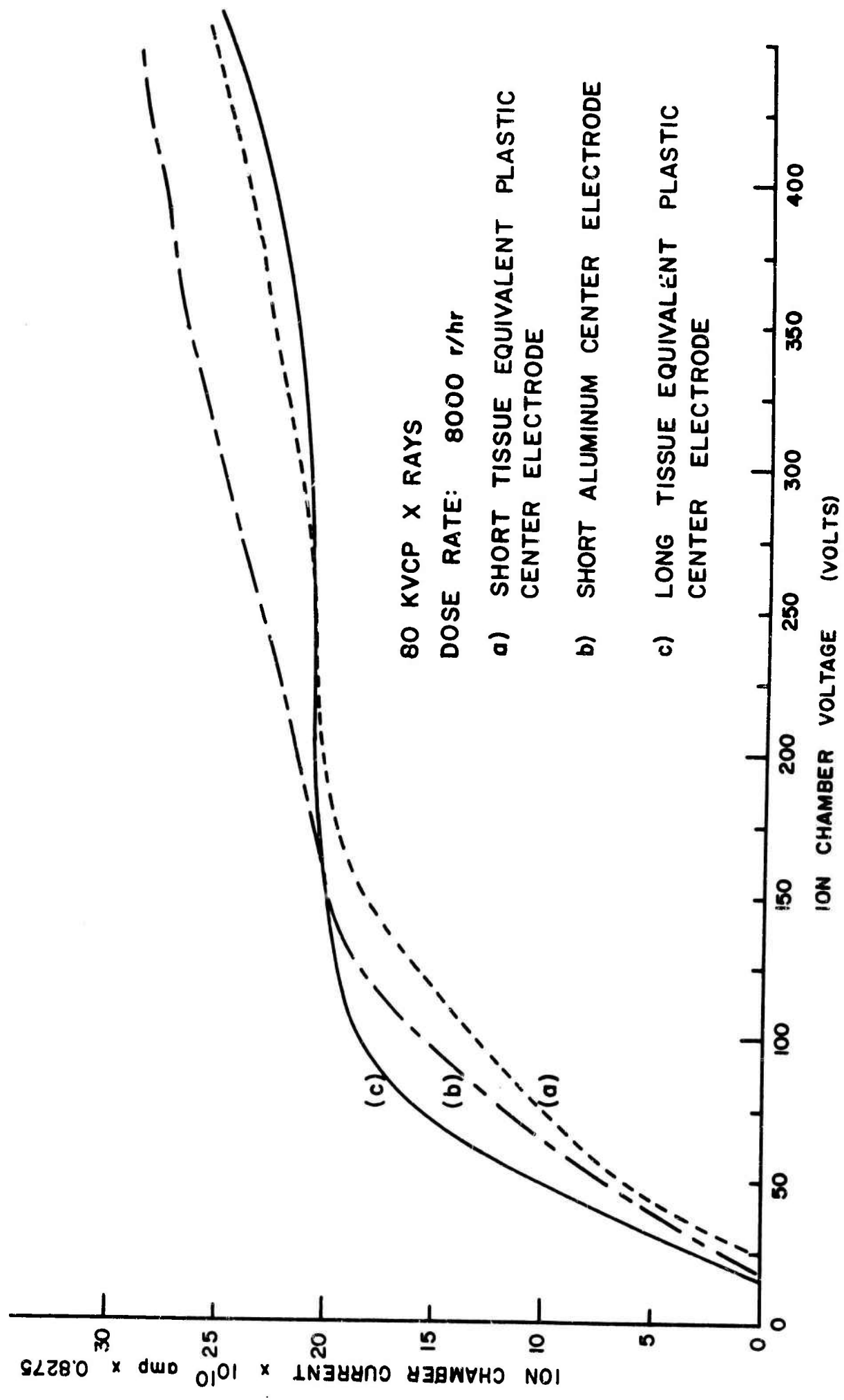
Figure 46. Collection Current versus Chamber Voltage for 80 KVCP X Rays

95
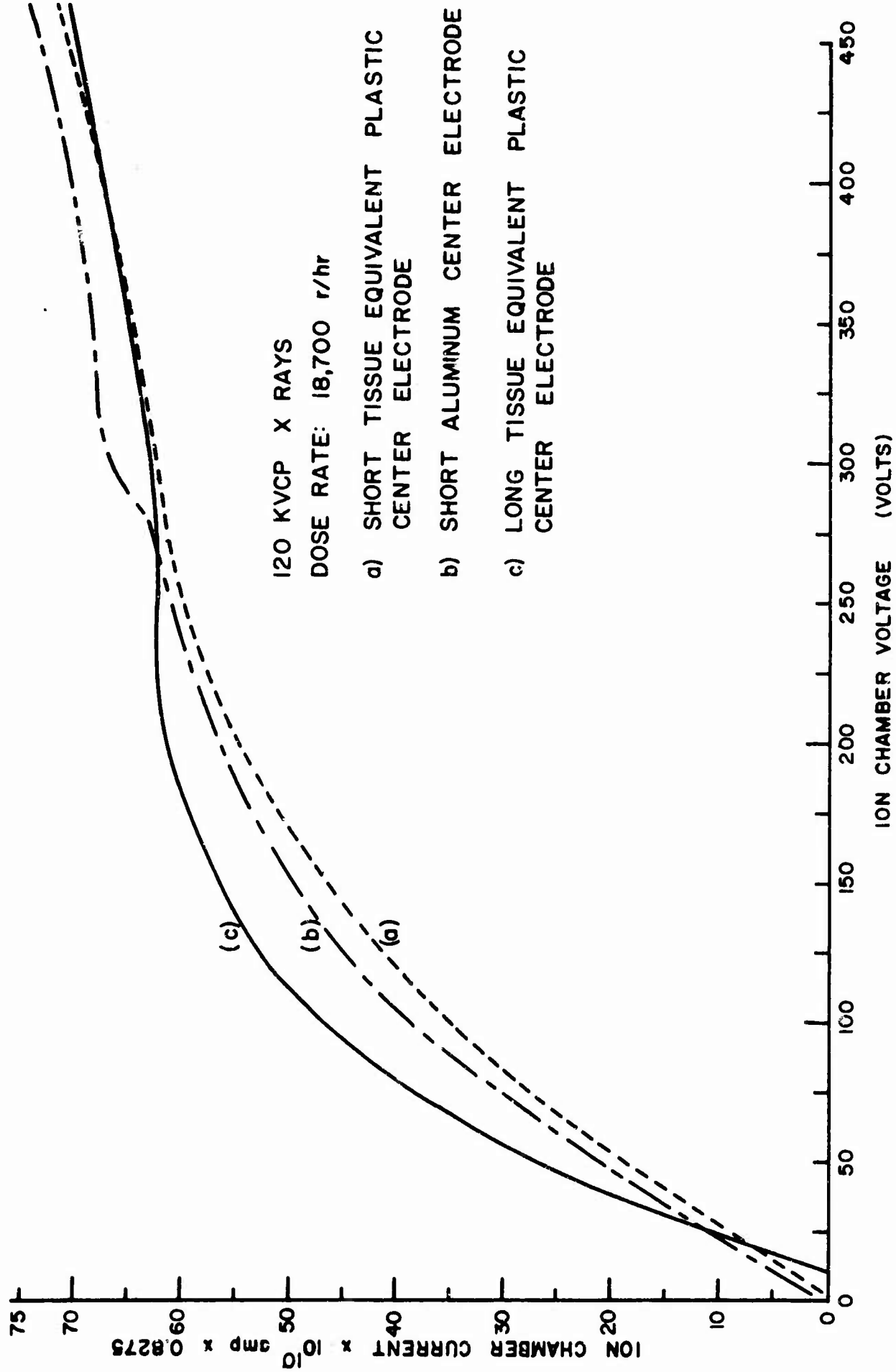
Figure 47. Collection Current versus Chamber Voltage for 120 KVCP X Rays

96

The electronics were tested during assembly to determine the core design of the magnetic amplifiers. Each test consisted of an induced voltage in which each set of windings were exposed to twice the normal operating voltages for a period of operation comparable to the expected operating time on the Gemini Missions. After the induced voltage tests, each amplifier was subjected to a stability test to determine the expected rate of drift with time in use. The results of a representative test for the Gemini SST coarse amplifier is shown in Figure 48. Since the electrometer circuit is the most critical element in the active dosimeter electronics, extensive tests were run during initial design to establish the proper aging time commensurate with operating currents and voltages established for this experiment. Figure 49 and 50 illustrate life aging tests performed on ten 5889 electrometer tubes of the type used in the Type I and Type V charge-sensitive preamplifier circuitry.

During design of the mounting and packaging configurations for the active dosimeters a series of directional response plots for each of the three mutually perpendicular planes of rotation illustrated in Figure 51 was generated for X Rays of 60 and 200 KVP energy levels. The relative dose rate for 348 directions of irradiation for the Type I instrument with 60 kvp X rays and no filter is shown in Table IV where it may be seen noticeable X-ray attenuation occurs only for rays passing through the electronics, even at these low energies.

Start of Test 8-7-64
Electronics S/N 1

TEIC 450, TYPE II STABILITY TEST

	Position											
	1		2		3		4		5		6	
Time	E_{oc}	E_{of}	E_{oc}	E_{of}	E_{oc}	E_{of}	E_{oc}	E_{of}	E_{oc}	E_{of}	E_{oc}	E_{of}
T = 0	2.95	4.9	2.21	1.30	1.90	4.67	1.65	3.50	1.45	2.50	0.035	0.130
T + 64 hrs	2.90	4.59	2.19	1.12	1.85	4.45	1.60	3.25	1.41	2.20	-0.005	-0.015
T + 232 hrs	2.90	4.55	2.19	1.0	1.85	4.31	1.59	3.12	1.42	2.25	0.015	0.070
T + 280 hrs	2.89	4.40	2.17	0.92	1.86	4.29	1.62	3.12	1.43	2.15	0.035	0.130

E_{oc} = Coarse output voltage

E_{of} = Fine output voltage

Positions 1, 2, etc. are fixed points on a 1 millicurie Strontium-90 calibration jig.

Figure 48.

98
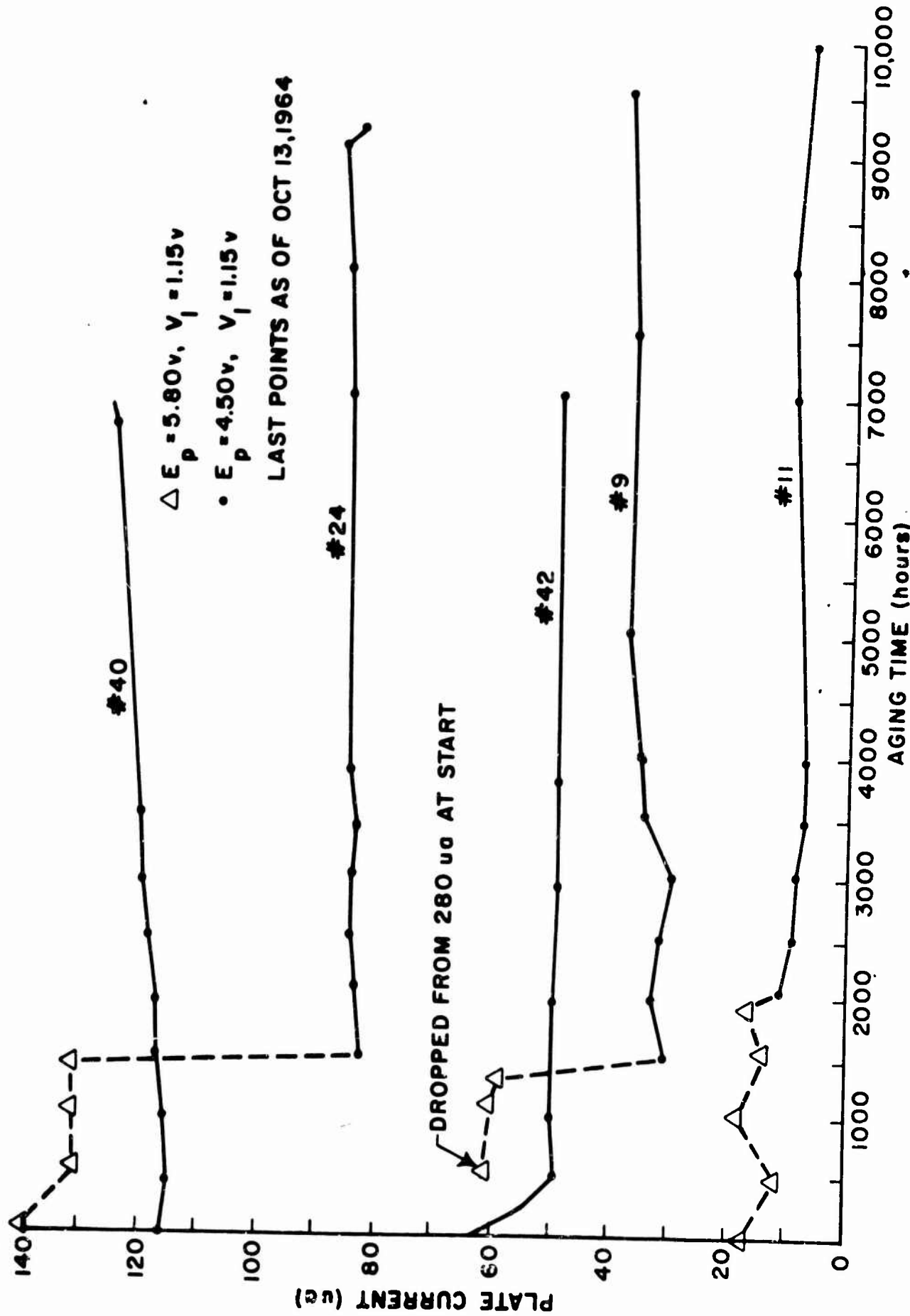
Figure 49. 5889 Life Aging Test
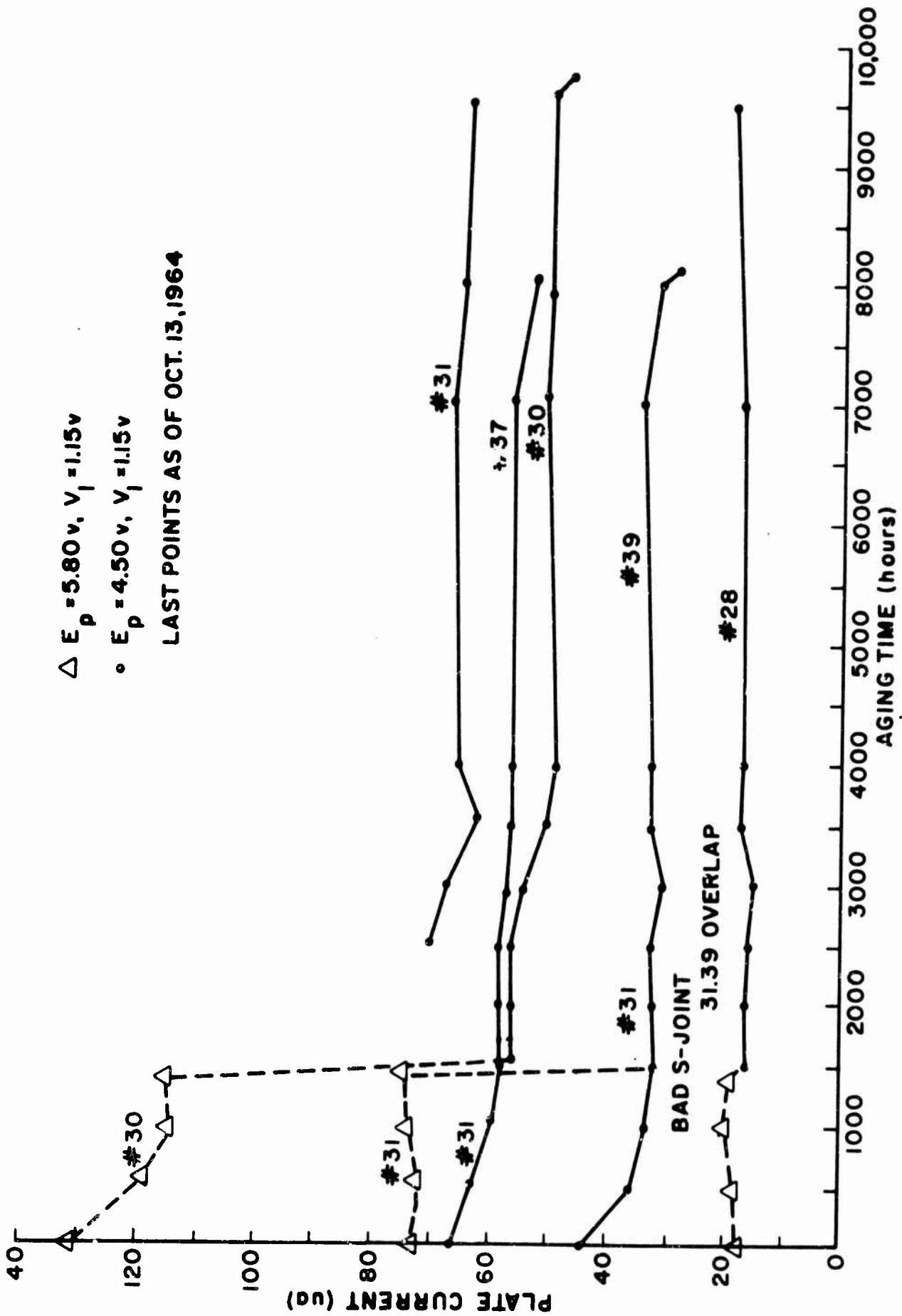
Figure 50.   5889 Life Aging Test

100
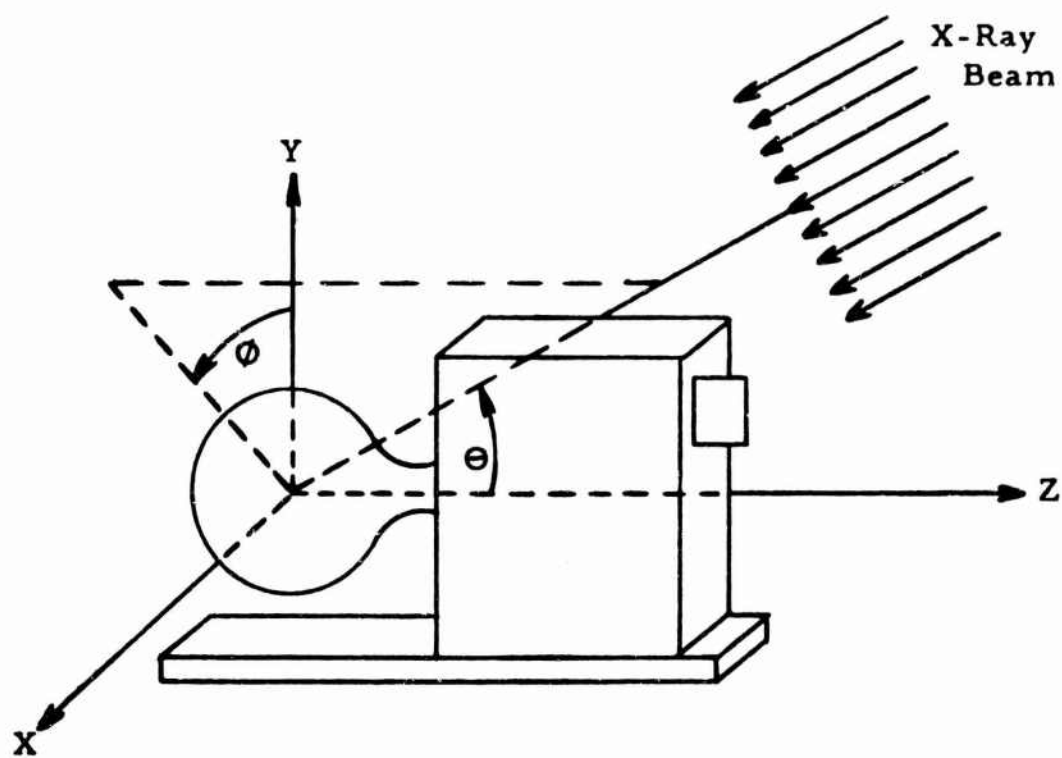
Three Planes of Ionization Chamber Rotation

Figure 51.

Table IV,

Relative Dose Rate for 348 Directions of Irradiation (Type I Instrument)

60 KVP, no filter

() means corrected for shielding mounting plate

Theta	Phi 0	30	60	90	120	150	180	210	240	270	300	330
180	1	1	1	1	1	1	1	1	1	1	1	1
175	1	1	1	1	1	1.	1	1	1	1	1	1
170	1	1	1	1	1	1	1	1	1	1	1	1
165	1	1	1	1	1	1	1	1	1	1	1	1
160	1	1	1	1	1	1	1	1	1	1	1	1
155	1	1	1	1	1	1	1	1	1	1	1	1
150	1	1	1	1	1	1	1	1	1	1	1	1
145	1	1	1	1	1	1	1	1	1	1	1	1
140	1	1	1	1	1	1	1	1	1	1	1	1
135	1	1	1	1	1	1	1	1	1	1	1	1
130	1	1	1	1	1	1	(.98)	(.99)	1	1	1	1
120	1	1	1	1	1	(.98)	(.91)	(.95)	1	1	1	1
110	1	1	1	1	1	(.93)	(.84)	(.87)	1	1	1	1
100	1	1	1	1	1	(.86)	(.77)	(.80)	1	1	1	1
90	1	1	1	1	.968	(.80)	(.70)	(.73)	.821	1	1	1
80	1	.986	1	.992	.950	(.75)	(.66)	(.69)	.809	1	1	1
70	.968	.968	.986	.992	.908	(.66)	(.58)	(.63)	.758	.986	1	.968
60	.840	.858	.893	.930	.809	(.56)	(.46)	(.52)	.671	.908	.908	.821
50	.630	.658	.729	.758	.658	(.43)	(.31)	(.40)	.546	.790	.740	.630
45	.515	.556	---	---	.569	(.34)	(.24)	(.30)	.475	.690	.644	.524
40	.411	.446	.530	.580	.483	(.25)	(.18)	(.22)	.411	.592	.546	.420
35	.303	.349	.432	.483	.394	.175	.123	.158	.335	.502	.446	.328
30	.214	.262	.335	.385	.315	.135	.0938	.123	.272	.394	.349	.224
25	.131	.172	.257	.296	.237	.0991	---	.0938	.202	.312	.278	.148
20	.0691	.0975	.176	.214	.161	.0691	.0539	.0749	.148	.227	.194	.0830
15	.0386	.0539	.110	.137	.101	.0496	.0475	.0636	.106	.148	.131	.0539
10	.0375	.0446	.0662	.0796	.0610	.0457	.0496	.0598	.0765	.0991	.0830	.0446
5	.0446	.0475	.0468	.0525	.0468	.0475	.0561	.0572	.0610	.0662	.0585	.0457
0	.0585	.0572	.0550	.0580	.0539	.0529	.0585	.0572	.0550	.0580	.0539	.0529

Figure 52 shows the comparative response of the Type I dosimeter for 60 and 200 KVP X rays in the first plane of rotation. Figure 53 illustrates the same type of curve for the second plane of rotation. In these curves a relative response of 1.00 means that the omnidirectional response of the dosimeter is 100%.

From these data the net response of the instrument to radiation can be calculated and compared to the response that would be obtained if the response were purely omnidirectional. This is done as follows:

The net response is given by

$$\int_0^{4\pi} r(\Omega)d\Omega$$

where $r(\Omega)$ = dose rate when irradiated from the directions Ω to

$$\Omega + d\Omega$$

Ω = solid angle.

For polar coordinates, the well known relationship

$$d\Omega = \sin \theta \; d\theta \; d\phi$$

means the net response can be calculated from

$$\int_0^{\pi} \sin \theta \; d\theta \int_0^{2\pi} r(\theta, \phi) \; d\phi.$$

This integration is very simply performed numerically. A sample numerical integration over θ for the 60 KVP data is given in Table (V). Note that in the table the result of the numerical integration over ϕ is reported in the column "average relative dose rate." Note also the fact that the readings for small θ

103
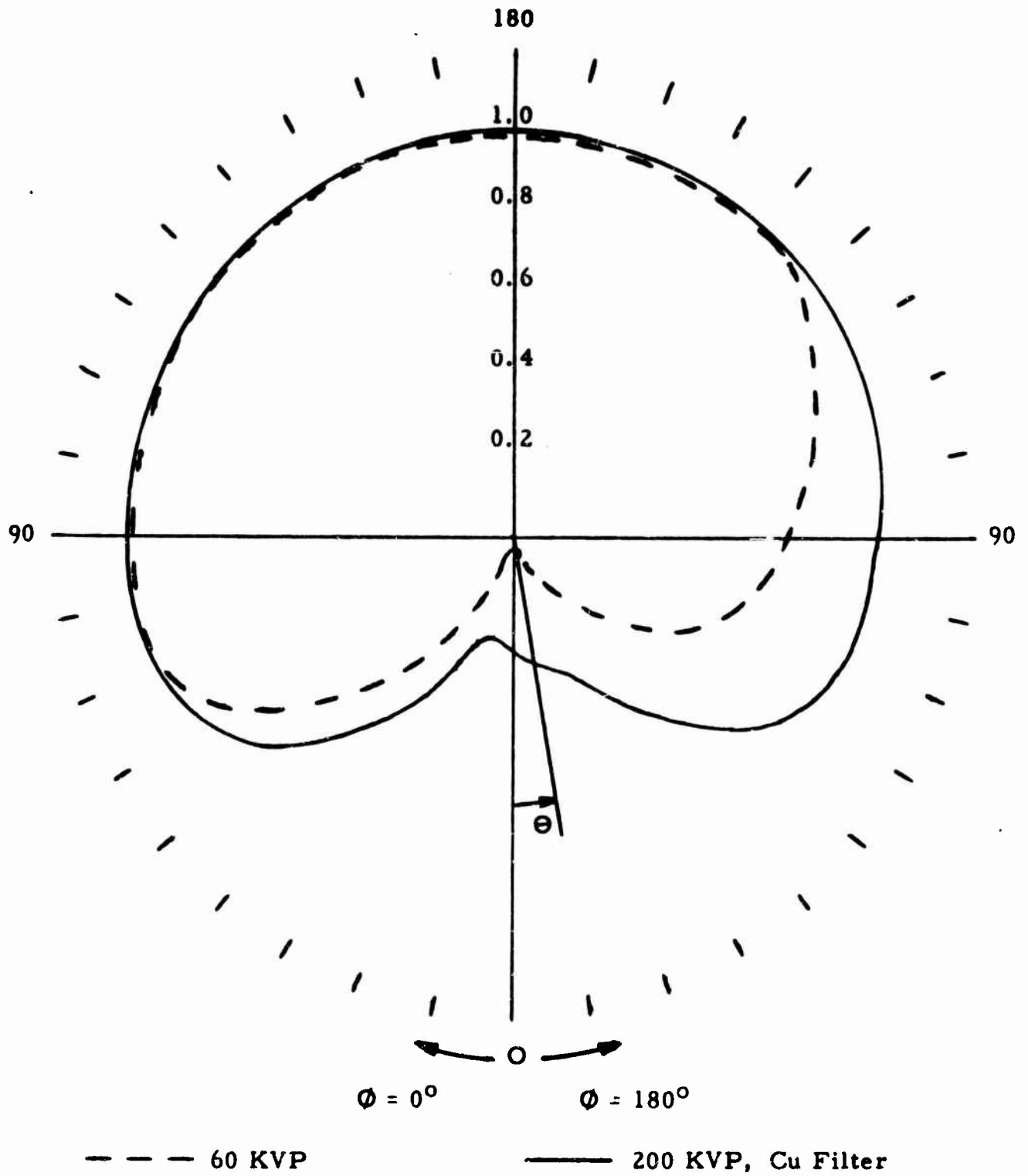
Comparison of 200 and 60 KVP Attenuation
in the First Plane of Rotation

Figure 52.
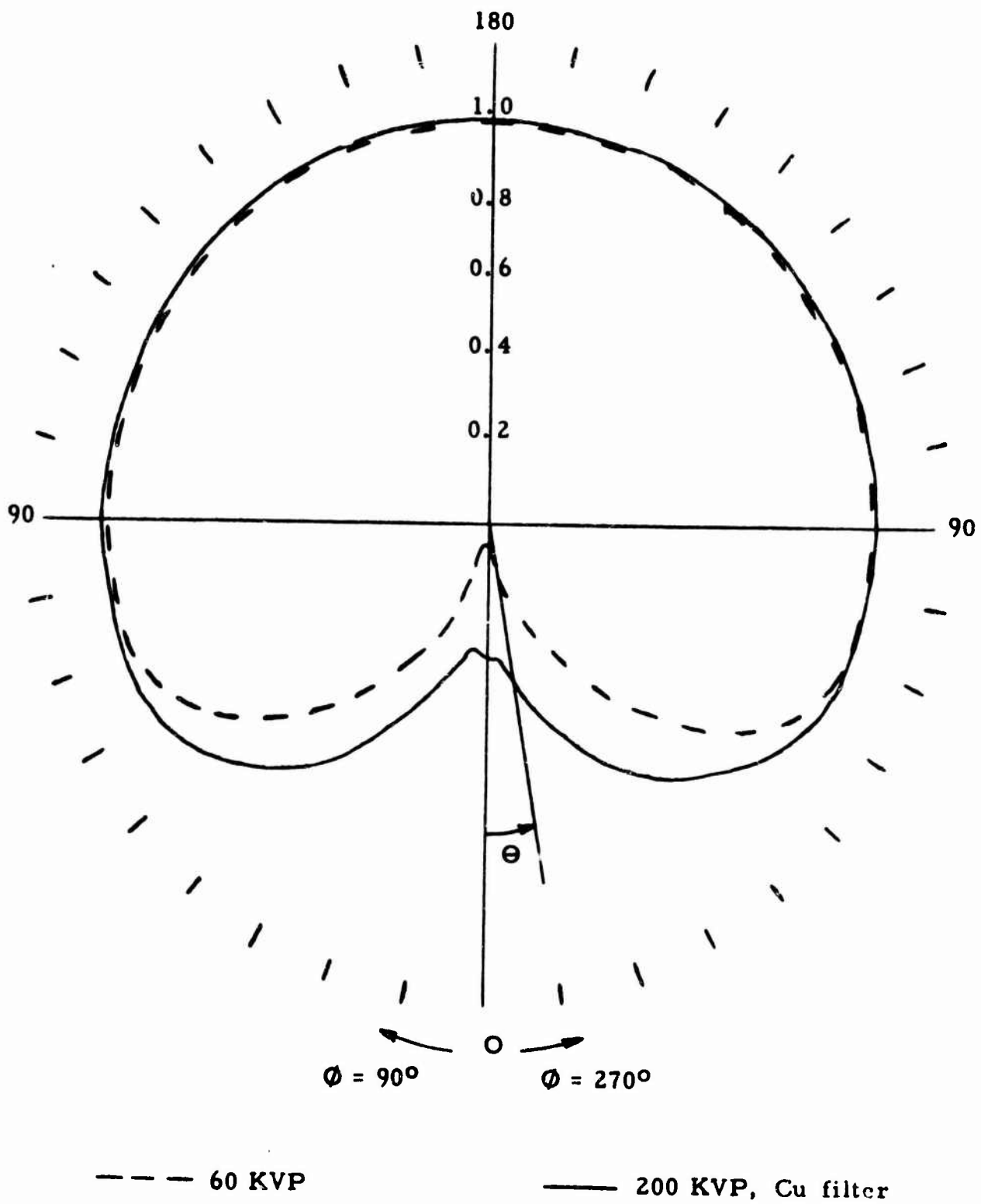
Comparison of 200 and 60 KVP Attenuation in the
Second Plane of Rotation

Figure 53.

TABLE Y

Calculation of Net Efficiency
(60 KVP, Type I Chamber)

Theta	Sin Θ $\Delta\Theta$	Average Relative Dose Rate	Product
180	0	1	0
175	.0092	1	.0092
170	.0152	1	.0152
165	.0226	1	.0226
160	.0298	1	.0298
155	.0368	1	.0368
150	.0436	1	.0436
145	.0500	1	.0500
140	.0560	1	.0560
135	.0616	1	.0616
130	.0668	.997	.0665
120	.147	.987	.145
110	.161	.971	.156
100	.170	.954	.162
90	.174	.918	.160
80	.170	.904	.1535
70	.161	.868	.140
60	.147	.765	.1125
50	.0668	.607	.0406
45	.0616	.515	.0318
40	.0560	.423	.0237
35	.0500	.334	.0167
30	.0436	.259	.0113
25	.0368	.191	.0070
20	.0298	.131	.0039
15	.0226	.087	.0020
10	.0152	.063	.0010
5	.0092	.053	.0005
0	0	.056	0
	1.9132		1.5719

$$\frac{1.5719}{1.9132} = 82.4\%$$

are of little importance relative to the readings at large θ because of the relatively small solid angle at small θ.

A net efficiency of 82.4 percent is calculated for the Type I instrument and unfiltered 60 KVP X rays. The results of similar calculations are given for a total of seven radiation qualities in Table VI. These figures were obtained by extensive measurements with the use of these results in performing the numerical double integrations. Consequently, the figures quoted are accurate, as indicated, in the tenths of percent. It is very gratifying that even for X rays as soft as the 60 KVP spectrum, the instrument is quite efficient as an omnidirectional sensor of radiation.

In Figure 54 is shown a comparison of the characteristics of seven radiation types available for use in calibration. The results of exposure of the Type I instrument to these seven radiation types, as well as the relative dose rate for each type at a given angle in the second plane of rotation is illustrated in Figure 55. Figures 56 through 57 illustrate the polar response of the Type I instrument in six planes of rotation for 60 KVP, 200 KVP X rays. Table VII shows the net efficiency of the Type I' shielding to a perfectly omnidirectional sensor for each of the seven radiation types. It is observed that a net efficiency of 96.6% was observed for the Type I instrument using γ radiation at only 1.25 Mev. The Type V instrument was tested for directional response in the same manner as the Type I dosimeter. A polar diagram of the angular response in two planes for three radiation types is shown in Figure 58 for the Type I instrument. The net efficiency of the Type V ionization chamber relative to a perfectly omnidirectional sensor is presented in Table VIII for all seven types of radiation. This table also shows the efficiency of the Type V sensor relative to the Type I sensor.

Type I Instrument
Net Efficiency Relative to a Perfectly Omnidirectional Sensor

Radiation	Efficiency
Cobalt-60 gamma rays	96.6%
200 KVP, 3 mm Cu filter	91.9%
160 KVP, 1.5 mm Cu filter	90.9%
160 KVP, 8.2 mm Al filter	89.6%
120 KVP, 1.6 mm Al filter	87.4%
80 KVP, no filter	84.6%
60 KVP, no filter	82.4%

TABLE VII

Type I Instrument, with Brass Shield
Net Efficiency Relative to a Perfectly Omnidirectional Sensor

Radiation	Brass Plate Attenuation	Estimated Efficiency
Cobalt-60 gamma rays	0.89	85-90%
200 KVP, 3 mm Cu filter	0.64	60-65%
160 KVP, 1.5 mm Cu filter	0.41	40%
160 KVP, 8.2 mm Al filter	0.26	25%
120 KVP, 1.6 mm Al filter	0.0786	10-15%
80 KVP, no filter	0.0123	4-8%
60 KVP, no filter	0.00376	1-3%

Figure 54.

109
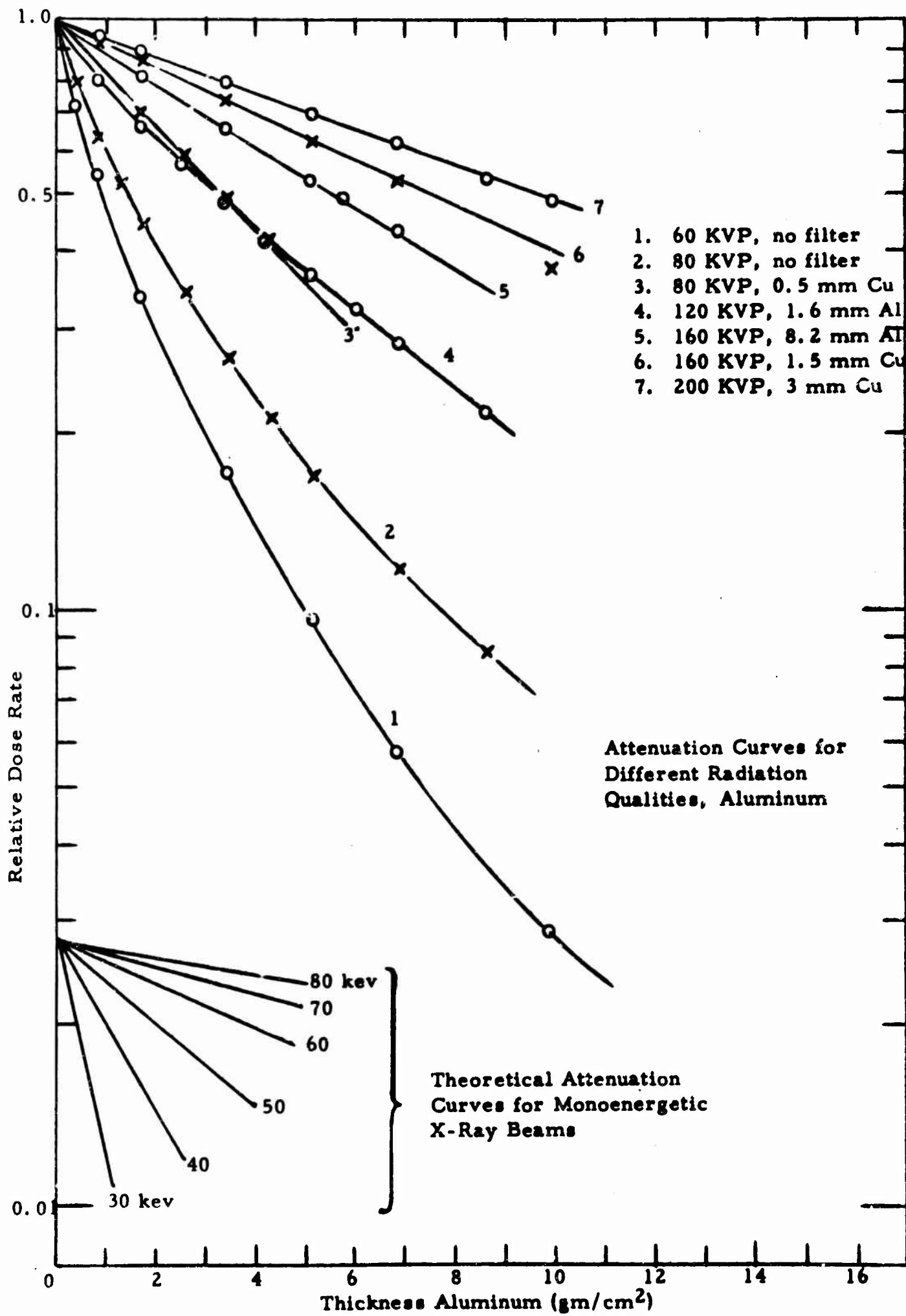
TABLE VIII

Type V Instrument
Net Efficiency Relative to a Perfectly Omnidirectional Sensor

Radiation	Efficiency*	Efficiency Relative to Type I
Cobalt-60 gamma rays	(93-95%)	(95-98%)
200 KVP, 3 mm Cu filter	86.6%	94.3%
160 KVP, 1.5 mm Cu filter	(84%)	(92.5%)
160 KVP, 8.2 mm Al filter	(82%)	(91.5%)
120 KVP, 1.6 mm Al filter	75.5%	86.5%
80 KVP, no filter	(71%)	(84%)
60 KVP, no filter	67.0%	81.4%

*( ) means the value is estimated; otherwise the values are obtained from detailed measurements.
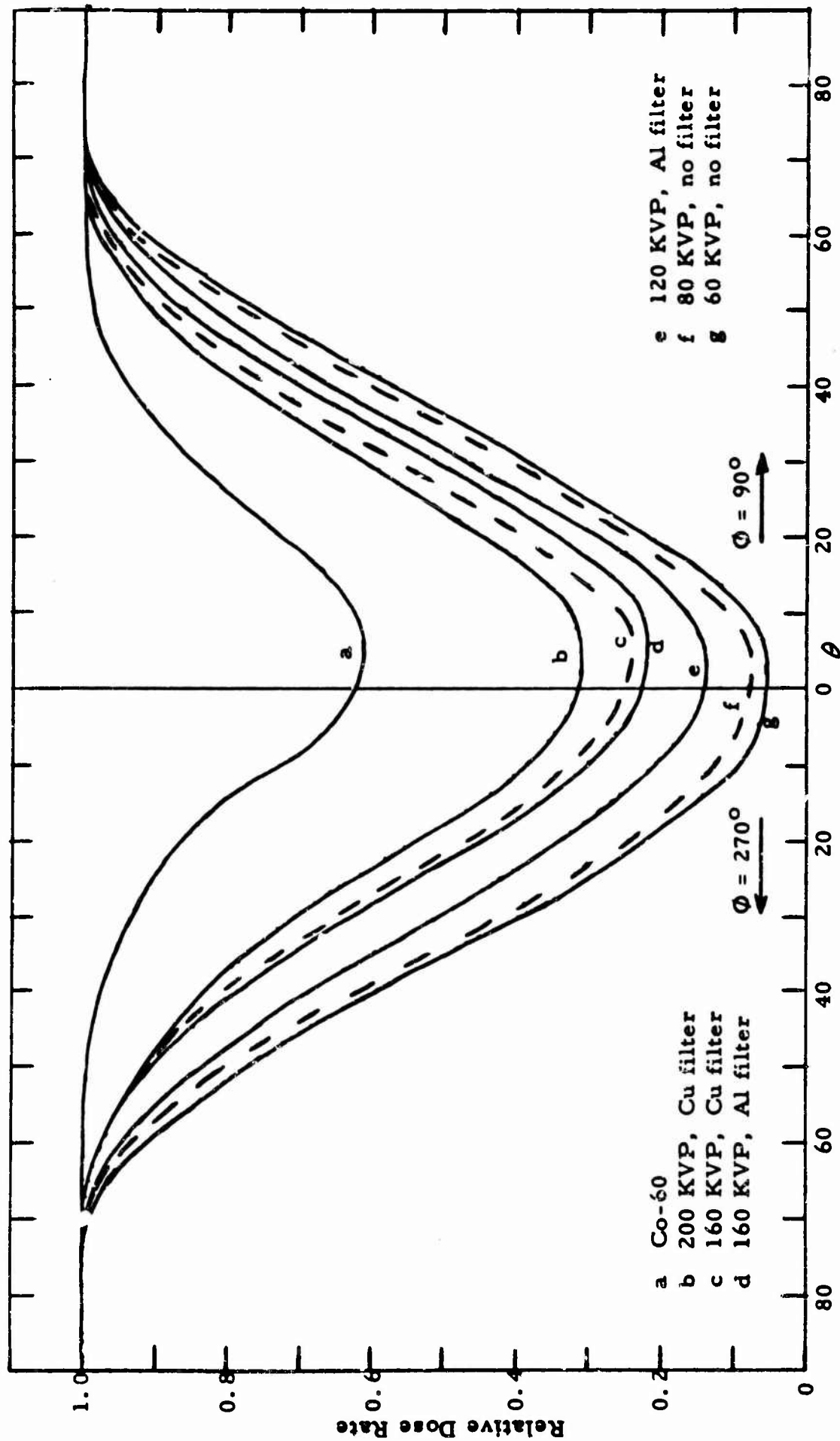
Comparison of All Radiation Attenuation in the Second Plane of Rotation

Figure 55.

111
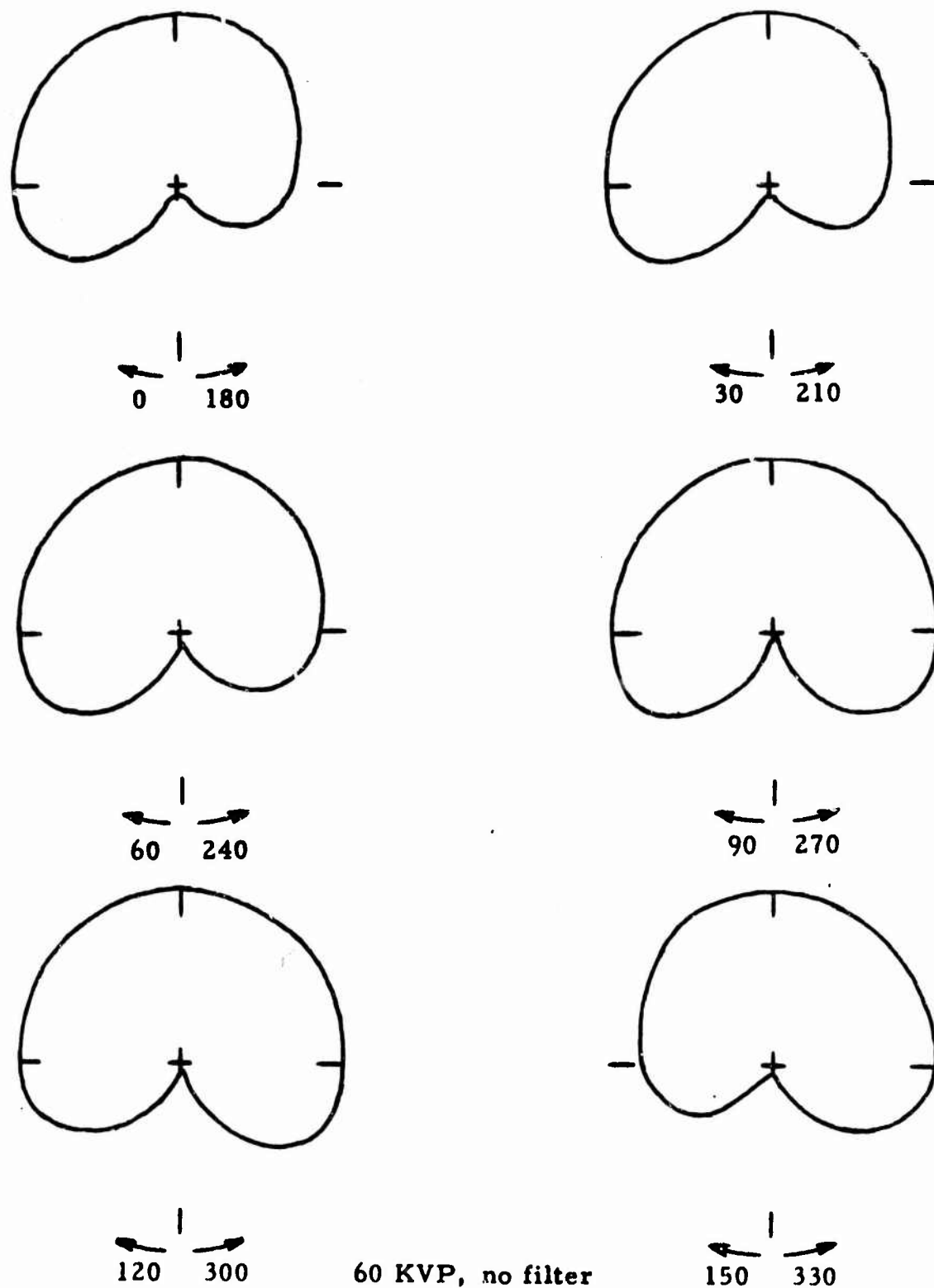
Polar Diagram of Theta Response in Six Planes of Rotation, 60 KVP

Figure 56.

0 180   30 210

60 240   90 270

120 300   150 330

200 KVP, 3 mm Cu filter
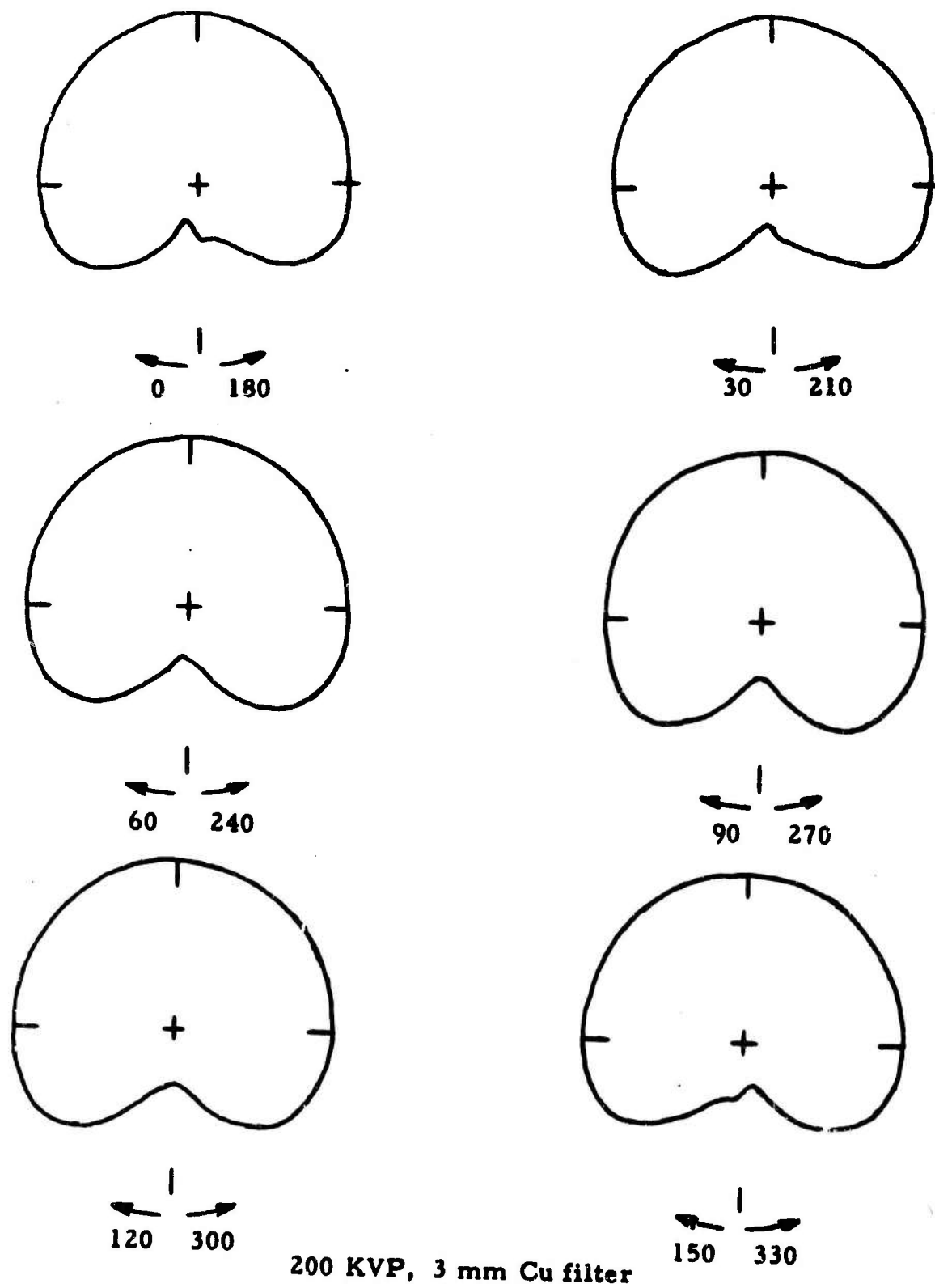
Polar Diagram of Theta Response in Six Planes of
Rotation, 200 KVP

Figure 57.

113
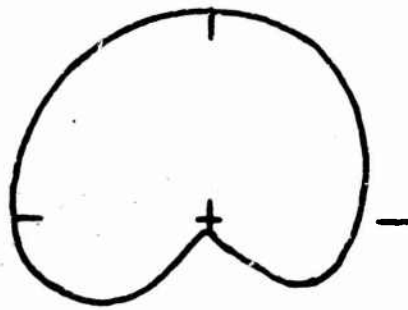
80 KVP, no filter
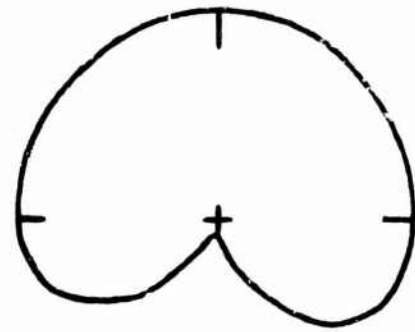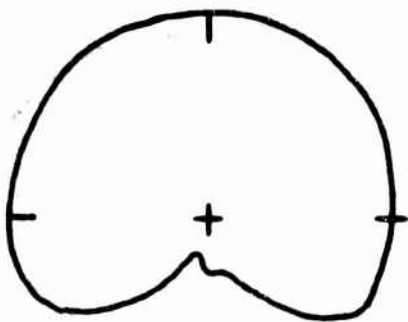
160 KVP, Cu filter
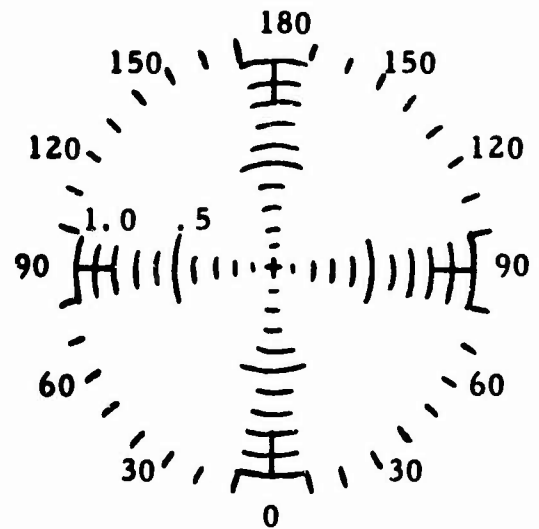
Graticule
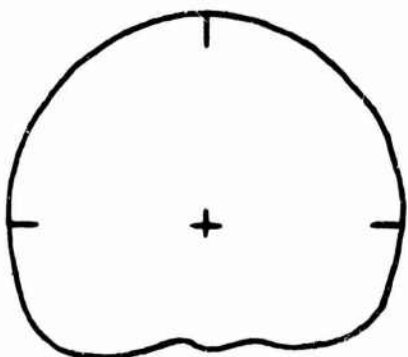
Cobalt-60 gamma rays
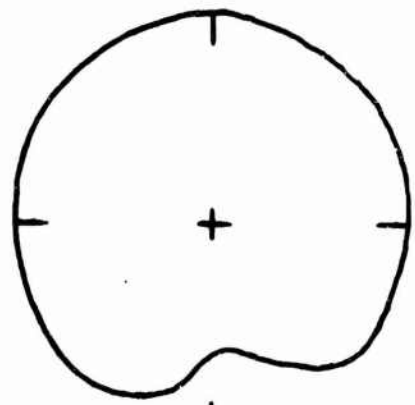
Polar Diagram of Theta Response in Two Planes
for Three Radiation Qualities, Type I Instrument
Figure 58.
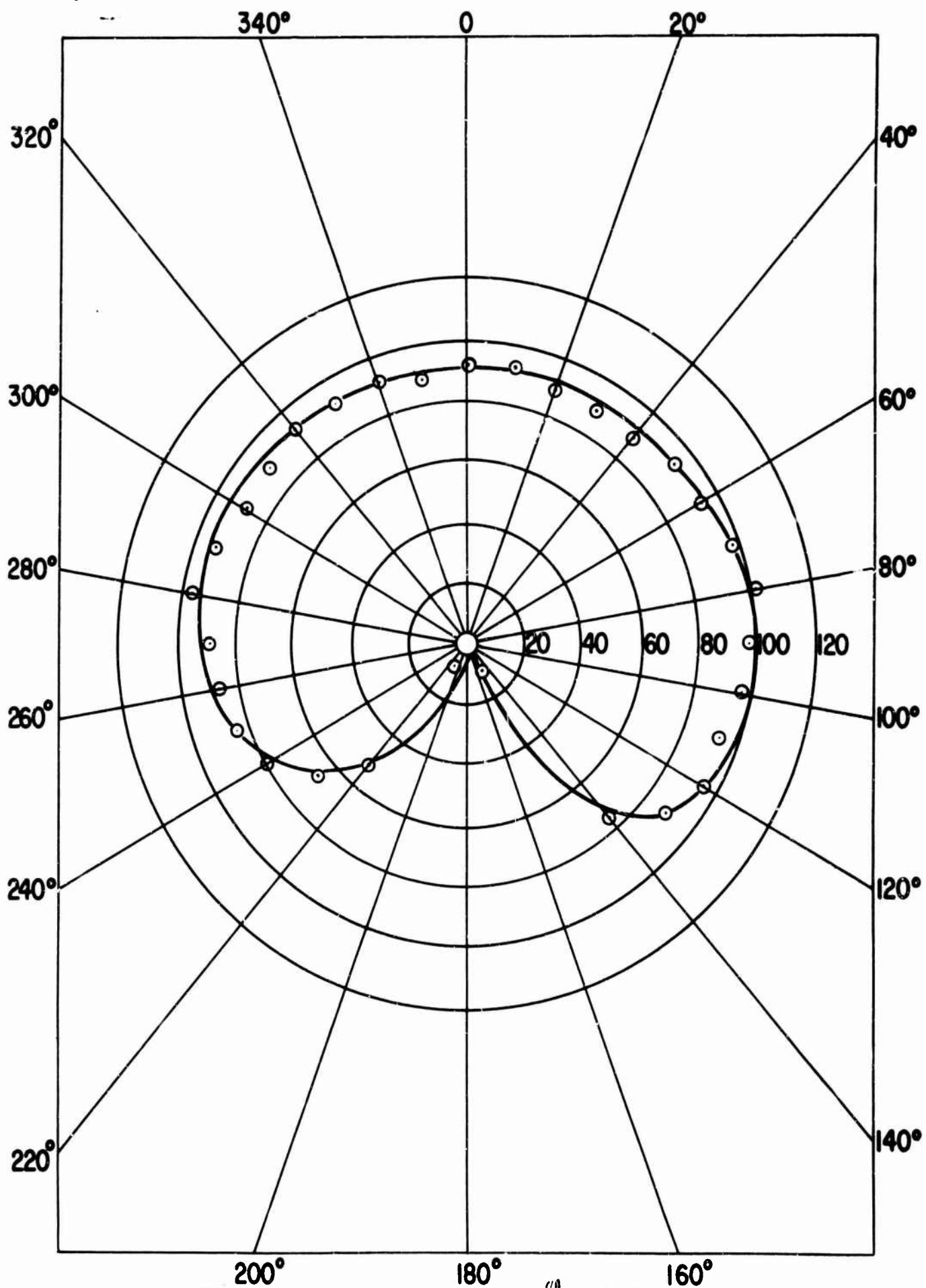
Type V Dosimeter Directional Response to 60 Mev Protons
Figure 59.
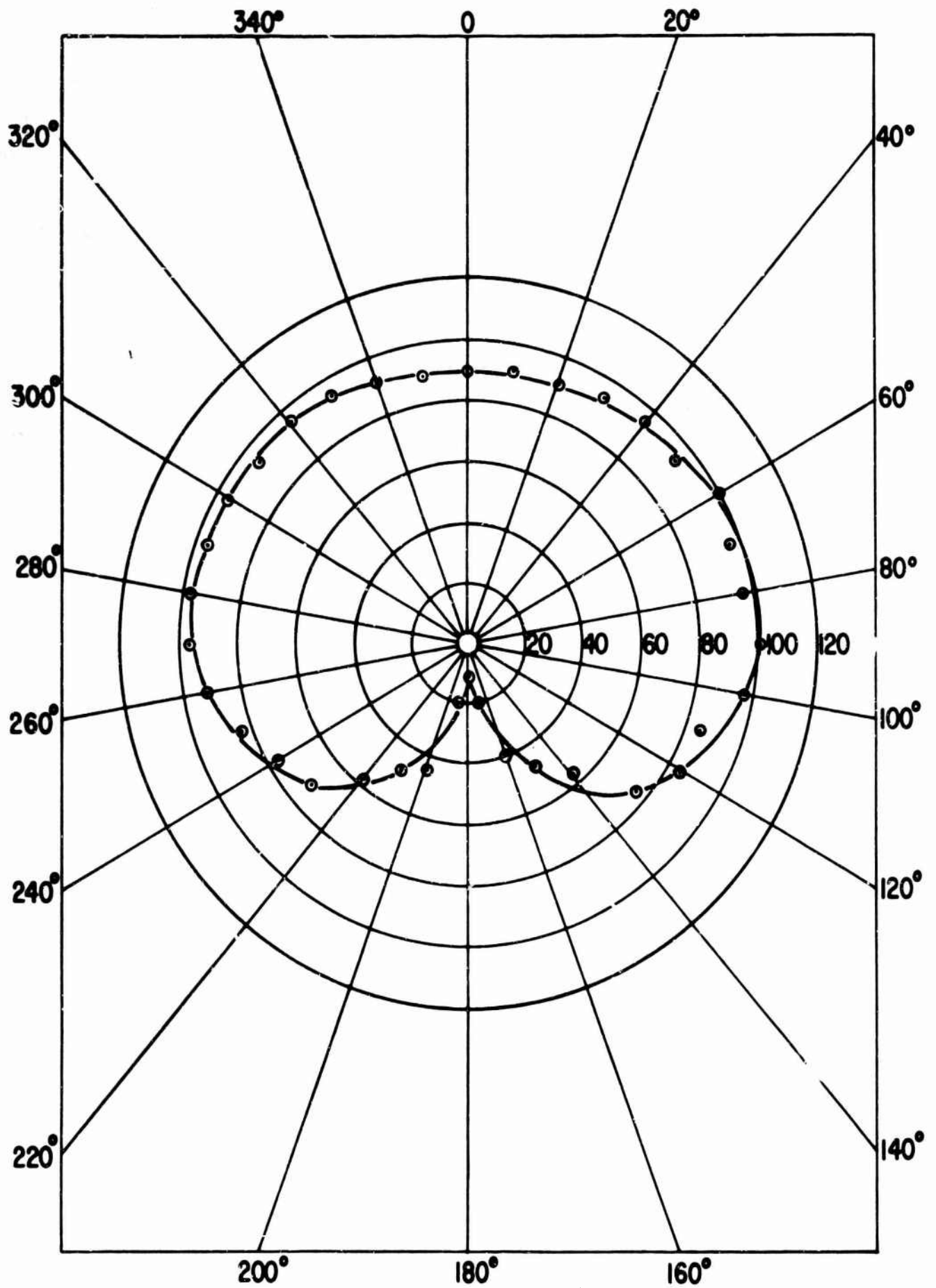
Type I Dosimeter Directional Response to 60 Mev. Protons
Figure 60.

116

IV.B.2.b. Calibration, Pre-Delivery, and Qualification Acceptance Testing.

Calibration of the flight active dosimeters consisted of a three-phased program to determine the radiation input-to-output voltage transfer functions, radiation response time at various radiation levels, and temperature-time effects on the transfer or calibration curves. Initial calibration was accomplished approximately 90 days before launch, using the AVCO Corporation Cobalt 60 gamma radiation facility at Tulsa, Oklahoma. Testing was performed prior to shipment of the Gemini 4 and Gemini 6 instruments to the Air Force Weapons Laboratory (AFWL) where recalibration was accomplished, with both Cobalt 60 and Cesium 137 gamma sources. Subsequently the units were delivered to McDonnell Aircraft for spacecraft integration. Recalibration was accomplished using the Gemini 4 dosimeters at AFWL approximately 20 days after the completion of the Gemini 4 missions. The test and calibration conditions and the results of each test are presented in two separate sections for: (1) calibration and testing at AVCO and (2) calibration and testing by the Air Force.

All gamma sources utilized in this effort were calibrated by the National Bureau of Standards in roentgens of exposure dose. Appendix (F) provides a set of suitable factors for conversion of the exposure dose defined in terms of the charge per unit mass to absorbed dose in energy deposition per unit mass.

(1) Test Conditions

The conditions for test of these instruments were delineated in the terms of the contract. The tests were accomplished in a specified sequence and all data recorded for each instrument tested. The testing sequence was as follows:

117

(a) Calibration and response

(b) Power requirement test

(c) Drift rate test

(d) Vacuum thermal and temperature

(e) Accuracy

(f) Sensitivity

The test equipment used was of good commercial quality, and all test equipment bore current calibration stamps.

The ion chamber instruments were calibrated using a 12 mc source of Co^{60}, and a range table approximately five feet long. Low level measurements were taken using an attenuator placed in front of the source. Measurements of response times were made with a strip chart recorder connected to the output of the TEIC instrument and the door to the source holder opened rapidly to produce a step function in radiation level. The response time is defined as 10 percent of the output change in voltage.

Power was measured at both extremes of the voltage range, 20 volts and 28 volts, at ambient temperature and under ambient radiation conditions. The Instrument outputs were periodically monitored for a drift rate test of 100 hours, including the time of succeeding vacuum thermal and temperature testing. The coarse and fine output voltage was recorded at the beginning of the test and again at the end.

Vacuum thermal testing was conducted by placing the instrument in a bell jar which in turn was placed in an environmental chamber adjusted to the required temperature. Temperature testing and Type I temperature sensor calibration was conducted in an environmental chamber at the specified temperatures with four hours of soak time at each temperature.

118

A functional check was performed on each instrument at the completion of the testing and before shipment of the instrument to McDonnell Aircraft.

The above tests were performed on all Gemini flight units.

Temperature limits were 160°F and 0°F and pressure was 3 mm Hg absolute.

(2) Calibration Curves.

The calibration curves for the four Gemini flight instruments, Type I SN-5 and SN-6, and the Type V SN-5 and SN-7, are shown in the following pages (Figures 61 through 64). The instruments were adjustable to different dose rates for the maximum 5.0 volts telemetry output. The characteristic shapes of the curves were all very nearly the same, the gain varying from 1.05 volt/decade to 1.3 volt/decade.

(3) Temperature Data.

The test data for the temperature run of the Gemini instruments are shown in Table IX. Each Type I Gemini instrument has a temperature sensor output voltage proportional to the internal temperature of the package. The output voltage from the temperature sensors was recorded for the Type I units at four points of temperature and ambient temperature after allowing the instrument to stabilize for four hours at each of four temperatures. A typical calibration curve of a temperature sensor is shown in Figure 65.

(4) Response Time Measurements.

A table of response time measurements of the Gemini instruments is shown in Table X. The measurements are taken from the 10 percent maximum to 90 percent equilibrium of the curve (Ref. 9). A drawing of a typical response time recording made on a Type V unit is shown in Figure 66.

119

TABLE IX

TEMPERATURE TEST DATA

(Unless noted, all readings positive and are in volts)

	-18°C	0°C	25°C	50°C	70°C
Type I S/N 5					
Coarse	0.0	0.02	0.10	-0.08	-0.02
Fine	0.0	0.10	0.35	-0.04	-0.02
Temp. Sensor	1.6	2.04	2.98	3.80	4.35
Type I S/N 7					
Coarse	0.15	0.20	0.35	0.55	0.60
Fine	0.70	1.00	1.60	2.25	2.50
Temp. Sensor	1.52	1.94	2.78	3.50	4.05
Type I S/N 6					
Coarse	0.02	0.09	0.18	0.27	0.31
Fine	0.09	0.40	0.80	1.35	1.47
Temp. Sensor	1.00	1.42	2.03	2.64	3.24
Type V S/N 5					
Coarse	0.20	0.25	0.32	0.37	0.40
Fine	0.95	1.20	1.70	1.80	2.00
Type V S/N 6					
Coarse	0.08	0.22	0.20	0.25	0.40
Fine	0.40	0.95	1.15	1.35	2.10
Type V S/N 7					
Coarse	0.15	0.25	0.10	0.20	0.40
Fine	0.75	1.25	0.35	1.10	2.00

TABLE X

RESPONSE TIME MEASUREMENTS

	100 mrad/hr		10 rad/hr	
	Rise time (sec)	Decay time (sec)	Rise time (sec)	Decay time (sec)
Type V, S/N 5	4.23	21.5	1.5	2.5
Type V, S/N 6	5.6	13.0	3.0	3.75
Type V, S/N 7	3.75	20.5	1.3	2.8
Type I, S/N 5	3.0	5.6	2.0	5.0
Type I, S/N 6	2.75	8.3	1.2	2.75
Type I, S/N 7	5.6	19.0	2.0	4.0

DOSE RATE (RADS/HR.)

VOLTS
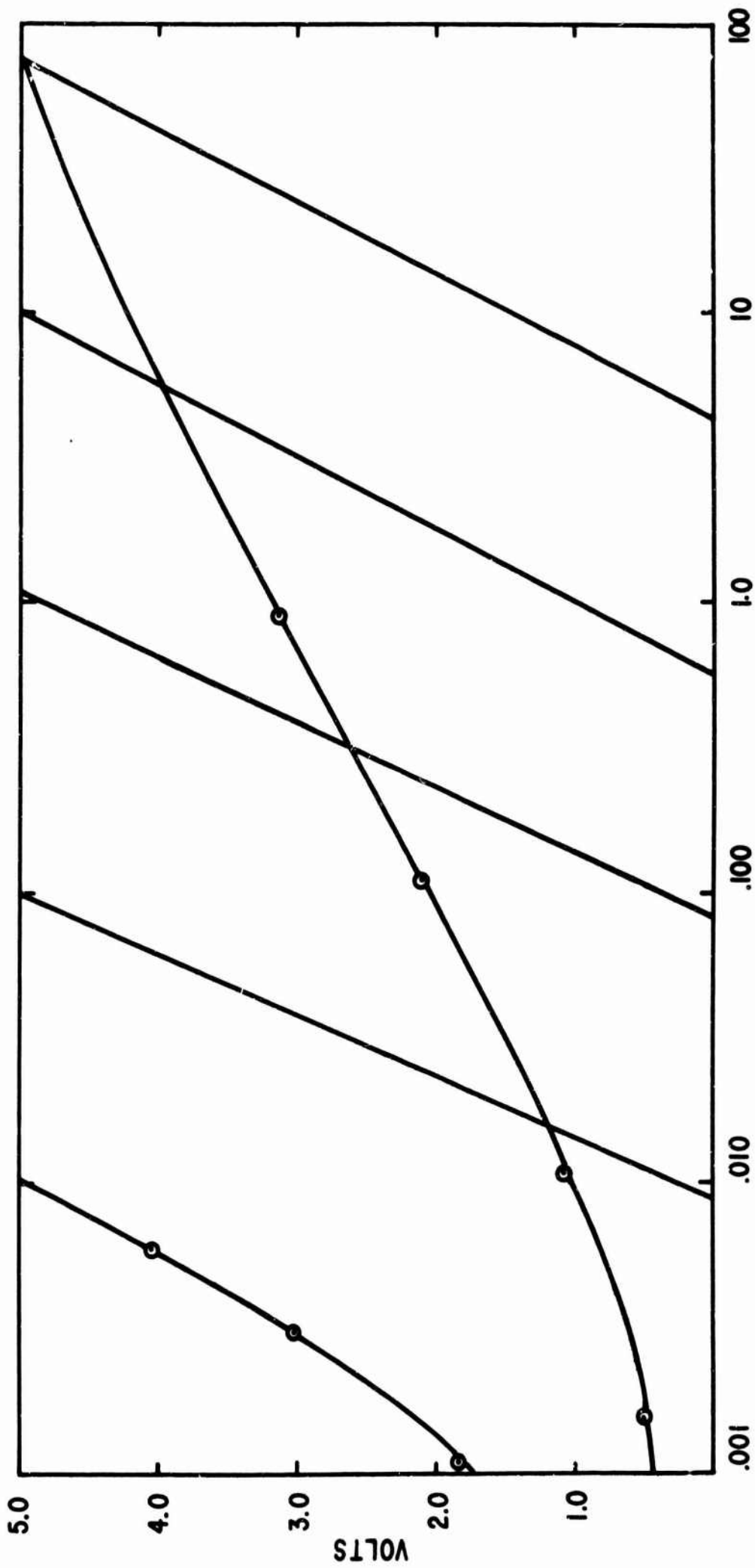
GEMINI TYPE I DOSIMETER
(SN-5)
Co^{60} CALIBRATION
17 FEB 1965

Figure 61

121
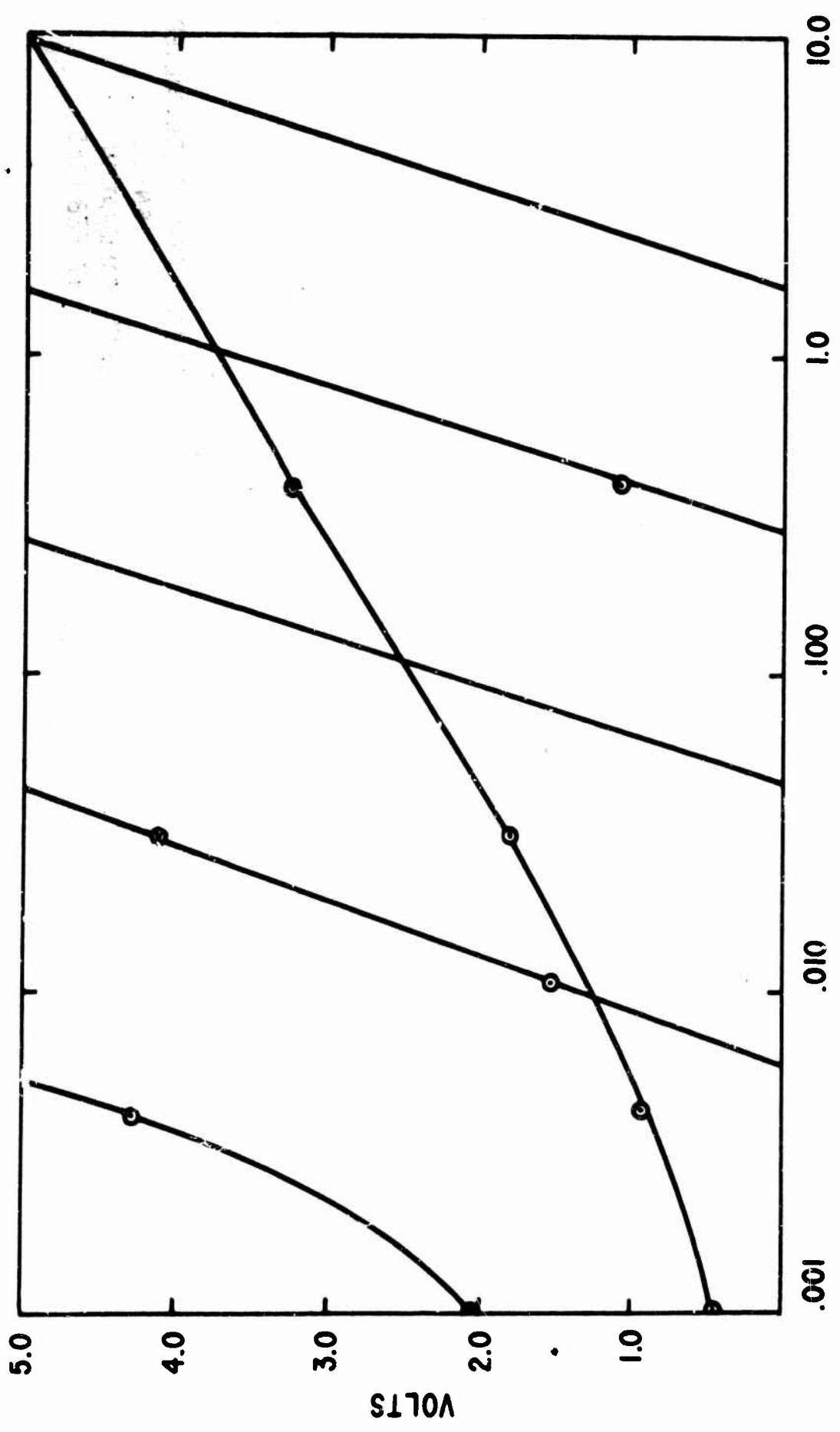
GEMINI TYPE I DOSIMETER
SN-7
Co⁶⁰ CALIBRATION
16 FEBRUARY 1965

Figure 62,

122

GEMINI TYPE 5 DOSIMETER
(SN-5)
CALIBRATION Co^{60}
17 MARCH 1965

DOSE RATE RAD/HR.

VOLTS
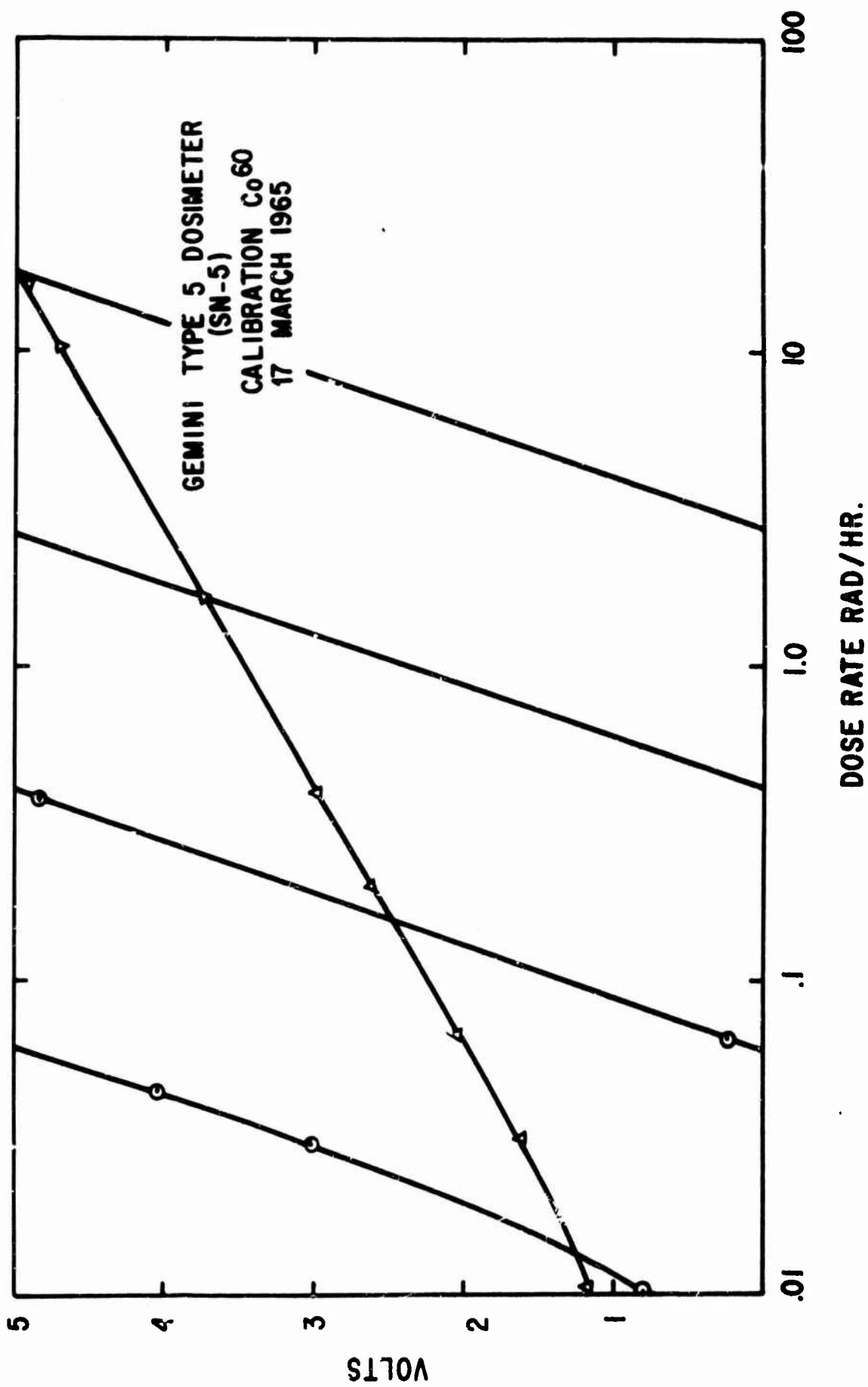
Figure 63.

123
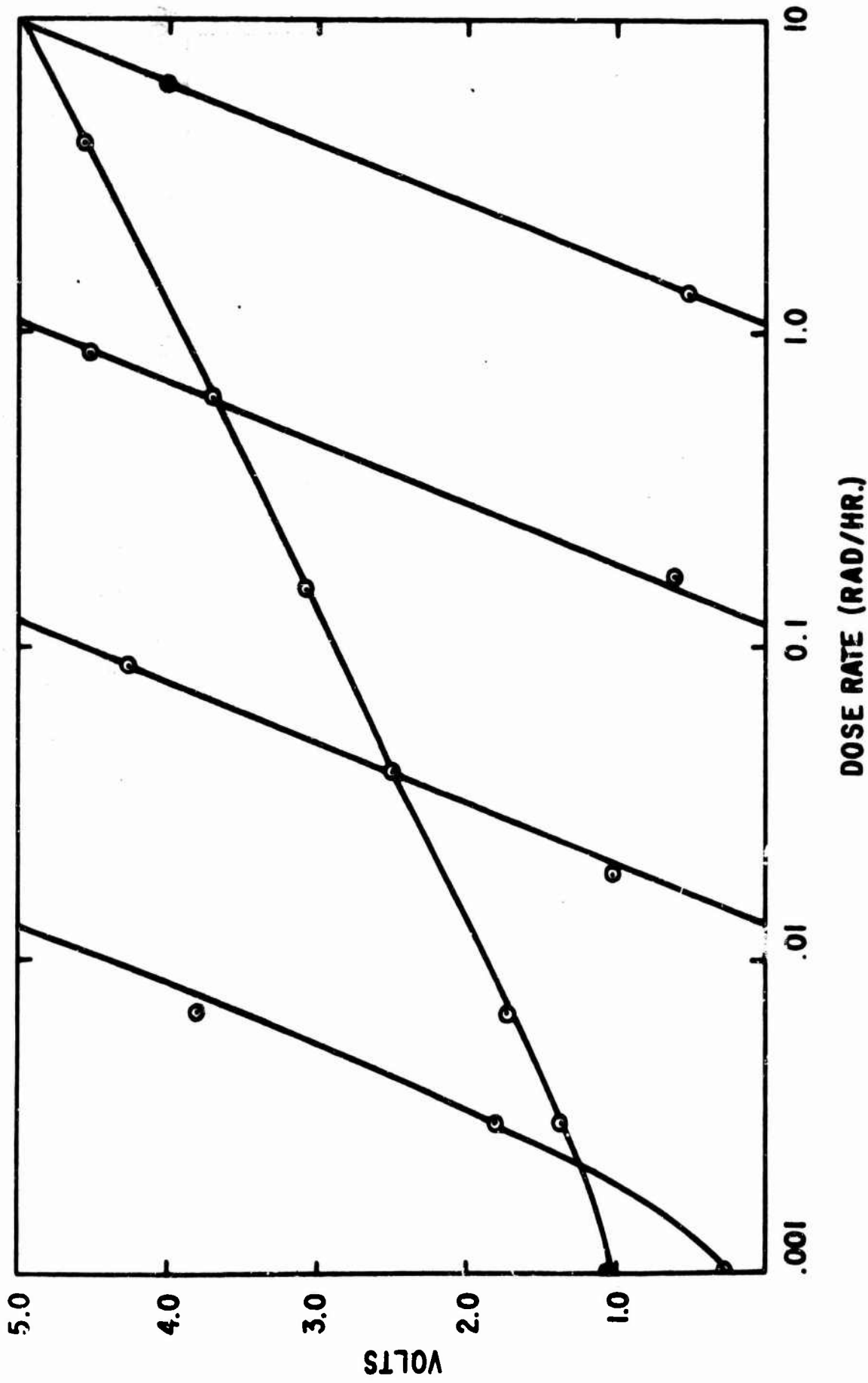
GEMINI TYPE V DOSIMETER
(SN-6)
CALIBRATION Co⁶⁰
18 MAR 1965

Figure 64

124
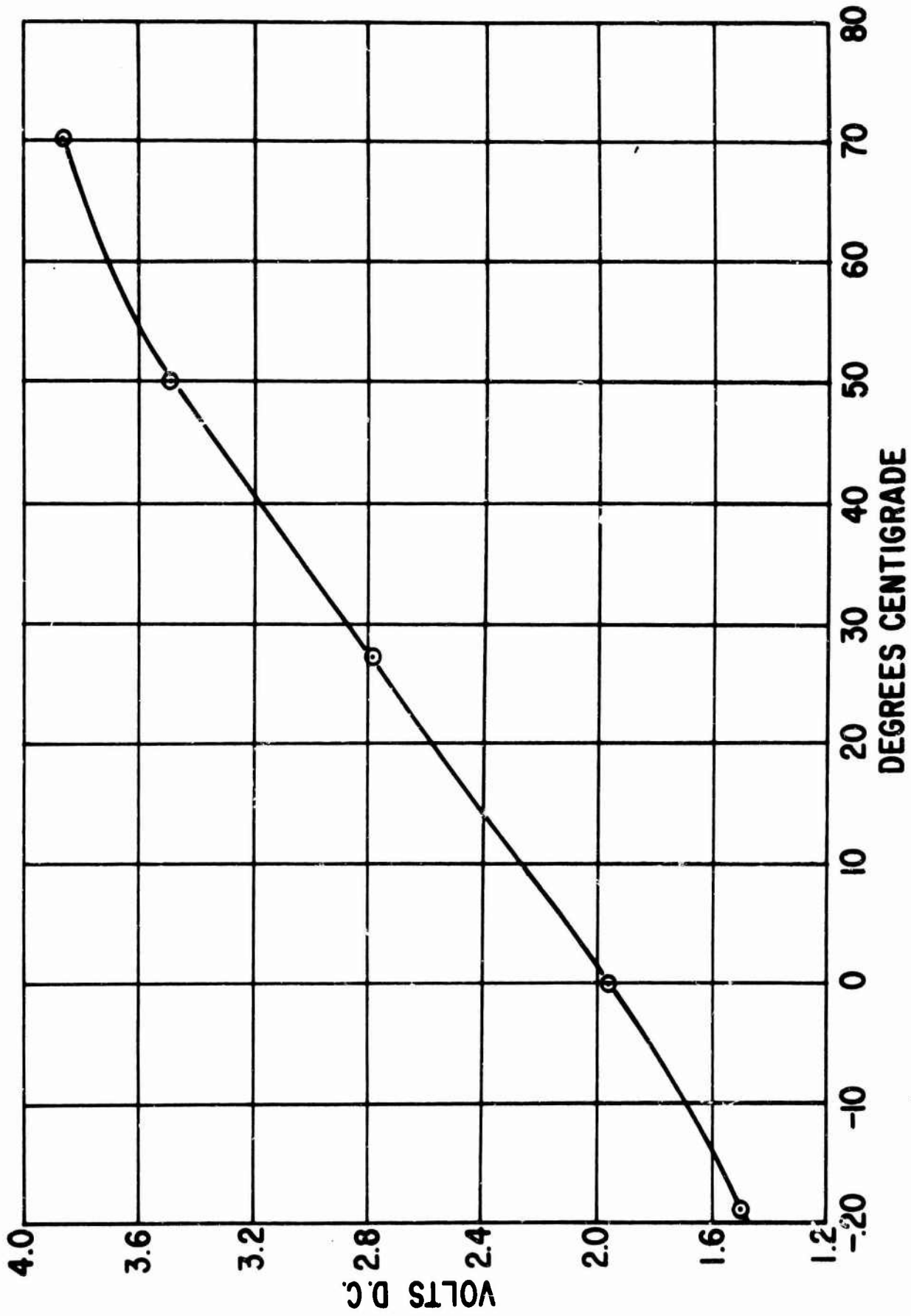
Gemini Temperature Sensor Calibration Curve
Figure 65,

125
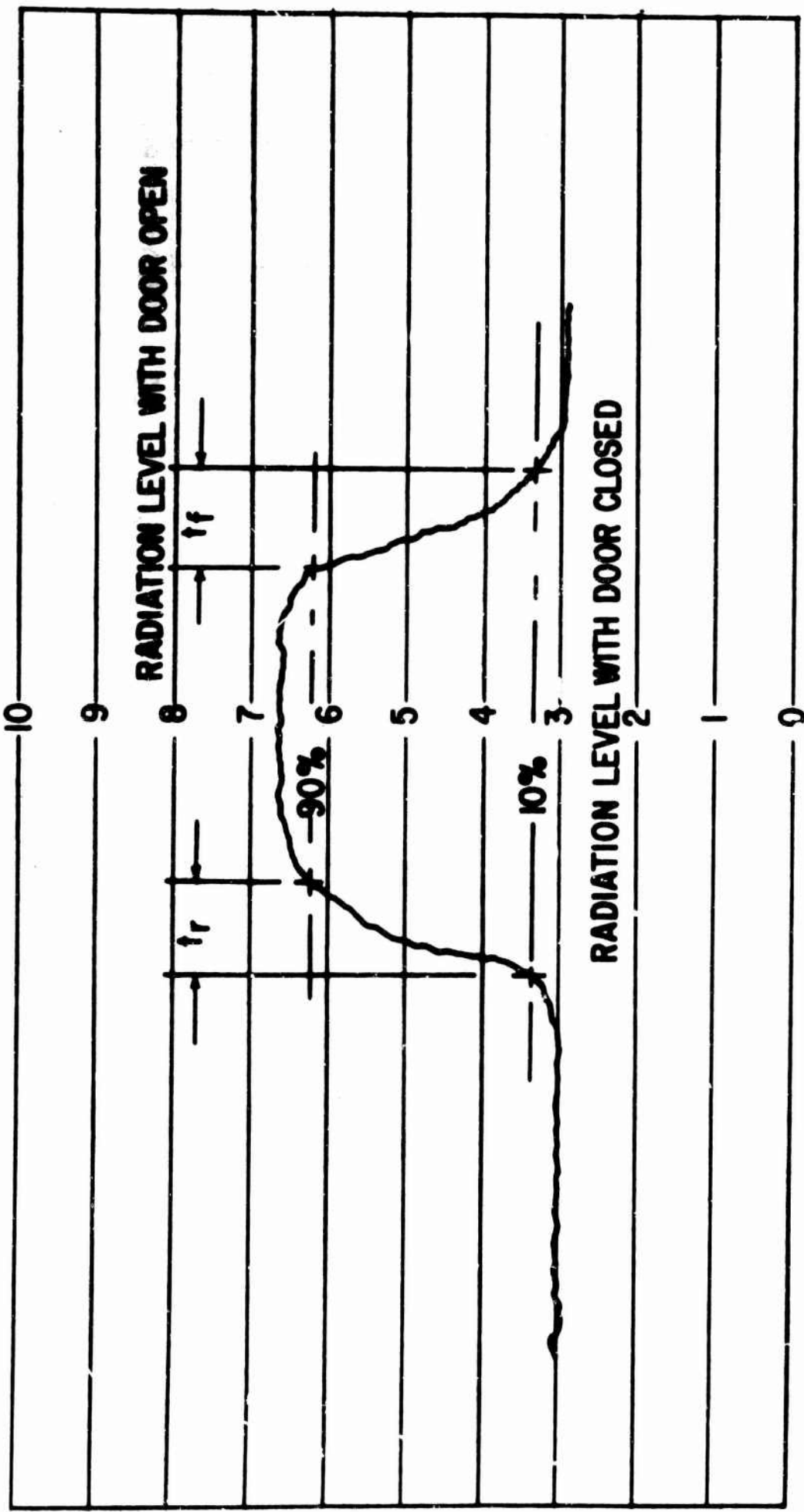
A Typical Response Time Measurement for the Type V Unit

Figure 66.

126

(5) Power Measurements.

Power requirements for each Gemini instrument are shown
in Table XI,

(6) Drift Rate Measurements.

The 100-hour drift rate data for Gemini instrument is
shown in Table XII.

(7) Vacuum Thermal Test.

The results of the vacuum thermal tests are included in
Table XIII,

(8) Automatic Calibration Data.

Automatic calibration of each Type I Gemini unit is
accomplished by introducing a pulsed step change to the ionization chamber
collection potential. A fixed charge is thus introduced into the collecting
grid of the electrometer which establishes a relationship between the transfer
function Q_{in} and E_{out} of the system; and, at the same time, provides a linear
rather than logarithmic measurement of the ambient radiation via observation
of the rate of change of the output signal. Actual strip chart recordings of
these calibrations under different radiation levels are shown in Figure 66, and
graphical representations of time intervals for these instruments for the various
levels of absorbed dose rates are shown in Figures 67 and 68. The time intervals
are obtained by measuring the time for the positive pulse to fall to half maxi-
mum (Figure 66) value and the projection of the negative slope near its maximum
value to the quiescent level. When the sensor is subjected to radiation, the
duration of these pulses becomes less. The durations may then be plotted against
radiation intensities. These points follow a straight line on log-log plot, but
the frequency characteristic of the magnetic amplifier and the pen type recorder
make the curve bend at the higher dose rates. Figure 69 for a Gemini Instrument
Dose rate response indicates the character of the higher dose bending.

TABLE XI

POWER TABULATION IN MILLIWATTS

| | Type I | | | | Type V | |
	S/N 5	S/N 6	S/N 7	S/N 5	S/N 6	S/N 7
20 V	208	223	212	179	202	186
24 V	223	235	230	189	183	194
28 V	236	253	246	201	198	207

TABLE XII

DRIFT RATE DATA

| | Type I | | | | Type V | |
	S/N 5	S/N 6	S/N 7	S/N 5	S/N 6	S/N 7
Ambient						
Coarse	0.20	0.22	0.15	0.29	0.30	0.28
Fine	1.00	1.05	0.15	1.35	1.50	1.40
100 hours						
Coarse	0.26	0.15	0.25	0.25	0.15	0.28
Fine	1.22	0.70	1.30	1.30	0.70	1.40

TABLE XIII

VACUUM THERMAL TEST

| | Type I | | | | Type V | |
	S/N 5	S/N 6	S/N 7	S/N 5	S/N 6	S/N 7
Ambient						
Coarse	0.02	0.27	0.25	0.30	0.34	0.28
Fine	0.05	1.40	0.80	1.55	1.65	1.15
High Temp.						
Coarse	-0.07	0.27	0.60	0.35	0.50	0.34
Fine	-0.06	1.50	3.00	1.55	2.60	1.45
Low Temp.						
Coarse	0.0	0.025	0.15	0.26	0.08	0.15
Fine	0.0	0.130	0.70	1.26	0.40	0.75
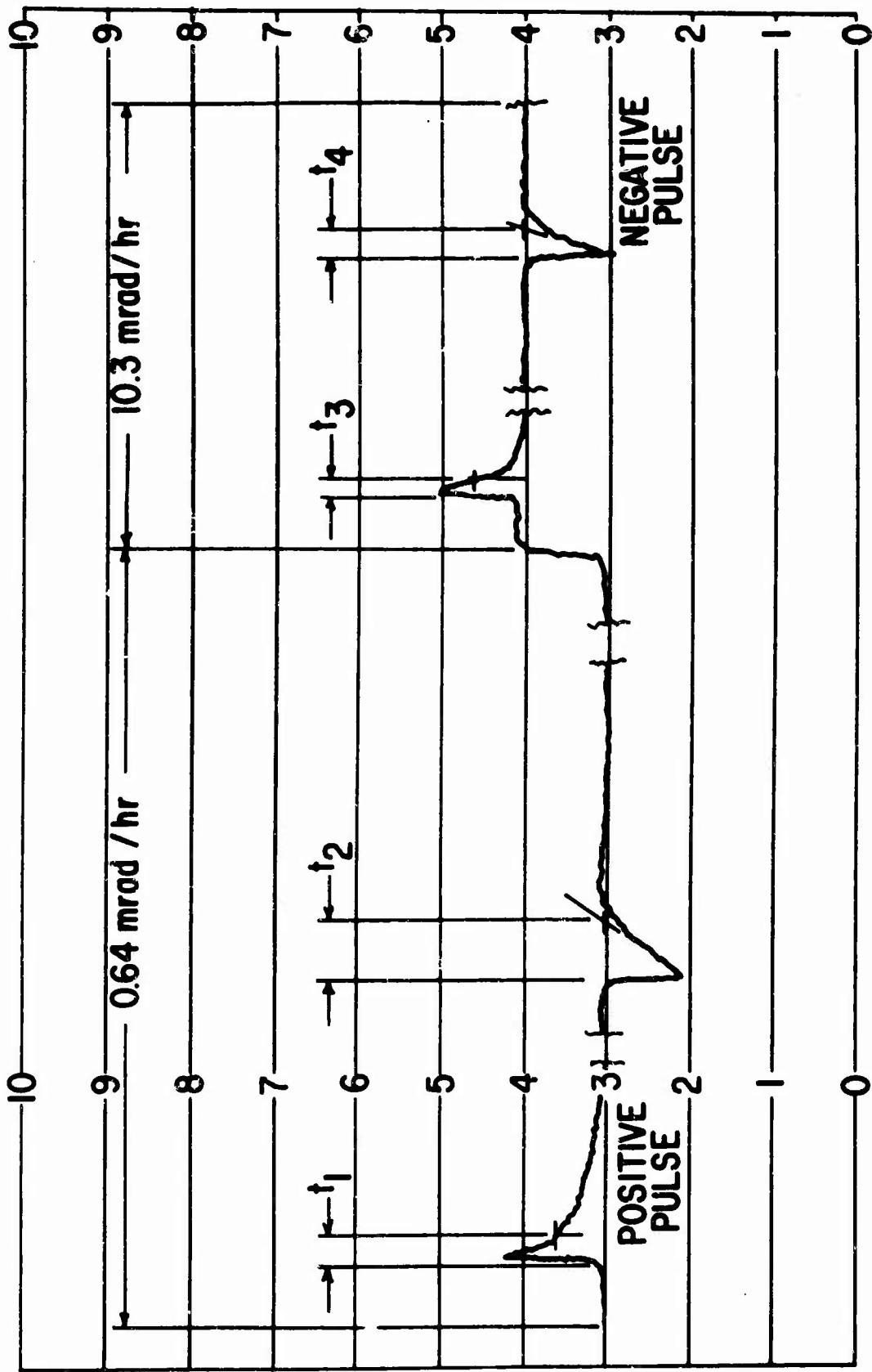
A Typical Automatic Calibration Sequence for the Type I System

Figure 67.

129
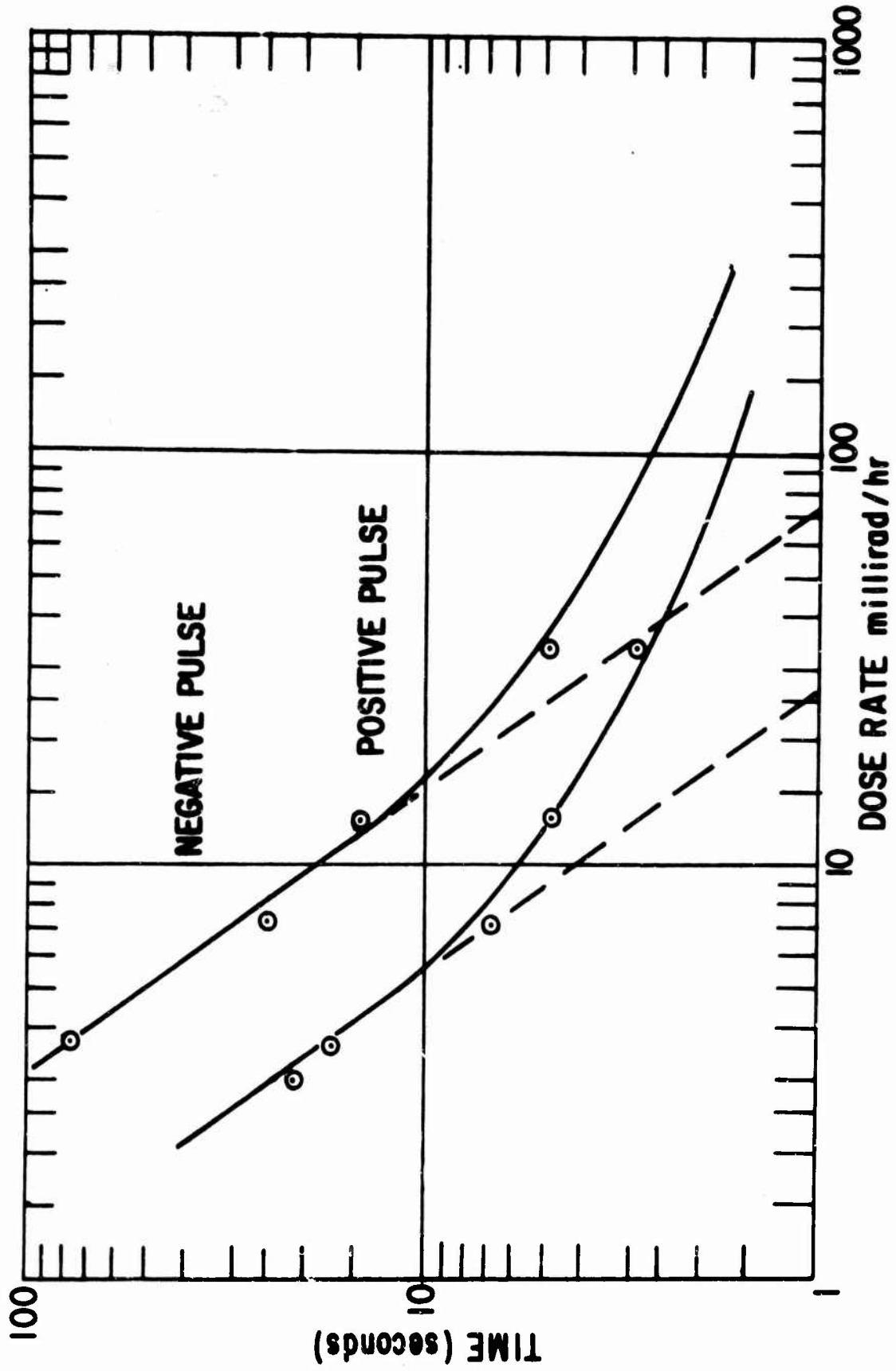
Typical Dose Rate versus Time Curve for the Gemini Instrument

Figure 68.

130
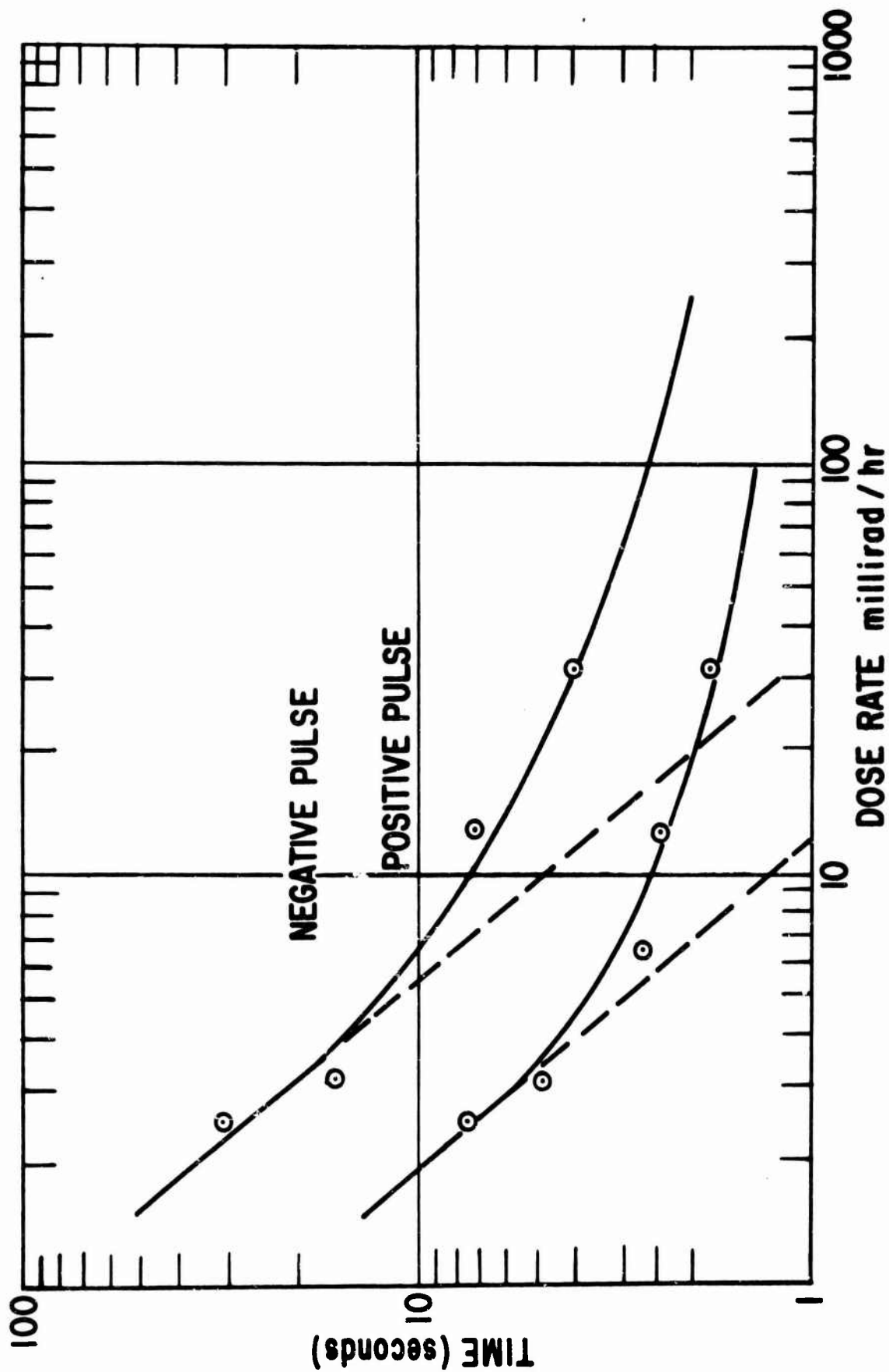
Typical Dose Rate versus Time Curve for the Gemini Instrument
Figure 69.

131

IV.B.2.c. Air Force Calibration and Recalibration of the Active Dosimeters.

Calibration tests were performed on the completed active dosimeters
at AFWL on 20 February 1965 prior to shipment to McDonnell Aircraft in St. Louis.
Cesium 137 was utilized as the standard radiation excitation source for both in-
struments. The calibration curves for the five instruments are illustrated in
Figures 70 through 74. The fine voltages XB02 and XB18 were monitored only
in the first decade because this decade was used exclusively in data analysis
below 1.0 volt. The active dosimeters flown on Gemini 4, both ser. no. 5, were
recalibrated at AFWL on 1 July 1965 using both Cobalt 60 and Cesium 137 gamma
radiation. Recalibration was performed to insure realization of the highest
accuracy in the voltage to dose conversion. The recalibration data for the Gemini 4
dosimeters is shown in Figures 75 and 76. A slight shift in the Type I calibration
curve was noticed between the February calibration and the July voltage to dose data.
This appears to have resulted from electrometer tube drift which occurred after the
final check at the pad at launch minus seven days. Additional error could have
occurred due to noise in the transmission lines at Cape Kennedy during the time
of final checkout at the pad. A high noise level in the lines on the power sys-
tem could have resulted in a general increase in the ambient voltage readings of
the Type I dosimeter. No changes in the Type V readings occurred between calibra-
tion and recalibration indicating that the problems associated with the other
dosimeter did not appear in it. The Gemini 6 active dosimeter recalibration was
carried out the day after touch down of the spacecraft and no shifts in either
the Type I and Type V Units were observed. These curves were shown in Figures 77
and 78. A Strontium 90 sealed portable beta emitter was used to accomplish PIA
and SST testing and final checkout at Cape Kennedy. The portable radiation
source was encased in a brass tube fitted with a removable cap which allows for

GEMINI TYPE 5 DOSIMETER
(SN-5)
AFWL CALIBRATION-CESIUM 137
22 FEB 1965

DOSE RATE (RAD/HR)

VOLTS

Figure 70.

133

GEMINI TYPE 1 DOSIMETER (SN-5)
AFWL CALIBRATION-CESIUM 137
23 FEB 1965

DOSE RATE (RAD/HR)

VOLTS

Figure 71.

134

GEMINI TYPE 1 DOSIMETER
(SN-6)
AFWL CALIBRATION-CESIUM 137
17 MARCH 1965

DOSE RATE (RAD/HR)

VOLTS

Figure 72.

135

GEMINI TYPE 5 DOSIMETER
(SN-6)
AFWL CALIBRATION - CESIUM 137
17 MARCH 1965
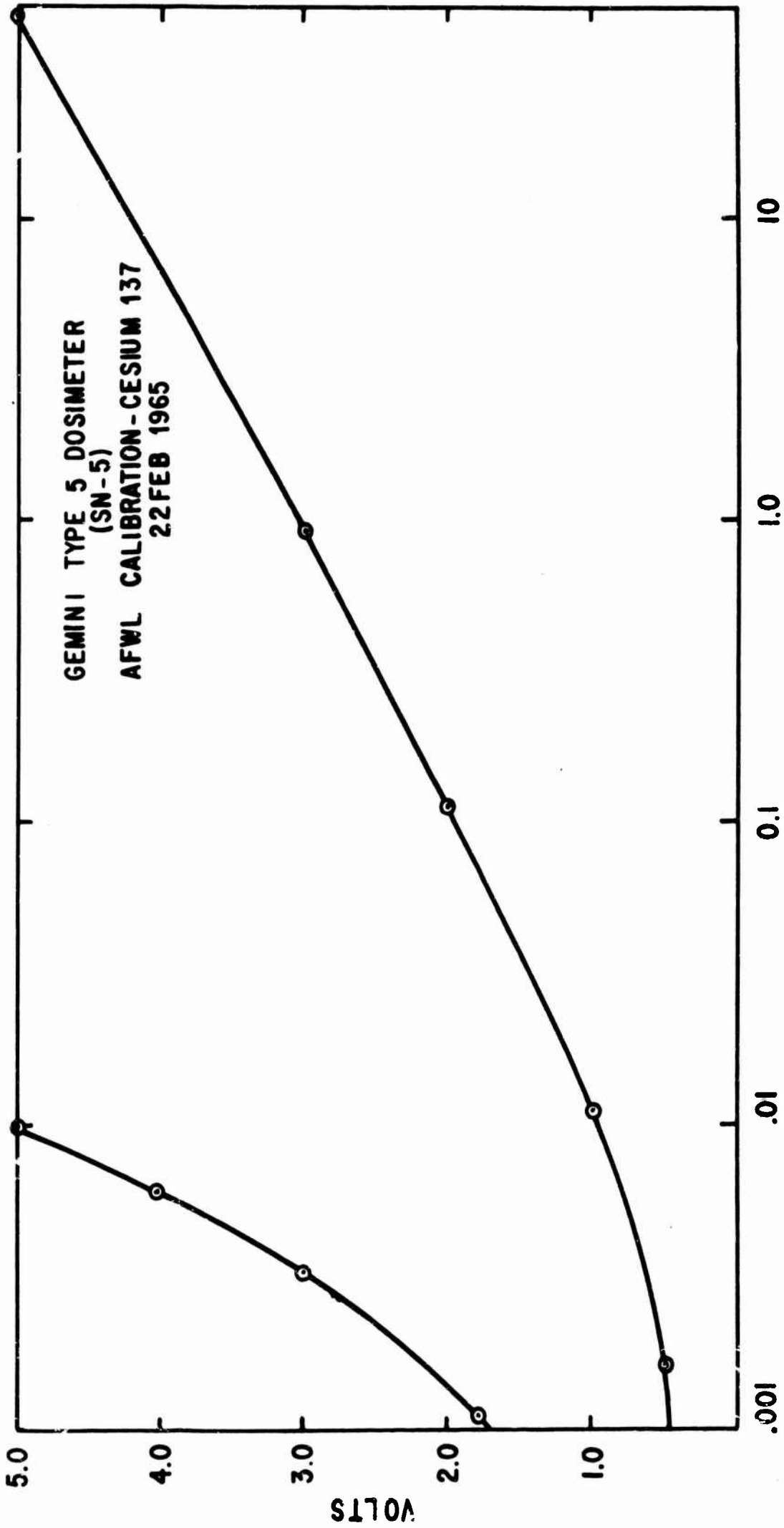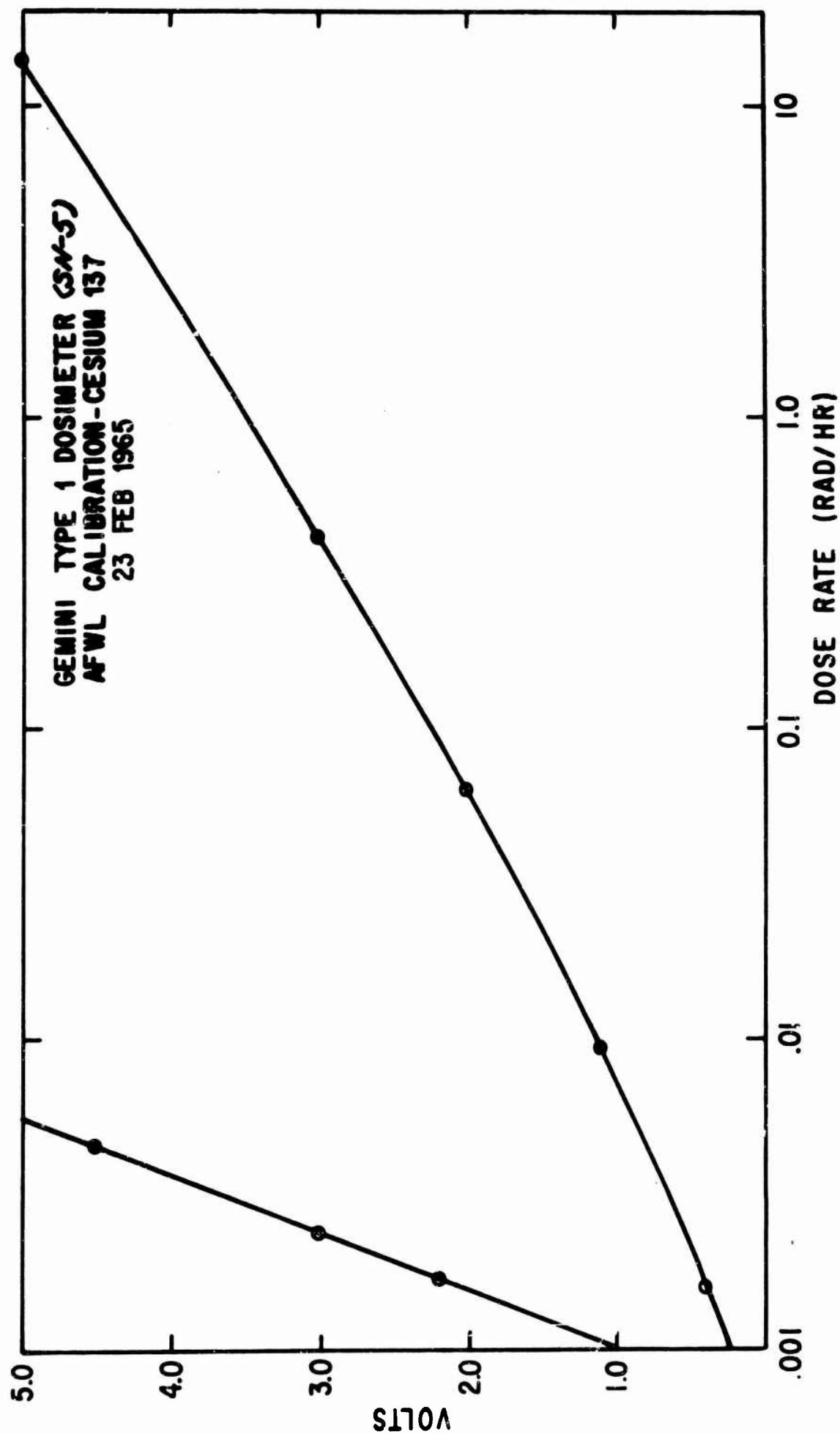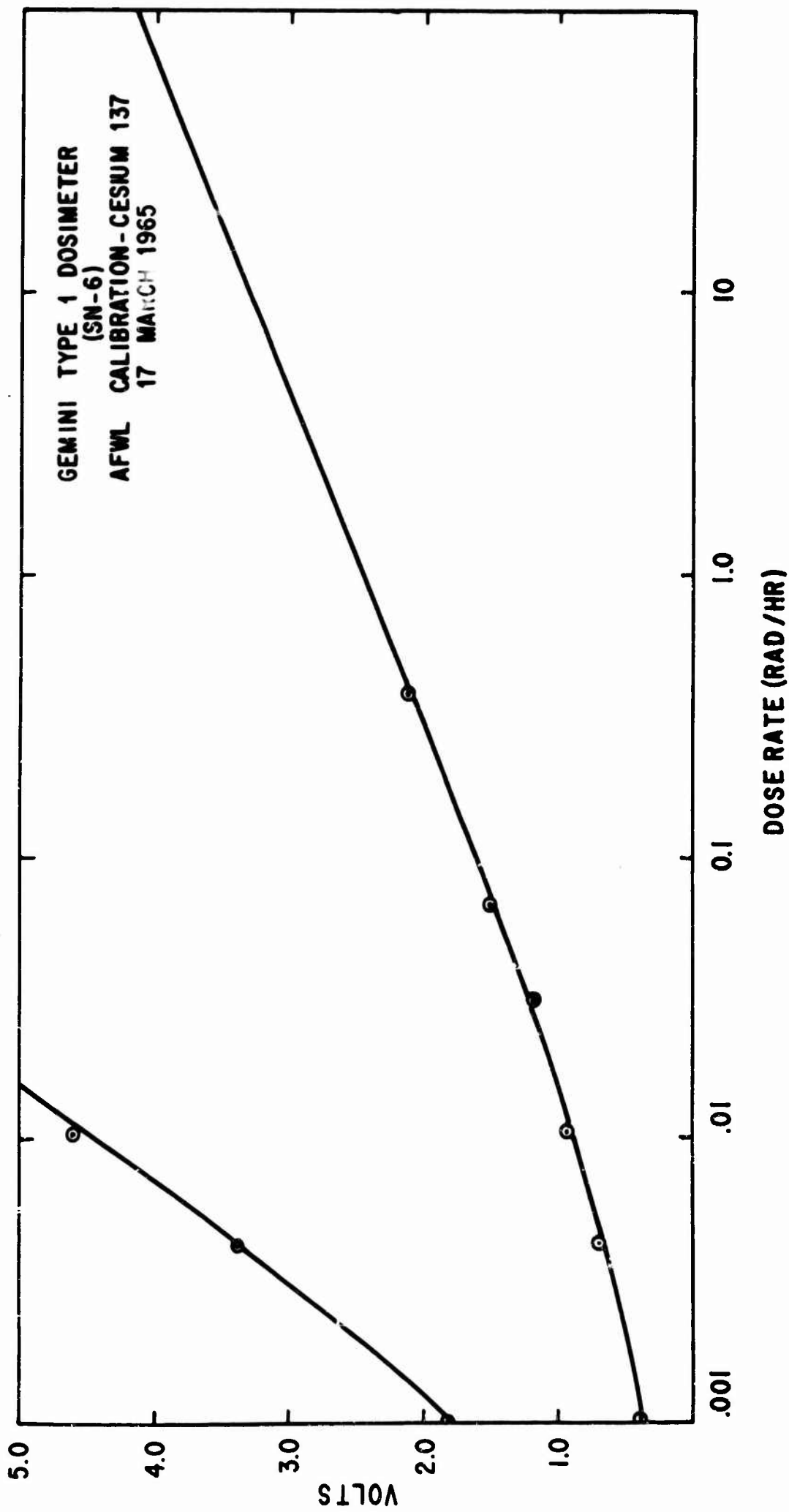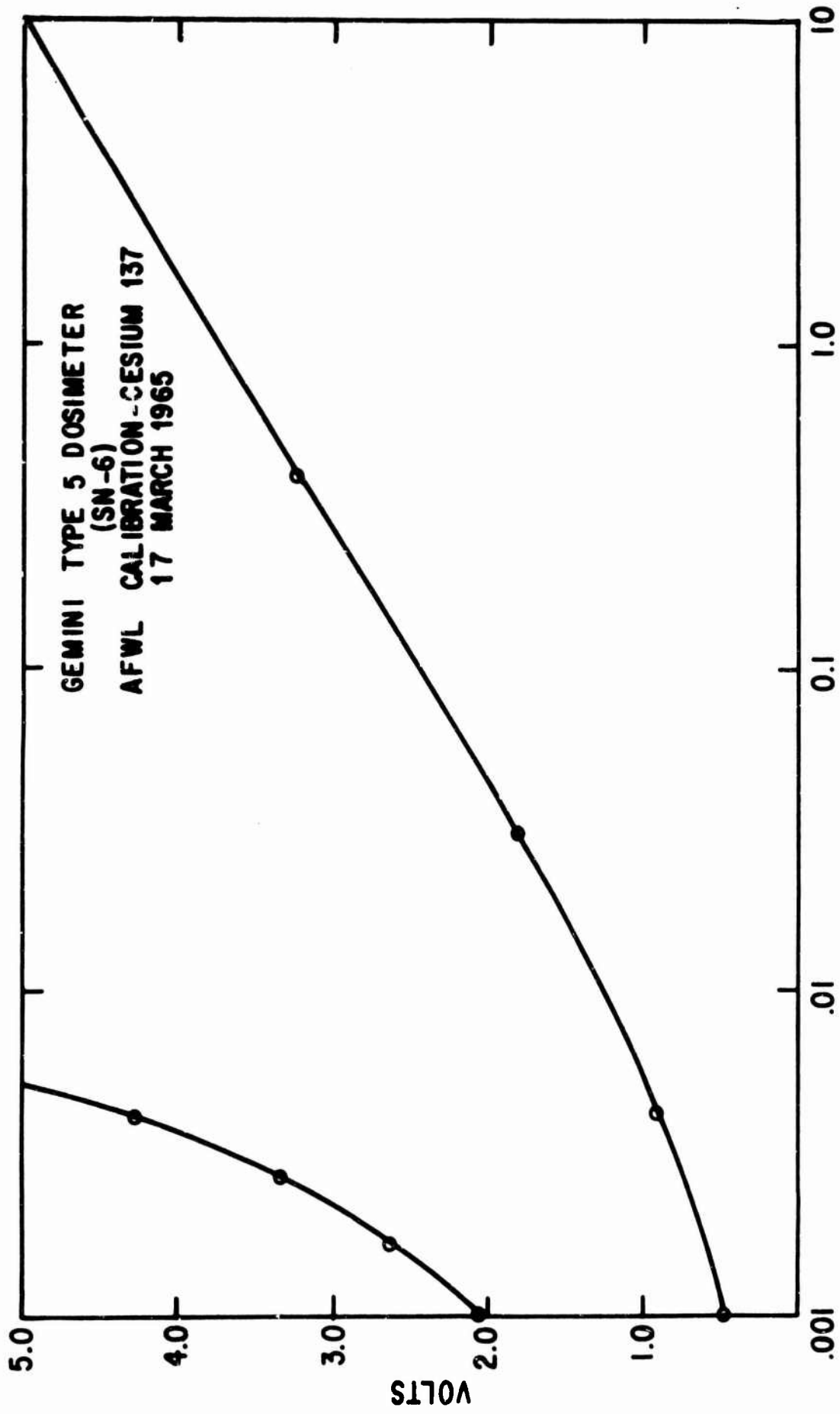
DOSE RATE (RAD/HR)

Figure 73.

136

Figure 74,

137
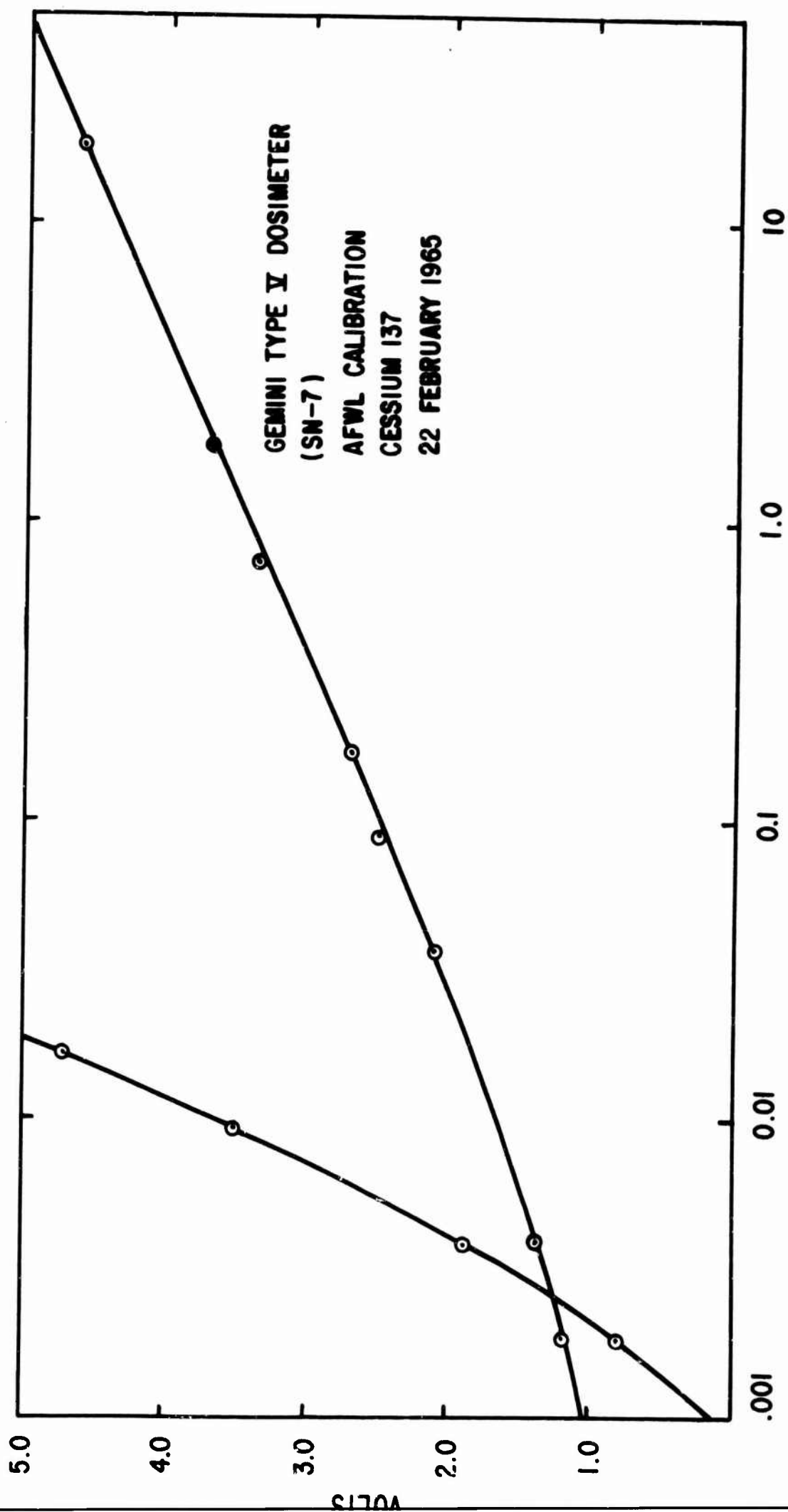
CESIUM 137 ◉
COBALT 60 ▼

GEMINI TYPE 5 DOSIMETER
AFWL RECALIBRATION
1 JULY 1965

DOSE RATE (RAD/HR.)

VOLTS

Figure 75.

138

CESIUM 137 o

COBALT 60 ▽

GEMINI TYPE 1 DOSIMETER
AFWL RECALIBRATION
1 JULY 1965

DOSE RATE (RAD/HR)

Figure 76.

VOLTS

139
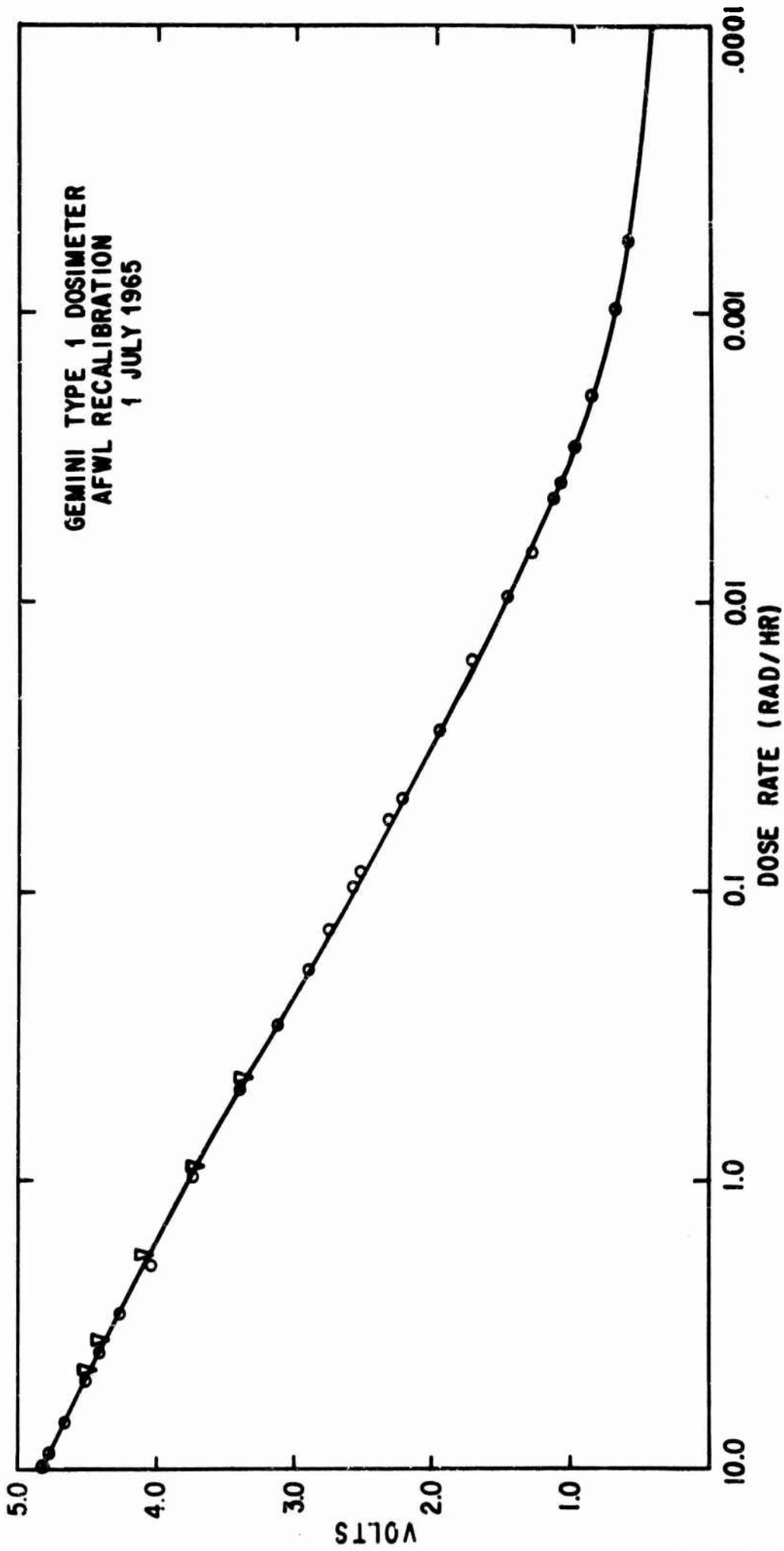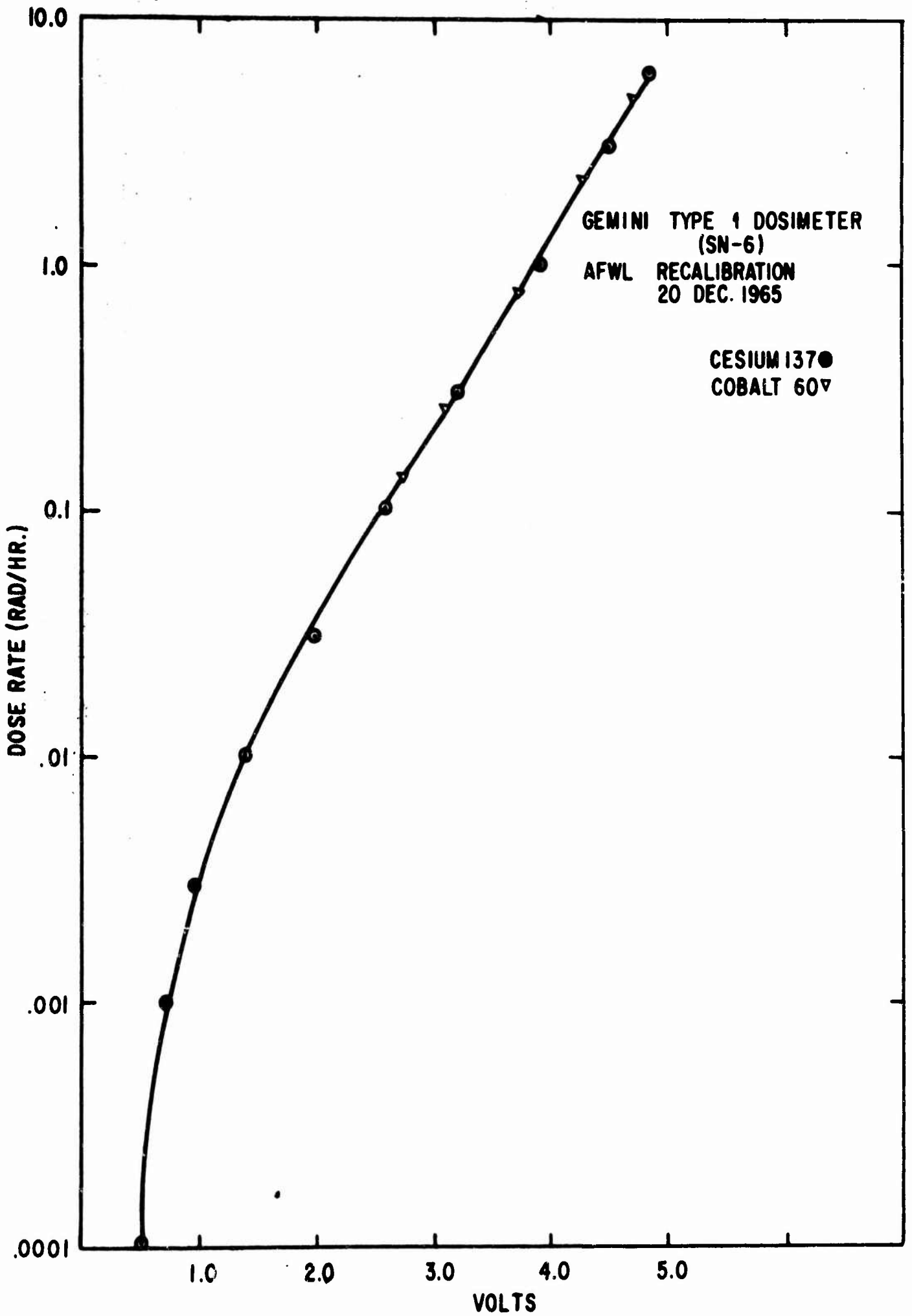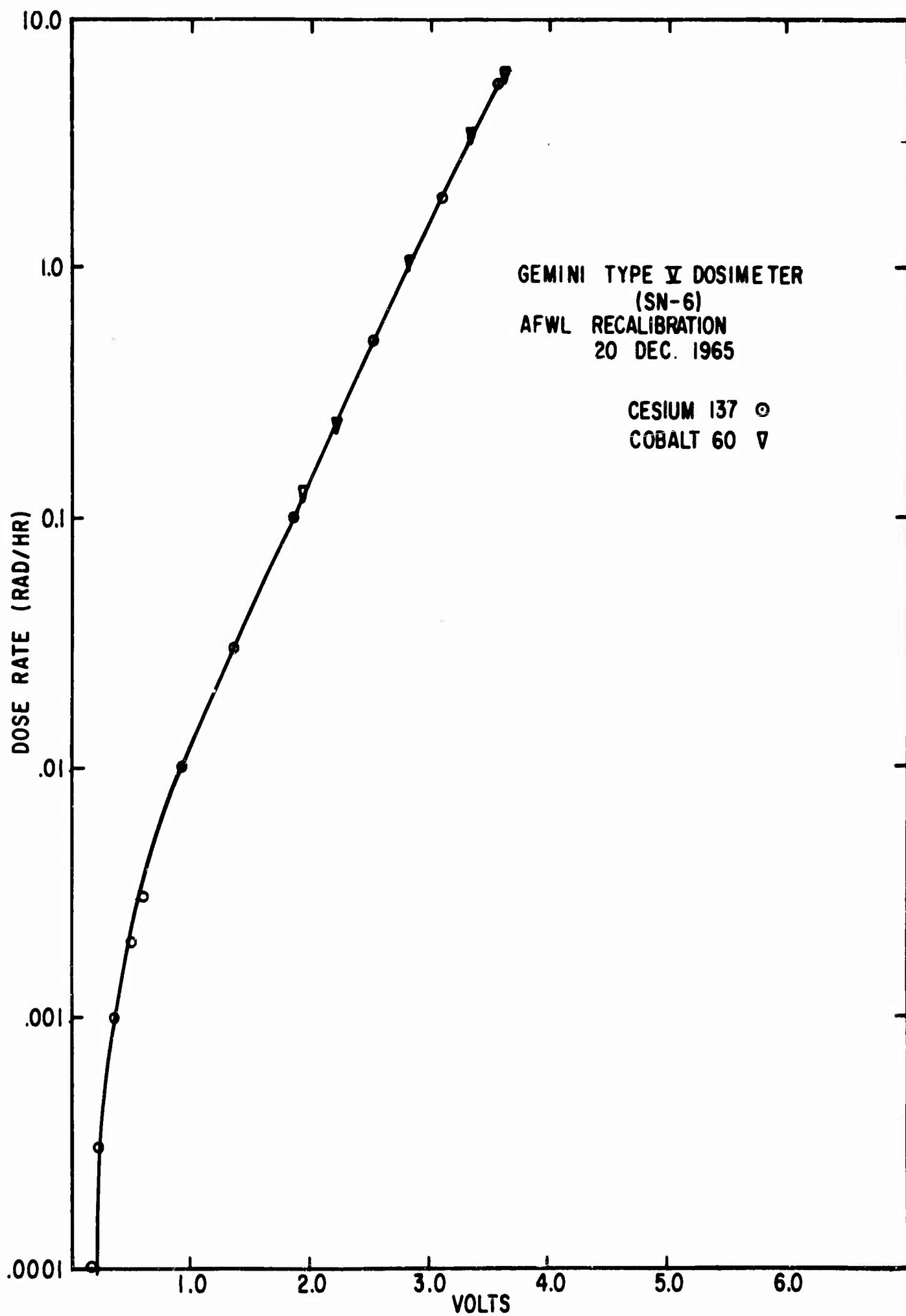
Figure 77.

Figure 78.

the emission of radiation from one end of the brass tube. The other end of the tube is fitted with a plastic source positioning device which allows for placement of the beta source at five locations within the brass tube to provide various radiation field strengths at the active dosimeter sensor heads. The source strength is 0.1 millicuries which allows for convenient shipment of the source on commercial carriers and passenger aircraft. Since the source is a beta emitter the radiation from it is absorbed in a few yards of air. As it is directional it may be safely utilized to perform calibration in areas where other activities are being carried out. This feature was designed into the source to remove limitations imposed by the crowded working areas of the Gemini spacecraft. During calibration at the launch pad, the health and safety officer monitored the radiation levels produced by this source at various locations both in the White Room and the spacecraft, and found them to be negligible.

IV.B.2.d. Spacecraft Qualification Testing:

Qualification testing was performed on the active dosimeters utilizing Spacecraft 6 SST instruments. Testing was accomplished using the facilities of the Test Directorate, Air Force Special Weapons Center, Kirtland Air Force Base, New Mexico, and the Systems Engineering Section at Wright-Patterson Air Force Base, Ohio. All tests were performed in accordance with the applicable portions of McDonnell reports A-531 and 8433. Testing was initiated on 12 August 1964 and completed on 28 October 1964.

The following series of tests was completed on the active dosimeters:

(1) High Temperature

(2) Low Temperature

(3) Pressure

(4) Temperature Pressure

(5) Relative Humidity

(6) Oxygen Atmosphere

(7) Shock

(8) Acceleration

(9) Acoustic Noise

(10) Radio Interference

(11) Vibration

The following environmental tests were not performed for the reasons stated:

Salt sea atmosphere environmental tests outlined in Mil-E-5252C, Procedure I and Procedure II: These tests were omitted because the active units are completely hermetically sealed. Therefore, they would not be affected by the atmospheric conditions existing at the Cape prior to launch. Since all useful data was already to be collected by the active ionization chambers prior to landing, the post landing requirements concerning salt sea atmosphere could also be waived without consequence.

Sand and dust environmental tests outlined in Mil-E-5272C, Procedure I: This phase of environmental testing was eliminated because the hermetic seal of the active units precludes the possibility of any effects from a sand or dust environment.

Fungus tests delineated in Mil-E-5272C, Procedure I: This test was not performed because the active equipment including connectors consists entirely of materials which are non-nutrients to the fungi listed in paragraph 4.8.1.1 of Mil-E-5272C.

Since the Type I and Type V ionization chambers are identical except for the physical size of the sensor heads, not every environmental test was performed on both units. However, the unit which was considered more susceptible to failure

in each test was subjected to that test, on the assumption that the stronger of the two units would automatically qualify for a given test if its weaker counterpart qualified. All units qualified successfully in accordance with the appropriate specifications of McDonnell Reports A-531 and 8433.

IV.B.2.e.. Qualification Test Results for the Passive Dosimetry Units:

The passive dosimetry units were subjected to thorough environmental testing to guarantee that the integrity of each unit would be maintained before, during, and after the Gemini flights. The guidelines for these tests were taken from the appropriate sections and tables of McDonnell Report 8433. All tests, with the exception of the acoustic noise test, were performed using the facilities of the Test Directorate, Air Force Special Weapons Center, Kirtland AFB, New Mexico. The instruments tested were identical to those which were actually placed aboard Gemini. The following environmental tests were performed on the passive dosimetry units:

(1) High Temperature

(2) Low Temperature

(3) Pressure

(4) Temperature Pressure

(5) Relative Humidity

(6) Oxygen Atmosphere

(7) Rain

(8) Salt Spray

(9) Shock

(10) Acceleration

(11) Acoustic Noise

(12) Sea Water Immersion

(13) Vibration

The following two environmental tests were not performed for the reasons stated:

Sand and dust environmental tests were eliminated because the hermetic seal of each passive unit eliminates the possibility of any adverse effects from a sand or dust environment.

Fungus tests were not performed because the materials from which the passive units are constructed are non-nutrients to the fungi listed in paragraph 4.8.1.1 of Mil-E-5272C.

Since the five passive dosimetry units are identical in all respects, it was not considered necessary to place all five units in each specified test environment. The units tested were identical in all respects to those which were delivered to McDonnell Aircraft Corp. on 23 November 1964. Since, in many cases, the specifications to be passed by the dosimeter outside the pressurized cabin were more rigorous than the similar requirements for those within the cabin, all dosimeters were tested to the stricter requirements, since each unit qualified in the more severe environment would certainly have passed the less severe testing procedures. All units were thus successfully qualified in an environment which was generally more severe than that called for.

Since the passive units require no power or telemetry, no electrical connections of any kind are required. As a result, this report will contain no output curves, voltage readings, or other data which was associated with the test results of the active units. Thorough visual observations before, during, and after each test were made to insure that no crushing, distortion, opening of seals; or other deleterious effects took place. Tests were also designed to guarantee both the firm mechanical attachment of the lid to the body of the units, and to check the hermetic seal.

IV.B.2.f Pre-Installation Acceptance Tests:

PIA: The pre-installation acceptance test plan was submitted by AVCO Corporation to McDonnell Aircraft Company on 15 June 1965, and assigned SEDR PIA Number 322. This procedure proved unsatisfactory during initial SST-4 instrument testing because of differences in the operating ranges of the various SST and flight instruments programmed for delivery. In order to eliminate this problem SEDR 322 was modified on 23 November 1965 to provide an adequate and flexible means of testing the instruments. Since there were a different set of operating conditions associated with each type of active dosimeter, separate procedures were established within the main SEDR to cover PIA testing of both the Type I and Type V units.

The units were weighed and inspected beforehand to insure that no mechanical flaws in mounting dimensions, finish, or connector condition existed. Each dosimeter was mounted on a suitably grounded table and connected to a specially designed test set designated TEIC Test Set No. 1 Model 52E440073. Both dosimeters were subjected to a chassis grounding test to insure that proper ground existed between the mounting base and the spacecraft. After grounding was established a specially sealed B.ta source, designated 453, was placed in five locations including ambient background to establish voltage readings with which to compare the PDA test results. Each radiation reading was fixed to correspond to points on the anticipated Gemini mission radiation level spectrum. The Type I dosimeter was also monitored to determine the proper operation of the calibrate monitor circuit. This was accomplished by simply monitoring the activating flip-flop voltage from Pin XB-17 and securing an alternate 3.5 or -0.5 volt d.c. reading. Appendix G provides the complete PIA Procedure.

All units successfully passed initial PIA testing with the exception of the first SST units for Spacecraft 4 which failed the test because of leaks in

146

the sensor heads. This has been discussed previously in the design and fabrication section of this report.

There were no explicit PIA procedures for the passive dosimeter since they had no electrical interface with the spacecraft and were as such only visually inspected by McDonnell to insure sealing integrity.

IV.B.3. Quality Assurance and Control:

This Quality Assurance Program was carried out under Air Force Regulation MIL Q 9858A which is incorporated in the NASA Quality Assurance and Control program for the G$_e$mini and Apollo Manned programs.

The Quality Assurance System which was employed on Contract AF29(601)-6346 is presented in Appendix (H). This manual is maintained by the contractor to assure that quality goals and requirements were realized in all phases of the c ontract performance including that of design, development, manufacturing, test, packaging, shipment and maintenance. A breakdown of personnel comprising the organization is presented in addition to the responsibilities associated with the quality program delineated for each.

The Quality Assurance System is implemented by written procedures, operating instructions, and training programs all of which readily lead themselves to the compliance by the contractor personnel and audit by both Contracts Management and Technical Management personnel of the Government.

The Quality Assurance System at the contractor's facility was as required by regulation and was effective in the control of quality on all systems specified in the subject contract with the Government. This program was carried out under three manuals published by the Contractor, AVCO/Tulsa.

Volume I is presented here since it contains the basic outline of the Quality Control Program. Vommues II and III present a complete and detailed list of all technical details associated with the Quality Control effort and may be obtained upon request from the contractor.

The Air Force Quality Control Program for the passive dosimeters that was utilized in the design, fabrications, and testing is outlined in Appendix (I).

IV.B.4.a. Technical and Scientific Contributions Test Development:

The major scientific and technical accomplishments associated with the
D-8 active dosimetry development were:

a. Design of a completely tissue equivalent ionizing cavity for
space use.

b. Successful use of a log triode electrometer tube and magnetic
amplifiers to detect ionizing currents down to 10^{-15} amperes.

c. Design of the self-calibration feature in the Type I Unit.

d. Evaluation of the directional sensitivity in three planes for
widely varying electromagnetic radiation exposure.

The design of the sensor element was the first use of space ruggedized
material tissue equivalent to all known radiation. No previous dose instrumen-
tation on board manned spaceflight were able to respond equally well to all forms
of electromagnetic and charged particle radiation for all energies present in
space. The design of the Type V chamber incorporated for the first time a sensor
element that could be used to survey localized areas of different shielding
within a manned space vehicle during passage through the radiation environment.
The sensor design also provided the first ionization chamber capable of with-
standing over 100 g's of shock while remaining operative. This extremely high
load design was dictated by the hatch location of the dosimeter which required
that the units survive more than 85 g's of force.

By coupling a log triode electrometer with a set of specially designed
magnetic amplifiers which operate on magnetic hysterisis phenomena, stable
operation in both types of ionization chambers was achieved at currents ranging
down to 10^{-15} amperes. This means that doses as low as 0.1 millirad/hour could
be assessed through the use of small portable ionization cavities with dimensions

148

as small as 100 cubic centimeters. Such low doses previously required cavities which were much larger in volume to perform stable measurements. Furthermore, with the magnetic amplifier arrangement of signal conditioning electrons accuracy in reading the telemetered data was increased by a factor of five. This was a result of the fine magnetic amplifier arrangement which allowed for each one volt change in the coarse amplifier to be magnified on a zero to five volt scale. Another extremely important development under this effort was to provide flight qualified hardware of small, rugged, and compact size which could cover seven decades or radiation exposure. Such dosimetry systems will be of great value in the future where space radiation will fluctuate even more than it did on the Gemini mission.

The design of the self-calibration feature in the Type I Unit was another major contribution to scientific and technical design of dosimetry equipment. This feature allowed the monitoring of the ambient conditions within the sensor as well as the electrometer tube amplification characteristics by use of the rate of charge method of radiation detection. Not only did this self-calibration feature allow for system monitoring, but also provided a means of detecting minutely small currents of ionization which were below the threshold of instantaneous detection. This could be accomplished by measuring the time required for each instrument to reach the ninety percent response points.

This effort also marked the first time that extensive research had been carried out on the directional sensitivity of spaceflight instrumentation. In this effort up to 348 directions of irradiation of the Type I instrument were utilized with seven types of radiation (six electromagnetic and one beta emitter). It was shown for the first time that the net efficiency to low energy X-Rays and Gamma rays were greater than 92% for all angles and directions of exposure.

149

IV.B.4.b. MILITARY CONTRIBUTIONS FROM DEVELOPMENT:

While only two active dosimeters were utilized on the Gemini flights, there evolved a system of four tissue-equivalent sensors of different geometric size coupled with the Gemini electronics which extended the range of measurement from .0001 to 40,000 rad/hour. This extended range system has been incorporated as a result of the qualifying work on Gemini Experiment D8 into unmanned Air Force Radiation Research Satellites WL-413 and OV 1-9 programmed to pass deeper into the Van Allen Belts. The four sensors with associated depth dose shielding are illustrated in Figure 79. Another ultra-sensitive cosmic radiation ionization chamber was developed as a result of the Gemini program of radiation experiments. This dosimeter is capable of assessing the cosmic ray from .05 millirad/hour to 10 rad/hour on polar orbiting satellites and is shown in Figure 80. The portable, hand-held, and self-powered manned spacecraft dose rate indicator is shown in Figure 81. This instrument is another variation of the basic Gemini Active Dosimeter Design in that it also uses the same sensor and signal conditioning electronics as the original hardware.

The electronics and sensors for these systems required stability of operation not available before the Gemini experimental radiation effort. From this effort emerged hardware able to meet the most rigorous experimental and environmental specifications ever placed on a dosimetry system.

The development of the D8 dosimetry system has now made it possible for the Air Force to have on-the-shelf hardware which meets all the environmental parameters of any manned or unmanned spacecraft. This hardware can be used to assess the radiation hazard in any situations which could arise on short notice such as assessing an area of space contaminated by nuclear burst particles from high altitude weapon detonations. This capability in both manned and unmanned systems did not exist in the Air Force prior to Experiment D8 which has now provided military readiness in a critical area of endeavor.

Unmanned Air Force Dosimetry System and Depth Dose Shields
Figure 79
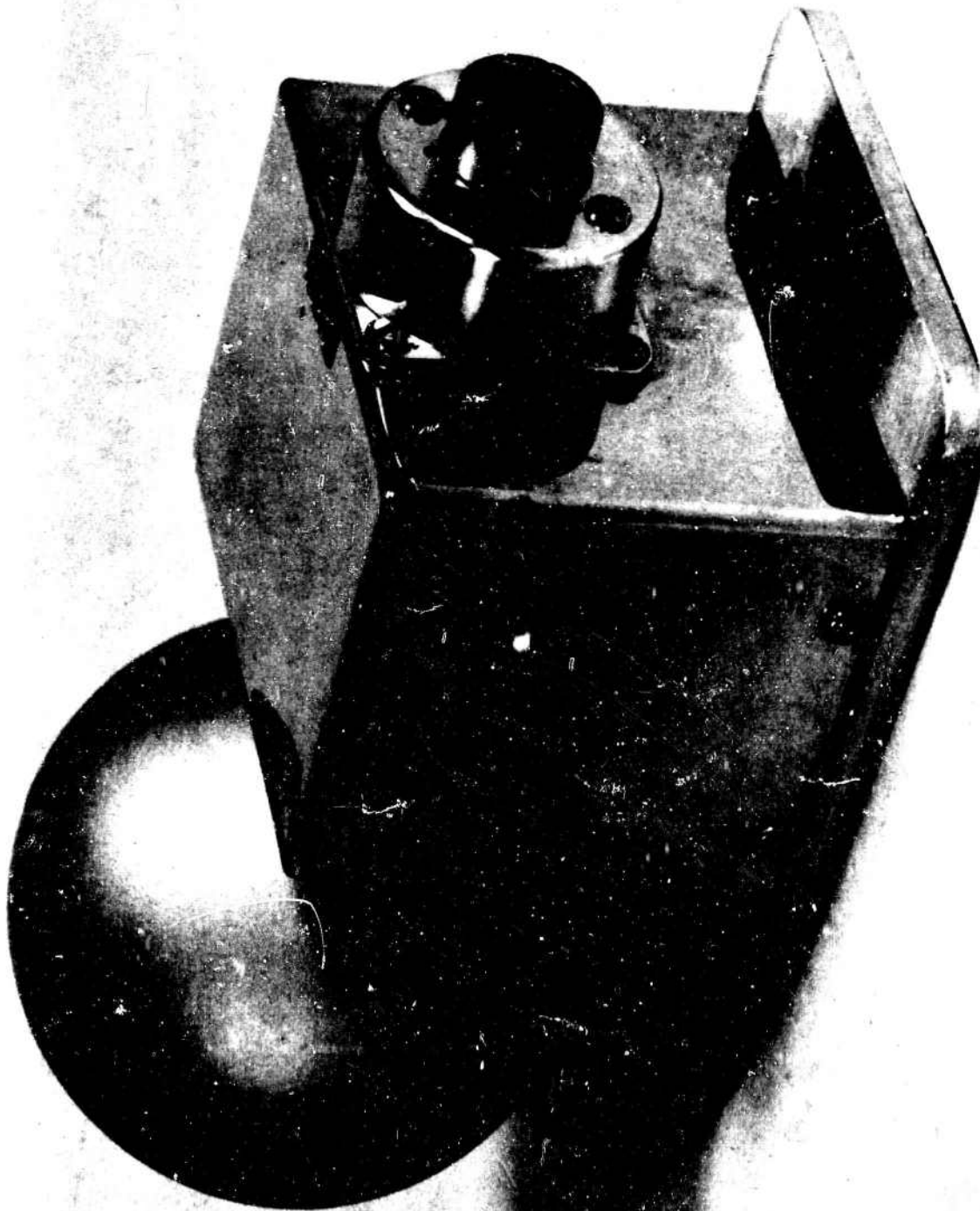
Cosmic Radiation Dosimeter for Manned and Unmanned Satellites
Figure 80

Page 152

Manned Systems Portable Survey Meter
Figure 81

Page 153

IV.C. INTEGRATION:

Integration of the active and passive dosimeters for Experiment D8 was controlled by Report A-531, "Interface Requirements Document for DOD and NASA Gemini Experiment D-8". This document defines all equipment interface requirements, testing criteria, aerospace ground equipment requirements, and delegated responsibility relating to the integration of experiment into the Gemini Spacecraft 4 and 6. This document was prepared under order 63-01, of the general contract NAS 9-170, DOD/NASA Gemini Experiments Program. All equipment with the exception of the mounting and attaching hardware and the electrical bundles and interconnectors was supplied by the Air Force. The items that were not GFE were supplied by McDonnell. The mounting of the units into the spacecraft was accomplished for both the passive and active dosimeters through McDonnell drawings 52-81155 and 52-81226 for spacecraft 4 and 6 respectively.

Verification of the electrical interface of the active dosimeters into Gemini Spacecrafts 4 and 6 was accomplished through sequences of 08-000 through 08-016 of SEDR C 321-6, which defined the Spacecraft Systems Testing Procedure. Initial mounting of the active and passive dosimeters onto the spacecraft was begun in May, 1964, when mock-up items of these units were installed for form-fit checks and astronaut-handling review. At that time mechanical design of all hardware was determined to be acceptable for astronaut handling in a simulated space environment.

IV.C.1. Schedule:

No limitations to passive or active dosimeter integration for Experiment D8 were observed for Spacecraft 4. Following a reduction of data from Gemini-4, the need to fly a depth-dose shield on the active Type I Dosimeter for Spacecraft 6 was evolved and did create design problems with that unit. Since the results of Gemini-4 were not reduced until after Spacecraft 6 had been delivered to the

Cape, all stowage space had been utilized and it was necessary to modify the Type I
unit so that the shield could be flown with it during launch. This required com-
plete mechanical requalification of the unit before reintegration by SEDR C 321-6
onto the spacecraft.

IV.C.2. Testing:

The SST Test Procedure is presented in Appendix (D). This procedure con-
sisted of a three-point strontium-90 beta calibration with the same source used
in the PreInstallation Acceptance (PIA) Procedure. Each position was run for a
period of one minute with the exception of the ambient readings, which were carried out
for fifteen minutes to insure that the negative and positive calibrate pulses as moni-
tored on pin B-17 were functioning. The outputs of each of the active units were
read out at the PCM ground station to insure that all telemetry channels and
dose-rate monitor outputs were functioning. No SST retesting was performed on
the modified Type I active dosimeter. The operational checkout at the Cape
at launch minus seven days was provided as a substitute for SST retest because
of the extremely late date at which modification had to be performed and because
the SST and Cape checkouts had previously determined that all telemetry points
were operating correctly. The SST-6 checkout procedure was the same as the checkout
for Spacecraft-4, but with the additional radiation settings being utilized for the
shielded Type I sensor.

The Cape Kennedy checkout of the active dosimeters was accomplished at launch
minus seven days for both spacecrafts 4 and 6. This test was similar to the SST
testing, except for the greater warm-up time allowed as a result of the long time
elapsed between SST testing at St. Louis and Cape checkout. The procedure is out-
lined in Appendix (E). Since the launch of Spacecraft 6 was postponed once, two
checkouts at the Cape were carried out for that flight.

IV.C.3. Technical Problems:

Several technical problems were discovered as a result of the SST Testing for Spacecrafts 4 and 6. On Spacecraft 4, a faulty design in the B + power line to the Type V unit was discovered when no power reached this unit. The wiring flaw was eliminated and the unit functioned properly thereafter. It was also discovered during SST testing that the large number of personnel who worked in the spacecraft would come into physical contact with the sensor heads of the active dosimeters and remove the outer insulating paint cover which led to ambient operation drift in the units. This was remedied by the building of special nylon AGE covers which were placed over the final flight units to eliminate this problem. The last problem discovered during hardware integration was that the AGE egress seat would not allow the hatch to close without bending the back portion of the Type I electronics. The SST Type I electronics suffered a rather large indentation as a result of the flaw in seat design. An MR was written to preclude using this temporary seat further for various spacecraft fit checks.

Only two problems were encountered on Gemini 6. One was that the Type I shield could not be removed due to an obstruction in the spacecraft wall when it was mounted on the left egress door. In order to eliminate this problem, the Type V and the Type I unit were relocated on the right and left hatches, respectively. The other major problem encountered with the Type I modified unit was that the base plate on the right hatch was warped and produced a strain in the shield. This problem was solved by inserting rubber washers in the four mounting holes to eliminate the strain.

156

V. FLIGHT TEST:

The data gathered in the experiment consisted of 97 hours and 45 minutes and 25 hours and 30 minutes of dose rate and depth dose rate measurements on Gemini 4 and 6. The dose rate data included a measurement of the cosmic radiation and trapped Van Allen radiation throughout both Gemini Missions. This Experiment recorded the instantaneous tissue dose in a manner never before accomplished on a manned spacecraft. The measurements marked the first time that dose rate surveys were performed at many shielded locations within the spacecraft during Van Allen Belt passage. This instantaneous data was also complemented by accumulated records of the particle profile and energy within the interior of the spacecraft from the passive dosimeters flown at the same location. This data has allowed the establishment of experimentally determined attenuation factors of the radiation field which can be extrapolated to operations in a Gemini spacecraft at other altitudes.

V. A. First Flight of Experiment : GT-4

1. Mission as Planned

Operational procedures:

All equipment in this experiment was automatic and required no switches or turn-on from the ground. Each active dosimeter was activated whenever the spacecraft was fully powered. The passive dosimeters were fixed at various locations within the spacecraft and were also completely automatic in that they required no switches or activation levers of any kind. It was necessary only for the co-pilot to remove the active sensor from the Type V instrument and to survey five locations about the spacecraft cabin during one of the passes of the spacecraft throught the Inner Van Allen belt. After the survey the astronaut was required to replace the sensor in its mount. No other equipment operation whatsoever was required in this experiment for GT-4.

157

The operational procedures were integrated into the flight plan by requesting the required times and locations of the survey through the Flight Crew Support Division at MSC. The required astronaut time was then programmed by this section into the flight plan for the spacecraft. These requirements were first submitted to the Air Force Systems Command Field Office in the Definitive Experiment Outline of June 1964, approximately eleven months prior to the launch of the spacecraft. They were then forwarded to the Flight Crew Support Division and other mission planning sections of NASA. Since it was anticipated that the spacecraft would make at least four passes per day into the anomaly, no definite revolutions were called for. It was specified, however, that at least three spacecraft passes through the anomaly be reserved for radiation surveys. Three survey passes were called for in order to insure that consistency in readings could be obtained and to determine whether any differences in effective spacecraft shielding resulted at different locations in the anomaly. With more than one radiation survey it would be possible to better determine the effects of spacecraft orientation on dose levels produced by the radiation field entering the cabin. In order to determine the best possible passes for the survey, an isoflux plot of the South Atlantic Anomaly was given to the Flight Crew Support Division. This plot gave the anticipated anomaly radiation intensities as a function of latitude, longitude, and altitude over the possible range of Gemini positions. With this chart it was possible for the crew support personnel to determine which passes would penetrate most deeply into the anomaly for survey use. No requests were made for any changes in orbit or for maneuvers to be accomplished in this experiment since the sensors were designed to be omnidirectional and little could be obtained that was not given by natural spacecraft motion such as normal tumble and roll.

V.A. 2. <u>Astronaut Training</u>:

a. The astronaut training schedule called for one formal briefing approximately six weeks before the launch of the spacecraft. Training units were used in the mission simulators and mission simulation training was undertaken several times before flight time. All astronaut training was accomplished with active dosimeter hardware since the astronauts were not required to participate in the passive dosimeter experiment.

b. The formal astronaut training period required less than an hour and consisted of a briefing by the project officer and a technical monitor from the Air Force Systems Command Field Office. The astronauts, key personnel from the Flight Crew Support Section of NASA, and the back-up crews were present. Each briefing consisted of a short background presentation of the problem, the nature of the experiment, and the anticipated results. Following this, the astronauts were trained in the operation of the active dosimeter with the portable sensor. This operation was demonstrated and mastered in a matter of minutes due to its simplicity. After each astronaut had correctly handled the sensor, it was positioned in the various specified body and spacecraft locations to demonstrate the performance of the experiment. After this demonstration the astronauts were requested to repeat the sensor placement and any corrections or questions that resulted from their performance were cleared up. The astronauts were then given written handouts of the briefing which gave a summary of the experiment and the items covered in the briefing, such as sensor operation, sensor placement, the time required for each placement, and the format for recording experiment data in the flight log book.

c. Informal briefings were held with the flight primary crew by the AFSCFC technical monitor on several occasions during the four weeks before launch. These informal briefings led to the performance of the experiment a total of five times during the mission instead of the three required. This was a very fortunate occurrence because the data from three of the five surveys was lost due to the manner of telemetry recovery handling on the Pacific recovery ship near Hawaii and had the extra surveys not been performed all survey data might have been lost.

d. Mockups of the active dosimeters for astronaut training were delivered to NASA Flight Crew Support Division in July 1964, approximately 11 months before the flight, for inclusion on the spacecraft mission simulator. During the formal briefing an SST unit, an identical model of the flight units, was used to demonstrate sensor removal and placement. The use of this unit provided a more realistic means of testing the use of the flight units since the locking mechanism, sensor weight, and the spring tension in the retractable cord were identical to those of the flight hardware. Passive dosimeter mockups were provided as a means of acquainting the astronauts with the complete experiment.

e. There was limited use of the training units in the simulator under the auspices of the NASA flight crew support section on several occasions before the spacecraft launch. It was not necessary for the Air Force project officers to participate in this test, as the astronauts had previously been briefed on all phases of handling of the dosimeters. The project personnel were present at the altitude chamber tests at McDonnell. The astronauts had experienced no trouble at that time in handling or positioning the actual flight units under simulated flight conditions.

V.A.3. Mission as Flown - GT-IV

The active dosimetry portion of Experiment D-8 was activated immediately when the spacecraft was powered up for launch. The active dosimeters remained on during the entire mission and recorded all ionizing radiation that entered the spacecraft at the hatches.

During five selected passes through the central portion of the South Atlantic anomaly, the sensor head of the protable Type V unit was removed from its mount on the hatch and placed at the following locations by the Gemini co-pilot:

        a. Against the chest, the sensor covered with a glove. (Figure No. 82)

        b. Between the legs in the area of the groin. (Figure No. 83)

        c. Under the left armpit. (Figure No.84)

        d. In front of the cabin window. (Figure No.85)

        e. In front of the instrument panel about midway between the floor and the ceiling. (Figure No.86)

        f. On the floor between the feet. (Figure No.87)

The sensing element was fixed at each of the pictured locations for a period of 1.0 m³ . te to insure that the full response of the instrument to the given radiation field was attained during the measurement.

The dose rate levels were thus measured as functions of position in the capsule and depth in the astronaut, using portions of the astronaut's body as a shield. The dose rate level beneath the left hatch of the spacecraft was obtained as a function of time from the fixed Type I dosimeter and this data were used as a base line from which to compare the measurements made by the portable unit.

161

Portable ionization chamber against chest and glove-covered.
Figure 82

Portable ionization chamber between legs, groin area.
Figure 83
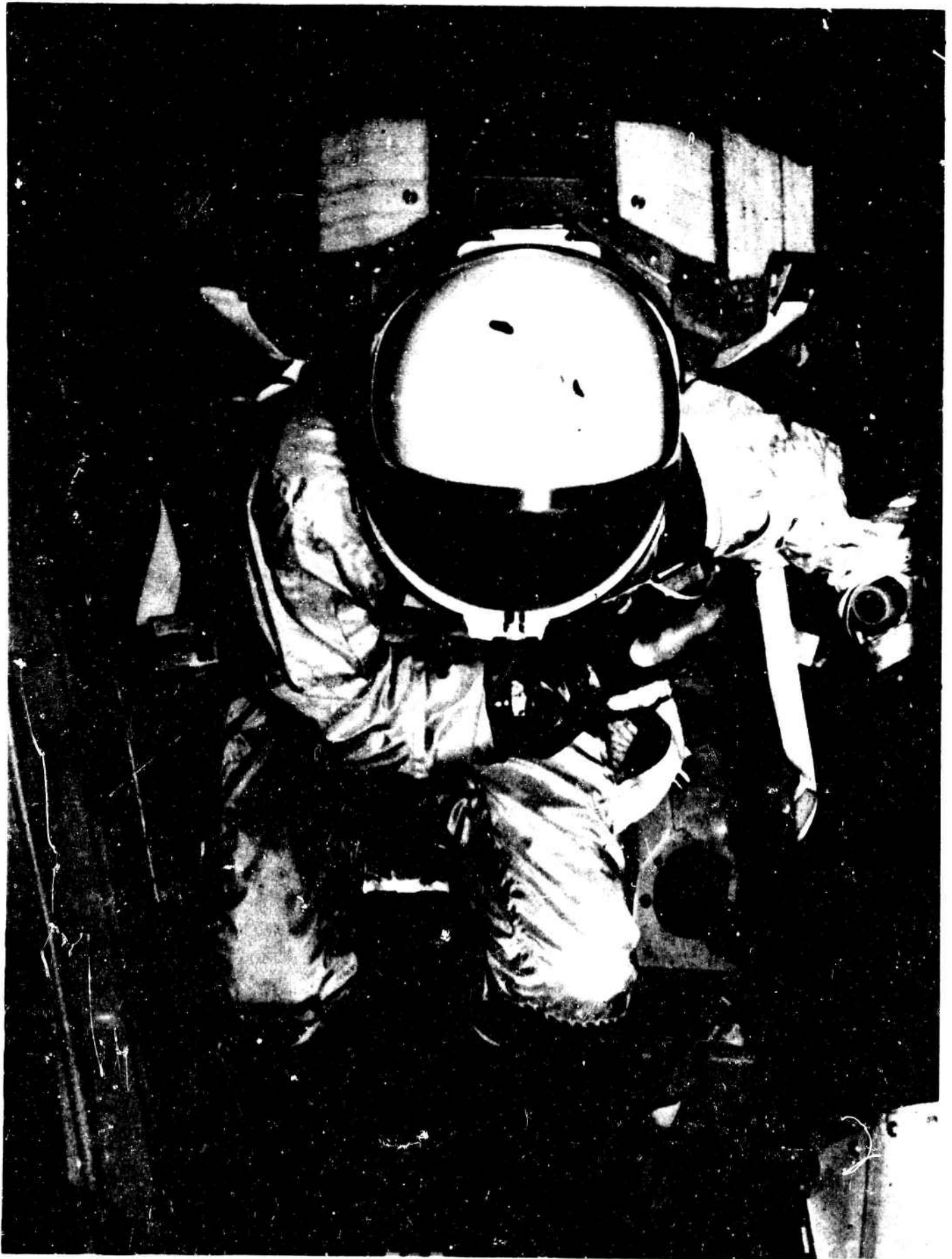
Portable ionization chamber under left armpit.
Figure 84

Portable ionization chamber in front of window.
Figure 85

Portable ionization chamber in front of instrument panel
Figure 86
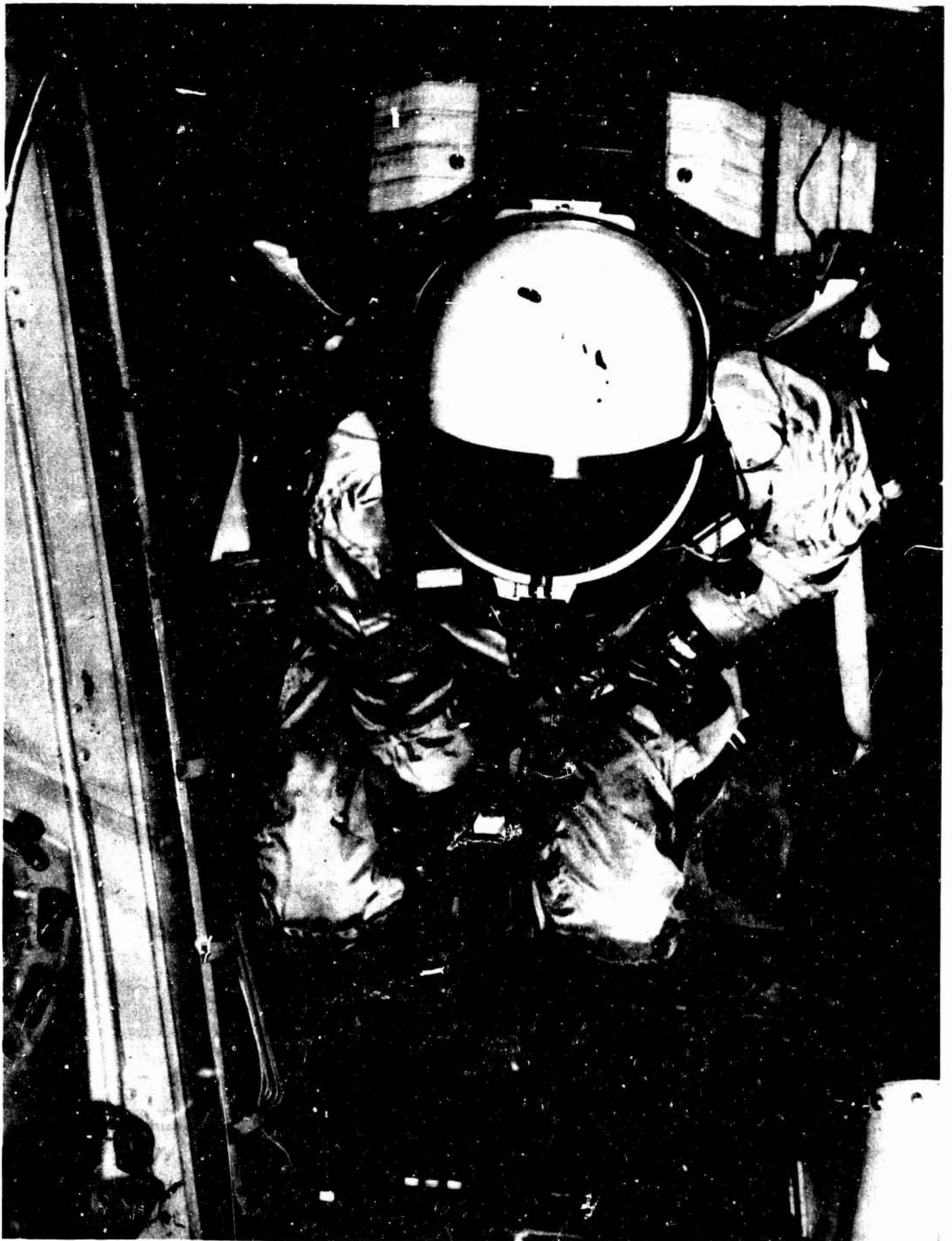
Portable ionization chamber on spacecraft floor
between the feet.

Figure 87

No experimental procedures in flight were associated with the passive dosimeter portion of the experiment. All units were mounted as previously described and remained at these positions from launch to touchdown when they were removed for shipment to the Air Force Weapons Laboratory.

V.A.4. Flight Equipment Performance:

All Experiment D-8 flight equipment performed flawlessly throughout the entire mission of Gemini 4.

V.A.5. Data and Results - Gemini Flight 4:

V.A.5.a. Active Dosimeters:

The active portion of Experiment D-8 is most conveniently discussed in terms of two general areas of interest: (1) experimental determination of the dose levels obtained outside of the South Atlantic Anomaly, and (2) measurement of the radiation characteristics during spacecraft passage through the anomalous region of the inner radiation belt. The active radiation sensors functioned perfectly throughout the mission; and the five scheduled radiation level surveys within the cabin by the co-pilot were performed during anomaly passes of the spacecraft.

. 1) Cosmic Radiation Dose Measurements:

Outside of the Brazilian or South Atlantic Anomaly, the principal contribution to the biological dose received by the astronaut was from cosmic radiation. The average, maximum and minimum dose levels obtained during nineteen revolutions of the spacecraft through regions excluding the Anomaly are presented in Table XIV. The average dose rate was obtained by mathematical determination of the average voltages as obtained every 3.2 seconds for each revolution. The maximum and minimum dose levels were determined respectively as the highest or lowest readings observed during at least a 1.0 minute period ofr each revolution. The average dose rate for all non-anomaly revolutions analyzed here was found to be 0.15 millirad/hour.

Since the revolutions selected for analysis covered the entire span of the Gemini-4 mission, the average dose rate presented for these selected passes may be readily extended to obtain excellent approximations of a total integrated dose for the flight, and projected to determine predictions of the cosmic radiation levels for extended missions at Gemini-operating levels. Using the average dose rate of 0.15 millirad/hour yields a total integrated dose due to cosmic radiation for the four-day mission of approximately 15.0 millirad. The cosmic radiation levels are generally very low and constitute a quite permissible exposure dose for extended periods at Gemini-operating altitudes.

Assuming a nominal period of 90 minutes for each revolution, the total accumulated tissue dose was found to be approximately 0.23 millirad for a one-revolution time span. The average daily radiation level received inside the cabin of the Gemini spacecraft due to cosmic radiation was then approximately 3.5 millirad/day. These radiation levels were very low and constituted a permissible magnitude of exposure.

The right hatch remained open during astronaut egress, exposing the Type V portable dosimeter to an essentially external space radiation environment during a portion of Revolution 3. The radiation levels measured by the Type V instrument during egress at no time exceeded those obtained by the Type I unit. This clearly indicates the total absence of softer or trapped corpuscular radiation in the regions of astronaut egress. Figure 88 illustrates the cosmic radiation dose profile as a function of orbital elapsed time and corresponding L-shell values. The dose profiles indicate a buildup to approximately 0.5 millirad/hour at higher L values, and a rapid drop below 0.1 millirad/hour for L values of near 1.0 earth radii. This effect is consistent with the predicted magnetic cutoff values encountered by Gemini spacecraft. Since the spacecraft traversed only lower geomagnetic latitudes, dose was less than polar or free-space values which nominally run as high as 14 millirad/day in solar minimum periods.

2) Anomaly Dose Levels:

Dose-rate data obtained from the Brazilian Anomaly show a rapid and pronounced rise in magnitude over cosmic radiation levels. The anomaly dose rate experienced during Revolution 7, for example, rose two orders of magnitude to more than 100 millirad.hour. Figures 89 through 97 indicate the dose levels encountered by the two active dosimeters for nine passes of the Gemini spacecraft beginning with the seventh revolution and running through the 54th revolution. The peak dose levels varied from 107 millirad/hour on Revolution 7 to only 20 millirad/hour for Revolution 51.

TABLE XIV

DOSE RATES OF COSMIC RADIATION FOR SELECTED REVOLUTIONS

OF GEMINI-4 OUTSIDE OF THE SOUTH AMERICAN ANOMALY

TABLE (XIV)

Revolution	Average Dose Rate Millirad/Hour	Maximum Observed Dose Rate	Minimum Observed Dose Rate
1	.25	.65	<.1
2	.25	.64	<.1
3	.20	.30	<.1
14	.15	.30	<.1
15	.15	.30	<.1
16	.18	.30	<.1
17	.15	.30	<.1
18	.22	.50	<.1
29	.12	.45	<.1
30	.18	.40	<.1
31	.12	.50	<.1
32	.12	.30	<.1
44	.15	.30	<.1
45	.12	.40	<.1
46	.12	.30	<.1
48	.15	.30	<.1
59	.10	.15	<.1
60	<.10	.10	<.1
61	<.10	.10	<.1
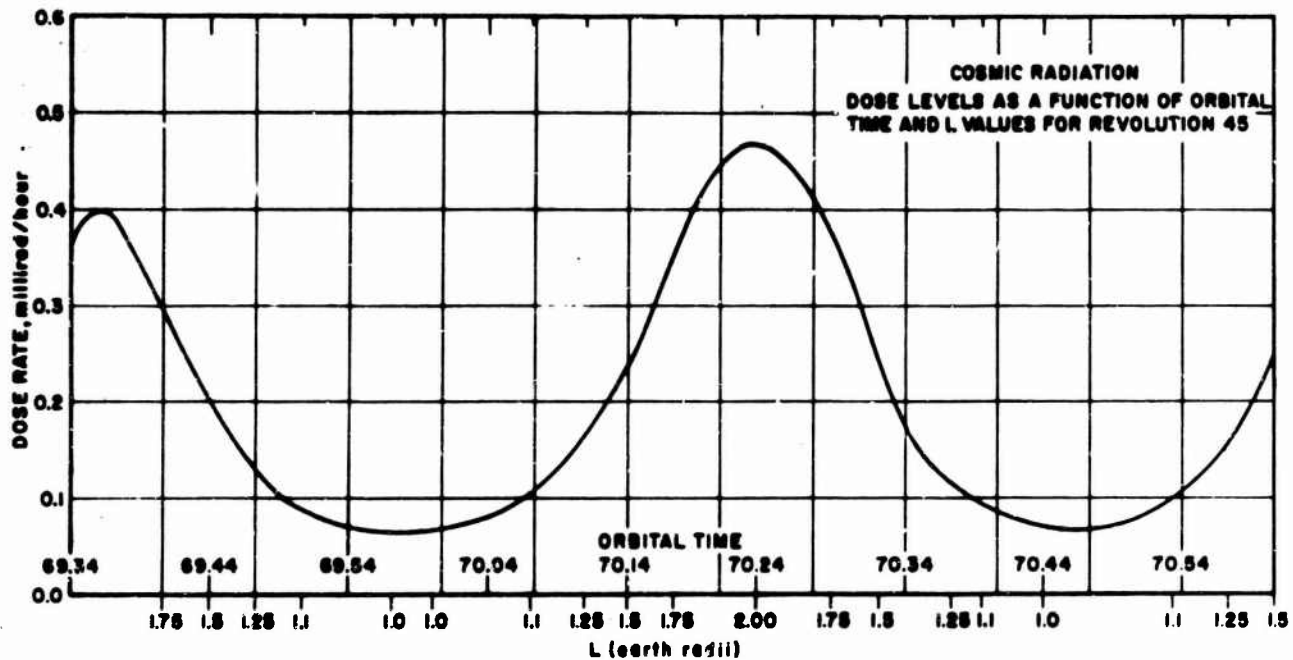
Cosmic Radiation Dose Levels Within Gemini-4
As a Function of Orbital Time and L Values for
Revolution 45.

Figure .88
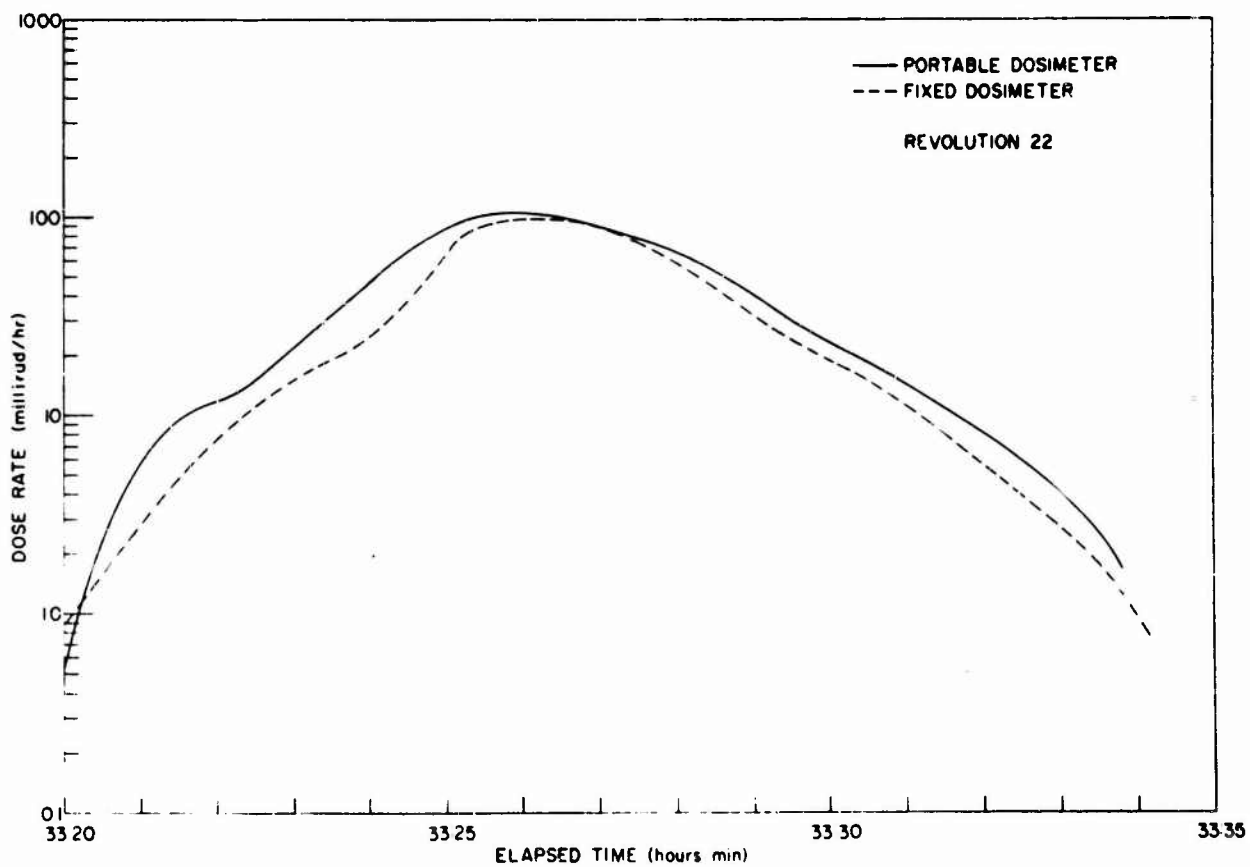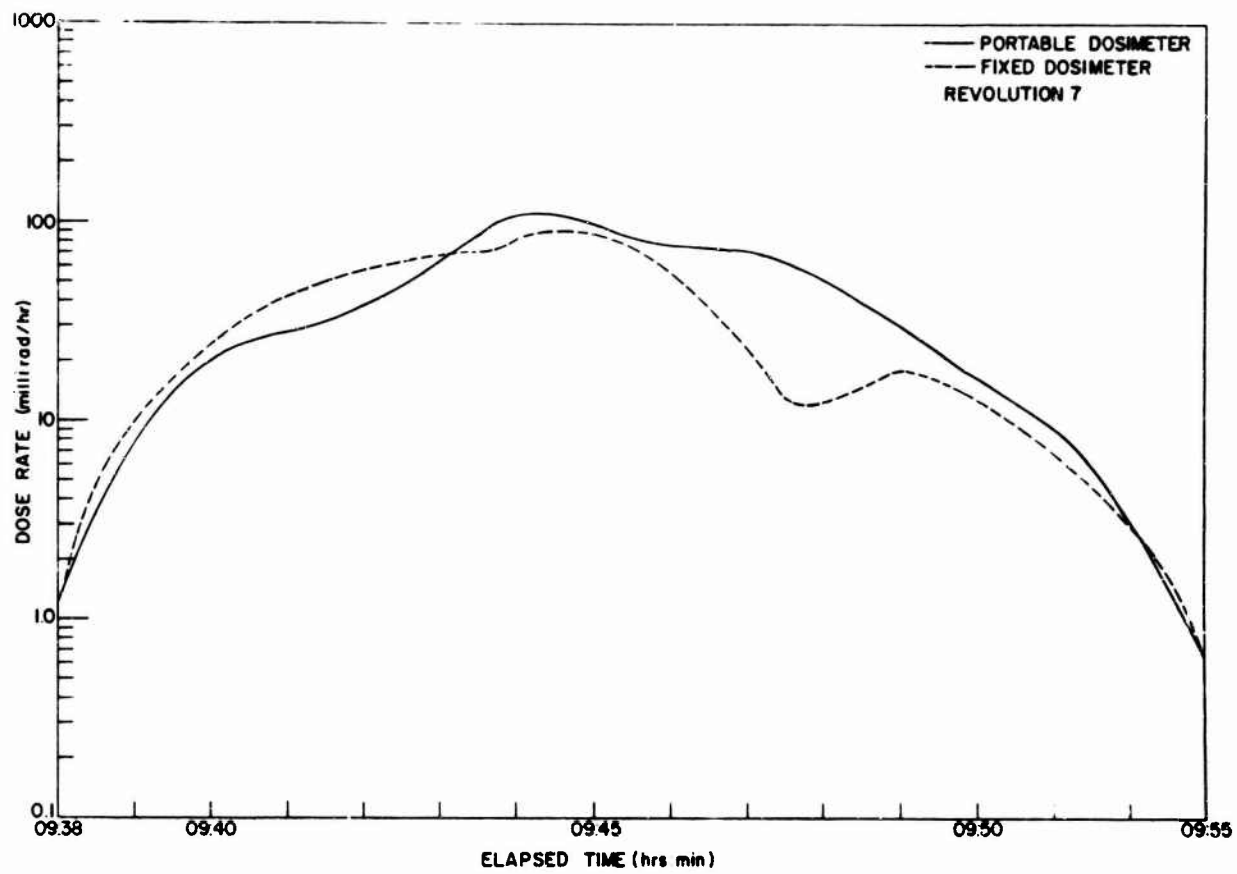
Instantaneous Dose Rate Revolutions 7 and 22

Figures 89 and 90

173
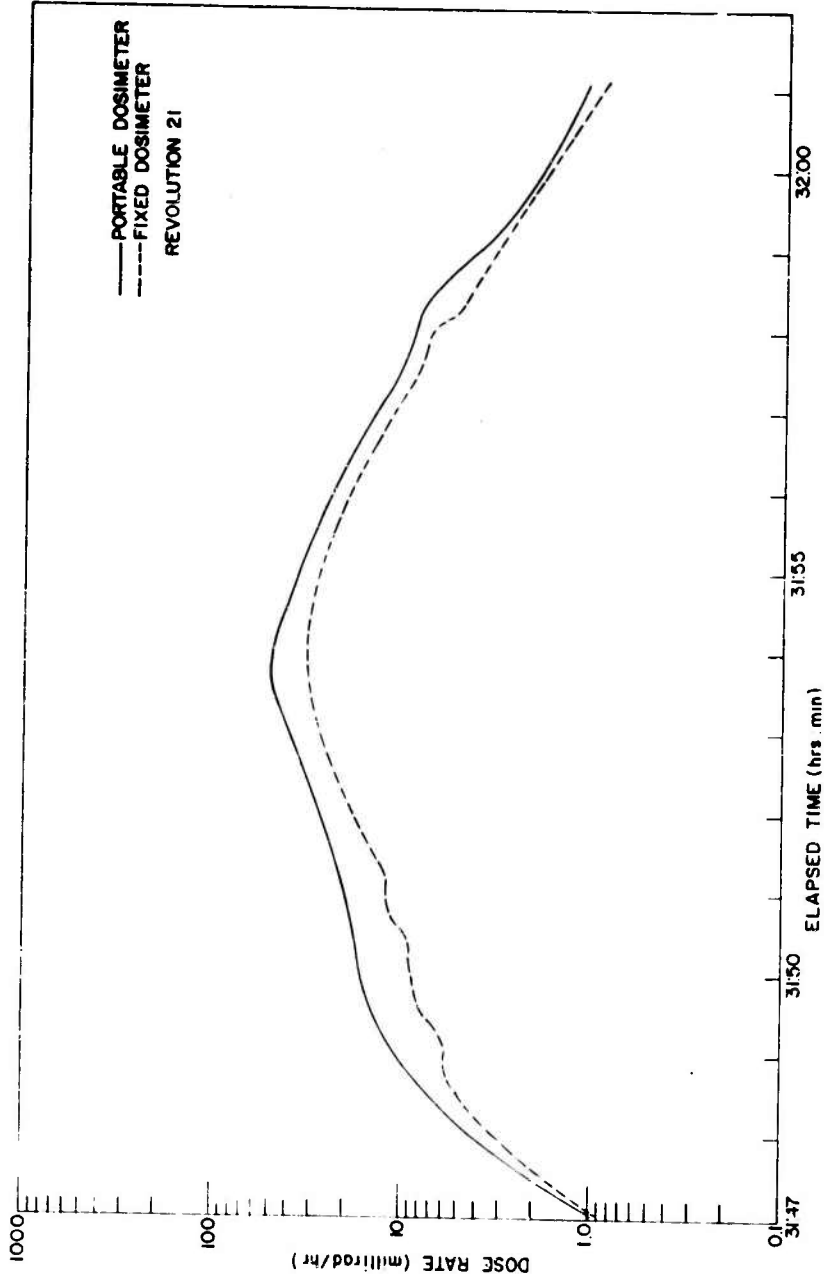
Instantaneous dose rate, revolution 21

Figure 91
174
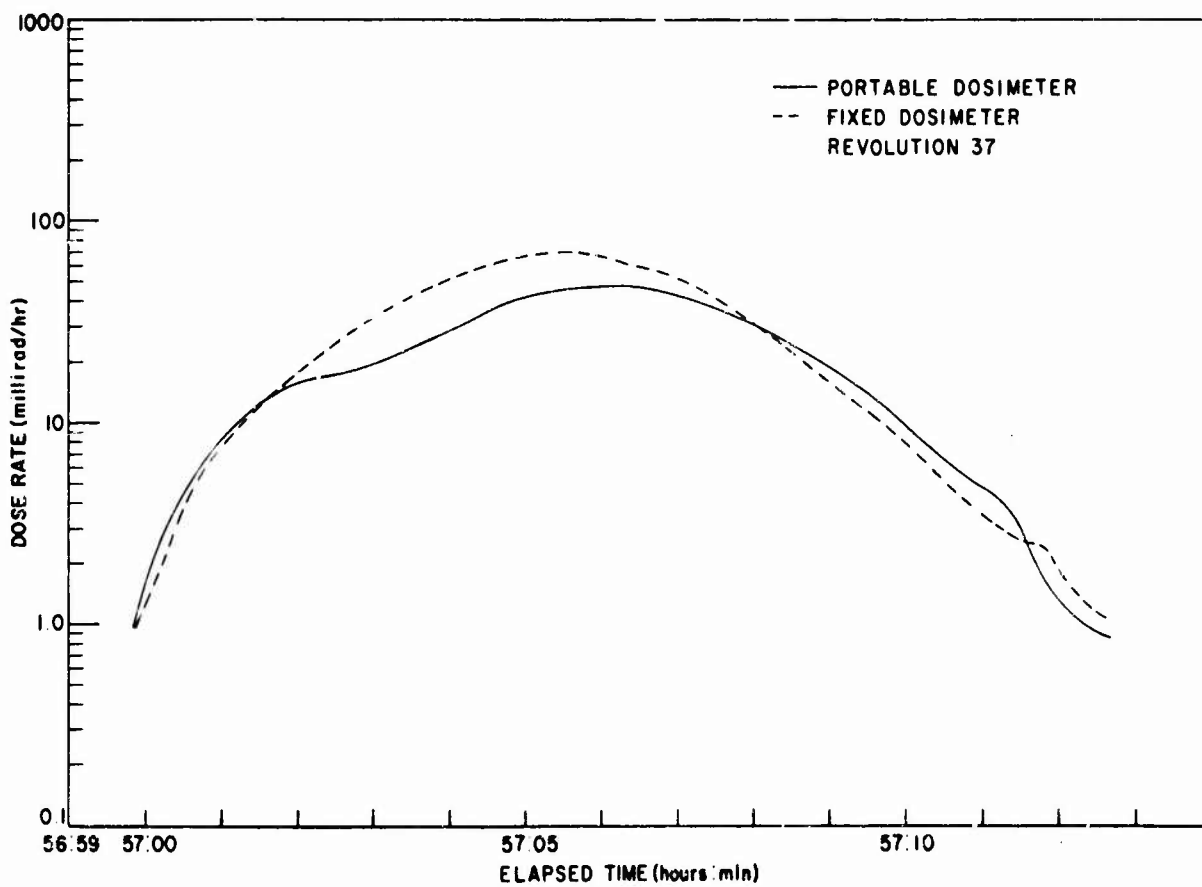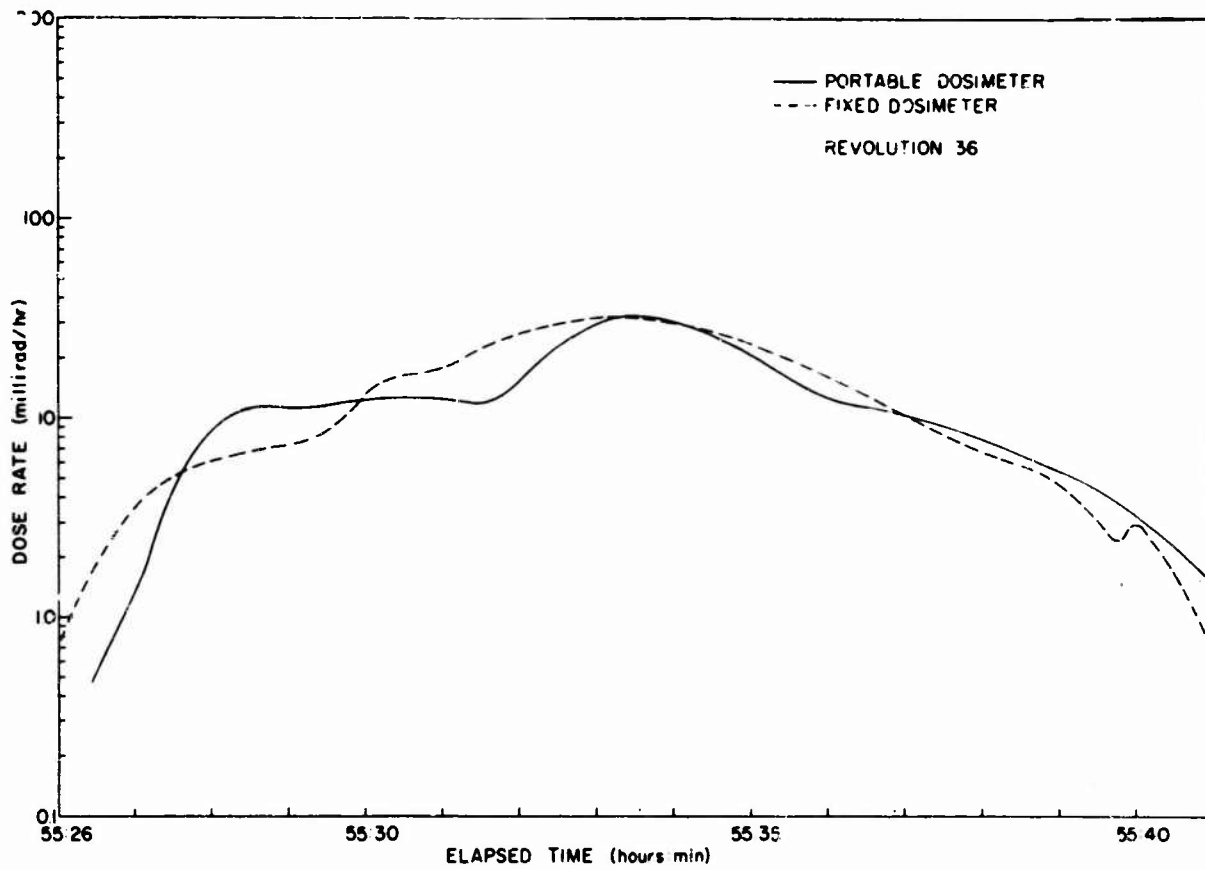
Instantaneous Dose Rate Revolutions 36 and 37

Figures 92 and 93
175
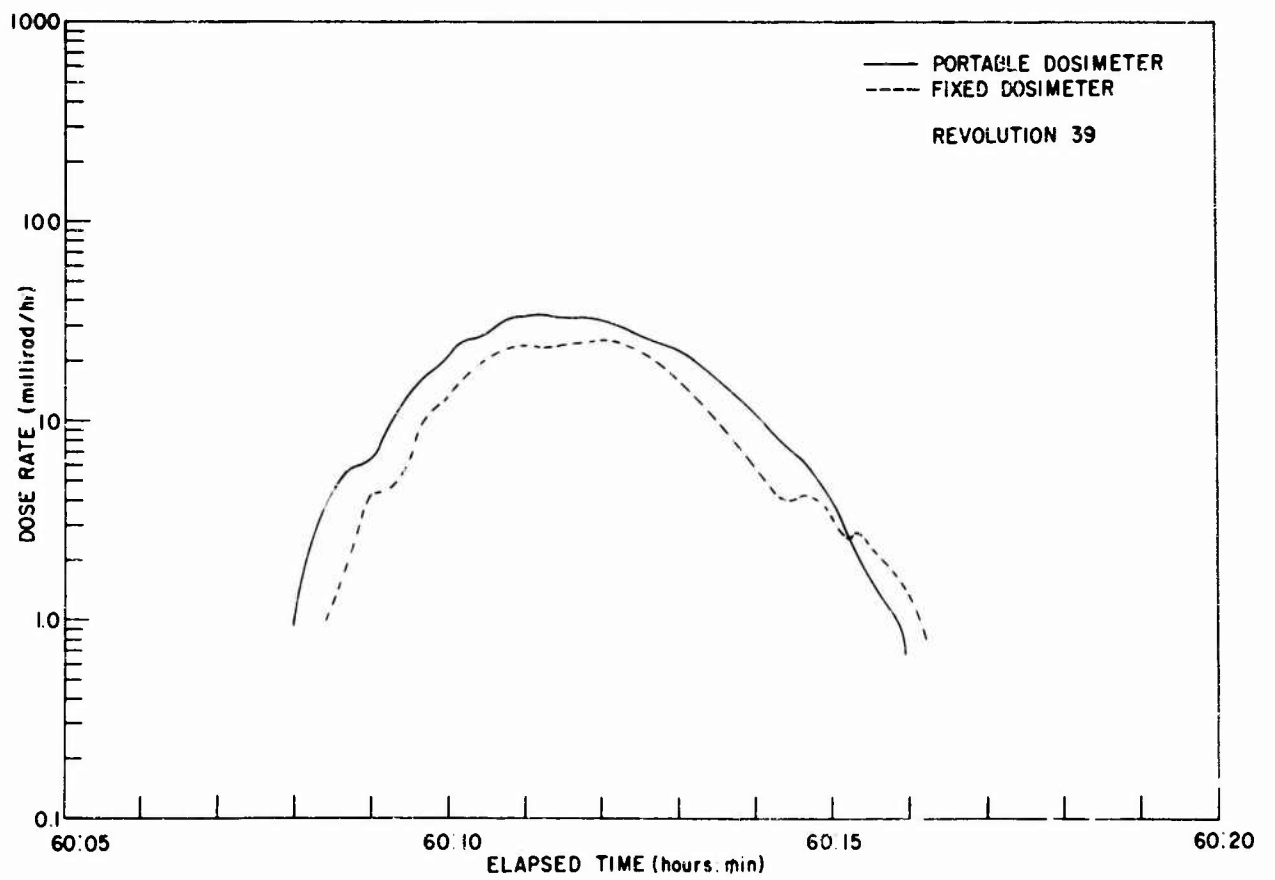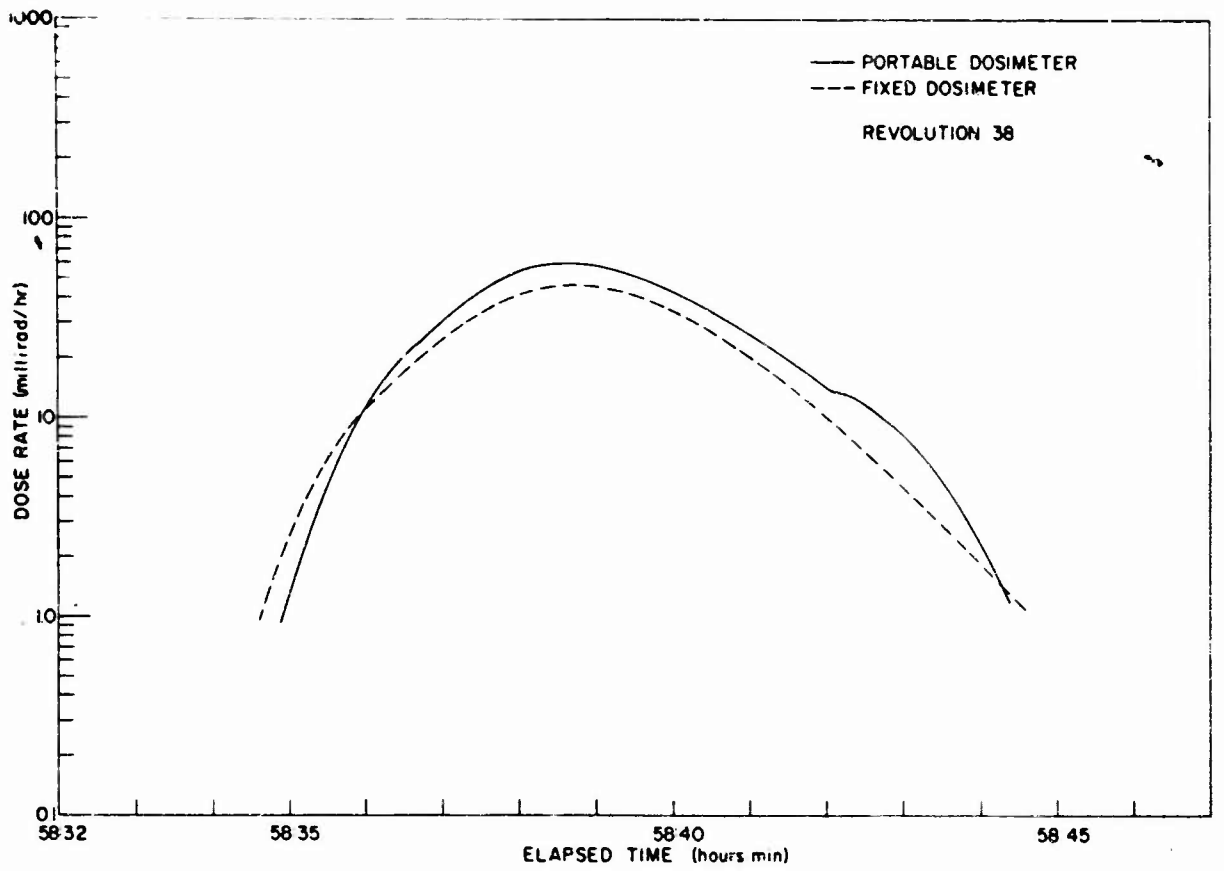
Instantaneous Dose Rate Revolutions 38 and 39

Figures 94 and 95
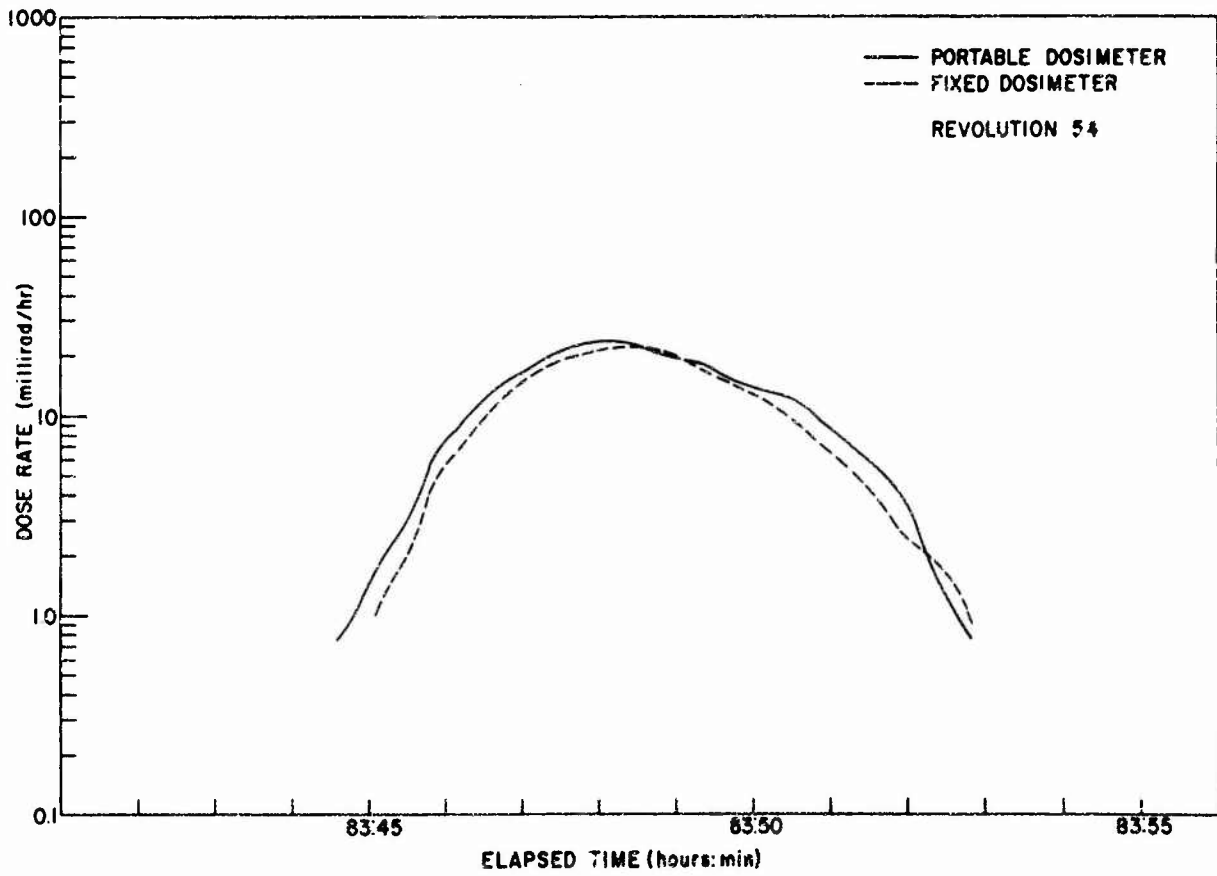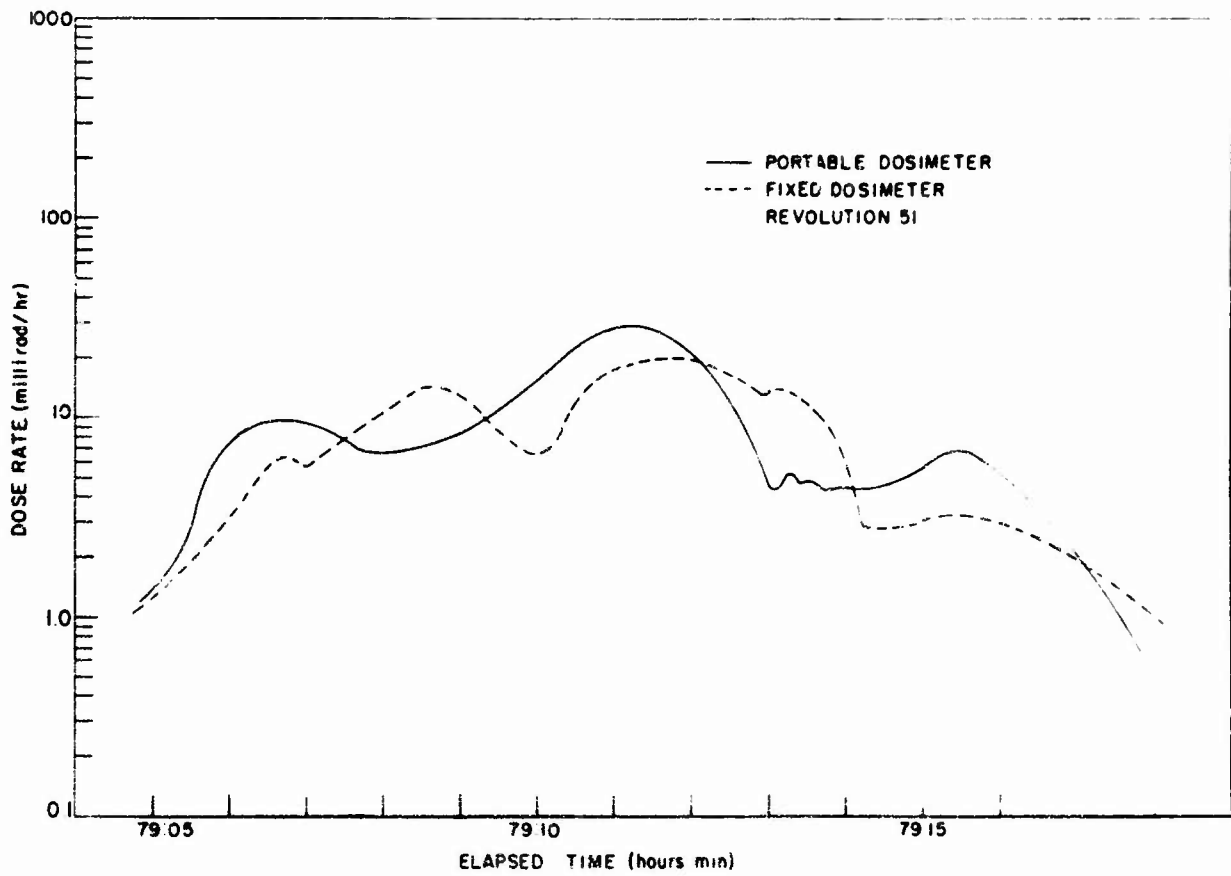
Instantaneous Dose Rate Revolutions 51 and 54

Figures 96 and 97

The curve in Figure 89 shows that an appreciable dose level existed for a period of fifteen minutes for Revolution 7, a deeply penetrating orbit. For a grazing orbit such as Revolution 39, the anomaly transit time was less than seven minutes. For most passes the transit time averaged approximately twelve minutes.

The dose rate differences between the two chambers show the effects of shielding differences interposed between the various sensing elements and the radiation field being measured. The Type V portable dosimeter generally read slightly higher than the Fixed Dose-Rate Meter. Revolutions 7, 21, 22, 38, 39 and 54 were passes in which the Type V dosimeter read slightly higher than the Type I dosimeter for the duration of the anomaly penetration. Revolutions 36 and 51 which were very similar types of revolutions show an interchanging of readings between the two dosimeters. On Revolutions 36 and 51, for example, five distinct intersection points between the fixed and portable dosimeter readings are seen. It is interesting to note that during Revolution 51, attitude control was exercised on the spacecraft so that it executed only yawing motion. These two curves clearly demonstrate the degree of directionality associated with the radiation entering the Gemini spacecraft. Generally, tumble and attitude data were not available for analysis. It can, however, safely be concluded that the radiation field had appreciable directionality associated with it at a number of given regions in the anomaly, since spectrometer measurements performed in this region indicate essentially the same results.

Colonel Edward White performed the series of radiation surveys shown in Figures 82 through 87 during five separate anomaly passes. Only the Revolutions 8 and 52 data are available for analysis. Figures 98 and 99 illustrate the results of the survey for Revolutions 8 and 52, respectively. It is apparent that considerable reduction in the dose levels was realized if the sensing element was buried beneath only a few grams per cm^2 of material. As the spacecraft approached the anomaly, the portable dosimeter indicated

178
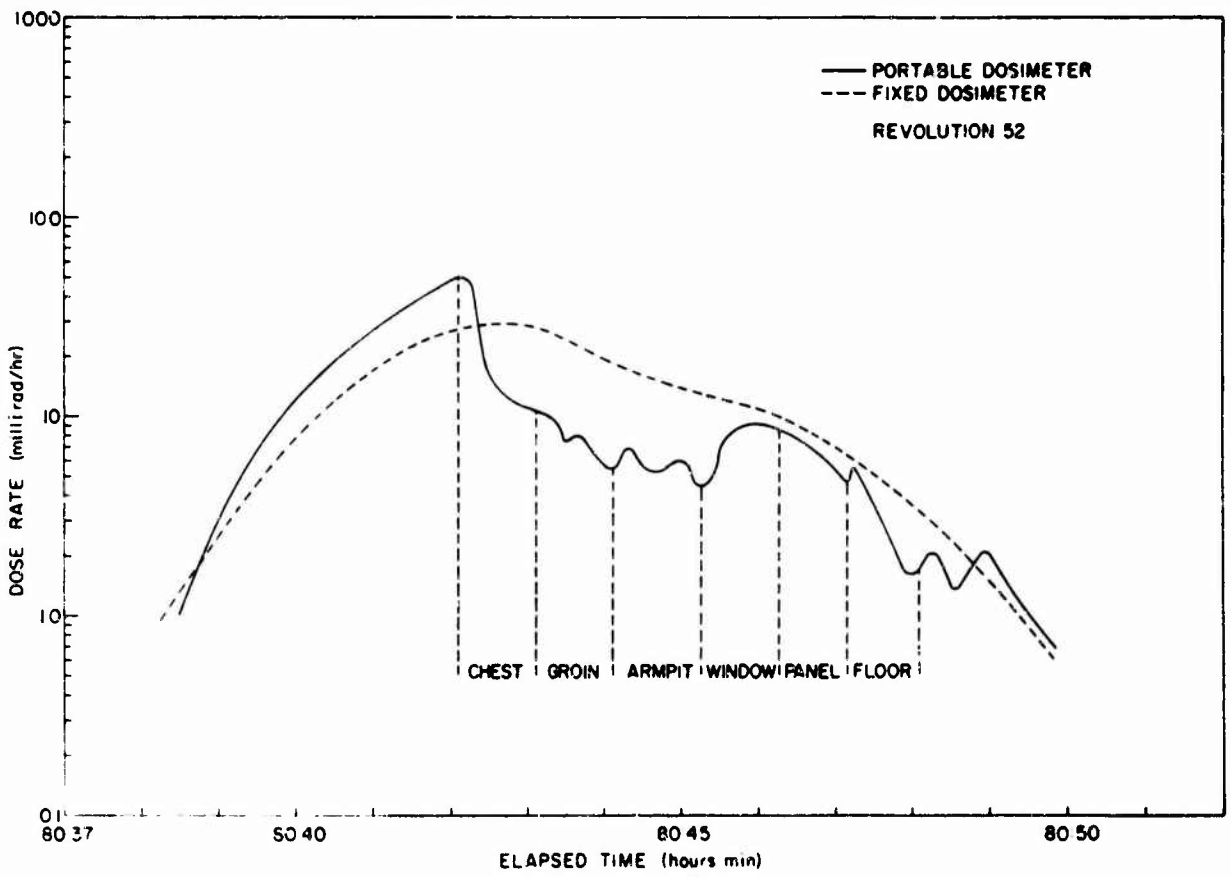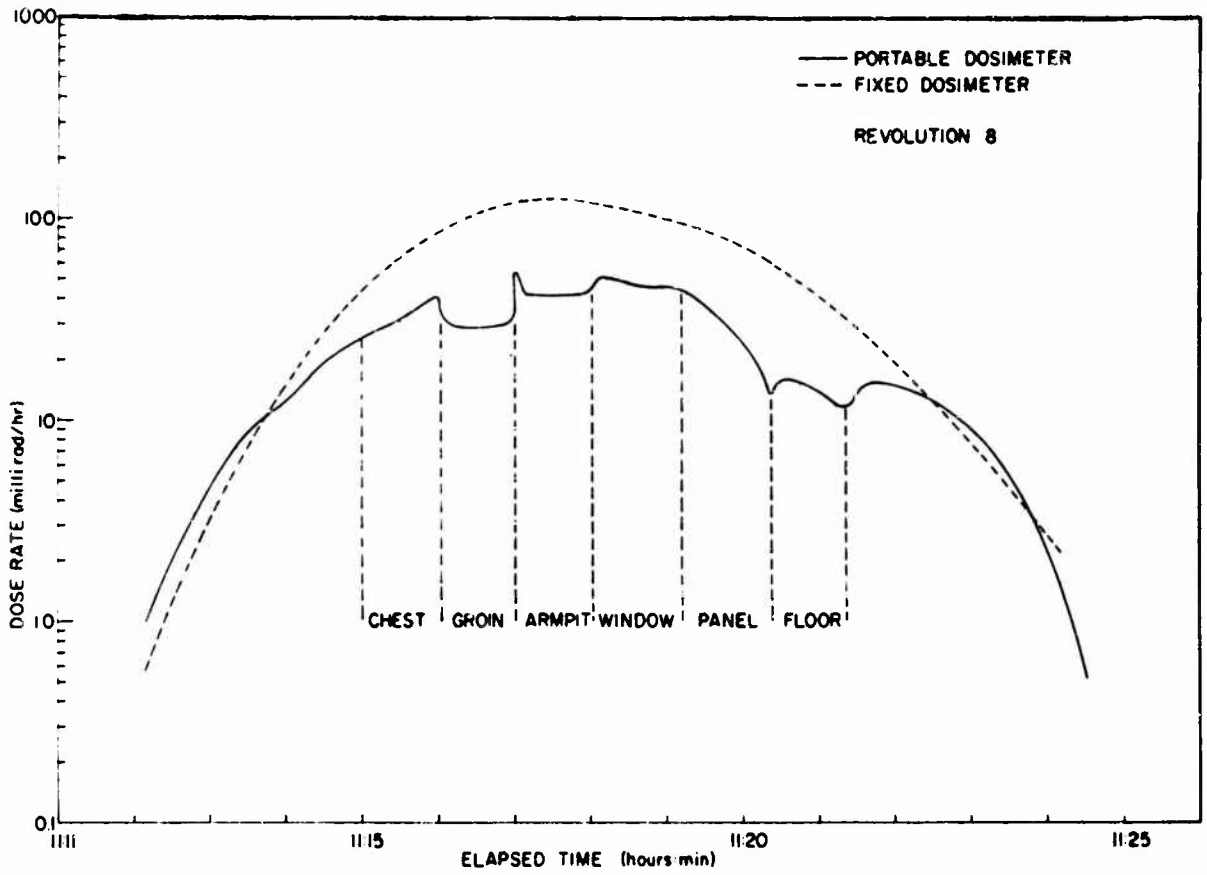
Radiation Surveys for Anomaly Revolutions 8 and 52

Figures 98 and 99

179

slightly higher dose levels than the fixed base-line instrument. When the sensor was moved to the chest position with the gloved hand covering the sensing element, a reduction in dose level of 50% was measured. Placement of the sensor at the groin and under the armpit led to an even greater attenuation in the dose level. In these two areas the dose was reduced to one-third of the fixed dosimeter levels. With the sensor head placed in front of the window, the dose level was reduced to approximately one-half of the base-line reading. The panel and floor areas are much better shielded and the dose rates observed there were, again, only one-third of the hatch area values. During Revolution 52, the hatch values of the dose were attenuated by approximately the same magnitude as they were on Revolution 8 at the chest, groin, and armpit locations. The window, panel, and floor areas appear to have been somewhat less effective in attenuating the radiation than they were during the eighth pass. The survey of the window, panel, and floor areas were performed at the edge of the anomaly region where the radiation levels are so low and poorly defined that a comparison between the base-line data and the portable dosimeter data is very difficult to accomplish accurately. The excellent agreement in attenuation between the two orbits at the chest, groin, and armpit, which were performed deeper in the anomaly region, however, indicated that passes similar to Revolution 8 would have produced the same attenuation in dose levels at the window, panel, and floor, respectively. Tables (XV) and (XVI) show the tabular values obtained at the various locations of survey compared to the base-line or hatch readings at the same instant in time for Revolutions 8 and 52. The survey readings were taken 30 seconds after the sensing element had been fixed in place at a given location to insure that equilibrium response had been reached there.

TABULAR VALUES OF CABIN RADIATION SURVEY

REVOLUTION 8

TABLE (XV)

(All dose-rate levels in millirad/hour)

Location	Portable Dose Rate	Fixed Base-Line Dose Rate
Chest	27	58
Groin	30	100
Armpit	36	105
Window	50	100
Panel	30	90
Floor	15	45

TABULAR VALUES OF CABIN RADIATION SURVEY

REVOLUTION 52

TABLE (XVI)

(All dose-rate levels in millirad/hour)

Location	Portable Dose Rate	Fixed Base-Line Dose Rate
Chest	15	29
Groin	9	27
Armpit	6	14
Window	9	12
Panel	6	9
Floor	2.2	4.5

181

The total integrated dose for Gemini anomaly passes is 67.28 millirad. The total extrapolated dose for other passes near the fringe areas of the anomaly did not exceed 2.0 millirad. The Type V portable dosimeter dose rates were not integrated because during five passes through the anomaly, surveys were being performed which would obviously have an appreciable effect on the dose readings.

Figure 100 illustrates an isodose mapping of the Brazilian Anomaly for a 280 kilometer altitude for Gemini Spacecraft-4. The contours were mapped by taking the highest dose rate reading from either instrument. The isodose contours have their maximum values at 37° of west longitude and 32.5^o south latitude. Revolutins 7 and 8 were, thus, shown to penetrate more deeply into the belt than other passes. Revolutions 22, 23, 37, 38, 52, and 53 follow a pattern similar to at least one of the revolutions shown in Figure 100 .

3) Comparison of Data with Computer Code Information:

One of the main objectives of the D-8 Experiment was to compa - ⁔⁔ dose rate measured by the active instruments with the dose rate predicted by ⁔ existing computer codes in order to test the validity of the codes. Predicted dose rates were computed using the actual Gemini trajectories. Radiation flux maps compiled by Dr. James Vette of Aerospace to describe the radiation environment were utilized in conjunction with a 720 sector analysis of the Gemini vehicle supplied by McDonnell Aircraft Corporation to describe the vehicle shielding. Figures 101 and 102 show comparison of the measured dose rate with the anticipated electron and proton environment for the pass through the anomaly region during Revolution 7. The measured dose rate is the average dose reading of the two active insturments. It is evident from these curves that the dose rates are highly dependent on the proton component of the radiation belt and fairly independent of the electron spectra at the same region in space. The data from the film emulsion flown in the passive portion of the experiment support this conclusion. It is felt that the electron component could not have exceeded ten percent of the total dose for the mission, which is consistent with the active dosimeter results.

182

An integration of the dose rate for the Type I (fixed) base-line dosimeter was performed for all anomaly passes during the mission.

DOSE RATES, INNER VAN ALLEN BELT RADIATION,

FOR SELECTED REVOLUTIONS

TABLE (XVII)

Revolution Number	Integrated Dose Per Anomaly Revolution (millirads)
6	3.0
7	8.4
8	10.45
9	3.5
21	2.87
22	7.10
23	6.0*
24	3.0*
36	3.32
37	5.90
38	3.26
39	2.50
51	1.72
52	2.26
53	2.0*
54	2.0

Total (Millirads)   67.28

*These data are not measured, but are extrapolated from dose-rate plots of similar type revolutions.
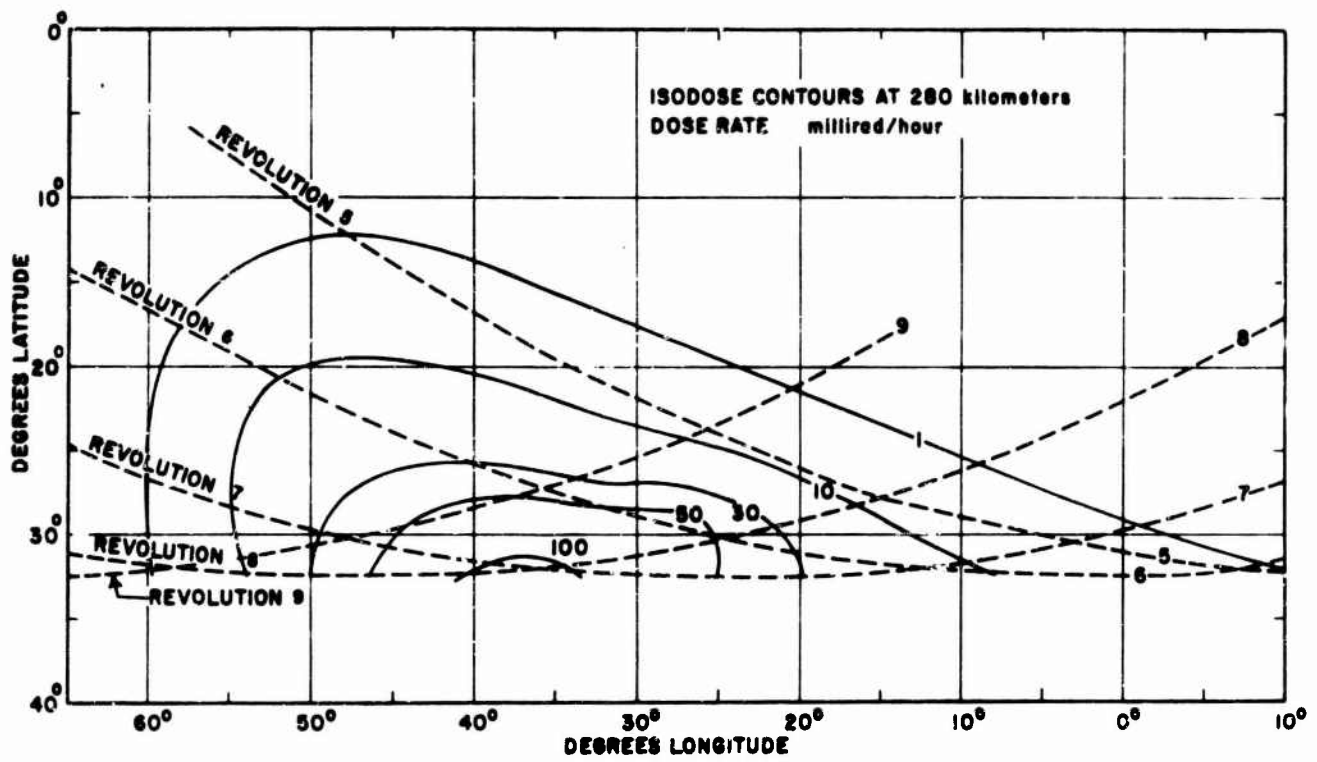
Isodose Contours at 280 Kilometers Obtained From
the Active Dosimeters Mounted on Each Hatch of the
Gemini-4 Spacecraft.

Figure 100
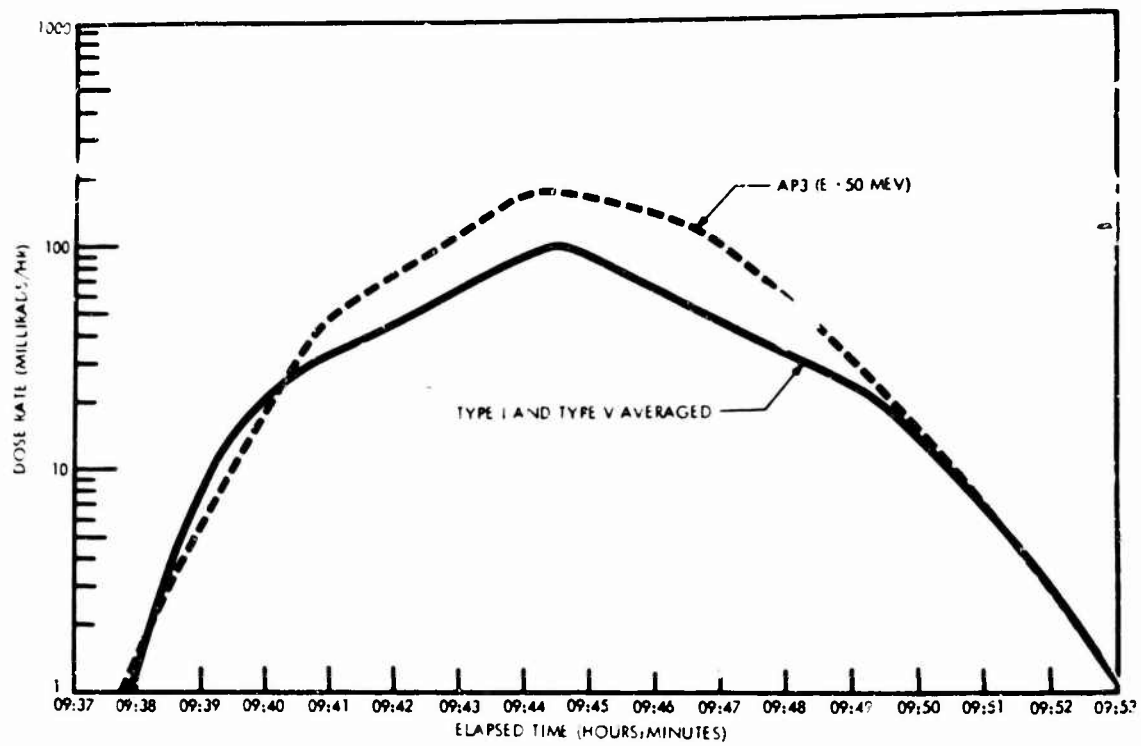
Comparison of dose rate profiles with proton spectrum.
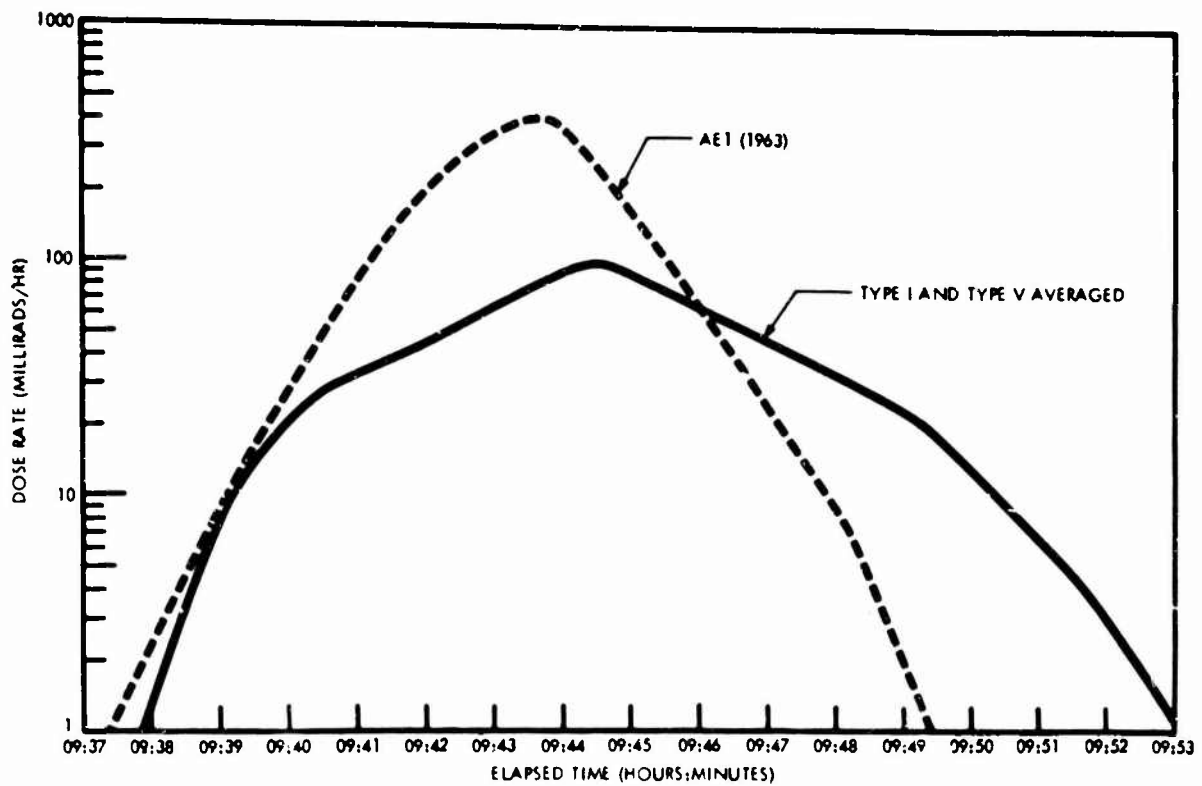
Comparison of dose rate profiles with electron spectrum.

Figures 101 and 102
185

Initial theoretical predictions of the dose levels carried out with the computer code using the Vette grid provide dose values approximately three times as great as the measured values for the Gemini anomaly orbits. Since these values depend on the flux map generated from the data gathered early in 1963, when the electron population was much greater than it was at the time of the Gemini-4 Flight, the present measured values would be expected to be much lower at the time of the Gemini-4 mission.

If only the proton dose rate is considered in working with the codes, a much better agreement is realized between the measured and the predicted values. The differences that do arise between the predicted and measured values are quite possibly a result of the poorly defined proton maps that are available for the region of the anomaly under consideration. Simultaneous spectral measurements were performed by NASA (MSC Experiment 2), which will be employed in updating the input spectral maps for both protons and electrons. With these corrected inputs, it will be possible to achieve much more accurate prediction capability than now exists.

V.A.5b. Passive Dosimeters,

The results of the passive portion of the experiment are summarized in Table (XVIII). The glass needles, because of their poor sensitivity at small doses, did not give statistically-significant results. The more sensitive Toshiba Glass Units registered low readings, which were in part a result of shielding by other passive dosimeters within the same package. Dose comparison between the two types of lithium fluorides indicated that within the limits of the experimental error -- about 40% at doses as low as 10 mr -- no neutron dose occurred. This lack of neutrons was further substantiated by the activation foils. This result is reasonable in that the only neutrons expected would come from secondary radiation produced by the interaction of high energy protons with the spacecraft and its occupants. Preliminary results from the film

186

SUMMARY OF THE PASSIVE-DOSIMETRY RESULTS ABOARD GEMINI-4 SPACECRAFT*

TABLE(XVIII)

Location (Figure 7)	1	2	3	4	5
Li^6F	$50 \pm 10(Li^6)$		$44 \pm 19(Li^6)$		$53 \pm 18(Li^6)$
Li^7F		$52.5 \pm 19(Li^7)$	$43 \pm 12(Li^7)$	$50 \pm 14(Li^7)$	$59 \pm 14(Li^7)$
CaF_2, Unshielded		49.4 ± 6.1		57.9 ± 6.5	49.4 ± 4.7
CaF_2, Unshielded	54.7 ± 7.0	47.1 ± 4.1	55.3 ± 5.4	55.7 ± 5.1	48.5 ± 6.1
CaF_2, Shielded	53.6 ± 5.7	48.9 ± 3.8	49.0 ± 3.8	55.9 ± 5.9	
Pocket Ionization Chamber	73 ± 5.1	45 ± 2.3	46 ± 3.2	54 ± 3.8	47 ± 3.3
Toshiba Glass:** Unshielded	52 ± 23	27 ± 15	42 ± 20		37 ± 18
Shielded	37 ± 18	17 ± 12	37 ± 18		12 ± 10
Emulsion***	68				35

* With the exception of the emulsion, all readings in this table are in milliroentgens equivalent exposure.

** The Toshiba Glass was calibrated using Co^{60}; all other calibrations used Cs^{137}.

*** The emulsion readings are in millirads. The error is less than 5 per cent.

187

emulsion packs indicate that over 95% of the tracks were caused by protons, with only residual electron, alpha, and heavy particle tracks. Less than 2 mr of dose was caused by particles other than protons.

Temperature Dependence. Since many of the dosimeters flown were to some extent temperature dependent in their response and dose fading, the temperature profile of the hatch area has been obtained using data gathered in the Type I active ionization chamber. Temperatures at the other four locations in which passive dosimeter packs were located are not expected to differ significantly. The extreme temperatures were never more than two degrees on either side of the mean, and were usually much less. At present, temperature profiles are available only for those revolutions listed.

GT-4 TEMPERATURE PROFILES ON LEFT HATCH

TABLE (XIX)

Revolution	Mean Temperature Degrees (C°)
6	22.6
7	23.8
8	23.8
21	20.9
22	20.9
36	20.4
37	20.9
38	20.4
45	20.9
50	26.2
51	25.6
52	25.0

188

V.B. Data and Results, Gemini Flight 6

Active Dosimeter Data;
_____

The two active dosimeters flown on Gemini 6 recorded dose readings that were generally in excellent agreement with the measurements carried out on Gemini 4. The noticeable difference of course occurred in the Type I unit which was shielded by a brass cover to provide the depth dose in 2.5 grams/Cm^2 of tissue. This unit was designed so that the electronics and shield provided this attenuation factor over at least 95% of the solid angle viewed by the omnidirectional sensor. The 5% radiation leak that could have occurred in shielding would have been straight through the back of the electronics and the barrel where less than one gram of shielding is seen. However, for all practical purposes the shielding is considered to surround the sensor omnidirectionally in the discussions that follow.

The cosmic radiation levels recorded on Gemini 6 were quite close to those on Gemini 4. No significant buildup was noted in the shielded chamber from cosmic radiation. Table XX shows the results of the cosmic radiation dose sampling performed on this flight for selected revolutions not passing through the anomaly. The average cosmic radiation dose for Gemini 6 is approximately .2 millirad/hour which gives a dose of 4.8 millirad for a 24-hour mission. Again, as on Gemini 4 these values of dose were quite insignificant when compared to the anomaly values which range several orders of magnitude above this level.

Five passes of Gemini 6 into the anomaly were recorded in which the data was recovered. Revolutions 5, 6, 7, 8, and 9 penetrated the anomaly in sufficient depth to provide measurable dose well above the cosmic radiation within the Gemini cabin. The highest dose level recorded on Gemini 6 was only 73 millirad/hour measured on revolution 6 which was the most penetrating pass of the spacecraft into the Inner Belt. This reading was recorded by the Type V

189

TABLE (XX)

Cosmic Radiation

Cosmic Radiation Dose Rate for Specific
Revolutions of Gemini 6 Outside of the
South American Anomaly. (millirad/hour)

Rev.	Average	Max.
3	.20	.7
4	.20	.7
10	.25	1.0
12	.15	.6
13	.20	1.0

TABLE (XXI)

Anomaly Peak and Integrated Dose - Gemini 6

Revolution	Peak-Dose (millirad/hour)	Integrated Dose (millirad)
5	21	1.0
6	73	6.0
7	62	5.5
8	44	2.5
9	20	1.5
TOTAL		16.5

unshielded unit as was anticipated. The Type I shielded unit also recorded its
highest dose of the mission during this revolution which was 42 millirad/hour.
Revolution 9 was the weakest pass into the belt made by the spacecraft. Here,
both dosimeters recorded their lowest anomaly dose rates of the mission with the
Type V unit recording a high mark of only 21 millirad/hour and the Type I measuring
only 16 millirad/hour. Table XXI shows the peak and integrated dose for all anomaly
passes observed in the mission. All values were recorded by the Type V unshielded
unit. The total anomaly dose was 16.5 millirad/hour for all passes. This was the
main contributor to the total dose in the mission accounting for approximately 80%
of the mission accumulated dose. It is quite interesting to note that if one
multiplies the Gemini 6 one-day mission anomaly dose value by four to account for
the four days of passes through anomaly experienced by the Gemini 4 spacecraft,
a figure of 66 millirad results which differs by 1.28 millirad from the integrated
dose on Gemini 4 in that region.

Shielding Effects on the Type I Dosimeter

For all the anomaly passes in which the Type V unit remained fixed to the
hatch, this unit recorded higer dose readings than its shielded counterpart on
the other hatch. On Revolution 6, the Type V unit read at 0809 hours a 50%
higher dose rate than the Type I unit. At 0811 hours the Type I unit was reading
only one-half the Type V Dosimeter. At 0813 hours the Type V unit read a 43%
higher dose value than the Type I unit. At 0814 hours, a 40% higher reading
was realized by the unshielded dosimeter. The period between 0814 and 0819 hours
was the only time during the mission that the Type I shielded unit read a higher
dose level than the Type V unit. During this short time span the Type I shielded
unit read from 20% to 30% higher dose values than the unshielded unit. This
unusual behavior is attributed to several possible causes: One of the astronauts
could have been positioned in such a manner within the cabin that he cut off
an appreciable portion of the radiation reaching the Type V sensor omnidirec-
tionally. No exact recording of the astronaut position has been available up to
now so this proposition cannot be verified. It is doubtful from the measurements
that were carried out on Gemini 4 and the remaining measurements carried out on
Gemini 6 that these reductions in dose could have resulted entirely from the
directional characteristics of the radiation field exterior to the spacecraft.
Even though the Gemini 6 spacecraft was in close proximity to the Gemini 7
spacecraft at this time, the small solid angle subtended by the Gemini 7 space-
craft would not have been large enough to affect the omnidirectional reading as
much as was recorded in a uniform field. If, however, the field was extremely
non-uniform, then it would be possible that the position of the astronaut
combined with the proximity of the Gemini 7 spacecraft would product the unusual
readings obtained here.

On Revolution 7 the dose level of the Type I unit was 43% less than the
unshielded unit at 0946 hours. From 0948 hours to 0954 hours, or for over 6
minutes, the dose level of the Type I unit remained at a level of one-half of

the unshielded unit. Thus, it appears that the shield for this pass cut the dose in half. This behavior in the dose profile indicated that the spectrum of protons producing it are generally quite flat with no build-up in dose with depth. This means that the number of particles entering the shielded sensor is reduced by more than 50%. This follows since the stopping power of particles of lower energy increases and would tend to increase the dose as the energy was lowered so that the number of particles entering the counter must have actually been reduced by a factor of more than two.

If we examine Revolution 8, it is seen that at 1120 hours the shielded dosimeter read 33% less dose than the unshielded unit. At 1121 this difference was still 33%. At 1123 the difference was only 25%. From 1124 to 1126 the difference between the two dosimeters held a very constant value of approximately 30%. From the dose measurements, it would appear that the proton spectrum is harder here than on the previous pass.

The shielding characteristics of the Type I dosimeter are somewhat different for the grazing revolution 9 of this mission. This revolution was within the anomaly at most for seven minutes, with a dose of only 10 millirad/hour being recorded for four minutes. At 1255.5 hours, the shielded unit read approximately 40% less than the bare dosimeter. At 1257 hours the difference was only 22%; at 1258 hours, the dose difference had climbed to 30%; at 1259 hours, the two units were recording an 18% difference; and at 1300 hours, the difference was again 27%. Thus, for this revolution the effect of shielding on the dose rate appears to oscillate from in excess of 30% attenuation to less than 20% over one minute intervals. The variations in attenuation here appear to be a result of the difference in shape of the proton spectrum entering the spacecraft because the oscillations are seen to also occur in the bare chamber dose readings simultaneously with the shielded unit readings. A possible explanation is that the

193

spectrum is subject to considerable variation especially at lower energies in
the fringe portion of the anomaly. The fact that the oscillations are seen in
both dosimeters would tend to indicate that there is little directional varia-
tion at this region. If one examines the data from Revolution 39 and Revolution
54 of Gemini 4, we see that a similar behavior pattern in the dose rates is
realized. These revolutions are approximately of the same anomaly duration and
are located in the same areas of the anomaly as Revolution 9 is on Gemini 6. If
these types of dose rate profiles are compared to Revolutions 7, 36, and 51 of
Gemini 4 where there is clearly a directional influence on the dose rate, there
is observed no pattern of simultaneous high or low readings for both dosimeters,
but rather a definite intersection of curves is evidenced.

An analysis of the data from all of the above revolutions established that
the dose was definitely predominately due to protons and possibly to a lesser
degree derived from bremsstrahlung. There could have been only a trace of elec-
trons penetrating the spacecraft shielding to make up the dose, for 2.5 g/cm^2
of brass would stop up to 3.5 MeV of electron energy, which is of course the
region of energy in which most of the anomaly electrons are found. There
is a possibility that a small number of the very high energy electrons found in
the upper end of the spectrum could have penetrated into the ionization chamber
volumes, but these particles are so few in number that they would be totally
swamped out in the proton background. As on Gemini 4, the film packs on Gemini VI showed
little evidence of electrons and attribute over 90% of the dose to protons.

Figures 103 through 106 display the results of the dose measurements
described above for Revolutions 6 through 9.

A radiation survey similar to the one described for Gemini 4 was performed
on Gemini 6. Figure 107 shows the results of this survey performed on
Revolution 6. One position was changed in this survey, that being to place
of the portable sensor next to the other sensor to determine how closely the

194

two dosimeters would read at approximately the same location. It was intended as mentioned that this survey be performed with the shield removed from the fixed active dosimeter on the other hatch so that base line readings similar to those obtained on Gemini 4 could be generated. Since the shield was not removed, an extrapolation of the base line data for the survey was necessary. This was accomplished by extending a dotted line as shown in Figure 107, the shape of which was determined from the Gemini 4 baseline curvature to the two survey initiation and termination points on the abscissa. The chest showed a 35% reduction from the unshielded values of the dose. The armpit dose level recorded was only 50% of the unshielded value. The groin area showed a reduction of almost 75%. Placing the sensors side by side reduced the dose to only 40% of the unshielded dose. This reduction was reasonable because the thickness of the brass shield reduced the solid angle of incoming radiation by 50% so that the Type V detector viewed only a 2π steradian rather than a 4π steradian solid angle. The shield actually provided 5.0 g/cm^2 of shielding over 2π steradians because both walls were acting as a shield. The panel shows a 50% reduction in the base line dose rate, and the floor shows almost 80% cut-off in the omnidirectional dose levels as measured at the hatch or base line. This survey generally agreed with the survey performed on Gemini 4, with somewhat more attenuation being realized at the groin and floor areas. These results tend further to support the hypothesis that the spectra vary rather rapidly with location during fringe passes and are considerably softer than the spectra recorded deeper in the belt as during Revolutions 8 and 52 on Gemini 4.

The shielded dosimeter for the survey revolution displays the small oscillation in dose levels characteristic of the fringe passes on Revolutions 7 and 8. The shielded dosimeter reads about 30% more than the chest, armpit or groin areas, indicating that these areas are roughly 30% more effective as a shield than the 2.5 g/cm^2 of brass. This finding is consistent with the

Instantaneous Dose Rate Revolution 6

Figure 103

-196
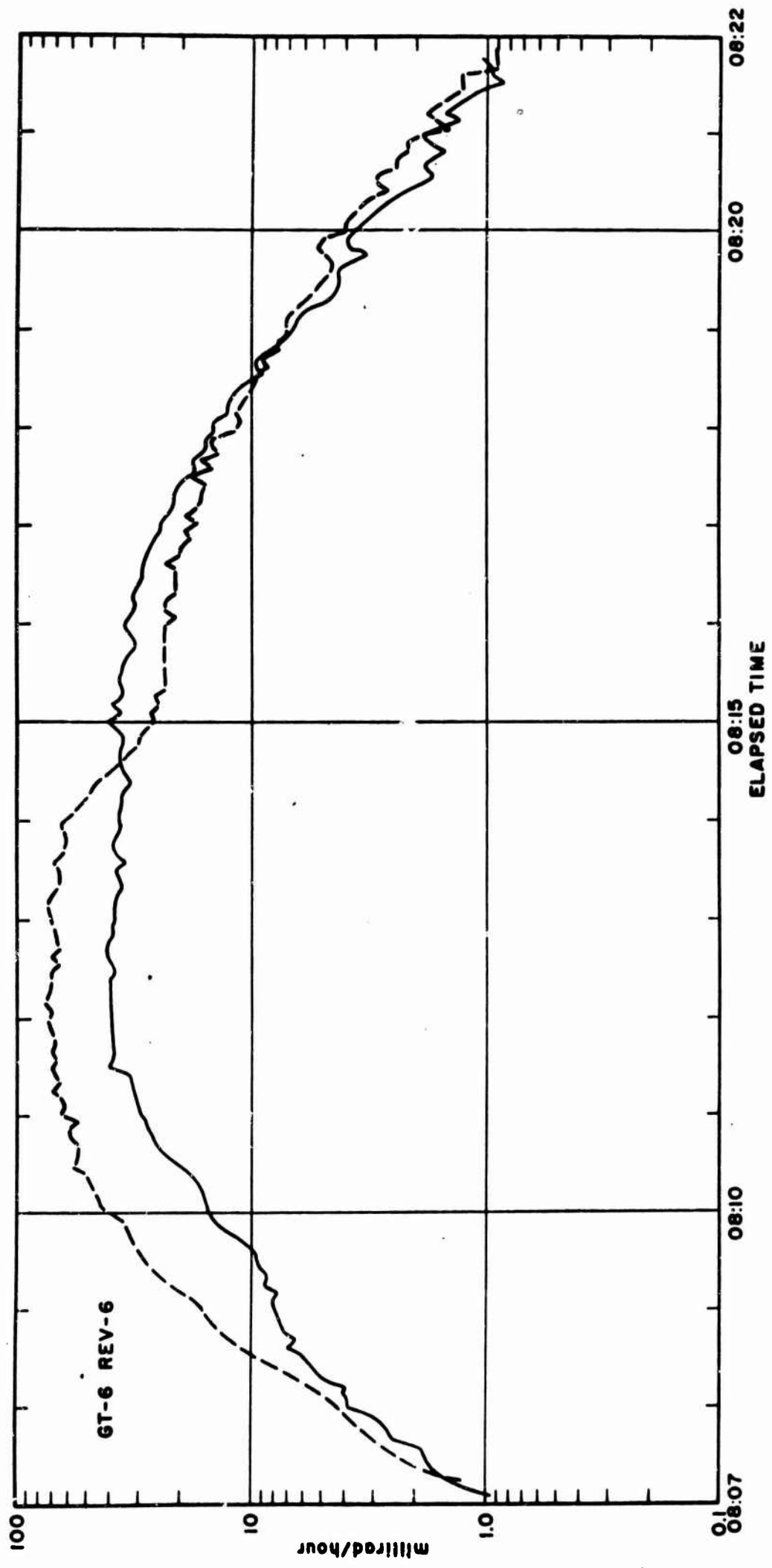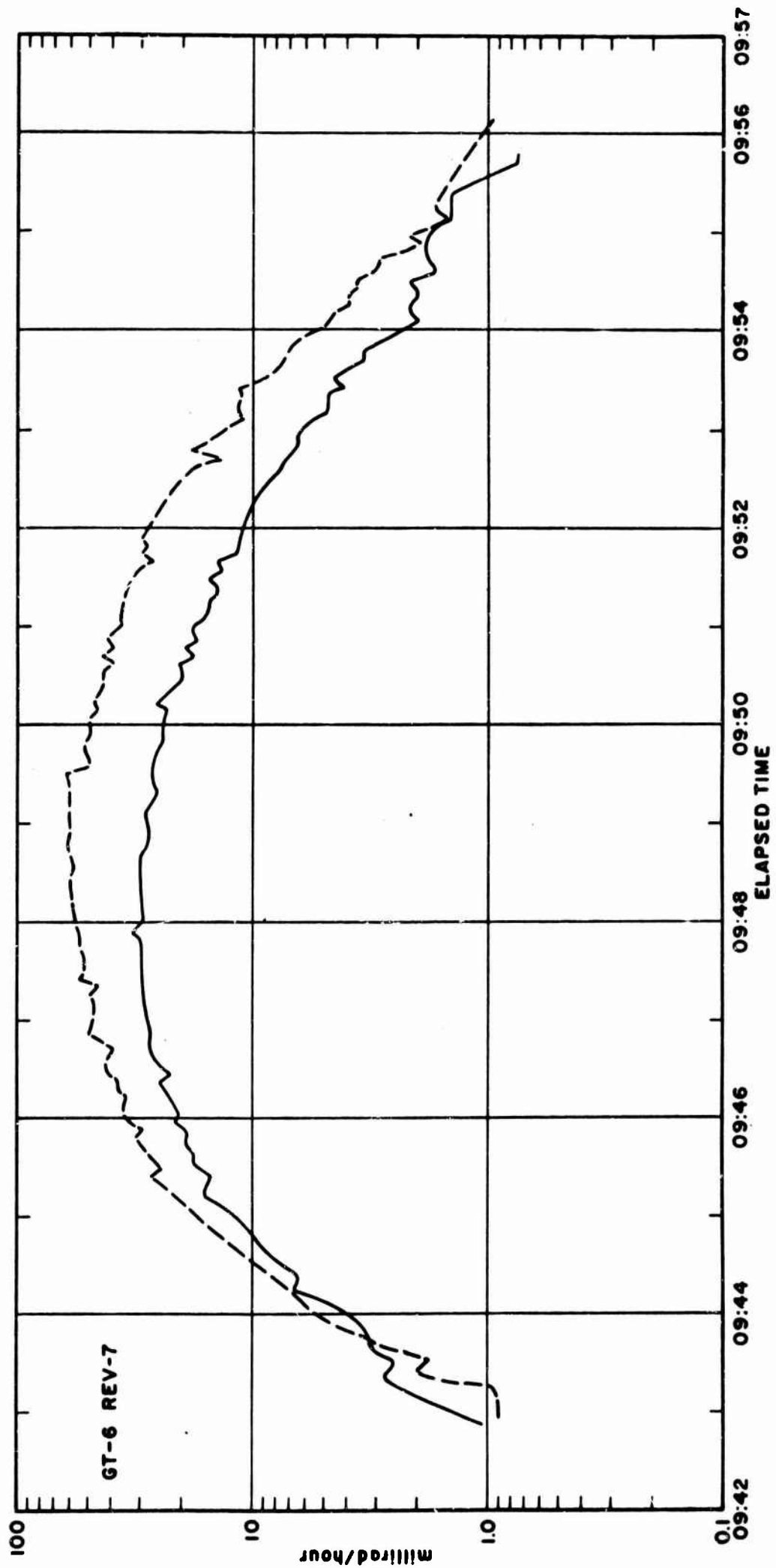
Instantaneous Dose Rate Revolution 7

Figure 104

197
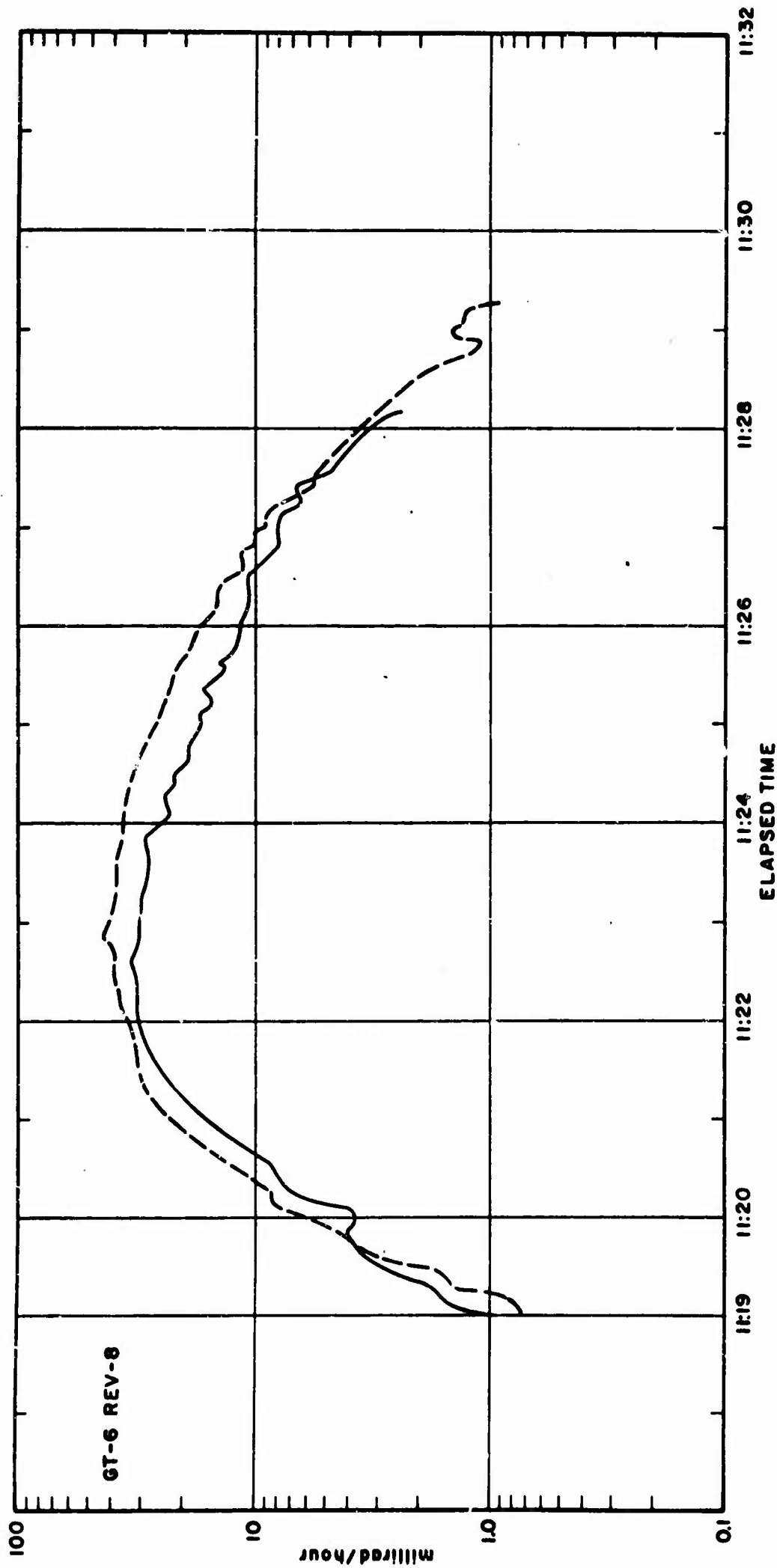
Instantaneous Dose Rate Revolution 8

Figure 105

198
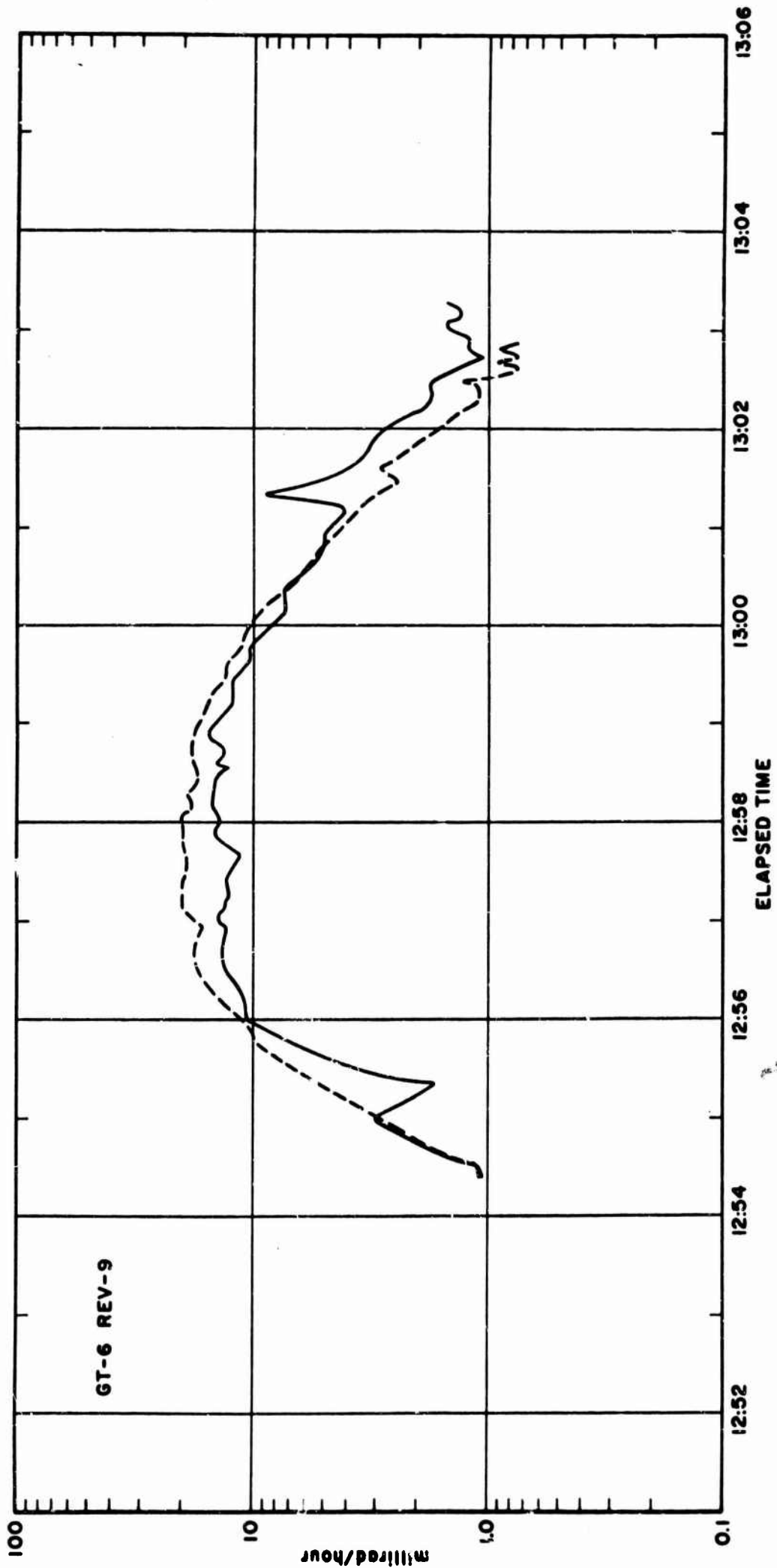
Instantaneous Dose Rate Revolution 9

Figure 106

199
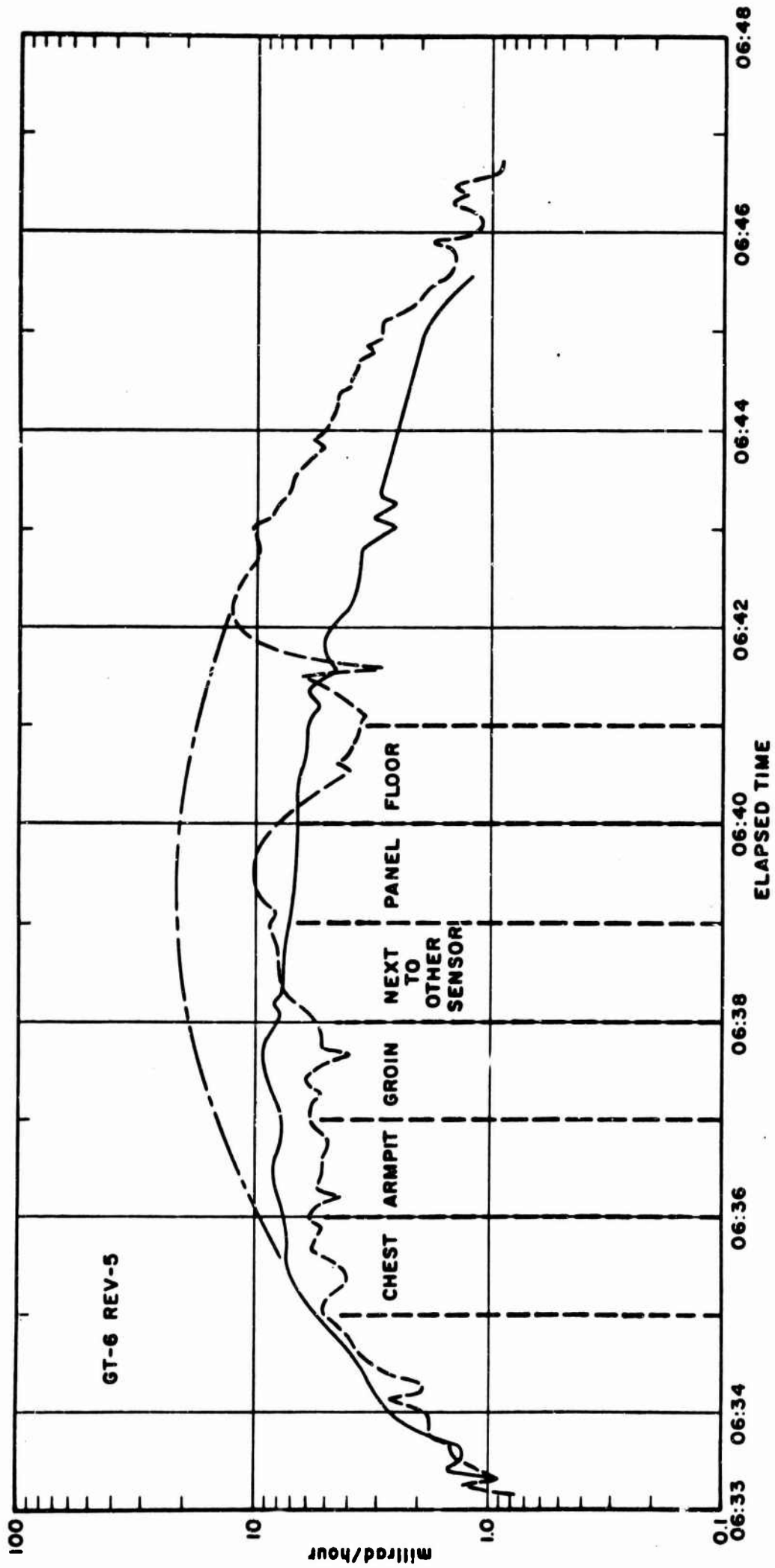
Instantaneous Dose Rate Revolution 5

Figure 107

200

geometric considerations of shielding at each of the positions recorded above. When the portable sensor was placed next to the brass shield, it was observed that both units read the same dose values. For the spectrum of exposure on this revolution, it can be seen that the shielding of a 2.5 g/cm^2 shield over a 4π solid angle is at least as effective as the 5.0 g/cm^2 shield over a 2π solid angle. The 2.5 g/cm^2 could have actually been more effective since the barrel and gloved hand of the astronaut performing the survey provided additional shielding to the portable unit, and without this the unit would have read higher than recorded here. We were not able to establish whether this relationship in shielding and dose held for deeper regions of the belt since this was the only survey of this type performed.

It is probably safe to assume that for grazing passes where the spectrum is soft, the above relationship in dose and shielding does hold. At the panel the dose level was recorded as 30% higher than behind the 2.5 g/cm^2 shield at the baseline. At the floor, however, the dose is 30% less than that behind the brass baseline shield. This indicates that the spacecraft floor is a much more effective shield than 2.5 grams of material at the hatch. The survey performed on Gemini 6, while incomplete, does confirm the fact that there is no buildup whatever in dose behind shielding. It also established the fact that many of the radiation sensitive organs of the body such as the blood forming organs are shielded sufficiently to cut the dose by a factor of two from the skin dose within the spacecraft geometries of the Gemini type in the inner belt where the spectra are not too steep. There is no experimental data to show that this type of attenuation will hold for solar flare radiation or for cosmic radiation. However, for spectra characteristic of the inner belt, it will be a good approximation to the dose attenuation factor with shielding at higher altitudes. This result agrees with attenuation factors computed by the shielding codes for the inner belt spectra.

201

Experiment D-8 allowed for the first time a comparison of recovered
passive dosimeter data with the time integrated dose from active tissue equivalent
ionization chambers. This data showed that certain passive dosimeters, parti-
cularly discharge ionization chambers, calcium fluoride thermoluminescent dosi-
meters, and film emulsion packs can provide a total dose which is sufficiently
tissue equivalent when they are exposed to the spectrum of particles that were encoun-
tered on the Gemini missions. Since the passive units do accurately assess integrated
dose for the type of radiation found in the Inner Belt, they may be employed with
full confidence in measurement of dose on future manned flights where the dose rate
is not an important consideration.

Data from this experiment served to provide empirical data to test exist-
ing computer codes for space radiation prediction capability. Initial comparison of
these measured data with calculated results using the AFWL Radiation Environment and
shielding code show that this code is not able to predict the dose within a space-
craft to more than an order of magnitude of accuracy. This poor agreement between
the predicted and measured values is attributable to to two main causes: errors in
the electron transmission coefficients and errors in the input spectra used in
the codes. The proton spectrum that caused the cabin dose was measured by MSC
Experiment 2 up to 80 Mev, but this input spectrum cannot be used to provide total
dose calculations because many particles exist above 80 Mev which also contribute
to the dose and cannot be determined from MSC-2. If accurate proton measure-
ments of the entire spectrum had been accomplished on the Gemini 4 Mission then
a true comparison of the codes performance could be made using comprehensive
input data. Since the input data to the codes is in doubt at high energies, no
direct comparison of the codes performance could be made using comprehensive input

202

data. Also, since the input data to the codes is in doubt at high energies, no direct comparison can be made of the proton transmission factors of the code. Until the code can be updated in the areas of electron transmission and input data, it is not possible to predict higher altitude, reliable, theoretical dosage interior to a spacecraft close than to a factor of two. The data from the experiment was very important in that it did establish that inaccuracies in the code existed. This was the first time that a radiation computer code had ever been checked with instantaneous dose and depth dose data gathered in a manned spacecraft.

VI. CONCLUSIONS:

The Experiment served to meet all major scientific and military objectives as planned. It can be concluded from the active dosimeter data that a negligible magnitude of dose producing biological effects exists for short term operations at less than 300 kilometers. The data also establishes the possible dangers associated with prolonged operations at altitudes above 550 kilometers with the Gemini shielding profile.

VII. RECOMMENDATIONS:

While the Gemini type of dosimetry system was designed to measure radiation fluxes such as found in solar flares and natural and artificial radiation belts, it does not have a suitable response time for the measurement of prompt radiation, e.g., microsecond pulses as are generated by nuclear explosions. Further development in the important field of pulsed radiation dosimetry detection is recommended to support future military space missions where all possible sources of radiation must be considered.

Theoretical computer codes evidently cannot predict radiation doses to better than an order of magnitude unless exact shielding breakdowns in conjunction with highly reliable input data are provided. Even then, unpredictable

203

sources such as solar flares and natural radioactivity of space bodies exist and could not be theoretically predicted even if the spacecraft shielding parameters were exactly known. Radiation computer codes should be used as mission planning guides but are not substitutes for dose measuring and radiation warning devices carried aboard a spacecraft.

In producing biological effects it has been mentioned that two quantities are of importance. These are the dose or dose rate, and the microscopic or local distribution of the dose which is called the Linear Energy Transfer or LET. Measurement of the Linear Energy Transfer of the radiation field becomes important in determining the dangerous effects when the dose or total energy deposited in a system approaches the lower limit for producing biological effects. Also, evidence shows that the number of times a man can be subjected to sub-lethal dose is directly related to LET of the radiation to which he is exposed. It is therefore most important when the radiation field is on the order of 10 rads or more, when solar flares are anticipated, or when long exposure to cosmic radiation of high specific ionization is indicated that LET instruments be included in the dosimetry system to insure total coverage of the radiation conditions. Development programs for a LET system are not needed since such hardware now exists on the shelf in the Air Force inventory of radiation equipment for spaceflight.

It is most strongly recommended that active dosimetry systems such as developed for Gemini be augmented with LET and pulse radiation measurement instruments and be carried on future manned space missions.

APPENDIX (A)

BRAGG-GRAY THEORY

Let a block of material be irradiated with gamma rays. A flux of secondary electrons M(E) from pair production, Compton, and photoelectric electrons will be produced. In the interior of this piece of material, consider a small region T with a certain linear dimension a.
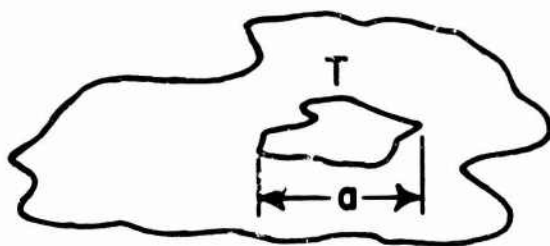
The energy lost by an electron crossing this region will then be $(a)(dE/dx)$. The energy lost per second by the entire spectrum is

$$E_{solid} = M(E,\theta)\, a(\theta)\, \frac{dE}{dx}_{solid}\, d\theta\, dE$$

Make T small enough so that its removal will not change M(E). If the solid material in the region is now removed, and the resulting cavity filled with a gas, the energy lost per second in the gas is

$$E_{gas} = \int M(E,\theta)\, a(\theta)\, \frac{dE}{\partial x}_{gas}\, d\theta\, dE$$

The ratio of the two integrals is the relative stopping power S.

$$\frac{\dfrac{dE}{dx}\,solid}{\dfrac{dE}{dx}\,gas} = \frac{E_{solid}}{E_{gas}}$$

or

$$E_{solid} = SE_{gas}$$

The energy per cubic centimeter of gas may be written as

$$E_{gas} = WJ$$

where W is the energy to produce an ion pair in the gas, and J is the ion current in ion pairs per cubic centimeter per second. Combining the above two

equations gives the Bragg-Gray principle

$$E_{solid} = SWJ_{gas}$$

An alternate method of writing is

$$E_M = S_M WJ_M$$

where E_M = energy absorption of ev/gm sec

. S_M = mass stopping power of the wall material relative to the cavity gas

J_M = ion current in ion pairs per gm per second.

APPENDIX (B)

Optimization of Electrometer Operating Point

It has been theoretically shown [7,8] and experimentally measured that a floating grid logarithmic triode obeys the current transfer relationship

$$i_p = (s \, \log_{10} i_g + q)^a$$

where

i_p = plate current

i_g = grid current

s, q, are determined by operating conditions and tube construction. The value of "a" in the above expression can be made close to one by the addition of sufficient (24 K ohms in the case of the CK5889) plate resistance to cause linear negative feedback to the preamplifier. In the case of the actual selected conditions for the sensor electrometer:

a = 1.10

s = 4.0 $\pm$ 0.2 for i_p expressed in microamps

q = 70.0 $\pm$ 7.0

Reading Resolution:

To obtain a greatest resolution in grid current, i_g for a fixed percentage reading error in plate current, i_p, define an error k such that

$$\frac{di_p}{i_p} = k$$

from

$$i_p = s \, \log_{10} i_g + q \quad \text{where } a \to 1$$

differentiating:

$$\frac{di_g}{i_g} = \frac{di_p}{s}$$

207

since:

$$di_p = ki_p$$

The percentage error of i_g is

$$\frac{di_g}{i_g} = \frac{ki_p}{s}$$

To maximize ion current reading resolution, a low ratio of i_p/s should be picked. It has been determined experimentally that the logarithmic gain per decade, s, is only slightly affected by operating plate current or voltage, and that smallest i_p/s occurs at the lowest possible plate current, i_p.

Drift Error:

Again using the original logarithmic transfer function, and calculating error referred to input as a function of changes in the tube operating parameters, s and q:

$$\frac{di_g}{i_g} = \frac{-sdq - ds(i_p - q)}{s^2}$$

$$\% \text{ error} = \frac{di_g}{i_g} = \frac{q}{s}\left(\frac{ds}{s} - \frac{dq}{q}\right) - \frac{i_p}{s}\left(\frac{ds}{s}\right)$$

As shown above, $(ds)/s \approx (dq)/q$, and furthermore the coefficient i_p/s is the most significant; therefore, the drift error equation can be reduced to:

$$\% \text{ error} = \frac{di_g}{i_g} \approx \frac{-i_p}{s}\left(\frac{ds}{s}\right)$$

Again, the input error is least significant for the highest ratio of (i_p/s) or for small plate currents.

Temperature Dependence:

For triodes with essentially planar geometry, such as the CK5889, Langmuir shows that initial electron velocities modify the plate power relationship in the following manner:

208

$$i_p = G\left(kT \log \frac{i_g}{i_{go}} + \frac{1p}{u} - V_m\right)^a \left\{ 1 + 2.66 \left[\frac{kT}{1\left(kT \log \frac{i_g}{i_{go}} + \frac{1p}{u} - V_m\right)} \right]^{1/2} \right\}$$

Where V_m is the minimum potential between plate and cathode, it can be shown from the preceding expression that

$$kT \log \frac{i_g}{i_{go}} + \frac{1p}{u} - V_m$$

can be set to a proper value so that a change in filament temperature, T, will introduce offsetting errors in the plate current terms. The balancing factor (1p/T) must be experimentally selected to null tube temperature and emission dependence. Thus, the selection of a low operating plate voltage, e_p, enables tube operation at a lower filament temperature, thus increased element lifetime and reduced power dissipation.

APPENDIX (C)

BENCH TEST PROCEDURE
EXPERIMENT D-8

A. **Test Equipment Requirements:**

1. Power supply - Hewlett-Packard Model 721A or equivalent.

   Requirements - $24 \pm .3$ VDC at 21 ma max.

2. Tektronic 545A oscilloscope with Type L preamp.

3. Voltmeter - Hewlett-Packard Model 412A or equivalent to read

   0-20 mv d.c. signal. Input must be floating.

4. Test fixture - Avco supplied.

B. **Test Preparations:**

Connect instruments to test circuit shown in Fig   Power switch S_1
should be in the "off" position. Switch S_2, S_3 and S_4 should be in
position 1. Set the VTVM to the .030 VDC scale. Set oscilloscope
amplitude to .050 volts/cm and sweep speed to 50 us/cm.

C. **Tests:**

1. Input current: Turn power switch S_1 to the "on" position. Read
   and record input current on meter M_1. Requirements: 31 ma max.

2. Type IV output #1: Read and record E_0 on the VTVM for switch
   S_2 in positions 1, 2 and 3. Requirements: E_0 should be as
   follows:

S_2 Position	E_0 (millivolts d. c.)
1	0.0 ± 0.2
2	10.0 ± 0.4
3	20.0 ± 0.7

3. Type IV output #1 ripple: Read and record the P-P ripple on
   the oscilloscope. Requirements: 50 mv P-P max.

4. Type I output #1: Place switch S_2 in position 1 and switch S_4 in position 2. Read and record E_o on the VTVM for all 9 positions of switch S_3. Requirements:

S_3 Position	E_o (millivolts d. c.)
1	0.0 ± 0.2
2	2.5 ± 0.2
3	5.0 ± 0.3
4	7.5 ± 0.3
5	10.0 ± 0.4
6	12.5 ± 0.4
7	15.0 ± 0.5
8	17.5 ± 0.6
9	20.0 ± 0.7

5. Type I output #2: Place switch S_4 in position 3 and record E out on the VTVM for all 9 positions of switch S_3. Requirements:

S_3 Position	E_o (millivolts d. c.)
1	0.0 ± 1.5
2	12.5 ± 1.5
3	5.0 ± 2.0
4	17.5 ± 2.0
5	10.0 ± 2.5
6	12.5 ± 2.5
7	15.0 ± 3.0
8	7.5 ± 3.5
9	20.0 ± 4.0

6. Type I output #1 ripple: Place switch S_4 in position 2 and switch S_3 in position 9. Read and record the P-P ripple on the oscilloscope. Requirements: 50 mv P-P max.

7. Type I output #2 ripple: Repeat test 6 with S_4 in position 3.

8. Type I output #3 calibration: Place switch S_4 in position 4. Read and record the peak amplitude and period between pulses. Requirements: The peak amplitude should be 3.0 ± 1 volt d. c. The period between pulses should be 4.0 ± 1 min.
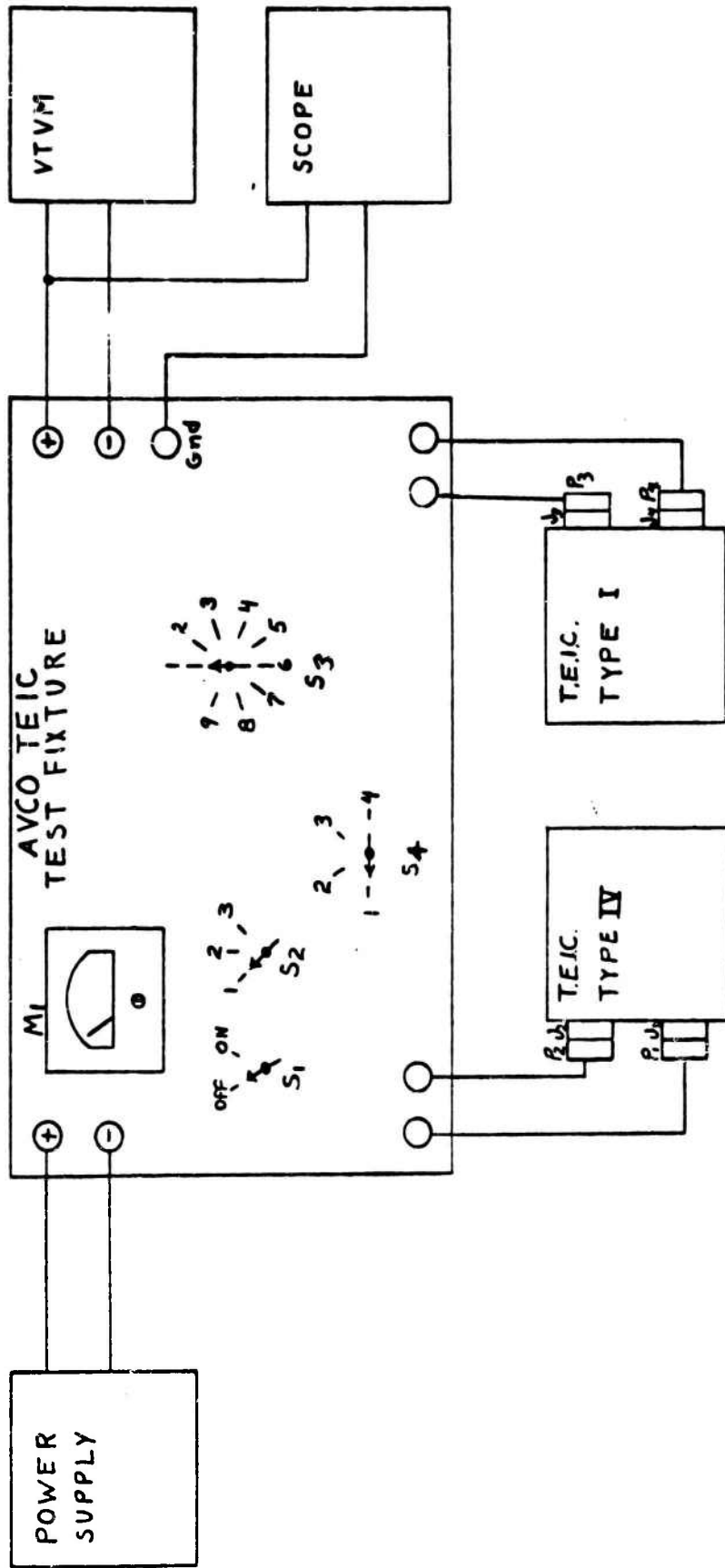
Pench Desk Fixture

Figure 108

212

APPENDIX (D)

SST TEST PROCEDURE

TIME	COMM CH	SEQUENCE	SYSTEM AREA	Description	REMARKS
		08-000		**DOD EXPERIMENT NO. 8 TEST**	
				The purpose of this is to verify the operation of the dose rate chambers.	
		08-001	TE	All stations report status on command	
				SCO/1 TM/2 RE N1 M1 NLE	
		08-002	TE	TM/2	Verify PCM ground station setup per test prep sheet No. 4. Verify patch from hardline to bit synchronizer. Setup brush recorder to record XB01, XB02, XB03, XB18, XB17 and XB06.	
		08-003	TE	SCO/1	Bio-med inst C/B - on /verify/	
				SCO/2	DC-DC Conv SW - PR1 DC-DC Conv C/B - ON	
		08-004	TE	TM/2	Make a 15 minute brush recording of XB01, XB02, XB03, XB18, XB17 and XB06.	

NOTE

The brush recorder recordings will be evaluated by the radiation engineer at end of this sequence.

NOTE

The location of the radiation source in reference to the dose rate chambers will be determined by the radiation engineer.

INSP.

213

TIME	COMM CH	SEQUENCE	SYSTEM AREA		Description	REMARKS
		08-005	TE	RE	Position radiation source plunger to the No. 3 position with it in a position to excite the fixed unit.	
		08-006	TE	TM/2	Make a 15 minute /max/ brush recording of XB01, XB02, XB17 and XB06.	
		08-007	TE	RE	Position radiation source to excite the removable unit.	
		08-008	TE	TM/2	Make a 1 minute brush recording of XB03 and XB18.	
		08-009	TE	RE	Position radiation source plunger to the No. 5 position with it in a position to excite the fixed unit.	
		08-010	TE	TM/2	Make a 15 minute /max/ brush recording of XB01, XB02, XB17 and XB06.	
		08-011	TE	RE	Position radiation source to excite the removable unit.	
		08-012	TE	TM/2	Make a 1 minute brush recording of XB03 and XB18.	
		08-013	TE	RE	Return radiation source to safe position.	
		08-014	TE	RE	Evaluate brush recordings and verify operation of XB01, XB02, XB17, XB06, XB03 and XB18.	
				RE	Brush recording evaluated and correct operation of XB01, XB02, XB17, XB06, XB03 and XB18 verified.	
		08-015	TE	SCO/1	DC-DC Conv C/B - OFF	

ACTIVE OSIMETER CAPE CHECKOUT PROCEDURE SEDAR H453-6

TIME	COMM CH	SEQUENCE	SYSTEM	AREA	Description
		08-021			D8 RADIATION CALIBRATIC
	59	08-021A	TM	TMH	Record all decimal read ts on PCM Table 5. *
	59	08-022	TM	PL	Verify following switch settings conditions. 　DC-DC Conv sel SW - primary or secondary. 　DC/DC Conv C/B - on
	59	08-023	TM	PL	Remove protective covers from the Type 1 and Type V dose rate chambers.
	59	08-024	TM	TMH	Make a 15 minute brush recording of XB01, XB02, XB03, XB06, XB17 and XB18. Make decimal readouts of foregoing.
	59	08-025	TM	RE	Position radiation source plunger to the No. 1 setting and place radiation source in a position to excite the removable dose rate chamber.
	59	08-026	TM	TMH	Make a 1 minute brush recording of XB03 and XB18. Make decimal readouts of foregoing.
	59	08-027	TM	RE	Place radiation source plunger to the No. 5 setting and place radiation source in a position to excite the removable dose rate chamber.
	59	08-028	TM	TMH	Make a 1 minute bruch recording of XB03 and XB18. Make decimal readouts of foregoing.
	59	08-029	TM	RE	Position radiation source plunger to the No. 1 setting and place radiation source in a position to excite the fixed dose rate chamber.
	59	08-030	TM	TMH	Make a 1 minute brush recording of XB01, XB02, XB06 and XB17. Make decimal readouts of foregoing.

TIME	COMM CH	SEQUENCE	SYSTEM	AREA	Description
	59	08-031	TM	RE	Place radiation source plunger to the No. 5 setting and place radiation source in a position to excite the fixed dose rate chamber.
	59	C8-032	TM	TMH	Make a 15 minute brush recording of XB01, XB02, XB06 and XB17.

Make decimal readouts of foregoing.*

*Decimal readouts can be interpreted from recorder data using as basis:

$$0\% = 001 \text{ counts}$$
$$100\% = 254 \text{ counts}$$

TIME	COMM CH	SEQUENCE	SYSTEM	AREA	Description
	59	08-033	TM	RE	Remove radiation shield.
	59	08-034	TM		Repeat seq's 029 thru 032
	59	08-035	TM	RE	Replace radiation shield.
	59	08-036	TM	RE	Return the radiation source plunger to the safe position.
-1260	59	08-037	TM	PL	Reinstall protective covers.

NOTE

Final removal of covers is planned for F minus 145 minutes on (SEDAR H463, H452).

TIME	COMM CH	SEQUENCE	SYSTEM	AREA	Description
	59	08-038	TM	STE	Experiment tests satisfactorily completed.

APPENDIX (F)

DOSE FACTORS

Since gamma radiation sources are utilized as the primary standard for all voltage to dose conversions performed for the Active Dosimeters, suitable conversion factors must be applied to obtain the absorbed dose from the exposure dose. The standard Cobalt-60 and Cesium-137 gamma radiation sources utilized in experiment D-8 were calibrated by the National Bureau of Standards using Victoreen R meters which provide the exposure dose in Air at STP.

The exposure dose of X or γ radiation is defined to be the ion charge ΔQ of either sign produced in air by the secondary electrons, which are produced by the primary X or γ radiation in a small mass Δm of air divided by Δm The standard unit of exposure is the Roentgen which is defined: One roentgen of X or γ radiation is equal to the production of air os 1 esu of ions of either sign along the tracks of electrons generated in 1.293 x 10^{-3} gram or 1 cubic centimeter of dry air at STP at a point by X or γ rays whose energy is less that 3 Mev.

The absorbed dose of any ionizing radiation at a point is defined as the ionizing energy absorbed per gram of irradiated material at the point of interest. The fundamental unit of absorbed dose is the RAD which is defined as the absorbtion of 100 ergs of energy per gram of material.

The Bragg-Gray Cavity Relation relates the absorbed dose to the ionization produced in a small gas-filled cavity inserted in the medium under equilibrium conditions at the place of interest in the material irradiated:
The Bragg-Gray relationship may be written:

$$\frac{dE}{dm} \text{(tissue)} = S_m wJ$$

For tissue the mass stopping power witn respect to dry air is taken as (1.11). w is taken to be 34 electron volts per ion pair in accordance with the ICRU recommended value (NBS Handbook 62, 1957).

217

$$J = \left(\frac{1 \text{ esu}}{1.293 \times 10^{-3} \text{ g of air}} \right) \left(\frac{1}{4.80 \times 10^{-10}} \quad \left| \frac{\text{ion pair}}{\text{esu}} \right| \right)$$

$$= \quad (1.6 \times 10^{12} \text{ ion pairs/gram air}) (1.6 \times 10^{-19} \frac{\text{ergs}}{\text{ion pair}})$$

$$= \quad 2.58 \times 10^{-7} \text{ coulomb/gram}$$

Substitution of these values into the Bragg-Gray formula gives following result:

$$\frac{dE}{dm} = \frac{(1.11)(34.0)(2.58 \times 10^{-7})(1.60 \times 10^{-12})}{1.60 \times 10^{-19}} = 96 \text{ ergs/gram}$$

Thus the absorbed dose D is proportional to the exposure dose in roentgens which we will call R.

$$D \text{ (rad)} = kR \text{ (roentgen)}$$

$$\therefore \quad k = .96 \frac{\text{rad}}{\text{roentgen}}$$

One roentgen of exposure dose is therefore seen to equal 0.96 rad of absorbed dose in tissue. This conversion factor was utilized throughout the calibrations performed in this effort. For materials other than tissue such as bone and air this attenuation factor will not apply. Also where the photon energy falls below 0.1 Mev., the photoelectric absorption processes dominate and this factor falls to a lower value than at the higher energies of calibration. Figure 109 illustrates the behavior of the proportionality factor for several materials and useful range of photon energies of irradiation.

ABSORBED DOSE IN RADS PER ROENTGEN OF EXPOSURE DOSE, f, VERSUS PHOTON ENERGY
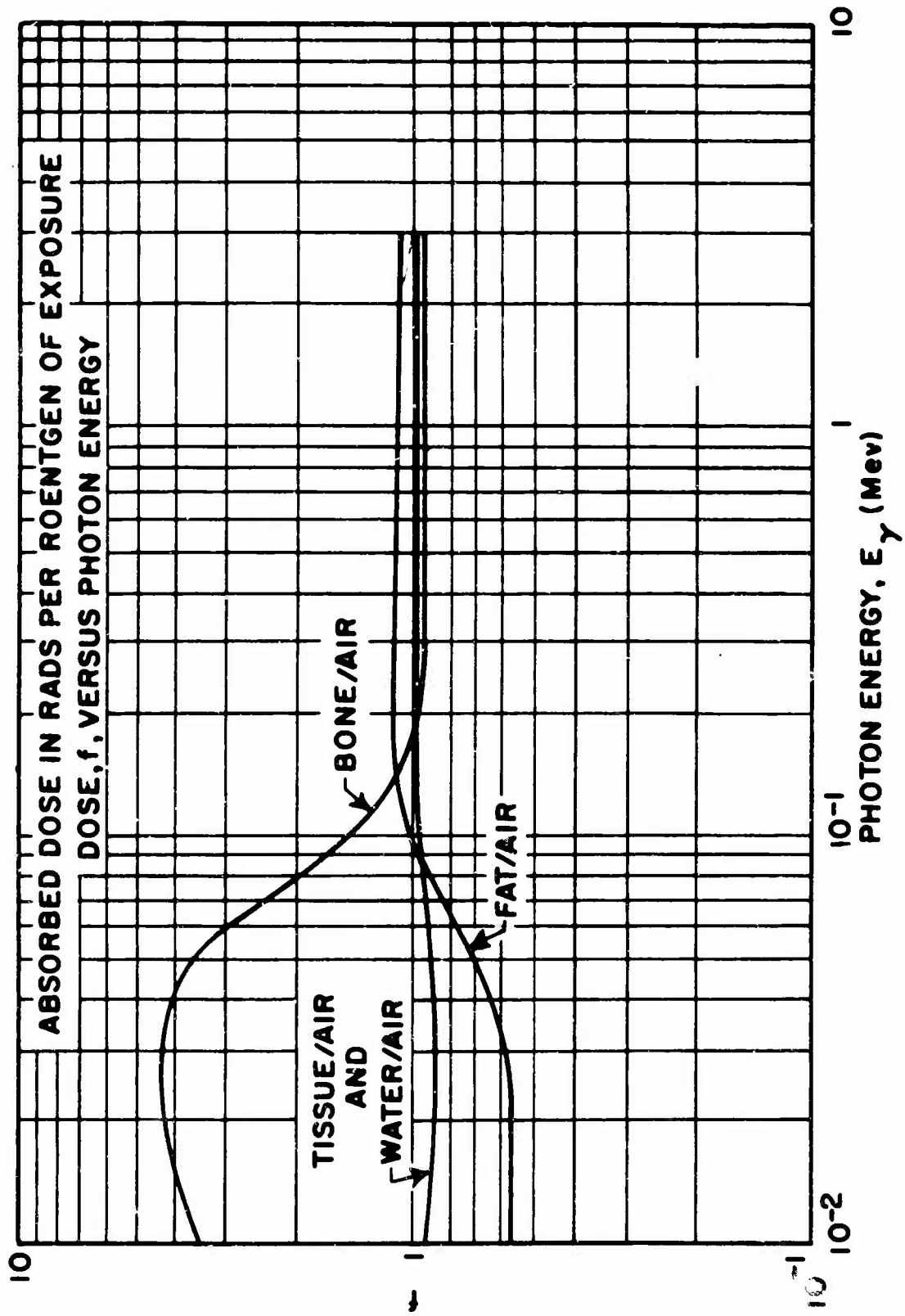
Figure 109

219

APPENDIX (G)

PRE-INITIATION ACCEPTANCE TEST PROCEDURE RADIATION

EXPERIMENT D-8 SEDAR 322

PART I

ACTIVE DOSIMETER PIA TEST EQUIPMENT

GEMINI FLIGHTS 4 & 6

AGE REQUIRED		SER NO.	PREV. SEDR USAGE	OPEN PAPERWORK			
PART NUMBER	NAME			DR'S MRR'S	MPR's	EO'S	OTHER
Model 297	Chart Recorder, Sanborn (Or Equivalent)						
Model 850-1300B	Pre-Amplifier, Sanborn (Or Equivalent) (2 each)						
Model 52E440073-1	TEIC Test Set (Supplied by Vendor)						
Model V-35	Digital Voltmeter, NLS (Or Equivalent)						
Model CR36-8	D.C. Power Supply, NJE (Or Equivalent)						
Model SM36-15M	D.C. Power Supply, KEPCO (Or Equivalent)						
Model SM26-15M	D.C. Power Supply, KEPCO (Or Equivalent)						
Model 453	Radiation Source, AVCO (Supplied by Vendor)						
N/A	Calibration Curve for Active Dosimeter Unit S/N (Supplied by Vendor)						

220

PART II

TEST PROCEDURES

2.1.1.1   TISSUE EQUIVALENT IONIZATION CHAMBER

TYPE V

2.1.1.2   EQUIPMENT REQUIRED

REFER TO TEST PREPARATION SHEET NO. 1; AGE TEST READINESS SUMMARY

FOR TISSUE EQUIVALENT IONIZATION CHAMBER SERIAL NUMBER.

2.1.1.3   FACILITY REQUIREMENT(S)

115 ($\pm$6) VOLTS AC, 60 ($\pm$1%) CPS, 15 AMPERES MAXIMUM

2.1.1.4   TEST SET-UP

(A)   VERIFY TEST EQUIPMENT IS VALIDATED PER PART I.

(B)   MOUNT TEIC TEST SET (52E440073-1) IN PLACE OF BLANK PANEL

NO. 2 OR NO. 9 OF S/C INSTRUMENTATION TEST SET (52E440040-3)

RACK # 215.

NOTE

STANDARD COMMERCIAL EQUIPMENT MAY BE

USED IN LIEU OF INSTRUMENTATION TEST

SET (52E440040-3, RACKS 215 AND 216).

(C)   SET TEIC TEST SET SWITCHES AS FOLLOWS:

(1)   POWER SWITCH - OFF

(2)   CHASSIS ISOLATION TEST SWITCH - INDICATOR TEST

(3)   CURRENT MONITOR SELECT SWITCH - OFF

(4)   OUTPUT SELECT SWITCH - VOLTAGE MONITOR

(5)   ROTATE FINE AND COARSE ADJ DIALS FULLY CLOCKWISE.

(D) CONNECT RECORDER HARNESS (52E440040-3) FROM TEIC TEST SET COARSE OUTPUT SBRN TERMINALS TO CHANNEL B PRE-AMPLIFIER INPUT CONNECTOR ON FRONT PANEL OF 2-CHANNEL RECORDER IN RACK #215 OF S/C INSTRUMENTATION TEST SET. ADJUST THE VOLTAGE SENSITIVITY ON RECORDER SO THAT RECORDING CHART WILL SHOW 0.05 VOLTS/MM.

(E) CONNECT VOLTAGE MONITOR OUTPUT OF TEIC TEST SET TO THE D.V.M. INPUT OF THE TAPE TEST PATCH PANEL (RACK #216).

(F) CONNECT TEIC TEST SET 24 VDC POWER INPUT TERMINALS TO RACK #216 POWER SUPPLY FRONT PANEL OUTPUT TERMINALS. SET POWER SUPPLY SWITCH ON AND ADJUST VOLTAGE TO APPROXIMATELY 24 VDC.

(G) PLACE TEIC TO BE TESTED ON ANY INSULATING SURFACE.

NOTE

TEIC CHASSIS IS TO BE ISOLATED

FROM RACK #216 CHASSIS

(H) CONNECT CABLE HARNESS (52E440073-5) BETWEEN TEIC TEST SET (J1) AND TEIC.

(I) SET VOLTAGE MONITOR SELECT SWITCH (ON TEIC TEST SET) TO 24 VDC POSITION.

(J) SET POWER SWITCH (ON DIGITAL VOLTMETER AND RECORDER) TO ON POSITION.

NOTE

ALLOW 15 MINUTES FOR EQUIPMENT TO WARM-UP

(K) ROTATE DC POWER SUPPLY DIAL UNTIL DVM INDICATES 24 ± 0.1 VDC.

NOTE

ALLOW 60 MINUTES FOR TEIC TO WARM-UP

(L) THIRTY (30) MINUTES BEFORE WARM-UP TIME HAS ELAPSED, REMOVE ENDS FROM RADIATION SOURCE FIXTURE AND PLACE AGAINST TEIC.

CAUTION

HANDLE RADIATION SOURCE FIXTURE WITH CARE

(1) PLACE CALIBRATE JUG UP TO SPHERE WITH ALL THREE (3)
POINTS OF FIXTURE TOUCHING SPHERE.

(2) EXTEND LUCITE ROD, HOLDING SOURCE, OUT TO MAXIMUM POSITION
AND DROP PIN IN POSITION AT THIS POINT.

1.5   CHASSIS ISOLATION TEST

(A) SET CHASSIS ISOLATION TEST (ON TEIC TEST SET) TO INDICATOR
     TEST POSITION. VERIFY CHASSIS ISOLATION TEST INDICATOR
     ILLUMINATES.

(B) SET CHASSIS ISOLATION TEST SWITCH TO CHASSIS FLOATING POSITION.
     VERIFY CHASSIS ISOLATION INDICATOR EXTINGUISHES.

(C) SET CHASSIS ISOLATION TEST SWITCH TO ISOLATION TEST POSITION.
     CHASSIS ISOLATION INDICATOR SHOULD REMAIN EXTINGUISHED. RECORD
     RESULTS ON TEST DATA SHEET.

                          NOTE

          CHASSIS IS NOT ISOLATED FROM POWER RETURN

          IF CHASSIS ISOLATION INDICATOR IS ILLUMINATED

(D) SET CHASSIS ISOLATION TEST SWITCH TO INDICATOR TEST POSITION.

1.6   CURRENT MONITOR AND POWER INPUT

(A) SET CURRENT MONITOR SWITCH (ON TEIC TEST SET) TO ON POSITION.
     RECORD CURRENT (I_{IN}) INDICATION ON TEST DATA SHEET.

(B) CALCULATE POWER INPUT: $P_{IN} = 24\ I_{IN}$. RECORD CALCULATED POWER
     P_{IN} ON TEST DATA SHEET.

1.7   RADIATION RATE CALIBRATION AND DUTY CYCLE TEST

       AMBIENT (ZERO) RADIATION TEST

(A) REMOVE RADIATION SOURCE FIXTURE FROM TEIC.

(B) ROTATE VOLTAGE MONITOR SELECT SWITCH (ON TEIC TEST SET) TO
     COARSE POSITION.

1.8   RADIATION CALIBRATE SOURCE POSITION #1 (CONTINUED)

(E) REFER TO CALIBRATION CURVE FOR TYPE V UNIT. OBTAIN RADIATION
     MEASUREMENT CORRESPONDING TO VOLTAGE READING IN STEPS (B) AND
     (D). READ AND RECORD CORRESPONDING RAD/HR ON TEST DATA SHEET.

1.9   RADIATION CALIBRATE SOURCE POSITION #2

      (A) SET RADIATION RATE CALIBRATION SOURCE FIXTURE TO POSITION #2.

      (B) RECORD DVM VOLTAGE INDICATION ON TEST DATA SHEET.

      (C) ROTATE VOLTAGE MONITOR SELECT SWITCH TO FINE POSITION.

      (D) RECORD DVM VOLTAGE INDICATION ON TEST DATA SHEET.

      (E) REFER TO CALIBRATION CURVE FOR TYPE V UNIT. OBTAIN RADIATION
MEASUREMENT CORRESPONDING TO VOLTAGE READING IN STEPS (B) AND
(C). READ AND RECORD CORRESPONDING RAD/HR ON TEST DATA SHEETS.

2.0   RADIATION CALIBRATE SOURCE POSITION #3

      (A) SET RADIATION RATE CALIBRATION SOURCE FIXTURE TO POSITION #3.

      (B) RECORD DVM VOLTAGE INDICATION ON TEST DATA SHEET.

      (C) ROTATE VOLTAGE MONITOR SELECT SWITCH TO COARSE POSITION.

      (D) RECORD DVM VOLTAGE INDICATION ON TEST DATA SHEET.

      (E) REFER TO CALIBRATION CURVE FOR TYPE V UNIT. OBTAIN RADIATION
MEASURE CORRESPONDING TO VOLTAGE READING IN STEPS (B) AND (D).
READ AND RECORD CORRESPONDING RAD/HR ON TEST DATA SHEET.

2.1   RADIATION CALIBRATION SOURCE POSITION #4

      (A) SET RADIATION RATE CALIBRATION SOURCE FIXTURE TO POSITION #4

      (B) RECORD DVM VOLTAGE INDICATION ON TEST DATA SHEET.

      (C) ROTATE VOLTAGE MONITOR SELECT SWITCH TO FINE POSITION.

      (D) RECORD DVM VOLTAGE INDICATION ON TEST DATA SHEET.

      (E) REFER TO CALIBRATION CURVE FOR TYPE V UNIT. OBTAIN RADIATION
MEASUREMENT CORRESPONDING TO VOLTAGE READING IN STEPS (B) AND
(D). READ AND RECORD CORRESPONDING RAD/HR ON TEST DATA SHEETS.

2.2   RADIATION CALIBRATE SOURCE POSITION #5.

      (A) SET RADIATION RATE CALIBRATION SOURCE FIXTURE TO POSITION #5.

      (B) RECORD DVM VOLTAGE INDICATION ON TEST DATA SHEET.

      (C) ROTATE VOLTAGE MONITOR SELECT SWITCH TO COARSE POSITION.

(D) <u>RECORD</u> DVM VOLTAGE INDICATION ON TEST DATA SHEET.

(E) SET THE FOLLOWING POWER SWITCHES OFF: TEIC TEST SET, DIGITAL VOLTMETER & D.C. POWER SUPPLY.

2.3 REFER TO CALIBRATION CURVE FOR TYPE V UNIT. OBTAIN RADIATION MEASUREMENT CORRESPONDING TO VOLTAGE READING IN STEPS (B) AND (D). READ AND <u>RECORD</u> CORRESPONDING RAD/HR ON TEST DATA SHEET.

2.4 DISCONNECT ALL EQUIPMENT CONNECTED TO EQUIPMENT UNDER TEST. RADIATION MEASUREMENTS EQUIPMENT TEST PROCEDURES HAVE BEEN COMPLETED.

2.5 <u>RECORD</u> WEIGHT OF TEIC TYPE V UNIT ON TEST DATA SHEET.

226

HIGHEST PCN #_____   <u>P.I.A. TEST DATA SHEET</u>

NAME: <u>TISSUE EQUIVALENT IONIZATION CHAMBER</u>   NAA P/N: _____

MFGR. & P/N <u>67975 S/N</u>   <u>TYPE V</u>

DATE TEST PERFORMED:_____   TEST FACILITY: ____   OP. TIME THIS TEST_____

INSTRUCTIONS: THIS TEST DATA SHEET IS TO BE USED IN CONJUNCTION WITH THE APPROPRIATE SEDR <u>PIA ( )</u> UPON COMPLETION

WAS SPECIFIED TEST EQUIPMENT USED: YES___ NO___ IF NO, SPECIFY EQUIPMENT USED.

MFGR_____   MODEL_____   S/N _____

VALIDATION ACCEPTANCE (AGE) _____

                       MISSION EXPERIMENTER

PARA	TEST PARAMETER	RECORD	LIMIT	INSPECTION
1.5		-------		_____
1.6	(A) CURRENT, I_{IN}		12 MA MAX	_____
	(B) POWER, P_{IN}		300 MW MAX	_____
1.7	ZERO RADIATION			
	(C) COARSE VOLTS		0.2 ± 0.2 VDC	_____
	(E) FINE VOLTS		1 ± 1 VDC	_____
1.8	SOURCE POSITION #1			
	(B) FINE VOLTS		REFERENCE	_____
	(D) COARSE VOLTS		REFERENCE	_____
	(E) RADIATION MEASUREMENT			
	FINE		130 ± 52 MRAD/HR	_____
	COARSE		130 ± 52 MRAD/HR	_____

                                INSPECTION   DATE

HIGHEST PCN #_____   P.I.A. TEST DATA SHEET

DATE TEST PERFORMED:_____

PARA.	TEST PARAMETER	RECORD	LIMIT	INSPECTION
1.9	SOURCE POSITION #2			
	(B) COARSE VOLTS		REFERENCE	_____
	(D) FINE VOLTS		REFERENCE	_____
	(E) RADIATION MEASUREMENT			
	COARSE		250+100 MRAD/HR	_____
	FINE		250+100 MRAD/HR	_____
2.0	SOURCE POSITION #3			
	(B) FINE VOLTS		REFERENCE	_____
	(D) COARSE VOLTS		REFERENCE	_____
	(E) RADIATION MEASUREMENT			
	FINE		430+172 MRAD/HR	_____
	COARSE		430+172 MRAD/HR	_____
2.1	SOURCE POSITION #4			
	(B) COARSE VOLTS		REFERENCE	_____
	(D) FINE VOLTS		REFERENCE	_____
	(E) RADIATION MEASUREMENT			
	COARSE		850+340 MRAD/HR	_____
	FINE		850+340 MRAD/HR	_____
2.2	WEIGHT		4.5	_____

                                    _____   _____
                                    INSPECTION   DATE

228

APPENDIX (H)

AVCO Corporation Quality Assurance System for Contract AF 29-(601)-6346, Active Dosimeters for Gemini Experiment D-8.

BLOCK DIAGRAM OF QUALITY CONTROL MANAGEMENT EFFORT

```
                    ┌──────────────────┐
                    │     MANAGER      │
                    │ QUALITY ASSURANCE│
                    └──────────────────┘
                             │
          ┌──────────────────┼──────────────────┐
          │                  │                  │
 ┌─────────────────┐ ┌─────────────────┐ ┌──────────────────┐
 │    INCOMING     │ │   IN-PROCESS    │ │ QUALITY ASSURANCE│
 │QUALITY ASSURANCE│ │QUALITY ASSURANCE│ │      TEST        │
 └─────────────────┘ └─────────────────┘ └──────────────────┘
```
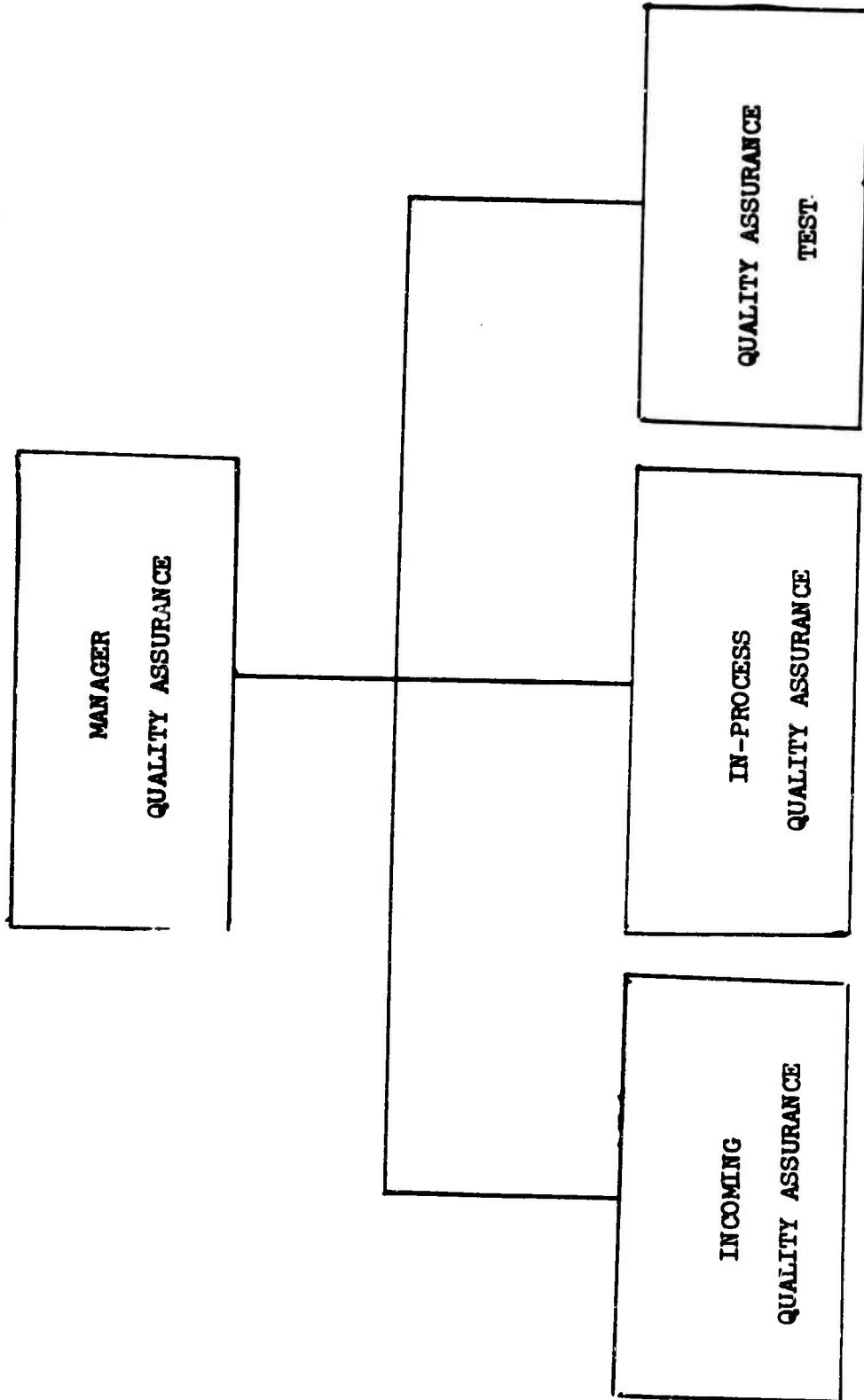
Purpose

Quality Assurance has the responsibility and authority for reviewing all specifications, documents, statement of work, etc., containin in the bid proposal package to determine the Quality Program necessary to meet or exceed proposal requirements to assure a quality product.

Contract Review

Quality Assurance has the responsibility and authority for reviewing and defining those portions of awarded contracts which pertain to quality and for promulgating, implementing, and enforcing such controls as are necessary for the successful accomplishment of the quality task stipulated by contract.

Quality Assurance is made aware of all contract awards by means of a contract synopsis form, issued from the Contract Administrator's office. Upon receipt of the contract synopsis form, Quality Assurance reviews the contract and supplements as applicable specifications for quality requirements. These requirements are compared with the Quality Assurance's bid proposal and informa-contained in the formal proposal request. Any disparities found to exist are brought to the immediate attention of the Contract Administrator for effective resolution with the customer. Quality Assurance management, after completion of contract review, authorizes and directs the implementation of the quality program described herein to the extent and the manner prescribed by the contract.

Design Review

Quality Assurance participates in the review and approval of engineering drawings and specifications on major contracts which specify AVCO/Tulsa design responsibility.

Procurement Control

On major contracts, a vendor selection board is established consisting of representatives from Quality Assurance, Purchasing, and Engineering. This board

prepares a list of potential vendors for major procurement items. A survey team consisting of representatives of the various departments or activities involved in the contract is formed and surveys of potential suppliers' facilities are made to determine their capabilities for delivering products which will meet all contractual requirements. The results of the survey are reviewed by the members of the board and recommendations are made to the Purchasing Department concerning the vendors considered best qualified as sources for the major procurement items.

Vendor Rating Program

A vendor rating program has been established by procedure which objectively evaluates vendors on the basis of the quality of products they are supplying to AVCO/Tulsa. Monthly vendor rating reports are issued to Purchasing and Management which states each vendor's quality rating. An approved list of vendors is maintained by Quality Assurance for the guidance of procurement actions by the Purchasing Department.

A special vendor summary report is prepared and distributed to Purchasing Department for each vendor who receives repeated unsatisfactory quality ratings. Purchasing is then required to answer in writing the action being taken to correct the quality problem.

Surveillance of Subcontractors

At the discretion of Quality Assurance, AVCO source inspection may be required in order to establish and maintain control over the quality of items being purchased from vendors and subcontractors which cannot be adequately inspected upon receipt; or to accelerate inspection, acceptance, and delivery of items.

It is the policy of the Government to keep Government source inspection to a minimum. The Government Quality Assurance representative at his discretion approves requests for Government source inspection if the item is an important or

critical element in the end product, and then only if one or more of the follow-ing factors apply:

It is the policy of the Government to keep Government source inspection to a minimum. The Government Quality Assurance representative at his discretion approves requests for Government source inspection if the item is an important or critical element in the end product, and then only if one or more of the follow-ing factors apply:

a. The determination of conformance of the supplies and services which at any other point would require an uneconomical disassembly or destructive testing to meet contract requirements.

b. Quality Assurance and inspection are closely related to production methods.

c. Inspection at any other point would destroy or acquire the replacement of costly packaging and packing.

d. Special instruments, gauges, or facilities required for inspection are available only at source.

e. Considerable loss would result from the manufacture and shipment of unacceptable supplies or from the delay in making necessary correc-tions.

f. Inspection at the subcontractor's plant is necessary to verify test reports, inspection records, certificates or other evidence of quality.

g. The applicable Government specification specifies that certain inspec-tions are to be made by a Government inspector and these inspections can only be performed at the subcontractor's plant.

Even if one or more of the above-enumerated conditions apply, except Paragraph g., Government source inspection is not required if test reports, inspection records, certificates or other suitable evidence of quality

233

accomplished by either AVCO/Tulsa or its subcontractor are available for use in lieu of the Government inspection at the subcontractor's facility.

Government source inspection can be requested only by and under the authorization of the Government Quality Assurance representative and does not relieve AVCO/Tulsa of any responsibility to furnish an acceptable end product or guarantee final acceptance; does not effect the prime contractor-subcontractor relationship; does not establish a contractual relationship between the Government and the subcontractor.

AVCO/Tulsa's source inspection may be performed regardless of the requirements of Government source inspection when determined necessary and desirable if and when any of the above-enumerated conditions apply.

Drawing and Change Control

The purpose of Drawing and Change Control is to establish a control of drawings issued for quotations, vendor fabrication, in-plant fabrication, customer approval, and interdepartmental approval or reference.

The following drawings are within the scope of this procedure: Drawings in conjunction with a Government contract; drawings produced for a research and development project; drawings produced for a standard product or commercial product; drawings furnished by a customer; drawings produced for proposal quotations.

The drawings are prepared, checked, and approved by the responsible project engineer from information developed or obtained from research and development, design criteria, contract sources, customers, etc. The original tracing is numbered and filed. The Program Manager or his designee then issues to the drawing control clerk a drawing issue memorandum (Form No. A/T 00-045-10-08/64).

Drawing Issue Memorandum is to contain the following information: Name of program area; vendor, or customer to receive prints; the purpose for which the prints are issued; the quantity of prints to be issued. The control of drawings is to be administered by the drawing control clerk. When this clerk receives the Drawing Issue Memorandum, he creates a drawing control card for the drawing (Form No. A/T 00-051-10-08/64). The clerk makes the necessary prints from the tracing, rubber stamping the prints with the appropriate issue stamp, dates them, and series numbers them from 1 to the number of prints made. The control card is then noted with the number of prints and distribution by number. The Drawing Issue Memorandum is then returned to the issuing program manager with the necessary prints. The memorandum is noted by the clerk reflecting the numbering assigned to the various recipients of the prints corresponding to that noted on the drawing control card.

The program manager issues the prints according to distribution number on memorandum.

Drawing changes are handled similarly to new drawings in which the revisions to tracings are ordered by the responsible Program Manager and he causes a Drawing Issue Memorandum to be prepared with this information and sent to the drawing control clerk. The program manager is responsible for collecting obsolete drawings and returning them to the control clerk who notes the control card appropriately. The obsolete prints are then destroyed unless otherwise instructed. The file copy of the obsolete print is stamped "Obsolete - Superceded by Revision" and retained in file. Customer drawings when received are delivered to the Program Manager who issues a Drawing Issue Memorandum and forwards it with customer drawings to control clerk. The prints are stamped with date of receipt and distributed as per memorandum, after being numbered and recorded on the control card. The drawings are recalled and records noted similarly to that of a new issue.

PRECISION TOOL AND GAUGE CONTROL

This procedure is applicable to the receiving and cyclical inspection of Government and Avco-owned inspection and test devices. The Quality Assurance Department is responsible for assuring that inspection and test devices are initially and periodically inspected.

All precision tools, gauges, test equipment, measuring devices, etc., whether Government, Avco, or employee-owned, will be inspected and checked to their respective standards with measurement standards that are traceable to the National Bureau of Standards or equivalent certified primary standards in accordance with frequency standard and method established.

Records of these inspections shall be maintained by the Quality Assurance Department (Form A/T 00-050-10-08/64). Any Government or Avco-owned tool, gauge, test equipment, measuring device, etc., that does not meet requirements is immediately removed from services and segregated from conforming equipment. An employee will be requested to take home any privately-owned equipment that is shown to be non-standard. A periodic surveillance will be performed to assure that the non-standard equipment has been removed from service.

Each time a device is checked or calibrated, the proper notation shall be made by the inspector on the permanent tool record.

Properly certified inspection sources may be employed for the contracting of tool and device testing and calibration. A list of such certified vendors will be maintained by the Quality Assurance Department. When a tool is so tested and calibrated, the test certification will become a part of the permanent tool record.

TRAINING

Quality Assurance inspection personnel, manufacturing , and other personnel who may have an effect upon or who are responsible for the determination of

quality will be required to successfully participate in whatever training programs are deemed necessary for them by Quality Assurance management with certifications issued in keeping with contract requirements.

STATISTICAL QUALITY ASSURANCE

The information received by inspection records and test results is summarized into statistical quality reports which are issued at regular intervals to management, manufacturing, and engineering departments, government inspectors if required by contract, and other necessary functionaries. Because of different types of data received, these reports will vary to some degree in arrangement, complexity, method of presenting data, and extent to which defects are detailed. Where possible defects will be compared with previous reporting periods to emphasize recurring discrepancies.

QUALITY ASSURANCE RECORDS

All quality control records shall be maintained as directed by Quality Assurance management in the Avco central files. Certain documents, such as tool and gauge records, may be maintained at other locations only when specifically delegated by Quality Assurance management.

All receiving inspection documentation, reject/rework tags, inspection records, etc., shall be forwarded to Quality Assurance when completed prior to filing in the Central Files.

Records shall be available at all times for review by Avco personnel and Government representatives, and copies of the records furnished them when requested.

Quality Assurance records become a prime basis for management action; therefore, entries on all forms must be legible, complete and clear. Entries such as "inoperable" when describing a discrepancy are not sufficiently descriptive and will be cause for management action.

237

Reject/rework tags are serialized and thereby controlled. Tags will be assigned to inspectors by serial number blocks and inspectors are responsible for maintaining the continuity and integrity of the system. Tags under any circumstances will not be destroyed. If a tag is rendered unusable for any reason, VOID will be written across it and the tag forwarded to the Quality Assurance department filing.

· Inspectors will maintain log books (Form A/T 00-048-10-08/64) of reject/rework tags issued. Log books will reflect serial number of tag, work order number to which tag was used, date tag was applied, and date tag was removed.

SYSTEM AUDIT

Quality Assurance performs routine periodic audits on all procedures contained in the Quality Assurance Manual to determine, (a) if necessity for procedure still exists, (b) if procedure is still adequate in all aspects, (c) if procedure is unnecessarily duplicated in part or whole by another procedure, (d) if procedure could be simplified, (e) if procedure is being followed.

Results of these audits are discussed with the program managers and are forwarded with their comments to the General Manager for appropriate action.

INCOMING QUALITY ASSURANCE

Quality Assurance is responsible for all activities incident to the quality of purchased items and materials. This responsibility includes the appropriate disposition of material through acceptance, rejection, recommendation for rework or submission to a higher authority for disposition.

Inspection of all received material will be assured by the following procedure:

a. Quality Assurance will indicate the inspector applicable to the commodity at the time of initiation of the purchase requisition by noting the inspector's name on the purchase requisition.

238

b. The Quality Assurance checklist on the reverse of the second copy of the purchase requisition will be completed at this time by Product Engineering and Quality Assurance by referencing applicable inspections and contract requirements.

c. Purchasing Department, in preparation of the purchase order, will insert the applicable inspector's name determined from the purchase requisition on the purchase order. In doing so, the receiving report will also reflect the inspector's name, since this report is part of the purchase order form.

d. The second copy of the purchase requisition containing the Quality Assurance checklist is forwarded to the Quality Assurance inspector by Purchasing. The inspector retains his copy of the purchase requisition with checklist in a suspense file for purchase requisitions awaiting receiving inspection.

e. Purchasing forwards the receiving report (part of the purchase order) to the receiving department who maintains the open reports in suspense by purchase order numbers.

f. When the material is received, the receiving department notifies the quality assurance inspector whose name appears on the purchase order copy.

g. Inspector will refer to the Quality Assurance checklist and obtain necessary inspection specifications including any characteristic sheets.

h. The inspector performs the receiving inspection according to requirements on the purchase requisition Quality Assurance checklist and documents his inspection and actions on this list. Rework/reject tags are used as necessary. Inspector signs off Quality checklist and forwards to Quality Assurance.

i. If a vendor or subcontractor certification and/or qualification is required, inspector will assure that certification and/or qualification is received and, in conjunction with Engineering, is correct and complete. Such certifications will be attached to purchase requisition checklist and forwarded along with it.

239

j. Inspector shall then allow approved material to be committed to stock.

k. Discrepant items are to be carefully segregated in an area designated by Quality Assurance, and held for Quality Assurance management action. This action will consist of orders to rework, scrap, return to supplier, or to submit to a higher authority for disposition.

l. The supplier of the defective material is notified through Purchasing by receiving a copy of a Vendor Defective Material Report that is issued by Quality Assurance.

IN-PROCESS INSPECTIONS

Assemblies and subassemblies will be subjected to inspection by Quality Assurance department. In-process inspections will be performed at any point in manufacture or assembly where progressive work will prevent subsequent inspection.

In-process inspections will be detailed on a characteristic sheet prepared under the responsibility of Quality Assurance in coordination with the responsible program manager.

In-process work will be accompanied by an inspection record prepared in advance in conjunction with the characteristic sheet. Work shall not proceed under the work release order until each check point detailed in the characteristic sheet has been inspected, accepted, and recorded in the inspection record.

If the inspected item is found to deviate from requirements, the item will be tagged as applicable. Discrepant items will be held for rework, rejection, or material review board action if applicable.

Material Review Board shall be constituted by members from Quality Assurance, program management, government representatives, and others at the direction of the Avco/Tulsa General Manager. The Material Review Board shall determine whether nonconforming items can be used in the present condition, if it can be satisfactorily reworked, or if it should be committed to scrap.

Reworked items will be reinspected and inspection recorded. Rework tag is to be removed only by the inspector and attached to the inspection record, thereby becoming a permanent part of the historical record of the work.

Inspections will be accomplished either by one hundred percent inspection or by sampling inspection subject to the approval of the Government inspector if required. All sampling inspection is performed in accordance with the provisions of MIL-STD-105 or other customer approved sampling plan.

FINAL INSPECTION

All completed work shall be subject to a final inspection detailed on the characteristic sheet and recorded on the inspection report. This inspection shall assure all contract, specification, standard, functional, dimensional, and visual requirements are met.

Reject/rework tags are to be used during the final inspection of the work. Final acceptance will be indicated by company inspection stamping along with, if required, Government approval stamp by Government inspector.

When the work is finally accepted, it shall be committed to packaging and shipping area for storage, packing, and subsequent shipping.

PACKAGING AND SHIPPING

Areas for storage, packaging and effecting shipment of completed work shall be established with the approval of Quality Assurance. Periodic inspections of the areas will be performed by Quality Assurance to assure that the areas are being maintained and that adequate precautions are being followed to assure prevention of damage of any nature or a compromise of quality to the stored goods.

Stored items shall be identified as required by contract in coordination with Quality Assurance.

Packaging and shipment shall be performed according to contract requirements detailed in the characteristic sheet and subject to a Quality Assurance inspection, acceptance, and documentation on the inspection record.

NONCONFORMING MATERIAL

All nonconforming material is identified as such and restricted from further processing until one or more of the following actions has been taken:

    a. Material is repaired to specification requirements.

    b. An engineering change is secured and documented.

    c. Authorized waivers are secured from the proper authority as designated by the individual contract.

All nonconforming material declared to be scrap material (cannot be reworked to specification requirements or is not suitable to waiver) is stored in an enclosed area under the cognizance of Quality Assurance until such time as final disposition is made by the Avco/Tulsa Property Administrator.

THE USE, CONTROL AND ISSUANCE OF INSPECTION STAMPS

Quality Assurance personnel responsible for inspection will be assigned identification numbers and furnished sets of rubber and/or metal stamps. These stamps reflect the inspector's identification number and the inspection status.

Stamps are to be applied to, (a) in-process and completed parts and/or their containers and related documents, (b) items procured under Avco/Tulsa source inspection and/or related documents, (c) items subjected to special processes such as X ray, magnetic particle inspection, etc., as required by Avco and a resident Government Quality Assurance representative or by contract.

Issuance of stamps will be documented by a control record (Form No. A/T 00-049-10-08/64) reflecting the inspector's name, signature, number, and other pertinent information. Issuance will be by Quality Assurance manager only.

Each inspector is responsible for the security, custody, serviceability, and use of the stamps issued to him. He will not permit the stamps out of his custody except by written authorization from the Quality Assurance manager. When stamps become unserviceable, inspector will advise Quality Assurance department that a new set is required and when issued to him, he will turn in the old set.

If the stamps are misplaced, lost, or stolen, Quality Assurance manager will be advised immediately. Control record will be so noted and affected inspector issued new number and stamp set. Should an inspector terminate employment, said inspector will turn in the stamps and append his signature to the control record reflecting this turn-in.

The method of stamping will be governed by the marking and specifications use applying the part number. Whenever practical, the material or item will be stamped adjacent to the part number. Whenever the direct use of the stamp is impractical due to shape, size, or quantity of parts, possible damage or mutilation of parts, or failure of drawing to specify marking method, then the stamp will be used on the package, tag, and/or labels accompanying the item.

CORRECTIVE ACTION

Prompt action is taken to correct conditions through all phases of procurement, manufacture, and testing which have resulted in, or might result in substandard or defective materials, parts, components, or services. Failures are analyzed by Quality Assurance, Product Engineering, and requested by suppliers when required. A failure report is issued by Quality Assurance on recurring failures which includes the following:

1. A clear statement of the problem.

2. A statement regarding the cause of the problem.

3. A statement regarding the action being (or to be) taken to correct the problem.

243

4. The effectivity date, or system, on which action will be effective.

Quality Assurance performs follow-up to determine if corrective action recommended is being applied and is effective.

APPENDIX (I)

Air Force Quality Control Program for Gemini Passive Dosimeter Units

1. AFWL, WLRB-1, Kirtland Air Force Base, New Mexico has initiated a quality control system which meets all necessary requirements. The government will perform quality inspections and buyoffs on the final Passive Dosimeter (PDX) flight units to insure that the highest standards of engineering and manufacturing quality have been met. Inspections and written approval will be performed at the completion of each major step involving the PDX units by the Kirtland Air Force Base Quality Control Group, the AFWL Project Officer (or his designated representative), and the supervisor of the responsible fabricating or assembly facilities. This program assures adequate quality throughout all areas of performance and includes design, development, fabrication, processing, assembly, inspection, test, packaging, shipping, and installation. Records and data essential to the effective operation of this program will be maintained. To achieve this goal, all steps leading to the production of the final PDX units will be prescribed with documented instructions dependent on existing circumstances.

2. Each of the following four major steps will be formally bought off by a Government Quality Control Inspector, the supervisor of the responsible shop, and the Project Officer or his designated representative: Material, Fabrication, Components, and Unit Integration.

3. The quality assurance program will include, but is not limited to, the following:

3.1. Material: All purchasing and handling will be done in accordance with AFSCM 74-1. These procedures are in standare usage in the procurement of all material used in the shops where the PDX units are fabricated.

3.2. Purchasing: The supplier of the 6061T6 Aluminum Alloy stock utilized in the fabrication of the PDX will provide suitable documented evidence of its

quality. A specimen may be tested chemically, mechanically, or as required to guarantee satisfaction in meeting design specifications. These documents are provided by the fabricating facility or shop at the time of delivery of the stock, and made available as required.

3.3. Storage: Until machining actually progresses, the selected stock will be plainly marked to preclude loss of its identity.

3.3.1. During the various fabrication procedures outlined in paragraph 3.4 below, the unit parts will be protected by appropriate storage procedures along with adequate identification data.

3.3.2. Upon completion of fabrication of the housing for the PDX units, they will be sealed in a polyethylene bag and appropriately marked to preclude contamination before integration.

3.4. Fabrication: The following items will be carefully controlled and checked: Tolerances on outside dimensions, wall thickness, lip thickness, bevel and seats, cleanliness, weight, final finish and appearance, anodizing uniformity and quality in accordance with MAC Drawing 52-90000, paragraph 4.1.1 (a), marking and serializations.

3.5. Machining: The machining process will be carried out on an appropriately sized stock of material approximately 1/8" oversize in all dimensions to insure adequate material for final product and supporting functions during machine operations. Any cut stock prepared for machining and stored for any period of time prior to machining operations, will be identified according to paragraph 3.3 above. The machining operations to be performed on the unit in accordance with the detailed blueprint N.A10-480-0-1, dated 10 February 1965, are as follows:

3.5.1. The sides and bottom, or cavity side, will be machined close to the final tolerances. The back or top is not machined until the last operation in order to provide adequate support during subsequent operations.

3.5.2. A vise support is provided for the outer sides to avoid flexure during the process of milling out the cavity of the body.

3.5.3. The bevel to provide sealing of the unit is now milled as well as the end seats to provide accurate seating of the lid.

3.5.4. The ends are cut out with fillet to form the mounting lips.

3.5.5. A plug is fashioned to insert in the cavity to provide rigidity in order to machine the back or top of the unit body.

3.5.6. The round edges of the body are machined and the lips are rounded.

3.5.7. The mounting holes are finally drilled to complete the basic machine operations on the PDX body.

3.5.8. The lid is fabricated from suitable sheet stock by cutting to size and shape and beveling the edge to provide the sealing channel.

3.6. Finishing: The finishing process includes polishing by hand to a standard surface finish as specified on the blueprints. Care is taken to insure the cleanliness of the finished product; i.e., absence of small metal particles, such as drillings, shearings, fillings, remaining on or imbedded in the material. Steel wool will not be used in the finishing processes.

3.6.1. Vacuum cleaning providing a strong suction should be used frequently during the machining operations to assure cleanliness.

3.6.2. Filing, polishing, or other additional machine operations will not be performed on the unit after inspections have been made and acceptance noted.

3.7. Anodizing: In accordance with MAC Report 52-90000, paragraph 4.1.1(a), all Aluminum Alloy parts visible and not painted shall be vapor degreased, and either liquid honed or barrel tumbled for two hours. The abrasive medium used is #3 triangular aluminum oxide chips. After tumbling,

the parts shall be given a 30-minute chromic acid anodizing and sealed in 190-210°F water adjusted to a PH of 4-6. The final appearance shall be a smooth uniform matte gray finish. All aluminum alloy parts will receive this treatment.

3.7.1. Specifically, the treatment which will be utilized is in accordance with MIL-A-8625A.

3.8. Marking: The finished and anodized unit will be labeled immediately after complete fabrication with Banner Rubber Stamp Co. #1448 ink (black). The label will be of the following form:

PASSIVE DOSIMETER UNIT

PART NAME: PDX   SERIAL NUMBER:

PART NUMBER: AF67983

3.8.1. The accepted flight units will be appropriately serialized.

4. Unit Integration: Integration of the PDX unit includes careful loading of the various dosimetry components into the body of the unit. To assure that no component will be broken in flight, each component will be loaded and surrounded by an acceptable form filling. This will be Nopcofoam (Type Lockform A-206), and is approved for use by MAC Report 6792. Pertinent logs or records will be maintained and will reflect the types, numbers, and array of components utilized in each serialized PDX unit. The weight of each unit will be recorded to assure that the weight limit of .2 pound is not exceeded.

4.1. Responsible personnel of the Biophysics Branch and other participating agencies have been designated for each component incorporated in the PDX. Due to their technical competence or interest, these personnel will be responsible for the preparation and provision of the components at the time of integration as well as post-flight processing.

4.1.1. Several of the dosimetry components which are being placed within the Gemini PDX units of Experiment D-8 are being supplied and analyzed by

laboratories other than AFWL. These laboratories are: The Naval Radiological Defense Laboratory (NRDL), San Francisco, California; and the Naval School of Aviation Medicine (NSAM), Pensacola, Florida.

      4.1.2. Specific dosimeter component responsibilities:

          4.1.2.1. Glass needle dosimetry: Airman Reinke, AFWL.

          4.1.2.2. Calcium Fluoride Dosimetry: Lt Joseph F. Janni, AFWL.

          4.1.2.3. Lithium Fluoride Dosimetry: Airman Edward Shope, AFWL.

          4.1.2.4. Activation foil analysis and counting: Lt LeRoy Hutzenbiler, AFWL.

          4.1.2.5. Ionization Chamber Dosimetry: Lt Joseph F. Janni, AFWL.

          4.1.2.6. The Film Dosimetry: Dr. Herman J. Schaefer, NSAM.

          4.1.2.7. Cubical block glass dosimeters: Mr. Eugene Tochilin, NRDL.

          4.1.2.8. Heavy Particle Dosimetry: Mr. Eugene Tochilin, NRDL.

4.2. Sealing: The PDX unit, completely loaded with the required components will be hermetically sealed by properly seating the lid in place and filling the beveled channel with an approved bonding epoxy. The final sealing of each unit will be inspected. Each PDX unit will be appropriately stamped and placed within a clean polyethylene bag for delivery.

5. Testing of integrated PDX units:

5.1. Complete environmental testing of the fully integrated PDX unit was performed as required by MAC Report 8433 in accordance with MIL-C-5272. All tests, with the exception of the acoustic noise test, were performed by the Test Directorate, Air Force Special Weapons Center, Kirtland AFB, New Mexico. The acoustic noise test was made at the Sandia Base Environmental Facility, Sandia Base, New

Mexico, under the auspices of the Test Directorate at Kirtland AFB. See Appendix I, "Qualification Test Results for the Passive Dosimetry Units," for results of tests performed.

5.2. It is certified that the final PDX flight units being deli_red are the same as those which were quality tested.

6. Installation and Recovery: Lt Joseph Janni, the AFWL Project Officer will personally deliver, monitor, and certify the proper installation and recovery of the PDX flight units. The flight units will be installed subsequent to T-1 day from launch.

1. This attachment contains specific details not contained in the Quality Control Document.

2. The following applicable documents, in ef·ct at the time of processing and/or inspection, form a part of this requirement.

SPECIFICATIONS

Federal

QQ-A-327   Aluminum Alloy, Plate and Sheet 6061

TT-C-595   Colors: (for) Ready Mixed Paints

Military

MIL-A-8625   Anodic Coatings, for Aluminum and Aluminum

Alloys

MIL-C-5541   Chemical Films and chemical film materials

for Aluminum and Aluminum Alloys

MIL-Q-9858   Quality Control System requirements

MIL-E-5272   Environmental testing, aeronautical and asso-

ciated equipment, general specifications for.

OTHER

McDonnell Aircraft Corporation

MAC Report 8433

--General Environmental Requirements for Model 133P

MAC Report 6792

--Physical Properties of non-metallic materials for manned space

vehicles

MAC Report 52-90000

--Finish specifications for Model 133P Gemini Spacecraft

MAC Report A531

--Interface requirements for DOD/NASA Gemini Experiment 11 (D-8)

APPENDIX (J)

Reliability Calculations for Advanced TEIC System

The table below is a collection of the realistic failure rates, λ, for all critical components in the advanced TEIC. The application factor, K_a, is the modifier of these data for the actual environment and operating stress levels under which the instruments are used.

Element	Number Used	Failure rate, λ, per 10^9 hours	Application Factor, K_a	Modified Failure rate λ_m per 10^9 hrs.
Transistor	26	140	0.062	226
Diode	30	45	1.0	1,350
Resistor	70	10	0.88	616
Capacitor	10	10	1.3	130
Capacitor, tantalum	15	50	1.1	825
Potentiometer	12	110	0.1	132
Choke	2	300	0.1	60
Transformer	3	500	0.1	150
Vacuum tube	1	189,000	0.12	22,680
Connector pins	9	5 per pin	3.0	135
TOTAL		178 COMPONENTS		26,174 fail. per 10^9 hrs.

The resultant total failure rate, 26,174 failures per billion hours, yields an average time between failures of 38,180 hours. The probability of a successful 4000-hour (6 month) mission may be calculated from the expression for reliability, R:

$$R = \exp - \lambda_m t$$
$$R = \exp - (26,174)(10^{-9})(4,000) = e^{-.1047}$$
$$= .9006 \text{ or } 90.1\% \text{ success probability.}$$

This figure can be shown to be larger, since failure of one component does not necessarily cause experiment failure. The MTBF of the TEIC system is tied very closely to the average operation time of the electrometer tube. Here a drift of 10 percent in accuracy has been denoted "failure."

REFERENCES

1. Stormer, C. Sur les trajectories des corpuscles electrises dans l'espace sous l'action du magnetisme terrestre avec application aux aurores boreales. Arch. Sci. Phys. Nat., 24, 1907.

2. McIlwain, C.E., "Coordinates for Mapping the Distribution of Magnetically Trapped Particles, " J.Geophys. Res., 66 (11), 3681,1961.

3. Jensen, D.C., and J.C. Cain, "An Interim Geomagnetic Field, "paper presented at the American Geophysical Union Meeting, Washington, D. C., April 1962.

4. Pizella, G., C.E. McIlwain, and J.A. Van Allen, "Time Variations of Intensity in the Earth's Inner Radiation Zone, October 1959 through December 1960,"J.Geophys. Res., 67 (4), 1235, 1962.

5. Holly, F.E., L. Allen, and R.G. Johnson, "Radiation Measurements to 1500 Kilometers Altitude at Equatorial Latitudes, "J. Geophys Res., 66 (6), 1627, 1961.

6. Tochlin, E., Private Communication presented with permission.

7. Chao, S.K., "Logarithmic Characteristics of Triode Electrometer Circuits," Review of Scientific Instruments, 38, December 1959.

8. Langmuir, I., "The Effect of Space Charge and Initial Velocities on the Potential Distribution and Thermionic Current between Parallel Plane Electrodes," The Physical Review, 21, 1923.

9. [1]Snell, A. H., Nuclear Instruments and Their Uses,Volume I, John Wiley & Sons, Inc., 1962.